AD NUMBER

AD480596

LIMITATION CHANGES

TO:

Approved for public release; distribution is unlimited.

FROM:

**Distribution authorized to U.S. Gov't. agencies and their contractors;
Administrative/Operational Use; MAR 1966. Other requests shall be referred to Rome Air Development Center, Griffiss AFB, NY.**

AUTHORITY

RADC ltr 27 Aug 1973

RADC-TR-66-61
Final Report

EVALUATION OF LENTICULAR SPIRAL ARRAY

F. J. Stimler

TECHNICAL REPORT NO. RADC-TR-66-61
March 1966

Communications Research Branch
Rome Air Development Center
Research and Technology Division
Air Force Systems Command
Griffiss Air Force Base, New York

EVALUATION OF LENTICULAR SPIRAL ARRAY

F. J. Stimler

AFLC, GAFB, N.Y., 18 Apr 66-120

FULL-SCALE SPIRAL ELEMENT

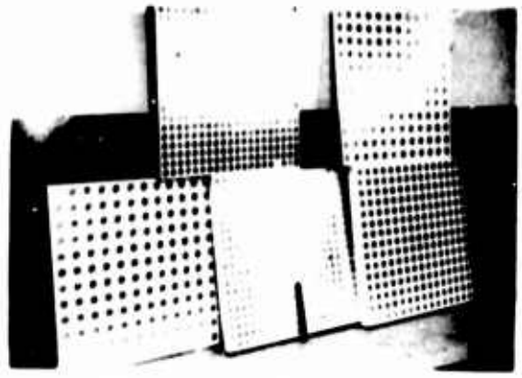

3 FT X 3 FT RF TEST MODELS

FLEXIBLE THERMAL COATING DEVELOPMENT

THIN FILM WELDING

ANECHOIC CHAMBER RF SETUP

RF RANGE TESTS

ARRAY SPACING (λ)	ANTENNA TERMINAL CONDITION					TYPE OF REFLECTING SURFACE (λ/2 THICK)	
	OPEN	SHORT	STUB SHORT (1.8 IN.)			POCKET OR CUP	PLANE
			x = λ/8	x = λ/16	x = 3λ/16		
0.75	A	B	C	L	N	A,B,C,L,N	H,I,J,K,P
1.0	-	D	-	-	-	D	
1.25	E	F	G	M	O	E,F,G,M,O	

TEST FREQUENCY = 5030 MC (λ = 2.348 INCHES)
USE CIRCULAR POLARIZATION
SPIRAL DIAMETER = 1.185 INCHES

MONOSTATIC TESTS - ALL MODELS
BISTATIC TESTS - MODELS B,D,F, AND I - 30 AND 60 DEGREES

SUMMARY OF 3 FT X 3 FT RF TEST MODELS

FOREWORD

Goodyear Aerospace Corporation (GAC), Akron, Ohio, conducted thermal studies and tests on flexible materials and theoretical and experimental rf evaluation of spiral array configurations under Contract AF30(602)-3486 from September 1964 through December 1965. RADC project number is 4519; task number is 451901; contractor's number is GER 12369.

Mr. Anthony F. Synder (EMCRR) was the RADC Project Engineer; F.J. Stimler of the Space Systems and Analytics Division was the GAC project engineer. The work was conducted as a cooperative effort by personnel from several divisions within GAC for the various specialties listed as follows:

Design	H.W. Barrett
Materials Development	W.B. Cross
Thermal Studies	J.N. Apisa
Model Fabrication	D.R. Thompson, E. Duplaga. J.A. Shannon and R.E. Welch
Microwave Consultant	B.M. Miller and J.C. Huber
Microwave Analysis	F. Fischer
Microwave Model Tests	W.D. Wheaton and G.M. Hazlip
Planning	H.T. Stewart
Contract Administration	D.H. Mitchell

Dr. E.M. Kennaugh and Mr. R.J. Garbacz of the Ohio State University Antenna Laboratory were consultants on the array scattering portion of the program.

This report is not releasable to CFSTI because it contains information prohibited for release by AFR 400-10.

This technical report has been reviewed and is approved.

Approved: [signature]
ANTHONY F. SNYDER
Project Engineer

Approved: [signature]
CHARLES A. STROM, JR.
Acting Chief
Communications Division

FOR THE COMMANDER: [signature]
IRVING J. GABELMAN
Chief, Advanced Studies Group

ABSTRACT

Goodyear Aerospace Corporation has conducted a research and development program in the areas of flexible thermal coatings, flexible solar sail materials, and theoretical and experimental rf evaluation of spiral elements and arrays.

A flexible thermal coating containing zinc oxide, silicone binder, Tinuvin "P", and toluene was rotoflex tested successfully up to 2000 cycles (see frontispiece) at test temperatures of -25, 23, and 100°C. An equivalent 1500 sun-hour ultraviolet exposure under high vacuum conditions resulted in an increase in solar absorptance and infrared emittance of less than 0.1. Sufficient information has been obtained from this development work to establish feasibility of the flexible thermal balance coating approach; however, additional characterization work must be done for any specific application.

A lightweight, packageable solar sail material possessing optical characteristics of low reflectivity and low infrared emissivity on one side (solar absorber side) and high reflectivity and high emissivity on the opposite side (solar reflector side) was fabricated and then tested under simulated space conditions. On top of a 1/4-mil Mylar substrate, alternate layers of aluminum and SiO (Haas "dark mirror" concept) were utilized to formulate the "solar absorber side" of the sail, resulting in the following optical characteristics:

Reflectivity = 0.28

Solar absorptance = 0.72

Infrared emittance = 0.05

A thick layer of SiO over an aluminized Mylar surface results in approximately the following optical characteristics for the "solar reflector side:"

Reflectivity = 0.8

Solar absorptance = 0.2

Infrared emittance = 0.7

Care must be taken to limit the thickness of the SiO coating to retain material flexibility.

Single-spiral elements were tested in an anechoic chamber for monostatic and bistatic angles at a frequency of 5030 mc for conditions of right-hand circular polarization (see frontispiece). Spiral elements with open circuit and direct short circuit between spiral terminals were investigated in addition to several lengths of stub short circuits in the form of a "U" attached to the terminals and perpendicular to the plane of the spiral. The effect of a reflecting surface (cup or plane surface) on the spiral back-scattering was also determined. Models with lengths of stub short ranging from $1/16\lambda$ to $3/16\lambda$ (0.15 inch to 0.44 inch) were tested to obtain the absolute maximum and minimum spiral radar cross section and in turn to determine the load dependent and load independent characteristics. Test results indicated that the load dependent scattering of the spiral antenna is far more significant than the load independent scattering.

Monostatic and bistatic scattering measurements were made on three-foot-square models of arrayed spiral antennas for array spacings of 0.75λ, 1.0λ, and 1.25λ and both cup-type and plane-type reflecting surfaces (see frontispiece).

The primary goal of the program was to use the experimental data to empirically determine mutual coupling effects between antennas and to compare the predicted far field pattern of the array to the measured array patterns, using the single-element pattern data.

An effort was made to adapt the single-port antenna scattering analysis to arrayed antennas. This included a method for computing the five unknown antenna parameters (A, B, γ, R_a, and X_a) of the following antenna equation.

$$\sigma = \left| Ae^{j\gamma} + B\left(\frac{Z_a^* - Z_e}{Z_a + Z_e}\right) \right|^2 = \text{measured radar cross section}$$

where

$Z_a = R_a + jX_a$ = antenna impedance,

$Z_e = R_e + jX_e$ = termination impedance,

under the assumption that the load impedance of the antenna was known. This effort was partially successful in that a Fortran computer program, which was not previously available, was developed using the fundamental equations of this technique to calculate these parameters. Due to problems of multiple roots, mechanical tolerances, uncertainties in the theoretical loads, or possibly measurement uncertainties, this program has not produced a useful set of antenna parameters from the measured antenna data. Correct results for hypothetical cases have been produced, and it should now be possible to refine either the computer program or the measurements to produce correct results for single elements. Additional fundamental work must be done in this field before a scattering approach can be applied to arrays.

TABLE OF CONTENTS

Section		Page
1	INTRODUCTION	1
2	TECHNICAL DISCUSSION	4
	A. Thermal Coating Development	4
	1. General	4
	2. Coating Formulations Considered	5
	3. Coating Application Procedures	12
	4. Effect of Rotoflexing	14
	5. Effect of Ultraviolet Exposure on Absorptance and Emittance	19
	6. Discussion of Results	20
	B. Solar Sail Materials Investigation	20
	1. Introduction	20
	2. Spectral Reflectance	21
	3. Solar Sail Solar Absorptance and Emittance Measurements	22
	4. Ultraviolet Exposure	23
	5. Results of Ultraviolet Exposure Tests.	23
	6. Discussion of Results	24
	C. RF Model Definition	25
	1. General	25
	2. Antenna Array Fabrication.	25
	3. Welding Considerations	30
	4. Test Panel Assembly	35
	D. RF Evaluation of Single-Spiral Antenna Elements	40
	1. General	40
	2. Model Description	41
	3. Measurements	43
	4. Data Analysis	56
	5. Conclusions	62
	E. RF Evaluation of Spiral Arrays	63
	1. General	63
	2. Model Description	63
	3. Measurements	64
	4. Data Analysis	72
	5. Conclusions	102
3	CONCLUSIONS	105
4	RECOMMENDATIONS	107
	REFERENCES	111

Appendix		Page
I	ROTOFLEX TESTING APPARATUS AND PROCEDURE.	I-1
II	ULTRAVIOLET IRRADIATION OF SAMPLES	II-1
III	SPECTROPHOTOMETRIC MEASUREMENTS	III-1
IV	OPTICAL PROPERTIES MEASUREMENTS	IV-1
V	GENERAL DESCRIPTION OF PHOTO-LIGHT PAINTING PROCESS	V-1

LIST OF ILLUSTRATIONS

Figure		Page
1	Lenticular Configuration Principle	113
2	Parameter Interaction of Scattering Antenna	113
3	Work Flow Chart for Coatings Investigation	114
4	Photographs of Coated Lens Material	115
5	Typical Cross Section of Panel	116
6	Cross-Sectional View of Absorptance-Emittance Sample	116
7	Photographs of Rotoflex Samples after 2000 Cycles	117
8	Solar Absorptance versus Exposure Time for Flexible Thermal Control Coatings	118
9	Emittance versus Exposure Time for Flexible Thermal Control Coatings	118
10	α_s/ϵ Ratio versus Exposure Time for Flexible Thermal Control Coatings	119
11	Optimum Solar Sail Material	119
12	Work Flow Chart for Solar Sail Investigation	120
13	Spectral Reflectance of Solar Sail Samples	121
14	Absolute Reflectance of Al-SiO Coating before and after Ultraviolet Exposure	122
15	Summary of Three-Foot-Square RF Test Models	122
16	Schematic of Three-Foot-Square Flat Panel Models for RF Evaluation	123
17	Design Details for Pocket or Cup and Plane Reflecting Types of Surfaces	124
18	Definition of Spiral Antenna Characteristics	125

Figure		Page
19	Master Patterns for 18-Inch-Square Quarter Panels with 0.75λ, 1.0λ, and 1.25λ	126
20	Sketch of Stub Short Details	127
21	Partially Welded Quarter Section Showing Protective Channels	128
22	Clean-Room Welding Installation	129
23	Close-Up of Welding Operation	130
24	Panel Division for Welding Operation	131
25	Welding Stub Shorts through Foam Cutouts	132
26	Electrodes in Welding Position as Viewed through Binoculars	133
27	Foot of Stub Short as Viewed through Mylar at 50X	134
28	Sectional View through Weld at 1000X	134
29	Test Panel Tools, Materials, Equipment, and Assemblies	135
30	Foam Support Preparation	136
31	Layout Procedure for RF Panel Array	137
32	Antenna Array Assembly	138
33	Assembly of Foam Backing to Array Panel	139
34	Reflector Face Assembly	140
35	Structural Back-Up for Parts A', D', and E'	141
36	Single-Spiral Antenna Element Design	142
37	Reflecting Surfaces for Single-Spiral Antennas	142
38	Nominal Dimensions of Single-Spiral Antenna Shorting Strip	142
39	Reflectivity Measurement Instrumentation for Single-Spiral Antennas	143

Figure		Page
40	Recorder, Receiver, Standard Targets, and Spiral Elements	144
41	A^2, B^2, $(A/B)^2$, and Shorted Element Pattern for Monostatic Return	145
42	A^2, B^2, $(A/B)^2$, and Shorted Element Pattern for 15-Degree Bistatic Return	146
43	A^2, B^2, $(A/B)^2$, and Shorted Element Pattern for 30-Degree Bistatic Return	147
44	A^2, B^2, $(A/B)^2$, and Shorted Element Pattern for 45-Degree Bistatic Return	148
45	A^2, B^2, $(A/B)^2$, and Shorted Element Pattern for 60-Degree Bistatic Return	149
46	Panel Configuration for Arrayed Elements	150
47	Reflecting Surfaces for Arrayed Elements	150
48	Shorting Strip Dimensions for Arrayed Elements	150
49	Monostatic Range Tests	151
50	System Block Diagram	152
51	Deviation of Panel Radar Cross Section from Reference Radar Cross Section	153
52	Sketch Illustrating Monostatic Scattering from Panel Array	154
53	Panel Distortion	154
54	Sketch Illustrating Bistatic Scattering from Panel Array	155
55	Thirty-Degree Bistatic Peak Returns	156
56	Sixty-Degree Bistatic Peak Returns	156
57	Isolated and Effective Spiral Element Patterns for Short Circuit Termination	157
58	Isolated and Effective Spiral Element Patterns for Open Circuit Termination	158

Figure		Page
59	Isolated and Effective Spiral Element Patterns for $\lambda/16$ Termination	159
60	Isolated and Effective Spiral Element Patterns for $\lambda/8$ Termination	160
61	Isolated and Effective Spiral Element Patterns for $3\lambda/16$ Termination	161
62	Input Data Format	162
63	Fortran IV Computer Program Listing.	163
64	Computer Results	168
65	Three-Dimensional Matrix	172
66	Rotoflex Test Apparatus	I-3
67	Rotoflex Sample in Test Apparatus	I-4
68	Ultraviolet Irradiation Apparatus	II-11
69	A-H6 Lamp Recirculating Cooling Water System	II-12
70	Filter Photometer Radiation Response	II-13
71	Diagram of Experimental Setup for Determining Filter Photometer Sensitivity	II-13
72	Spectral Reflectance Apparatus	III-3
73	Carbon Arc Solar Radiation Simulator Test Setup in Operation	IV-5
74	Diagram of Solar Simulator Test Setup	IV-6
75	Typical Heating and Cooling Curves for α_s and ϵ Measurement	IV-7
76	Dynamic Response Curves for Typical Sample	IV-7
77	Photo-Light Painting Flow Chart (Types I and II)	V-3
78	Type I Photo-Light Painting	V-4

Figure		Page
79	Type II Photo-Light Painting	V-5
80	Etching Clean-Up Technique	V-5

LIST OF TABLES

Table		Page
1	Pigmented Coatings Evaluated	6, 7, 8
2	Formulation Data for Candidate Coatings	11
3	Results of Rotoflex Tests on Candidate Coating I	15
4	Results of Rotoflex Tests on Candidate Coating II	16
5	Results of Rotoflex Tests on Candidate Coating III	17
6	Effect of Ultraviolet Exposure in Vacuum on Optical Properties of Candidate Thermal Control Coatings	18
7	Effect of Ultraviolet Exposure in Vacuum on Optical Properties of Solar Sail Type Coatings	24
8	Test Panel Assemblies.	36
9	Test Panel Subassemblies	37
10	Single-Spiral Antenna Elements.	42
11	Reference Target Power Ratio	47
12	Pattern Data of Spiral Mounted on Foam - No Reflector Backing	48
13	Pattern Data of Spiral Mounted on Small Cup	49
14	Pattern Data of Spiral Mounted on Large Cup	49
15	Pattern Data of Spiral Mounted on Plane Disk Reflector	49
16	Monostatic Return of Single-Spiral Antenna	51
17	15-Degree Bistatic Return of Single-Spiral Antenna	52
18	30-Degree Bistatic Return of Single-Spiral Antenna	53
19	45-Degree Bistatic Return of Single-Spiral Antenna	54
20	60-Degree Bistatic Return of Single-Spiral Antenna	55

Table		Page
21	Peak Single-Spiral Return Relative to Reference Target	61
22	Arrayed Antenna Elements Used in RF Tests.	64
23	Three-Foot-Square Array Pattern Data - Monostatic Return (5030 MC, Circular Polarization)	67
24	Three-Foot-Square Array Pattern Data - Thirty-Degree Bistatic Return (5030 MC, Circular Polarization).	70
25	Three-Foot-Square Array Pattern Data - Sixty-Degree Bistatic Return (5030 MC, Circular Polarization).	71
26	Comparison of Spectral Energy Distribution of A-H6 Lamp and the Solar Spectral Energy Distribution	II-3
27	Tabulated Phototube and Filter Transmission Data	II-5
28	Tabulated Values for Tungsten Lamp Radiance (N_λ) and Filter Photometer Radiation Response (S_λ)	II-7
29	Tabulated Values for A-H6 Lamp Energy Distribution (f_λ) and Filter Photometer Radiation Response (S_λ)	II-9

EVALUATION

Initially the contractor was concerned with a program in support of the launch of a pseudo passive solar sailing satellite. Problems concerned with the requirement of temperature stabilization of an active reflecting array in space through appropriate thermal coatings were investigated. The report presents the development of various thermal coating materials and test procedures used to evaluate each material under a simulated space environment. There were three (3) coatings developed that indicated acceptable performance for space application. The satellite was to have the capability of utilizing solar radiation for the purpose of orbital positioning. The report covers the development of a solar sail material that is flexible, lightweight, and has the required values of reflectivity, solar absorptance and infrared emittance. The material testing indicated that the dark mirror coating is well suited for the required application but further optimization will be required to achieve the coating for the high emittance surface.

The contractor was then directed to change program goals as the satellite requirements were eliminated. The primary goal of the new effort was to use experimental data to empirically determine mutual coupling effects between antennas and to compare the predicted far field pattern of the array to the measured array patterns, using single element pattern data. The first step was to determine the coefficients for the load dependent and load independent terms in the cross section equation for single elements. These coefficients were determined using the premise that the absolute maximum and minimum values of scattering cross section had been determined. This may have been true but could only be verified through many additional scattering measurements. Assuming that the load independence and dependence had been determined, an attempt was made to determine the value of the single element impedance. The equation for scattering cross section contains the antenna impedance and it was this equation that was programmed into FORTRAN IV computer language. The value of antenna impedance derived differed from its known value but it should be possible to refine either the computer program or the measurement procedure to correct the results. The use of the radar cross section measurements to determine the antenna impedance should be useful when the antenna terminals are not easily accessible or when known impedance measurement techniques cannot be used. The computer program developed can then be used to determine the impedance parameters of single port antennas. The attempt to extend the scattering theory developed for single port antennas to arrays in general was not successful as the array scattering equation is not of bilinear form. There may be arrays for which the equations satisfy the bilinear requirement or the resulting equations may just have a few significant terms. The negative results in this area does not mean that the scattering approach to array parameter determination is impossible. The work reported on is an attempt to extend the state of the art in antenna parameter prediction and further effort would be required before this technique can be applied to arrays.

ANTHONY F. SNYDER
Project Engineer

SECTION 1

INTRODUCTION

Early in the program, the goals were to develop a pseudo-passive communications satellite utilizing a spiral antenna array and tunnel diode amplifiers for the lenticular lens to enhance rf back-scattering. This satellite was to be packaged during launch and later deployed at orbital altitude as depicted roughly in Figure 1.

For this reason, it became necessary to develop a passive surface temperature control coating to maintain the array within close temperature limits to protect the diode and lens materials.

Preliminary thermal studies of the lenticular shape indicated that the lens surface should have a solar absorptance of approximately 0.3 and an infrared emittance of approximately 0.8 to maintain suitable material temperatures. Coatings having these optical properties are essentially white paints of the type being used on current space vehicles; therefore, it became necessary to develop a similar thermal coating that could be applied to non-metallic flexible surfaces of a packageable satellite.

Solar sailing techniques have been studied for station keeping of a lenticular satellite (Reference 1). As part of the material effort of this program, a flexible material having potential as a solar sail was evaluated briefly. This type of solar sail material must be developed for successful station keeping of large satellites with high area to mass ratios.

Manuscript released December 1965 for publication as an RADC Technical Report.

Work was performed to determine impedances through the study of scattering properties of isolated and arrayed spiral antenna elements. The approach that was taken to determine the spiral antenna parameters from scattering measurements was based on studies at the Ohio State University (OSU) Antenna Laboratory (References 2, 3, and 4). The form of the antenna radar cross section equation that was considered in the spiral antenna study is

$$\sigma = \left| Ae^{j\gamma} + B\left(\frac{Z_a^* - Z_e}{Z_a + Z_e}\right)\right|^2$$

where

Z_a (complex antenna element impedance) = $R_a + jX_a$ and

Z_e (fixed load impedance) = $R_e + jX_e$

and

σ = measured radar cross section,

$A(\theta, \phi)$ = load independent radar cross section coefficient,

$B(\theta, \phi)$ = load dependent radar cross section coefficient,

γ = phase angle between the two scattered components,

R_a = antenna radiation resistance,

R_e = load resistance,

X_a = antenna reactance,

X_e = load reactance.

The field components that result in this return are illustrated in Figure 2.

A procedure for determining isolated antenna parameters from three scattering measurements is outlined in the OSU reports (References 2, 3, and 4). One

measurement is made with a known load that is adjusted for minimum return, one is made with a known load that is adjusted for maximum return, and one is made with an arbitrary known load. The data from these three measurements is then plotted on a Smith Chart to obtain A, B, and R_a. But since the loads on the C band spiral antennas cannot be conveniently adjusted, the method that was chosen for evaluating the spiral parameters is the use of various shorting strips for loads. This requires five measurements to determine the five unknown parameters, A, B, γ, R_a, and X_a. However, some qualitative information about the scattering characteristics can be obtained with fewer measurements.

Although the OSU scattering measurement technique for determining antenna parameters had been applied only to single-port antennas, the application of this technique to determine mutual coupling effects of large antenna arrays appeared to be a logical extension of this approach. The steps that were considered for determining the antenna parameters with mutual coupling effects are to first measure the array patterns and then divide these patterns by the array factor. The single-element equation would then be applied to the resulting effective single-element patterns.

SECTION 2

TECHNICAL DISCUSSION

A. THERMAL COATING DEVELOPMENT

1. General

Passive surface temperature control is essential to the satisfactory operation of the pseudo-passive communications satellite concept. To obtain this temperature control, the thermal optical properties of the outer surface of the vehicle must be adjusted to within certain limits. Preliminary thermal studies of a lenticular satellite shape have indicated that lens surface with a low solar absorptance (α_s) to emittance (ϵ) ratio is required to maintain suitable material temperatures (see Reference 5). It is desirable to have a solar absorptance of approximately 0.3 and an emittance of approximately 0.8. Coatings having these optical properties are essentially white paints of the type being used on many current space vehicles. Available coatings, however, have not been designed primarily for application to non-metallic, flexible surfaces such as the type being considered in the present application.

The coating investigation was directed toward establishing a suitable thermal control coating system that meets the overall needs of the pseudo-passive communications vehicle. In general, the coating system required must have the following characteristics:

(1) $\alpha_s \approx 0.3$ and $\epsilon \approx 0.8$,

(2) Good ultraviolet stability

(3) Flexibility and good abrasion resistance

(4) Easily applied to Mylar with a tight bond without heat or pressure

(5) High ultraviolet opacity to protect substrate from ultraviolet damage

(6) Transparent to microwave energy

The procedure for obtaining a suitable coating was to screen a number of possible coating systems and from this group obtain the candidate systems that warranted further study. The three coatings chosen where then given a careful examination to establish their flex resistance and ultraviolet stability.

A flow chart showing the various steps taken in the coating investigation is shown in Figure 3.

2. Coating Formulations Considered

a. Preliminary Screening of Coatings. A series of screening tests was conducted to evaluate relative adhesion strength and flex resistance of potentially useful commercial and experimental thermal control coatings. All coatings except one were applied to Mylar film. Each coating was applied by spray techniques, using recommended application procedures, primers, etc. Both smooth and "vapor-blasted" Mylar film substrates were used to establish the effect of mechanical roughening on bond strength. The coatings evaluated and the results obtained are presented in Table 1.

Commercial coatings were selected for trial largely on the basis of optical properties and published space stability characteristics. The references used to obtain this information are given in Table 1. Experimental formulations were

Table 1. Pigmented Coatings

Coating No.	Type	Source	Pigment	Binder	Pigment-to-Binder Weight Ratio	Cure	Absorp (α_s)
1	White Skyspar (A423, color SA 9185)	Andrew Brown Co	TiO_2	Epoxy	Unknown	Room temp	0.22
2	White Kenacryl lacquer (M49WC17)	The Sherwin Williams Co	Unknown	Acrylic	Unknown	Room temp	0.28
3	White Silicone (Q-90-106)	Dow Corning Corp	ZnO (SP 500)	Silicone	Estimated to be approx 1.3	Room temp	0.282
4	White Silicone (RTV-11)	General Electric Co	Silica, calcium oxide, and calcium carbonate	Silicone	Unknown	Room temp	Unknow
5	White Silicone (GAC experimental) with ultraviolet absorber	The New Jersey Zinc Co General Electric Co Geigy Chemical Corp	ZnO (SP 500)	Silicone (RTV-602) Tinuvin "P" (absorber)	5	Room temp	0.32
6	White Acrylic (GAC experimental)	The New Jersey Zinc Co Leon Chemical Industries, Inc	ZnO (SP 500)	Leonite (acrylic)	5	Room temp	Unknow
7	White Acrylic (GAC experimental)	The New Jersey Zinc Co Rohm and Haas Co.	ZnO (SP 500)	Acriloid (acrylic)	5	Room temp	Unknow

tings Evaluated

bsorptance (α_s)	Emittance (ϵ)	$\Delta\alpha_s$ for 1000 Equivalent Sun Hours	Ref	Adhesion to Mylar	Remarks
.22	0.91	0.12	6, 7	Good adhesion to untreated surface; poor flexibility.	Not considered a good candidate for study.
.28	0.86	Unknown	7	Very good adhesion to untreated surface; brittle.	Unsuitable for application.
.282	Unknown	0.036	8	Fair to good adhesion to untreated surface; excellent flexibility.	Good candidate for study.
nknown	Unknown	Unknown		Very poor adhesion to primed, sand-blasted, and untreated surfaces.	Unsuitable for application.
.32	0.90	0.004	9	Very poor adhesion to primed, sand-blasted, and untreated surfaces.	Unsuitable for application.
nknown	Unknown	Unknown		Very poor adhesion to untreated surface; brittle.	Unsuitable for application.
nknown	Unknown	Unknown		Very poor adhesion to untreated surface; brittle.	Unsuitable for application.

Table 1. Pigmented C

Coating No.	Type	Source	Pigment	Binder	Pigment-to-Binder Weight Ratio	C
8	White Polyimide (GAC experimental)	The New Jersey Zinc Co DuPont	ZnO (SP 500)	Polyimide	5	12 at F
9	White Epoxy (GAC experimental)	The New Jersey Zinc Co Bee Chemical	ZnO (SP 500)	Logo EV-6184 (epoxy)	5	1 22
10	White Silicone (RTV-102)	General Electric Co	Unknown	Silicone	Unknown	Ro te
11	White Silicone (GAC experimental)	The New Jersey Zinc Co General Electric Co	Normal pigment + ZnO (SP 500)	Silicone (RTV-102)	1	Ro te
12	White Silicone (Silastic 731)	Dow Corning Corp	Unknown	Silicone	Unknown	Ro te

'igmented Coatings Evaluated (Continued)

nent-to-er ght Ratio	Cure	Absorptance (α_s)	Emittance (ϵ)	$\Delta\alpha_s$ for 1000 Equivalent Sun Hours	Ref	Adhesion to Mylar	Remarks
	12 min at 225° F	Unknown	Unknown	Unknown		Fair to good adhesion to untreated surface; fair flexibility; very good adhesion to Type H film.	Coating has slight yellow color due to binder properties.
	1 hr at 225°F	Unknown	Unknown	Unknown		Good adhesion to untreated surface; fair flexibility.	Appears to be good candidate based on adhesion and flex characteristics.
own	Room temp	Unknown	Unknown	Unknown		Very good; excellent adhesion to untreated surface; adhesion improved with primer.	Additional pigment required.
	Room temp	Unknown	Unknown	Unknown		Very good; excellent adhesion to untreated surface; adhesion improved with primer.	Excellent candidate.
own	Room temp	Unknown	Unknown	Unknown		Good; excellent adhesion to untreated surface.	About same characteristics as No. 10.

2

Table 1. Pigmented Coatings Evaluated (Cc

Coating No.	Type	Source	Pigment	Binder	Pigment-to-Binder Weight Ratio	Cure	Absorptance (α_s)	
13	Clear Silicone (RTV-140)	Dow Corning Corp	None	Silicone		Room temp		
14	White Silicone (GAC experimental)	The New Jersey Zinc Co General Electric Co	ZnO (SP 500)	 RTV-615	2	Room temp	Unknown	
15	White Silicone (GAC experimental)	The New Jersey Zinc Co Dow Corning Corp	ZnO (SP 500)	 Q-92-009 Silicone	3	Room temp	Unknown	
16	White Silicone (GAC experimental)	General Electric Co	Unknown	RTV-112	Unknown	Room temp	Unknown	

ıgs Evaluated (Continued)

Absorptance (α_s)	Emittance (ϵ)	$\Delta\alpha_s$ for 1000 Equivalent Sun Hours	Ref	Adhesion to Mylar	Remarks
				Available sample did not cure thoroughly after 24 hours.	Unsuitable for application.
Unknown	Unknown	Unknown		Available sample did not cure thoroughly after 24 hours.	Unsuitable for application.
Unknown	Unknown	Unknown		Fair to good adhesion.	About the same as No. 3; good candidate.
Unknown	Unknown	Unknown		Good; excellent adhesion to unprimed surface.	Same as No. 10, but lower in viscosity.

mostly blends of highly stable zinc oxide and selected binder materials. Reasonable care was taken to avoid the use of binders having known poor resistance to ultraviolet degradation.

As indicated previously, various reports on the subject of thermal control coatings were obtained and reviewed to form a background for coating selection. It was concluded that the particular application under consideration is somewhat unique in that, aside from other requirements, the coating must be flexible and be easily applied to Mylar without high heat or pressure. None of the reports reviewed except Reference 9 considered flexibility a basic requirement, since coatings are normally applied to metal substrates. In Reference 9 the use of thermal control coatings on flexible substrates is considered; however, test data is not reported on coatings applied to Mylar.

The primary purpose of the screening tests was to select three coating systems that displayed excellent adhesion and flex characteristics. After the selected coatings were subjected to extensive quantitative testing, as outlined in Figure 3, feasibility of the thermal coating approach could be established.

After considerable coating experimentation, it was found that because of poor adhesion and/or brittleness, most coating systems evaluated fell short of basic requirements. Of the coating systems examined, only two silicone-based formulations appeared to meet basic requirements. Both coatings were experimental formulations compounded by GAC. These formulations,No. 11 and No. 15 in Table 1, were found to have outstanding adhesion; also, the flexibility of both

coatings was excellent, imparting little stiffness to the Mylar. It was also noted that full bond strength was obtained without mechanical roughening of the Mylar surface. Of the two coatings selected, No. 15 appeared to be a particularly good candidate, since the formulation approximates that of No. 3, which was found to be highly ultraviolet stable in experiments reported in Reference 8.

b. Selection of Three Candidate Coatings. Original plans called for continued evaluation of the three best coatings resulting from preliminary screening tests. These tests, however, produced only two coating systems that warranted further consideration. In the absence of a suitable third candidate, it was thought desirable to create another coating by increasing the pigment-to-binder ratio of one of the two selected systems. Coating No. 15 was selected as the base formulation for modification. Selection of No. 15 rather than No. 11 was made because it was thought that the binder in No. 15 would perhaps be more ultraviolet stable. This conclusion was made on the basis of discussions with Dow Corning Corporation technical representatives, who indicated that DC-Q-92-009 was the binder used in DC-Q-90-106, a specially prepared thermal coating found to be very ultraviolet stable in Reference 8. Quantities of DC-Q-90-106 coating, however, were no longer available from Dow Corning Corporation.

The three formulations selected for continued evaluation are described in Table 2. These three coating systems, designated as coatings I, II, and III, are referred to in this manner throughout the report.

As discussed previously, coatings II and III are similar and differ only in the concentration of pigment. The pigment concentration of coating II has been adjusted

Table 2. Formulation Data for Candidate Coatings

Candidate Coating	Ingredients (parts by weight)		Pigment Volume Concentration* (percent)	Pigment/ Binder Weight Ratio*	Solids* (percent by vol)
I	RTV-102	100.0	16.5	1.0	19.0
	SP 500 Zinc Oxide	100.0			
	Tinuvin "P"	0.2			
	Toluene	400.0			
II	DC-Q-92-009	100.0	66.1	9.1	9.5
	SP 500 Zinc Oxide	300.0			
	Tinuvin "P"	0.4			
	Toluene	700.0			
III	DC-Q-92-009	100.0	39.4	3.0	9.0
	SP 500 Zinc Oxide	100.0			
	Tinuvin "P"	0.2			
	Toluene	390.0			

* Values are approximate and are based on limited information obtained from handbooks or manufacturers' data sheets.

close to the critical limit. The purpose of doing this was to determine the effect of very high pigment concentration on optical and physical properties and ultraviolet stability. Examination of coating III indicated a slight powderiness;however, the coating appeared to have sufficient strength for utility.

Slight formulation changes were made over the basic formulation used in screening. An ultraviolet absorber, Tinuvin "P", was incorporated in each of the candidate formulations. The use of Tinuvin "P" was thought desirable because of previous experimental results (Reference 9) that showed evidence that the absorber compound reduced ultraviolet degradation.

To assure compliance with microwave transmission requirements, coating I was tested for reflectivity in a standard S-band waveguide setup at 3120 mc. The sample showed essentially no reflectivity. Coatings II and III were not tested; however, it is estimated that these coatings would have about the same characteristics as coating I.

3. Coating Application Procedures

a. Coating Preparation. Equipment and procedures used to prepare the experimental coatings are discussed in the following paragraphs.

(1) Equipment. Coatings were ground in porcelain jar ball mills, using high-density porcelain rods. The jars, rods, and roller assembly were supplied by U. S. Stoneware Corporation.

(2) Pigment. High-purity, Type SP 500 zinc oxide, obtained from The New Jersey Zinc Company, was used in all compounding work. SP 500 was selected because of its excellent resistance to ultraviolet degradation (see References 8 and 10).

(3) Grinding. Coatings were prepared by first weighing out the required zinc oxide and blending the oxide with approximately half of the specified solvent. This mixture was then added to the ball mill. Following pigment addition, the required weight of binder was combined with the remaining solvent and added to the pigment. This mixture was then ground for 12 hours.

Special care was taken in the preparation of coatings I, II, and III, because binder materials cure from the reaction of moisture in the air. Moisture-free

solvent was used, and the ball mills, balls, and pigment were oven-dried to eliminate moisture inclusion. Also, the space above the liquid in the ball mills was purged with dry helium as additional protection. It was found that when the above procedures were followed, premature gelation did not occur.

b. Rotoflex Samples. Preparation of the rotoflex samples was accomplished in the following manner:

(1) Three 18 x 18 inch panels of 0.45-mil aluminum laminated to 0.5-mil Mylar were photo-etched to provide typical satellite lens material consisting of uniformly spaced spiral antenna elements bonded to Mylar film. Details of the etching process are given later in this section.

(2) Each 18 x 18 inch panel was mounted on a rigid cardboard with the plastic film side exposed. Dow Corning DC 4004 primer was then applied and allowed to dry.

(3) The final step in the process was to coat each panel with a different candidate coating. A Brinks spray gun with 35-psi air pressure supply was used. Sufficient coats were applied to provide a surface thickness of approximately 4 mils. After curing, nine 5.5-inch-diameter test samples were die cut from each panel.

Photographs of completed panels are shown in Figure 4. A typical cross-sectional view of the panel is shown in Figure 5.

c. Absorptance-Emittance Samples. Application of coating on prepared copper disks with Mylar bonded to each side was accomplished at the same time that

rotoflex samples were prepared. A cross-sectional view of the sample is shown in Figure 6. The same techniques used to prepare rotoflex samples were used to apply these coatings.

4. Effect of Rotoflexing

Coating adhesion tests were conducted using the rotoflex test apparatus described in Appendix I. This apparatus is designed to flex a 5.5-inch-diameter sample through rotary motion at various temperature levels. Tests were conducted at -25, 23, and 100°C on the three candidate coatings. Three samples per temperature condition, a total of nine per coating, were tested. Three tests for each temperature level were performed to assure reliability of the results obtained and to determine material consistency.

Test results supplied much needed information on the compatibility of the three candidate thermal control coatings with respect to flexing, cracking, and peeling. Since the samples also contained spiral antennas, they too were evaluated with respect to the above.

Results obtained from the rotoflex tests are given in Tables 3, 4, and 5. Photographs of the samples taken after 2000 cycles are presented in Figure 7.

Coatings I and II showed excellent flex resistance at all three temperatures (-25, 23, 100°C) through the 500-cycle level. Upon continued flexing, coating I was found to be slightly more degradation resistant than coating II. Both types, however, were not heavily damaged even after 2000 cycles at all three temperatures.

Table 3. Results of Rotof

Sample	Test Temperature (°C)	Condition of		
		50	100	200
1A	-25	Tore in jaw area; moved to new position.	No change	Etched array cracked.
2A		No change	No change	No change
3A		No change	No change	No change
1B	+23	No change	No change	Numerous small wrinkles
2B		No change	No change	Wrinkled; no separation.
3B		No change	No change	Wrinkled; no separation.
1C	+100	No change	No change	No change
2C		No change	No change	No change
3C		No change	No change	No change

sults of Rotoflex Tests on Candidate Coating I

Condition of Sample Following Cycles Noted				
200	500	1000	1500	2000
ed array ked.	Heavy wrinkles	Array cracked.	Small cracks in coating and slight separation	Increased cracking
nange	Wrinkled; cracks started in array.	No change	Cracks in coating; some separation.	Increased separation of coating
nange	Wrinkled	No change	Small hole in jaw area	Separation of coating in some areas
erous small kles	No change	Small separation in jaw area	No change	No change
kled; paration.	Heavy wrinkles	No change	No change	Some separation of coating and array noted.
kled; paration.	No change	No change	No change	Very wrinkled; no apparent separation.
nange	No change	1/32-inch cracks near center in both coating and array	No change; slight shrinkage of Mylar noted.	Cracks elongated slightly.
nange	Small cracks	No change	Small cracks in array	--
nange	No change	Cracks in jaw area	No change	Heavy wrinkles and small cracks

2

Table 4. Results of Rotoflex Tests on Candidate Coating II

Sample	Test Temp (°C)	Condition of Samples Following Cycles Noted				
		200	500	1000	1500	2000
1A	-25	No apparent damage	One crack in coating	(640) Tore at jaw.	--	--
2A		No apparent damage	No apparent damage	Three small cracks in coating	Two more small cracks in coating	(1900) Tore at both jaws.
3A		No apparent damage	Three small cracks in coating	Two pinholes in coating	Tore at upper jaw	
1B	+23	No apparent damage	Some separation and small cracks in coating	Some flaking of coating	No change	No change
2B		Minute cracks in coating	Cracks in coating; some separation of coating in jaw area.	More cracks and separation	No change	Coating flaked and separated in jaw areas
3B		Cracks and slight separation in coating	No change	Crack in antenna in jaw section	No change	--
1C	+100	No apparent damage	No change	No change	No change	Antennas on back side cracked in some areas.
2C		No apparent damage	No change	Signs of horizon creases; no cracks.	Several small pinholes in coating	Some creases, holes, and cracks
3C		No apparent damage	Crease plus few pinholes in coating	No change; new crack in coating near lower jaw.	No change in coating; crack in center on back.	--

Table 5. Results of Rotoflex Tests on Car

Sample	Test Temperature (°C)	Condition of Samples I		
		200	500	10
1A	-25	Small crack on coated side	Hairline crack on coated side; cracks in outside edge of one antenna.	Many hairl coated side antennas.
2A		Hairline cracks on coated side	Small crack in one antenna; cracking increased on coated side.	Hole in jaw
3A		Small crack in one antenna and one crack on coated side	More cracks on coated side	No apparen
1B	+23	No apparent damage except for tear in jaw area	Small cracks in antenna at jaw area	Some separ nas; hairlir coated side
2B		No apparent damage	Small cracks on coated side	Slight crac at jaw area
3B		No apparent damage	Small crack in one antenna; some cracking on coated side.	Some flakir and coating
1C	+100	No apparent damage	Peeling of antenna in jaw area	More peelir nas; some peeling on hole.
2C		(240) Cracks and separation on coated side; antennas started to peel.	More of same	Small holes on coated s peeling.
3C		(300) Cracks in antenna; no damage to coated side.	Small cracks on coated side	Small holes and more c antennas

*Substrate material used in sample fabrication was found to be chemically degraded Results should not be taken as an indication of poor coating performance.

ts of Rotoflex Tests on Candidate Coating III*

	Condition of Samples Following Cycles Noted		
	1000	1500	2000
ck on coated in outside ıntenna.	Many hairline cracks on coated side; no change in antennas.	Tear in upper jaw area; pinholes on coated side.	Tear in lower jaw area; crack in antenna apparantly same as at 500 cycles.
in one antenna; reased on	Hole in jaw area	Hole in jaw area; moved jaws; cracking increased on coated side.	Large tear in center of sample; slight separation and small crack in center antenna.
on coated	No apparent change	Small tear in center of specimen	Tear increased in size
in antenna	Some separation of antennas; hairline cracks on coated side.	No more apparent damage	No more apparent damage
on coated	Slight cracks in antenna at jaw area	Hairline cracks and some separation of coating	More cracks and separation on coated side; some extension of cracks in antenna.
in one antenıcking on	Some flaking of one antenna and coating	More of same; tear at jaw; moved sample.	More separation of coating; cracks in antenna increased.
ıtenna in jaw	More peeling of all antennas; some separation and peeling on coated side; one hole.	No apparent change	No apparent change
e	Small holes; more cracks on coated side; antennas peeling.	Some loss of antennas; more cracks on coated side.	Cracks through specimen; pieces of antennas missing.
on coated	Small holes in jaw area and more cracks in antennas	No apparent change	No apparent change

to be chemically degraded in etching solution.
ing performance.

2

Table 6. Effect of Ultraviolet Exposure in Vacuum on Optical Properties of Candidate Thermal Control Coatings

Candidate Coating No.	Ingredients (parts by weight)		Equivalent 1570 Sun-Hour Exposure							
			Before			After				
			α_s	ϵ	α_s/ϵ	α_s	ϵ	α_s/ϵ	$\Delta\alpha_s$	$\Delta\epsilon$
I	RTV-102	100.0	0.32	0.87		0.36	0.89		0.04	0.02
	SP 500 Zinc Oxide	100.0	0.30	0.85		0.31*	0.77*		0.01*	0.08*
	Tinuvin "P"	0.2	0.28	0.80		0.34	0.86		0.06	0.06
	Toluene	400.0	0.30 Avg	0.85 Avg	0.35 Avg	0.35 Avg	0.88 Avg	0.40 Avg	0.05 Avg	0.04 Avg
II	DC-Q-92-009	100.0	0.12	0.77		0.23	0.94		0.11	0.17
	SP 500 Zinc Oxide	300.0	0.13	0.77		0.22	0.86		0.09	0.09
	Tinuvin "P"	0.4	0.15	0.76		0.20	0.85		0.05	0.09
	Toluene	700.0	0.13 Avg	0.77 Avg	0.17 Avg	0.22 Avg	0.88 Avg	0.25 Avg	0.08 Avg	0.12 Avg
III	DC-Q-92-009	100.0	0.17	0.75		0.27	0.86		0.10	0.11
	SP 500 Zinc Oxide	100.0	0.16	0.75		0.27	0.88		0.11	0.12
	Tinuvin "P"	0.2	0.16	0.76		0.19**	0.86**		0.03**	0.10**
	Toluene	390.0	0.16 Avg	0.75 Avg	0.21 Avg	0.27 Avg	0.87 Avg	0.31 Avg	0.11 Avg	0.12 Avg

*Data questionable; not used to compute average.

**Sample was shadowed during exposure and received very little ultraviolet. Data was not used to compute average.

Note: Spray application method, room temperature cure, and DC-A4004 primer were used in these tests.

After completion of rotoflex tests on coating III, it was noted that the overall performance of this coating fell considerably short of the other two.

After careful study, it was determined that the poor performance of coating III resulted from the use of chemically degraded Mylar. This degradation is not easily detected but resulted from allowing the film to remain in contact with the etching solution for too long a time period. Degradation was confined only to the material used to prepare coating III samples.

Brief evaluations indicate that the performance of coating III is only slightly less than coating II when applied to undamaged Mylar.

5. Effect of Ultraviolet Exposure on Absorptance and Emittance

Coatings I, II, and III were exposed to 1570 hours of simulated space exposure, using the testing techniques outlined in Appendix II.

The optical properties (α_s and ϵ) of the samples were then remeasured and compared to the values obtained before exposure. Details of optical properties measuring techniques are discussed in Appendix IV.

Results of these tests are given in Table 6 and plotted in Figures 8, 9, and 10.

Change in solar absorptance of all three coatings, after 1000 sun hours of exposure, appears to be less than 0.1. A survey of results obtained by other organizations on other paint types of coatings applied to metal substrates indicates that 0.1 change for 1000 sun hours is about average degradation for a white coating.

6. Discussion of Results

Examination of the results obtained on the three candidate coatings indicates that the performance of all three coatings is sufficiently high to warrant their further consideration. However, of the three coatings tested, coating III appears to most closely meet the overall requirements as they are presently known. Although the optical properties of all coatings change with continued exposure, the rate of change considerably reduces with time. The solar absorptance of coating III is sufficiently low that even after extended exposure, sufficient degradation may not occur to bring solar absorptance above critical limits. The initial low value should not significantly affect vehicle performance.

It is believed that sufficient information has been obtained from the coating development work to establish the feasibility of the flexible thermal balance coating approach. However, since many factors affect the selection of an orbiting vehicle coating system, much additional characterization work should precede the final selection.

B. SOLAR SAIL MATERIALS INVESTIGATION

1. Introduction

Solar sailing techniques provide a unique method for keeping the psuedo-passive communications satellite on station. Therefore, as part of the materials effort, one potential solar sail material was briefly evaluated. Only limited work in this area was undertaken because of early program redirection.

The solar sail must have satisfactory optical and thermal properties to obtain

efficient momentum transfer from solar electromagnetic radiation. Properties required for optimum solar sail efficiency are shown in Figure 11.

After consideration of the requirements of a solar sail material, it was concluded that a dark mirror type of coating (see Reference 11) might be suitable for side 1. The dark mirror coating consists of multilayers of vapor-deposited metals and oxides and is extremely lightweight. Of particular interest is a type composed of Al, SiO, Al, SiO. With this approach, it was estimated that the practical value of R would be about 0.2 and the value of ϵ about 0.07.

An opaque coating of vapor-deposited aluminum with an overcoat of SiO was considered a satisfactory choice for side 2. Using this combination, values of R and ϵ on the order of 0.8 and 0.7 seemed realistic. Lightweight 0.25-mil Mylar was selected as the substrate material. The film serves as a carrier for the coatings as well as the basic structural member for transmitting load resulting from the reactions of the solar radiation. Weight of the above combination is approximately 0.35 oz/yd^2.

Three samples, 3 x 3 inches of the above described material, were prepared for GAC by Kinney Vacuum Division, New York Air Brake Co. The optical properties of the material were measured as received and remeasured after being exposed to simulated space conditions for an equivalent 2450 sun-hour exposure. The investigation procedure is outlined in Figure 12.

2. Spectral Reflectance

Total reflectance measurements were made on each side of the three especially

prepared solar sail samples. Date obtained in the wave length region between 0.3 and 0.8 micron is presented in Figure 13.

The data obtained shows general agreement with published data on similar coatings (Reference 11). It also provides an excellent means for determining the repeatability of the sample production process.

3. Solar Sail Solar Absorptance and Emittance Measurements

Measurement of the thermal properties (solar absorptance and emittance) of the solar sail material before and after ultraviolet exposure was accomplished by means of the dynamic thermal vacuum technique described in Appendix IV. Simulated solar radiation is used to heat the sample, which is subsequently permitted to cool. Sample temperatures are monitored as a function of time throughout the test. The coating emittance and solar absorptance were then derived from the time-temperature data as outlined in Appendix IV.

Test specimens were prepared in the same manner as the samples for coating analysis except that the coatings were applied to the Mylar substrate before bonding to the copper disk.

Solar absorptance and emittance of the dark mirror side were determined to be 0.72 and 0.050 respectively. The solar absorptance appears to be in line with values reported by other investigators. The emittance of 0.05, however, appears to be somewhat lower than the 0.08 normally reported for this type of coating.

Solar absorptance and emittance of side 2 were determined to be 0.224 and

0.055 respectively. It was determined that the thickness of the SiO coating on side 2 of the solar sail is about 0.2 micron and therefore would explain the low emittance characteristics. To obtain a higher emittance, the thickness of the SiO coating would have to be increased. Limited data indicates that about 5 microns would be required to provide an emittance of 0.7. It is very doubtful that the material could be folded if coated with this thick a layer.

4. Ultraviolet Exposure

Ultraviolet exposure tests were conducted to determine the space stability of the solar sail material. Samples disk prepared for optical properties measurement were irradiated with ultraviolet under high vacuum conditions, using the procedures outlined in Appendix II. Vacuum pressure during exposure was maintained in the range of 1 to 5 x 10^{-5} mm Hg. The temperature of the sample was held at approximately 70°F during exposure. Ultraviolet energy was supplied by a water-cooled, A-H6, high-pressure, mercury arc lamp. Ultraviolet intensity was monitored throughout the test. Intensity ranged between 4 and 5 times the level provided by the sun in space.

5. Results of Ultraviolet Exposure Tests

The effect of ultraviolet exposure on the optical properties of the solar sail material is shown in Table 7. In general, results indicate that the exposure of an equivalent 2450 sun hours did not bring about a large change in the optical properties of either coating. However, emittance of the dark mirror could not be measured because the sample overheated and was lost while making absorptance measurements.

A comparison of the absolute reflectance characteristics of the Al-SiO coated side before and after exposure was also made. This data is presented in Figure 14. Absolute reflectance measurements were obtained using the equipment described in Appendix III.

6. Discussion of Results

Although the solar sail material was examined only to a limited degree, it would appear that the dark mirror coating is very suited to the requirements. Further optimization of a coating system for side 2, however, will be required to obtain high emittance.

Table 7. Effect of Ultraviolet Exposure in Vacuum on Optical Properties of Solar Sail Type Coatings

Description	Equivalent 2450 Sun Hour Exposure				$\Delta\alpha_s$	$\Delta\epsilon$
	Before		After			
	α_s	ϵ	α_s	ϵ		
Dark mirror coating deposited on 0.25-mil Mylar, 4 layer type, SiO-Al-SiO-Al (Ref 11)	0.72	0.050	0.795	*	0.075	--
Vapor-deposited aluminum with SiO over coating. Substrate is 0.25-mil Mylar. SiO thickness is approx 0.25 micron.	0.224	0.055	0.280	0.108	0.056	0.053

*Emittance not measured because sample was damaged in making absorptance measurement.

C. RF MODEL DEFINITION

1. General

Single-element and three-foot-square models of the spiral antenna concept were required for rf anechoic and range tests respectively. A representative single-spiral element is shown in the frontispiece. Three types of single elements were made for the anechoic chamber tests; namely, the open circuit spiral, the short circuit spiral and the stub short spirals as defined on Figure 15.

Several spiral array spacings and types of reflecting surfaces were investigated for the rf range tests, as defined in Figure 15. The three stub short lengths of $\lambda/8$, $\lambda/16$, and $3\lambda/16$ were chosen as a result of the monostatic and bistatic rf tests of single-spiral elements in the anechoic chamber. The details of the test panels are shown schematically in Figure 16. The models basically consist of three to five separate layers depending on the type of reflecting surface incorporated. Details of material characteristics and sizes are also included. Basically 11 separate models were constructed primarily for the pocket or cup type of reflecting surface. Five of these models were adapted for the plane type reflecting surface by substitution of the back subassembly (see Figure 16). Figure 17 shows the design details for both types of reflecting surfaces under consideration.

2. Antenna Array Fabrication

a. Photographic Artwork Development. A model spiral pattern of etched copper on a fiberglass substrate was supplied to GAC by Sylvania Electric Products, Inc per RADC direction.

The spiral antenna characteristics are defined in Figure 18. The mathematical definitions are given for the spaces between the metallic elements for the spiral concept. Further theoretical treatment and overall analysis can be obtained from Reference 12. Arrays of these elements in conjunction with a tunnel diode circuit are being tested at X band at different spacings both at Sylvania (Reference 13) and RADC. Since GAC rf tests were to be conducted at a frequency of 5030 mcs, it was necessary to increase the Sylvania spiral size by a factor of 1.6.

The following steps were used to develop GAC's spiral pattern from Sylvania's etched copper sample:

(1) Sylvania's single spiral pattern was contact printed and a 1 : 1 scale negative was obtained as shown in the following sketch:

(2) Step 1 negative was enlarged by a factor of 1.6 to yield a size for 5030-mcs testing.

(3) Step 2 negative was enlarged to a 10 : 1 scale, and two positive cronaflex working copies were made for design A (open circuit) and design B (short circuit).

(4) Design A was reworked to obtain a 0.030 inch line width at a 1 : 1 scale at the inner two termination points.

(5) Design B was reworked to obtain a 0.030 inch line width at a 1 : 1 scale at the inner termination points.

DESIGN A - OPEN CIRCUIT

DESIGN B - SHORT CIRCUT

(6) Designs A and B were reduced from a 10 : 1 to a 5 : 1 scale and photo-light painted (Type II) (See Appendix V) together in order to keep them identical in size. The photo-paint was used to clean up the ragged edges.

(7) The artwork of designs A and B was reduced from a 5 : 1 to a 1 : 1 scale. (1.185 ±0.003 inch diameter). (Obtained one negative of each.)

(8) Photographically duplicated artwork from step 7, making the number required for all panel assemblies. (Obtained positive films at a 1 : 1 scale.)

(9) Positive films of the spirals were assembled onto an overlay of stable film (18 x 18 inches), using an accurate scribed guide as an assembly aid. This was done for each antenna array spacing (0.75λ, 1.0λ and 1.25λ), using an assembly tolerance of ±0.020 (see Figure 19).

(10) The film was contact printed, and an 18 x 18 inch negative (1 : 1 scale) was obtained as a completed master pattern.

b. Chemical Etching Procedure. The rf antenna array models for free space range tests were three feet square. For ease in handling, the array sections were made in four 18 x 18 inch pieces, which were later spliced together.

The following chemical etching procedure was used to etch the master pattern artwork on 0.00045-inch aluminum bonded to 0.0005-inch Mylar film.

(1) The aluminum-Mylar sheets were cut to 20 x 20 inches and taped onto mounting boards of aluminum (0.040 inch) with the aluminum side up.

(2) The aluminum surfaces to be etched were then cleaned, using a small block of styrafoam with fine pumice and water until unbroken water film was obtained during the rinse.

(3) The surface was air dried for 10 minutes, then heat dried for 5 minutes at 150 to 200°F.

(4) The photo-sensitive material was applied in a darkroom by dipping the mounting board into a large tray of Kodak Metal Etch Resist (KMER) by mixing 2 parts KMER thinner with 1 part KMER resist. The mounting board was laid in the tray with the aluminum surface up for 3 to 5 minutes. The mounting board was removed from the tray very slowly and allowed to drain and air dry for 10 to 15 minutes.

(5) When the air dry was complete, the resist coating was cured for 5 minutes at 150 to 200°F and cooled tc room temperature.

(6) The master pattern negative was then exposed for 8 minutes on the photo-resist surface.

(7) KMER Developer (full strength) was used to develop the unwanted resist away. Development time was 2 minutes.

(8) The developed panels were rinsed in cold running water and air dried at room temperature.

(9) The sheets of material were then removed from the aluminum mounting

and taped onto a plexiglass mounting board. (The aluminum mounting was used to withstand the curing temperature in the photo-resist process, and the plexiglass mounting was used to resist the next step etching process.)

(10) The chemical etching process was obtained by mixing 11 to 15 ounces of NaOH/gallon of water (by weight) in a dipping tank.

(11) The plexiglass panels were then placed in the tank and allowed to etch away the unwanted aluminum from the sheets for 30 minutes at room temperature.

(12) After the etching process, the sheets were rinsed in cold water for 30 minutes and air dried for 30 minutes. The sheets were then removed from the plexiglass mounting and placed in a cardboard folder with thin sheets of paper to separate each sheet.

c. Recommendations for Future Array Fabrication. The substrate materials to be used for fabrication of future arrays shall be selected to minimize all tolerances that build up in all steps of fabrication. The basic substrate should be of stable material and of such thickness as to prevent wrinkling in the photographic, etching, welding, and assembly processing.

For photographing any future master patterns of the spiral arrays, GAC's newly developed "pinhole camera" method should be considered. The advantages gained here are time and cost saving plus improved oriented spacings between spirals. This innovation is possible simply by photo-painting the pinholes to obtain a very sharp edge around the circumference of the hole. This factor greatly

improves the resolution of the image. This new development is also planned to be used for multilayer printed circuit boards and many electronic applications.

In the future, all photographic film used for the spiral master pattern shall be DuPont's Cronar Ortho S Litho Film or equivalent. This is a new stable film that is replacing photographic glass plates in most applications. Tests showed that it is three to four times as stable as any other film made to date.

To locate the metal cups in the same relationship as the master pattern, a photographic metal template should be made by contact printing directly from the master pattern onto the metal template. Then the centers of each spiral can be located and center-punched for drilling.

3. Welding Considerations

a. Background. The welding requirement was to join stub shorts of a suitable material to the spiral antennas. The characteristics required of this material are as follows:

(1) Good electrical conductivity

(2) Ductility (for small bend radii)

(3) Rigidity (to maintain its shape during handling and service)

(4) Welding compatibility (for joining to the aluminum foil)

(5) Minimum mass

Both strength and electrical conductivity were required of this joint without serious damage to the Mylar. Three welding processes - electron beam, laser,

and parallel gap - were considered. The first two involve very high initial equipment costs and would require special tooling. Also, it is likely that the use of these processes would result in Mylar damage. Electron beam welding can be accomplished only in a vacuum, and parts are therefore limited to the size of the chamber. Special safety precautions must be observed when using the laser welding process. However, this does not mean that these processes should not be considered for future work. It is doubtful whether ultrasonic welding would work with these materials, since the Mylar would tend to dampen the vibrations. Electrodes as they are now being made would not have access to the joint area.

Parallel gap welding is a resistance welding process wherein the heating necessary to the formation of a joint is effected by the resistance to the flow of current between two electrodes, both on the same side of the materials to be joined. Initial equipment costs are comparatively low, and no special tooling is required. The parallel gap method was chosen because the equipment was available and it seemed the most practical for this application.

b. Stub Short Material Selection. The stub width was established at 0.030 inch. Available foils under 0.010-inch thick were sheared into strips for weld tests. Cursory weld schedule searches were made to establish the degree of compatibility for welding to aluminum. Welding was attempted using the following materials:

(1) 0.0034-inch René 41

(2) 0.003-inch brazing stock (melting temperature 1200°F)

(3) 0.007-inch brass

(4) 0.003-inch stainless steel

(5) 0.002-inch copper

Of these, the 0.007-inch brass appeared to be the most weldable. Several single elements were welded and tested electrically. The conductivity across the joint was good. The parent material strength or its bond strength was evidently insufficient to support the mass of the 0.007-inch stub, since joint failure occurred during subsequent testing.

Further weld tests were conducted, and it was found that 0.003-inch stainless steel welded satisfactorily. A change was made to this material to reduce the stub mass. Even with the new material, parent material failures occurred during testing and handling. This was remedied by adding a small amount of [illegible] the joint after welding.

c. Equipment. The welding machine is a capacitor-discharge, parallel-gap, 40-watt-second Weltek (Wells Electronics, Inc). This has a force range of 3 ounces to 10 pounds, a variable working stroke, and a throat depth of 3 inches. Before welding the large test panels, the weld head was returned to the factory for modification. This included increasing the throat depth to 9 inches, calibrating the weld force, and adding a micro adjuster for easy and repetitive adjustment of the electrode gap.

d. Weld Schedule Development. A good weld in a material combination such as this should demonstrate the ability to pull out a 0.015 - 0.020 inch diameter slug of the thinner material when loaded in peel. This was accomplished with the brass stubs using 3.9 watt-seconds, 1.6-pound force, 0.003-inch electrode gap, and Class 2 (RWMA*) electrodes having a 0.020 x 0.040 inch face. When the change

*Resistance Welder Manufacturers' Association

was made to Type 302, 0.003-inch stainless steel, the schedule used was 300 units (approximately 1.1 pound) of force, 3.4 watt-seconds of energy, 0.007-inch electrode gap, and Class 2 electrodes having a 0.015 x 0.035 inch face. The back-up or base material has a definite bearing on the amount of weld energy required to effect a good weld. For example, more energy is required when using copper than when using glass. The electrode face size, the electrode gap, and the land area where the weld is being made are the most critical parameters.

e. Fabrication Techniques

(1) Shorting Stubs. The stainless steel foil was first sheared into strips 6 x 0.030 (±0.002) inches. These strips were then gripped at the ends and stretched beyond the yield point so that they would be flat and straight. The strips were placed, five at a time, in a two-stage forming tool. The first stage forced the material down to form the top and sides of the stub. The second stage bent the two feet over and sheared them off to the proper length (see Figure 20).

(2) Welding and Handling Fixtures. In the early portion of the program, the panels were welded in 18-inch-square quarters. With the new welding machine arms, which extended the throat depth to nine inches, it was possible to weld halfway across the quarter panel. An 18-inch-square aluminum table was attached to the weld head base to support the parts during welding. The Mylar sheet was positioned and taped to a 20-inch-square aluminum sheet that was free to move across the support table under the electrodes. After a row of stubs was welded in place, a channel was bolted down to protect the welded stubs during subsequent work and handling (see Figure 21). A Teflon-covered strip of metal was made to position

the stubs. It was an aid in welding but could not be removed after welding without damage to the parts.

(3) Welding (Panels C and G). Figure 22 shows the operator positioning a panel for welding. This clean-room installation shows the dual-range power supply, which discharges current through the electrodes of the dual-head. A foot pedal moves the electrodes vertically and triggers the current discharge when a preset weld force is reached. All welding is done with the aid of 10X Bausch and Lomb stereo binoculars and an illuminator. Stub shorts are positioned with tweezers and held manually until the electrodes apply sufficient force to fix the stub location. The electrodes are cleaned with a very fine (600-grit) emery board about every 10 welds. The electrodes are formed with a double bend, as shown in Figure 23. The upper bend gives clearance for the stub and permits good visibility; the lower bend makes the welding portion of the electrodes parallel. With this short portion being a constant section, the electrodes can be dressed repeatedly without changing the size of the contact face or the electrode gap. Following welding, a drop of Vitel* is applied with a hypodermic needle (0.010-inch hole) to the foot of the stub. The Vitel flows enough so that upon drying it helps distribute the load of the stub short mass to the adjacent Mylar and aluminum.

(4) Welding (Panels L, M, N, and O). The Mylar panels with the stub shorts attached presented a handling problem; therefore, it was decided that for the balance of the program, the Mylar should be bonded to the foam before welding. It was further decided that to minimize labor, the panels be made in three sections

*TM, The Goodyear Tire & Rubber Co, Akron, Ohio.

approximately 12 x 36 inches as shown in Figure 24, rather than in the original four 18 x 18 inch sections. The 36 x 36 inch panels were divided into three equal lengths and three equal widths as nearly as possible. The actual width was controlled by the antenna array spacing. The slit lines were made parallel to a line drawn through the inner antenna terminals. The section at the bottom of Figure 24 shows how the panels were reassembled and cemented together after the welding was completed. The remaining assembly procedure was the same as for panels A and E as far as cup spacers and back-up structure were concerned. A partially welded panel is shown in Figure 25. A new set of electrodes was made to provide better accessibility for welding through the foam panel and to accommodate the longer ($3\lambda/16$) stub shorts. Figure 26, a view of the electrodes in the welding position as seen through the stereo binoculars, shows what the operator sees when welding the rear foot of the stub short. Figure 27, a view of the stub short foot as seen from the bottom through the Mylar, shows where melting and resolidification of the Mylar have taken place. Figure 28, a sectional view through the weld, shows the stainless steel to aluminum bond. The sequence of operations incorporating the bonding of the Mylar to the foam sections before welding was very satisfactory throughout the fabrication processes. Special handling boxes and separator foam sheets were used to prevent panel damage during transportation from one area to another.

4. Test Panel Assembly

a. General. Figure 29 shows the equipment used to manufacture the test panels and examples of the separate components. Table 8 describes the test panels, and Table 9 identifies the various subassemblies of the test panels.

Table 8. Test Panel Assemblies

Panel Assembly	Subassemblies No. (See Table 9)		Antenna Array Spacing	Cup Reflectors	Type of Circuit	Stub Height Dimension (X)
	Front	Back				
A	1	4	0.75λ	Yes	Open	--
B	2	4	0.75λ	Yes	Direct short	--
C	3	4	0.75λ	Yes	Stub short	λ/8
D	5	6	1.0λ	Yes	Direct short	--
E	7	8	1.25λ	Yes	Open	--
F	9	8	1.25λ	Yes	Direct short	--
G	10	8	1.25λ	Yes	Stub short	λ/8
H	1	11	0.75λ	No	Open	--
I	2	11	0.75λ	No	Direct short	--
J	3	11	0.75λ	No	Stub short	--
K	12*	11	0.75λ	No	Stub short	λ/16
L	12*	4	0.75λ	Yes	Stub short	λ/16
M	15*	8	1.25λ	Yes	Stub short	λ/16
N	14*	4	0.75λ	Yes	Stub short	3λ/16
O	13*	8	1.25λ	Yes	Stub short	3λ/16
P	14*	11	0.75λ	No	Stub short	3λ/16

*Stub shorts welded to front face panel after assembly of Mylar to foam.

Table 9. Test Panel Subassemblies

Sub-assembly No.	Antenna Array Spacing	Cup Reflectors	No. of Cups	Hole Size in Foam (inches)	Foam Thickness (inches)	Covering on one Side	Type of Circuit	
1	0.75λ	No		1-7/16	0.375	Yes	Open	
2	0.75λ	No		1-7/16	0.375	Yes	Direct short	
3	0.75λ	No		1-7/16	0.375	Yes	Stub short	λ/8
4	0.75λ	Yes	400	1.350	0.375	No	NA	
5	1λ	No		1.7/16	0.375	Yes	Direct short	
6	1λ	Yes	225	1.350	0.375	No	NA	
7	1.25λ	No		1-7/16	0.375	Yes	Open	
8	1.25λ	Yes	144	1.350	0.375	No	NA	
9	1.25λ	No		1-7/16	0.375	Yes	Direct short	
10	1.25λ	No		1-7/16	0.375	Yes	Stub short	λ/8
11	--	No		NA	0.212	Al sheet	--	
12	0.75λ	No		1-7/16	0.375	Yes	Stub short	λ/16
13	1.25λ	No		1-7/16	0.375	Yes	Stub short	3λ/16
14	0.75λ	No		1-7/16	0.375	Yes	Stub short	3λ/16
15	1.25λ	No		1-7/16	0.375	Yes	Stub short	λ/16

b. Foam Support Preparation. The foam used to support the array and reflector components was rigid polyurethane foam having a nominal density of 2 lb/cu ft. The foam was cast in one 42 x 84 x 10 inch piece and then cut to 42 x 42 x 10 inches The block foam was sliced to the required slab thickness on a band saw. A 36 x 36 inch template and a sharp knife were used to trim the panels to size.

The trimmed panels were placed in the drill template (see Figure 30). Two of the side rails were adjustable to provide light clamping pressure on the foam

and to allow for slight dimensional variations of the foam panel. The template was then turned over so that the foam panel was down against a sheet of plywood (see Figure 30). The next operation was to pilot drill 1/4-inch-diameter holes through the drill template (see Figure 30). A collet was mounted on the drill bit to eliminate excessive drilling and to minimize wood chip debris from the plywood back-up board. The fixture was turned over again with foam side up. The enlarged holes were drilled as shown in Figure 30. The hole saws used had lengthened center bits to engage the 1/4-inch holes in the drill template before cutting the foam. A 1-7/16 inch-diameter hole saw was used for the panels to which the array was mounted. A hole saw ground to a 1.350-inch-diameter was used for cutting the panels in which the cups were mounted. The outside diameter of the cups was 1.359 inches, thus creating an interference fit of 0.009 inch.

c. Antenna Array Face Assembly. The etched quarter panel arrays were received untrimmed. Mylar film drawing material was used on a flat surface to lay out the centerlines for a 36 x 36 inch panel. The layout also included the centerlines for the outside row of arrays for each quarter panel. Figure 31 illustrates the layout procedure and defines dimensions for the three spacings involved.

Figure 32A shows the positioning of the first quarter panel, lining up with the layout centerlines, and then taping it down. Figure 32B shows the placement of the second quarter panel. Figure 32C shows all four quarter panels in position and prepared for trimming. The panels were trimmed on the centerlines only, and the trimmed-off material was removed as shown in Figure 32D. The butt edges of the panels were then seamed with pressure-sensitive Mylar tape as shown in

Figure 32E. All of the foregoing operations were performed with the etched side, or metal side, down.

At this point, the assembled array panel was turned over to put the etched side up and realigned with the layout in preparation for mounting of the foam panel. This procedure also served as proof of dimensional accuracy of the array assembly. Along the 36-inch-long sides, small wood battens were tacked down as guides for placing the rigid foam backing (see Figure 33A). One coat of a polyurethane elastomer adhesive was applied to the bonding surface of both the foam and the array sheet (see Figure 33B). Immediately after adhesive application, the foam backing was positioned. After the foam backing was in place, it was covered with a plywood sheet, which in turn was weighted with shot bags. The assembly was left in this condition for not less than 24 hours, the room temperature cure time for the polyurethane adhesive.

d. Reflector Face Assembly. One of the reflector face assemblies consists of a sheet of thin aluminum bonded to a foam spacer 0.212 inch thick. To further stiffen this panel, a 36-inch-square piece of 1/2-inch plywood was added to the back side of the aluminum.

The reflector panels using the aluminum cups for the reflector element were assembled as follows: Using the polyurethane elastomer adhesive, the foam was cemented with one coat over the contact area between the cup and foam (see Figure 34A). The cups were cleaned using acetone solvent. A wood holder with a groove cut to receive the open end of the cup was used to position the cups. The depth of

the groove in the holder was 0.355 (+0.000, - 0.010) inch. The cups were placed in the holder as shown in Figure 34B and positioned in the foam as shown in Figure 34C. The adhesive was allowed to cure for 24 hours at room temperature before any further handling.

e. Panel Tolerances and Flexural Stability. A common master was not used for the spacing of the antenna array sheets and the drill fixture. Therefore, there were situations where the cumulative tolerances were in opposite directions. Although no test panel was rejected because of this, better alignment could have resulted if a common master had been made.

Additional foam, as a hollow core structure, had to be provided to stiffen the test panels for field test conditions. Figure 35 shows the construction of this added stiffener and its position relative to the cup reflector panels.

D. RF EVALUATION OF SINGLE-SPIRAL ANTENNA ELEMENTS

1. General

The purpose of the single-spiral antenna patterns was to obtain data that could be compared to the corresponding data of the arrayed spiral antennas. As a result, single-element models were fabricated, and scattering measurements were made of the spirai antennnas with specified terminations. The effort was concentrated on evaluating the load independent coefficient, A, and load dependent coefficient, B, for the particular spiral antennas. The relative magnitude of these two quantities indicates the amount of interference that can be expected when the reflecting antenna is used in a communications system.

The following discussion of single-spiral antenna elements includes data first presented in Reference 14.

2. Model Description

The single-spiral antenna models and terminations that were used for the reflectivity measurements and analysis are presented in Table 10. The spiral antennas are copies of the Sylvania design discussed in Reference 13. Since the original antennas were designed for the 7.5 to 8 gc range, the scattering antenna models were enlarged by a factor of 1.6 to be compatible with the reflectivity range equipment that was available at 5030 mc. The spiral antenna supplied by Sylvania and an enlarged spiral antenna are shown in Figure 36. The diameter is about 0.5 wave length at the measurement frequency of 5030 mc. The radiating region of the antenna is approximately 1 wave length in circumference, and the radiation pattern rotates with frequency as the radiating region changes with frequency. Although the antennas were designed for an antenna impedance of 60 ohms, Sylvania deduced that the actual impedance was $\approx$ 62 ohms on the basis of the performance of their tunnel diode antennafier systems. They also determined that the elipticity ratio was less than 3 db over the half power radiation beamwidth. This beamwidth varied between 50 and 90 degrees, depending on the measurement plane, and had a nominal value of 75 degrees.

Cross-sectional views of the spiral antenna reflecting surfaces are shown in Figure 37, and a sketch indicating nominal dimensions of the shorting strips is shown in Figure 38. Since the single-element terminations were constructed by

Table 10. Single-Spiral Antenna Elements

Model	Bistatic Angle (degrees)	Spiral Termination						
		SC	OC	λ/16	3λ/32	λ/8	5λ/32	3λ/16
1. No Reflector Backing								
a. Terminals Horizontal	0	X	X			X		
b. Terminals 45°	0	X	X			X		
c. Terminals Vertical	0	X	X			X		
2. Plane Disk Reflector								
a. Terminals Horizontal	0	X	X			X		
b. Terminals 45°	0	X	X			X		
c. Terminals Vertical	0	X	X			X		
3. Large Cup (1.469" Dia)								
a. Terminals Horizontal	0	X	X			X		
b. Terminals 45°	0	X	X			X		
c. Terminals Vertical	0	X	X			X		
4. Small Cup (1.312" Dia)								
a. Terminals Horizontal	0	X	X			X		
b. Terminals 45°	0	X	X			X		
c. Terminals Vertical	0	X	X			X		
d. Terminals Vertical	0	X	X	X	X	X	X	X
e. Terminals Vertical	15	X	X	X	X	X	X	X
f. Terminals Vertical	30	X	X	X	X	X	X	X
g. Terminals Vertical	45	X	X	X	X	X	X	X
h. Terminals Vertical	60	X	X	X	X	X	X	X

NOTE: SC = short circuit. OC = open circuit. λ = wave length (2.348").

hand, the mechanical tolerances were somewhat greater than for the terminations that were used with the arrayed elements.

3. Measurements

a. General. An empirical study was conducted in an effort to separate the load dependent from the load independent scattering of a single-spiral element. The data acquired consists of scattering patterns of the element with various shorting configurations attached to the terminals.

b. Measurement Facilities. All single-element measurements were conducted in a C-band anechoic chamber lined with Emerson & Cumming Ecosorb CV-6 absorber material (≈ 0.1 percent maximum power reflection, i.e., -30 db).

Two conical horns were designed and fabricated with a dielectric card inserted to achieve right-hand circular polarization. The measured circularity in each horn was ≤ 0.35 db. The aperture diameter of each horn is 4.0 inch, hence the far field ($R = 2D^2/\lambda$) is 13.6 inches. The spiral elements, which have a diameter slightly greater than one inch, will have a much smaller minimum range requirement. The range length used was 31.0 inches. This more than doubled the minimum far-field requirement and facilitated convenient handling.

A small azimuth rotator was fitted with a 2.0-inch diameter foam cylinder target support. This cylinder was found to be essentially invisible at the test frequency (5030 mc, λ = 2.348 inch).

The equipment block diagram and photographs of the system that was used for monostatic measurements and the system that was used for bistatic measurements are shown in Figure 39. The block diagram portion enclosed by dashed lines is used for monostatic operation only. For bistatic operation, the two horns are connected as shown by the dotted lines. The operation of the bistatic system is straightforward and will not be discussed in detail. The operation of the monostatic system requires rather unique tuning, however, and will be discussed in the following paragraphs.

The klystron is locked on the test frequency by a crystal-controlled frequency-stabilizing unit. The frequency meter and oscilloscope are used for initial tuning of of the klystron. The frequency stabilizer ensures long-term frequency stability of one part in 10^6. The klystron output is fed through a tuner and a waveguide isolator to the E arm of the magic T. This energy is split between arms 1 and 2. The reflected energy received by the antenna is split between the E arm and the H arm. The isolator in the transmitter line prevents this received energy from reaching the transmitter system. The received energy from the H arm is fed through a tuner, an isolator, a precision attenuator, and to the mixer. A portion of the transmitter energy is taken out via a directional coupler and fed through an attenuator and a slotted line (used as a phase shifter) to the receive system. This energy is adjusted in amplitude and phase such that it cancels the undesired background reflections entering the receive system through the antenna. This yields a null condition and hence facilitates very accurate target measurements.

The monostatic system is initially tuned as follows:

(1) The background cancelling network is disconnected.

(2) The variable attenuator connected to the antenna is set for maximum attenuation.

(3) The receiver and a VSWR indicator are connected to the mixer on arm 1 of the magic T.

(4) The tuner in the transmit line and the tuner connected to arm 1 of the T are adjusted for a maximum on the VSWR indicator. (The attenuation was inserted in the antenna arm to minimize the effect of a mismatch at the horn, on the matching of the E arm and arm 1.)

(5) The attenuator connected to arm 1 is set for maximum attenuation to minimize reflections from the mixer.

(6) A detector is placed in the vicinity of the target mount.

(7) The attenuator in the antenna arm is set for minimum attenuation.

(8) The tuner in the antenna arm is adjusted for a maximum at the target position (this matches arm 2 and the antenna).

(9) The receiver and VSWR indicator are connected to the mixer in the receive line.

(10) A scattering device is placed on the target mount.

(11) The tuner on the H arm is adjusted for a maximum indication on the VSWR indicator.

This procedure was repeated several times to achieve a good match at each of the four ports of the magic T.

The background cancelling network was then connected and adjusted for a minimum on the recorder with no target on the mount. This tuning was repeated as required throughout the measurement effort. Figure 40 is a photograph of several of the spiral elements and the corner reflector reference targets as well as the receiver and recorder system.

c. Measurement Procedure. After the system was properly tuned and checked out, the following procedure was followed to obtain the data patterns:

(1) With the target mount in position (no target), the background cancelling network was adjusted for a null.

(2) The background return was then recorded as the empty mount was rotated.

(3) A reference target (dihedral corner reflector) was positioned on the mount and its return (±36 degrees from the peak) was recorded.

(4) With the reference positioned for peak return, i.e., normal incidence, calibration levels were recorded using the precision attenuator in the receive line (this records the system linearity).

(5) The element under test was positioned on the mount and its scattering pattern ($\pm 120^{o}$) was recorded.

(6) The target was removed and the background return was again recorded.

The reference target used was a dihedral corner reflector with a 1.5 x 1.5 inch aperture. A double reflection reference was required to illuminate and detect the return using a single or "same sense" antenna with circular polarization. Since the aperture dimensions are less than a wave length, the absolute radar

Table 11. Reference Target Power Ratio

Corner Reflector*	Measured (db)	Calculated (db)
σ_6/σ_4	7.05	6.00
$\sigma_4/\sigma_{1.5}$	17.04	15.80
$\sigma_6/\sigma_{1.5}$	24.09	21.80

*The subscripts refer to the aperture dimension.

cross section (σ in units of area) is not known; i.e., the standard equation for the radar cross section of a dihedral is valid only if the dimensions are large with respect to λ. In an effort to determine the absolute radar cross section for the reference used, two larger dihedral corner reflectors were also measured. The relative difference between the three corner reflectors as measured and as calculated using $\sigma = 8\pi\ a^2b^2/\lambda^2$ for each is given in Table 11.

If it can be assumed that the 6-inch dimension, i.e., $\approx 2.5\lambda$, is large enough for the radar cross-section equation to be valid, it appears that the actual radar cross section of the small corner reflector is 18.9 square inches or $3.42\lambda^2$. This is computed using the difference between the calculated ratio of the large to the small and the measured ratio between the large and the small corner reflectors. This difference is approximately 2.3 db.

In all reference target measurements, the corner reflectors were mounted such that the bend is normal to the axis of rotation. In this position, the pattern in the vertical plane is considerably broader and hence the mounting position is much less critical.

d. Measurement Results. To determine the optimum element orientation and the optimum backing, several preliminary experiments were conducted. Two cup reflectors (each $\lambda/4$ deep) were used in addition to a plane disk-shaped back and no reflector backing. The two cups were 1.31 and 1.47 inches in diameter. The smaller cup was the original design; however, since its circumference was very nearly 2λ, the larger size was also fabricated to determine the possible resonant ring effect. Three elements (open, short, and $\lambda/8$ stub) were measured with each of these four backing configurations and in each of three orientation positions. These three positions were such that (1) the line joining the terminals of the spiral was parallel to the axis of rotation, (2) the line was oriented normal to the axis of rotation, and (3) the line was oriented at 45 degrees to the axis of rotation. The results of these experiments are given in Tables 12 through 15. In each case, the 3-, 10-, and 13-db beamwidths are given as well as the peak gain relative to the peak of the reference target.

Table 12. Pattern Data of Spiral Mounted on Foam - No Reflector Backing

Beamwidth and Gain (db)	Element Configuration								
	Short			Open			$\lambda/8$ Stub		
									
3	60	55	52	46	59	40	61	57	54
10	113	97	106	82	107	71	111	101	98
13	129	109	139	91	124	80	130	116	113
Gain	-4.3	-3.7	-4.2	-5.1	-4.8	-5.0	-4.4	-4.0	-4.5

Table 13. Pattern Data of Spiral Mounted on Small Cup

Beamwidth and Gain (db)	Element Configuration								
	Short			Open			λ/8 Stub		
									
3	56	60	46	54	68	48	57	64	48
10	114	110	94	113	126	95	117	112	92
13	138	126	108	144	183	115	150	129	107
Gain	+0.8	+0.9	+0.8	-1.6	-2.6	-2.5	-1.2	-1.8	-1.6

Table 14. Pattern Data of Spiral Mounted on Large Cup

Beamdwidth and Gain (db)	Element Configuration								
	Short			Open			λ/8 Stub		
									
3	55	55	47	55	57	43	60	53	51
10	111	105	93	123	130	85	130	101	109
13	133	142	107	157	226	98	169	171	134
Gain	+1.3	+1.6	+1.5	-0.5	-1.2	-0.5	-0.2	-0.5	0.0

Table 15. Pattern Data of Spiral Mounted on Plane Disk Reflector

Beamwidth and Gain (db)	Element Configuration								
	Short			Open			λ/8 Stub		
									
3	50	50	51	47	50	48	49	53	56
10	96	89	90	84	93	82	104	91	97
13	110	101	100	94	106	89	119	104	108
Gain	+2.5	+3.0	+2.5	+2.7	+2.6	+2.0	+0.8	+1.0	+1.0

The following conclusions were drawn from the data in Tables 12 through 15.

(1) The smaller cup will be used for all future testing, since there is no apparent detrimental effect of the 2 λ circumference and since it exhibited the larger 3-db beamwidth.

(2) The spiral will be oriented with the line between the terminals parallel to the axis of rotation. This is a somewhat arbitrary choice; however, this orientation did, in most cases, exhibit the higher gain relative to the reference.

Each of seven spiral terminations was measured monostatically and at 15, 30, 45, and 60 degrees bistatic. The seven termination configurations were as follows: short, open, λ/16 stub, 3λ/32 stub, λ/8 stub, 5λ/32 stub, and 3 λ/16 stub.

The data has been reduced and is given in Tables 16 through 20. The return relative to the reference target peak is given in four-degree increments for each element at each bistatic angle.

In all cases, the peak target return and the peak of the reference target were >35 db above the average recorded background level. For this reason, the possible uncertainty due to background of any peak level is ±0.2 db. The absolute radar cross section of the target peak could then be in error by

$$\pm \left[(0.2)^2 + (0.2)^2\right]^{1/2} = \pm 0.28$$

due to background effects on both the target and reference, using the root-sum-square method of computing the combined errors. This assumes that the errors

Table 16. Monostatic Return* of Single-Spiral Antenna

Aspect Angle (degrees)	Element Configuration						
	Short	Open	λ/16 Stub	3λ/32 Stub	λ/8 Stub	5λ/32 Stub	3λ/16 Stub
0	+1.5	-2.2	-0.1	-1.0	-1.2	-3.0	-1.4
4	+1.5	-2.3	-0.2	-1.1	-1.3	-3.1	-1.5
8	+1.3	-2.4	-0.4	-1.4	-1.4	-3.4	-1.6
12	+0.9	-2.6	-0.7	-1.7	-1.8	-3.8	-1.9
16	+0.5	-3.0	-1.1	-2.0	-2.1	-4.4	-2.4
20	-0.1	-3.4	-1.7	-2.6	-2.8	-5.2	-2.9
24	-0.7	-3.9	-2.3	-3.2	-3.4	-6.0	-3.5
28	-1.4	-4.5	-3.0	-3.8	-4.1	-7.0	-4.2
32	-2.3	-5.2	-3.8	-4.6	-5.0	-8.0	-4.9
36	-3.0	-6.0	-4.8	-5.3	-5.9	-9.1	-5.8
40	-4.0	-7.0	-5.8	-6.4	-7.0	-10.4	-6.8
44	-5.1	-8.1	-6.9	-7.5	-8.4	-11.9	-8.0
48	-6.4	-9.1	-8.2	-8.8	-9.7	-13.4	-9.3
52	-7.8	-10.5	-9.8	-10.1	-11.2	-15.2	-10.9
56	-8.8	-11.5	-11.1	-11.8	-12.9	-16.8	-12.3
60	-10.6	-12.5	-12.8	-13.0	-14.4	-18.4	-13.8
64	-11.9	-13.4	-14.2	-14.3	-15.5	-19.1	-15.0
68	-13.1	-14.0	-15.4	-15.4	-16.3	-19.0	-16.0
72	-14.0	-14.3	-16.3	-15.9	-16.5	-18.2	-16.5
76	-14.7	-14.8	-16.8	-16.1	-16.5	-17.2	-16.6
80	-15.0	-15.0	-17.0	-16.1	-16.4	-16.4	-16.6
84	-15.5	-15.2	-17.2	-16.2	-16.4	-15.7	-16.6
88	-15.9	-15.6	-17.4	-16.4	-16.5	-15.0	-16.7
92	-16.3	-15.9	-17.8	-16.6	-16.8	-14.4	-16.9
96	-16.9	-16.3	-18.1	-16.9	-17.2	-14.1	-17.2
100	-17.7	-17.1	-18.9	-17.5	-17.7	-14.0	-17.7
104	-18.8	-18.0	-19.7	-18.4	-18.5	-14.1	-18.5
108	-20.0	-18.8	-20.6	-19.4	-19.5	-14.4	-19.5
112	-21.5	-20.0	-21.6	-20.4	-20.9	-15.0	-20.8
116	-23.1	-20.7	-22.4	-21.8	-22.0	-15.9	-21.9
120	-24.0	-21.0	-22.5	-22.7	-22.7	-16.8	-22.8

*Return relative to 1.5" x 1.5" corner reflector.

Table 17. 15-Degree Bistatic Return* of Single-Spiral Antenna

Aspect Angle (degrees)	Element Configuration						
	Short	Open	λ/16 Stub	3λ/32 Stub	λ/8 Stub	5λ/32 Stub	3λ/16 Stub
0	+1.0	-2.6	-0.9	-1.7	-1.8	-2.2	-2.8
4	+1.0	-2.6	-0.9	-1.7	-1.9	-2.3	-2.9
8	+0.7	-2.8	-1.0	-1.9	-2.0	-2.5	-3.2
12	+0.4	-3.1	-1.3	-2.2	-2.3	-2.7	-3.5
16	-0.1	-3.5	-1.7	-2.5	-2.6	-3.1	-3.9
20	-0.7	-3.9	-2.1	-2.9	-3.1	-3.6	-4.4
24	-1.4	-4.4	-2.6	-3.4	-3.7	-4.3	-5.1
28	-2.1	-5.1	-3.2	-4.0	-4.3	-5.0	-5.8
32	-2.8	-5.8	-3.9	-4.8	-5.2	-5.8	-6.6
36	-3.7	-6.6	-4.7	-5.6	-6.2	-6.8	-7.5
40	-4.7	-7.5	-5.6	-6.6	-7.2	-7.8	-8.6
44	-6.0	-8.6	-6.7	-7.8	-8.4	-9.1	-9.9
48	-7.2	-9.8	-8.0	-9.0	-9.8	-10.7	-11.4
52	-8.7	-11.2	-9.5	-10.6	-11.5	-12.3	-13.0
56	-10.6	-12.7	-11.1	-12.2	-13.2	-14.2	-14.6
60	-12.4	-14.3	-12.9	-14.2	-15.1	-16.6	-16.1
64	-14.3	-16.0	-14.8	-16.3	-17.0	-19.0	-17.1
68	-16.3	-17.3	-16.5	-18.2	-18.5	-21.2	-17.4
72	-17.6	-18.0	-17.7	-19.7	-19.3	-22.4	-17.1
76	-18.3	-18.1	-18.3	-20.3	-19.2	-22.2	-16.4
80	-18.3	-18.0	-18.3	-20.2	-18.7	-21.4	-15.7
84	-18.1	-17.7	-18.0	-19.7	-18.3	-20.5	-15.0
88	-18.0	-17.6	-17.9	-19.4	-18.1	-20.0	-14.5
92	-18.0	-17.6	-17.9	-19.3	-18.1	-20.0	-14.2
96	-18.2	-17.7	-18.0	-19.4	-18.2	-20.1	-14.2
100	-18.7	-18.0	-18.3	-19.7	-18.6	-20.6	-14.3
104	-19.6	-18.7	-19.2	-20.4	-19.4	-21.5	-14.8
108	-20.7	-19.7	-20.3	-21.5	-20.6	-22.9	-15.8
112	-22.6	-21.0	-22.0	-23.0	-22.2	-25.0	-17.0
116	-25.1	-23.0	-24.2	-25.2	-24.2	-27.2	-18.9
120	-27.9	-26.0	-26.7	-27.2	-26.6	-28.6	-22.0

*Return relative to 1.5" x 1.5" corner reflector

Table 18. 30-Degree Bistatic Return* of Single-Spiral Antenna

Aspect Angle (degrees)	Element Configuration						
	Short	Open	λ/16 Stub	3λ/32 Stub	λ/8 Stub	5λ/32 Stub	3λ/16 Stub
0	+0.4	-2.8	-1.1	-1.9	-2.0	-2.3	-3.0
4	+0.3	-2.8	-1.2	-1.9	-2.0	-2.4	-3.0
8	+0.1	-2.9	-1.3	-2.0	-2.1	-2.6	-3.2
12	-0.2	-3.1	-1.5	-2.1	-2.4	-2.8	-3.4
16	-0.6	-3.4	-1.8	-2.4	-2.7	-3.1	-3.8
20	-1.1	-3.7	-2.3	-2.8	-3.0	-3.5	-4.3
24	-1.7	-4.2	-2.8	-3.2	-3.5	-4.1	-4.9
28	-2.2	-4.8	-3.4	-3.8	-4.1	-4.9	-5.5
32	-3.0	-5.5	-4.2	-4.3	-5.0	-5.7	-6.3
36	-3.8	-6.3	-5.0	-5.1	-6.0	-6.5	-7.1
40	-4.7	-7.1	-6.0	-6.0	-7.0	-7.5	-8.1
44	-5.7	-8.2	-7.1	-6.9	-8.0	-8.6	-9.1
48	-6.9	-9.6	-8.3	-8.0	-9.3	-10.0	-10.4
52	-8.2	-11.0	-9.9	-9.1	-10.9	-11.4	-11.8
56	-9.8	-12.3	-11.6	-10.6	-12.5	-13.1	-13.1
60	-11.5	-13.9	-13.4	-12.2	-14.2	-15.0	-14.8
64	-31.3	-15.4	-15.6	-14.0	-16.1	-17.2	-16.0
68	-15.0	-16.8	-17.8	-15.9	-18.0	-19.2	-16.7
72	-16.7	-17.8	-19.6	-17.4	-19.1	-20.9	-17.2
76	-18.0	-18.4	-20.8	-18.7	-19.7	-21.6	-17.2
80	-18.5	-18.7	-21.1	-19.4	-19.7	-21.6	-16.9
84	-19.1	-18.8	-21.0	-19.9	-19.6	-21.4	-16.3
88	-19.5	-18.9	-20.9	-20.0	-19.6	-21.0	-15.8
92	-19.8	-19.1	-20.9	-20.1	-19.8	-21.0	-15.6
96	-20.4	-19.6	-21.0	-20.3	-20.2	-21.3	-15.6
100	-21.2	-20.3	-21.6	-20.9	-21.1	-22.0	-15.6
104	-22.5	-21.4	-22.6	-21.9	-22.2	-23.0	-16.0
108	-24.7	-23.2	-24.4	-23.2	-24.1	-25.0	-16.6
112	-27.5	-25.9	-27.0	-25.3	-26.8	-27.4	-17.9
116	-30.6	-29.5	-30.0	-28.4	-29.7	-30.5	-19.4
120	-29.5	-31.0	-29.7	-32.0	-28.9	-29.9	-22.2

*Return relative to 1.5" x 1.5" corner reflector.

Table 19. 45-Degree Bistatic Return* of Single-Spiral Antenna

Aspect Angle (degrees)	Element Configuration						
	Short	Open	λ/16 Stub	3λ/32 Stub	λ/8 Stub	5λ/32 Stub	3λ/16 Stub
0	-0.2	-3.1	-1.5	-2.3	-2.2	-2.7	-3.2
4	-0.3	-3.1	-1.5	-2.4	-2.3	-2.7	-3.3
8	-0.6	-3.3	-1.7	-2.5	-2.4	-2.8	-3.4
12	-0.9	-3.5	-1.9	-2.6	-2.7	-3.1	-3.6
16	-1.3	-3.8	-2.2	-2.8	-3.0	-3.4	-4.0
20	-1.7	-4.1	-2.5	-3.2	-3.4	-3.8	-4.4
24	-2.2	-4.6	-3.0	-3.5	-3.8	-4.3	-4.9
28	-2.7	-5.2	-3.5	-4.0	-4.5	-4.9	-5.5
32	-3.4	-5.9	-4.1	-4.5	-5.0	-5.7	-6.3
36	-4.2	-6.5	-5.0	-5.2	-5.8	-6.5	-7.0
40	-5.1	-7.3	-5.8	-6.1	-6.7	-7.3	-7.8
44	-6.2	-8.4	-6.8	-7.0	-7.7	-8.3	-8.8
48	-7.3	-9.5	-8.0	-8.1	-8.8	-9.5	-10.0
52	-8.7	-10.8	-9.3	-9.3	-10.2	-10.8	-11.4
56	-10.5	-12.3	-10.7	-10.7	-11.8	-12.3	-12.7
60	-11.9	-13.8	-12.3	-12.2	-13.3	-14.0	-14.2
64	-13.8	-15.7	-14.0	-13.8	-15.2	-15.9	-15.8
68	-15.9	-17.5	-16.0	-15.3	-17.1	-17.9	-17.3
72	-17.8	-19.5	-18.0	-16.9	-19.1	-19.9	-18.9
76	-19.7	-21.1	-20.0	-18.2	-21.0	-21.9	-20.3
80	-20.5	-22.7	-21.9	-19.6	-22.7	-23.5	-21.6
84	-22.9	-23.7	-23.3	-20.5	-23.7	-24.6	-22.4
88	-24.0	-24.5	-24.4	-21.1	-24.4	-25.2	-22.8
92	-25.2	-25.1	-25.1	-21.8	-25.0	-25.6	-22.7
96	-26.2	-25.9	-25.8	-22.4	-25.5	-26.0	-22.3
100	-27.7	-27.0	-26.6	-23.2	-26.1	-26.8	-21.9
104	-29.2	-28.2	-27.7	-24.2	-26.8	-27.8	-21.7
108	-30.3	-29.7	-29.0	-25.5	-27.5	-28.2	-21.8
112	-29.8	-29.7	-29.3	-26.9	-27.6	-28.3	-22.3
116	-27.2	-27.7	-28.0	-27.1	-26.6	-26.8	-23.5
120	-24.4	-25.6	-25.5	-25.8	-25.0	-24.8	-25.3

*Return relative to 1.5" x 1.5" corner reflector.

Table 20. 60-Degree Bistatic Return* of Single-Spiral Antenna

Aspect Angle (degrees)	Element Configuration						
	Short	Open	λ/16 Stub	3λ/32 Stub	λ/8 Stub	5λ/32 Stub	3λ/16 Stub
0	-0.5	-3.2	-1.7	-2.3	-2.4	-2.8	-3.3
4	-0.6	-3.3	-1.8	-2.4	-2.5	-2.9	-3.4
8	-0.7	-3.4	-1.9	-2.6	-2.6	-3.0	-3.5
12	-1.0	-3.6	-2.0	-2.7	-2.8	-3.3	-3.7
16	-1.3	-4.0	-2.2	-3.0	-3.2	-3.6	-4.0
20	-1.7	-4.5	-2.7	-3.3	-3.6	-4.0	-4.5
24	-2.2	-4.8	-3.1	-3.7	-4.1	-4.6	-5.0
28	-2.7	-5.4	-3.6	-3.5	-4.8	-5.0	-5.6
32	-3.3	-5.9	-4.2	-4.8	-5.3	-5.7	-6.2
36	-4.0	-6.7	-5.0	-5.6	-6.0	-6.3	-6.9
40	-4.9	-7.5	-5.7	-6.3	-6.9	-7.1	-7.7
44	-5.7	-8.5	-6.5	-7.2	-7.9	-8.1	-8.7
48	-6.8	-9.6	-7.6	-8.3	-9.0	-9.2	-9.9
52	-8.0	-10.8	-8.7	-9.5	-10.2	-10.4	-10.9
56	-9.5	-12.3	-9.9	-10.7	-11.6	-11.8	-12.0
60	-10.9	-13.9	-11.2	-12.0	-13.0	-13.2	-13.0
64	-12.6	-15.8	-12.8	-13.6	-14.7	-15.1	-14.0
68	-14.4	-17.6	-14.5	-15.2	-16.5	-17.0	-15.1
72	-16.4	-19.7	-16.2	-17.0	-17.3	-18.9	-15.8
76	-18.4	-21.8	-18.0	-18.8	-20.1	-20.9	-16.4
80	-20.2	-24.0	-19.7	-20.5	-21.8	-22.5	-17.1
84	-21.8	-25.8	-20.8	-22.0	-23.2	-23.9	-17.7
88	-22.7	-27.2	-21.7	-23.2	-24.3	-24.8	-18.4
92	-23.1	-27.6	-22.1	-24.0	-25.0	-24.9	-19.3
96	-23.1	-27.2	-22.2	-24.3	-25.1	-24.8	-20.1
100	-22.8	-26.3	-22.1	-24.1	-24.7	-24.1	-21.0
104	-22.2	-24.8	-21.7	-23.6	-24.0	-23.2	-21.7
108	-21.3	-23.1	-21.1	-22.6	-23.0	-22.2	-22.3
112	-20.3	-21.7	-20.3	-22.6	-21.7	-21.0	-22.7
116	-19.2	-20.1	-19.4	-20.3	-20.3	-19.7	-22.7
120	-18.0	-18.7	-18.3	-19.0	-19.1	-17.5	-22.1

*Return relative to 1.5" x 1.5" corner reflector.

are independent. The overall accuracy figure for each measurement (peak) would be the root-sum-square combination of the above plus the possible error due to the equipment etc.

A reasonable figure for the instrumentation is $< \pm 0.5$ db. The total error on any peak value for σ is

$$\Delta\sigma = \pm \left[(0.28)^2 + (0.5)^2\right]^{1/2} = \pm 0.6 \text{ db.}$$

The total error obviously increases for levels lower than the peak. However, as long as the return is no more than 10 db below the peak, the error due to background is better than

$$\pm \left[(0.2)^2 + (0.5)^2\right]^{1/2} = \pm 0.54 \text{ db,}$$

which when combined with the equipment accuracy, yields an overall possible accuracy of

$$\Delta\sigma = \pm \left[(0.54)^2 + (0.5)^2\right]^{1/2} = < \pm 0.74 \text{ db.}$$

4. Data Analysis

a. General. The equation,

$$\sigma = \left| Ae^{j\gamma} + B \frac{Z_a^* - Z_e}{Z_a + Z_e} \right|^2,$$

was examined in an effort to separate the load dependent coefficient, A, from the load independent coefficient, B, of the single-spiral element. It had been originally hypothesized that the interference between the two quantities as a function of shorting

position followed a simple function such as a sine curve. In this case, only three scattering measurements would have been necessary to determine the coefficients. From this examination, it was established that vector addition of the two quantities is not such a simple function and five measurements are necessary to be able to determine A and B along with the unknown parameters, γ (the phase between A and B), R_a, and X_a. As a result, several spiral antennas with different terminations were fabricated and tested before the initial attempt to solve for the five unknowns was found to be unsuccessful. The data from these measurements are shown in Tables 16 through 20. However, it was found that the two coefficients, A and B, can be determined from a pair of equations if absolute maximum and absolute minimum radar cross sections are measured. The derivation of these two equations is presented in the following paragraphs.

b. Load Dependent and Independent Coefficients. The measured radar cross section of an antenna with a reactive load can be expressed as

$$\sigma = \left| Ae^{j\gamma} + B\Gamma \right|^2$$

where

$$\Gamma = \frac{Z_a^* - Z_e}{Z_a + Z_e} = e^{j\eta}.$$

A minimum return results when $\eta = \pi + \gamma$. Then

$$\sigma_x(\theta,\phi) = \left[A(\theta,\phi)\right]^2 - 2\left[A(\theta,\phi)\right]\left[B(\theta,\phi)\right] + \left[B(\theta,\phi)\right]^2.$$

A maximum return results when $\eta = \gamma$. Then

$$\sigma_n(\theta,\phi) = \left[A(\theta,\phi)\right]^2 + 2\left[A(\theta,\phi)\right]\left[B(\theta,\phi)\right] + \left[B(\theta,\phi)\right]^2.$$

Adding the above equations,

$$\sigma_x(\theta,\phi) + \sigma_n(\theta,\phi) = 2\left[A(\theta,\phi)\right]^2 + 2\left[B(\theta,\phi)\right]^2 .$$

Subtracting the same equations,

$$\sigma_x(\theta,\phi) - \sigma_n(\theta,\phi) = -4\left[A(\theta,\phi)\right]\left[B(\theta,\phi)\right].$$

Then substituting for $\left[A(\theta,\phi)\right]^2$ gives

$$\sigma_x(\theta,\phi) + \sigma_n(\theta,\phi) = 2\left[\frac{\sigma_x(\theta,\phi) - \sigma_n(\theta,\phi)}{-4B(\theta,\phi)}\right]^2 + 2\left[B(\theta,\phi)\right]^2$$

or

$$16\left[B(\theta,\phi)\right]^4 - 8\left[B(\theta,\phi)\right]^2\left[\sigma_x(\theta,\phi) + \sigma_n(\theta,\phi)\right] + \left[\sigma_x(\theta,\phi) - \sigma_n(\theta,\phi)\right]^2 = 0.$$

Therefore,

$$\left[B(\theta,\phi)\right]^2 = \left\{8\left[\sigma_x(\theta,\phi) + \sigma_n(\theta,\phi)\right] \pm \sqrt{64\left[\sigma_x(\theta,\phi) + \sigma_n(\theta,\phi)\right]^2 - 64\left[\sigma_x(\theta,\phi) - \sigma_n(\theta,\phi)\right]^2}\right\} \div 32$$

$$= 0.25\left[\sigma_x(\theta,\phi) + \sigma_n(\theta,\phi)\right] \pm 0.5\sqrt{\sigma_x(\theta,\phi)\,\sigma_n(\theta,\phi)} .$$

Similarly,

$$\left[A(\theta,\phi)\right]^2 = 0.25\left[\sigma_x(\theta,\phi) + \sigma_n(\theta,\phi)\right] \mp 0.5\sqrt{\sigma_x(\theta,\phi)\,\sigma_n(\theta,\phi)} .$$

c. Relative Magnitude of Coefficients. The relative magnitudes of A and B are indistinguishable in their solution from the open and short circuit radar cross-section equations. The relative magnitude of these quantities can be established by computing A^2_{max}/B^2, which results from comparing the maximum load independent

radar cross section that can be obtained from the cup reflector (ignoring polarization) to the load dependent radar cross section of just the spiral antenna.

The maximum load independent radar cross section, σ_c, (ignoring polarization effects) that can be obtained from the cup reflector is

$$\sigma_c = \frac{4\pi}{\lambda^2} (\pi r^2)^2$$

where

λ = wave length,

r = radius of the cup.

As indicated in Reference 15, the load dependent radar cross section of the spiral antenna, σ_d, can be expressed as

$$\sigma_d = A_e \Gamma^2 G$$

where

A_e = effective aperture of the antenna,

Γ = target reflection coefficient,

$|\Gamma| = 1$, for a short termination,

G = gain of the antenna,

The maximum effective aperture, A_{em}, is related to the directivity, D, in Reference 16 by the equation

$$D = \frac{4\pi}{\lambda^2} A_{em}$$

where

$A_e = \alpha A_{em}$,

a = effectiveness ratio.

Since

$$G = aD,$$

then

$$A_e = \frac{\lambda^2}{4\pi} aD = \frac{\lambda^2}{4\pi} G \quad \text{and}$$

$$\sigma_d = \frac{\lambda^2}{4\pi} G^2.$$

The ratio of A^2_{max}/B^2 then becomes

$$\frac{A^2_{max}}{B^2} = \frac{\sigma_c}{\sigma_d} = \frac{4\pi (\pi r^2)^2/\lambda^2}{\lambda^2 G^2/4\pi} = \left[\frac{4\pi^2 r^2}{G\lambda^2}\right]^2 .$$

A spiral antenna has a gain of approximately 5 db. For r = 0.656 inch, G ≈ 5 db = 3.162, and λ = 2.347 inch,

$$\frac{A^2_{max}}{B^2} = \left[\frac{4(3.1416)^2 (0.656 \text{ in.})^2}{3.162 (2.347 \text{ in.})^2}\right]^2 = 0.951 = -0.2 \text{ db.}$$

This is the maximum ratio of flat plate return to the spiral antenna return. The actual ratio for the spiral-cup combination is expected to be much less than this number.

The measured results indicated that A^2/B^2 is either approximately +13.5 db or -13.5 db. In order for A^2/B^2 to be +13.5 db, G would have to be less than -1.8 db to satisfy the maximum ratio equation of A^2_{max}/B^2. Since this is not very likely, it appears that A^2/B^2 = -13.5 db and that $B^2 >> A^2$.

d. Calculated Results. The results of the numerical evaluation of A and B for the open and shorted terminals of the planer spiral antenna are plotted in Figures 41 through 45. Although A and B were calculated using this set of terminals, a precise computation of these coefficients requires that these calculations be performed for a set of terminals where the open and short circuited return is an absolute minimum and maximum. Even though many configurations with different shorted terminations were measured, it is not possible to state that the absolute minimum and maximum scattering has been measured. Only by additional measurements of various configurations can the true minimum and maximum be established and precise A and B values be computed.

A summary of the peak measurement results is shown in Table 21.

Table 21. Peak Single-Spiral Return Relative to Reference Target

Termination	Monostatic			Bistatic			
	Trial 1	Trial 2	Trial 3	15^{o}	30^{o}	45^{o}	60^{o}
Short circuit	+1.2	+1.4	+1.5	+1.0	+0.4	-0.2	-0.5
Open circuit	-2.3	-2.2	-2.2	-2.6	-2.8	-3.1	-3.2
$\lambda/16$ stub	-0.3	-0.8	-0.1	-0.9	-1.1	-1.5	-1.7
$3\lambda/32$ stub	--	--	-1.0	-1.7	-1.9	-2.3	-2.3
$\lambda/8$ stub	-1.5	-1.3	-1.2	-1.8	-2.0	-2.2	-2.4
$5\lambda/32$ stub	--	--	-3.0	-2.2	-2.3	-2.7	-2.8
$3\lambda/16$ stub	-2.5	-2.3	-1.4	-2.8	-3.0	-3.2	-3.3

With the exception of trial 3, the $5\lambda/32$ shorting stub consistently had a radar cross section that is at least 0.4 db greater than the corresponding open circuit termination that was used in the data reduction. With the exception of trial 3, only the $3\lambda/16$ shorting stub of the six shorting positions consistently had a slightly lower radar cross section (≤ 0.2 db) than the corresponding open circuit termination. This indicates that the data reduction termination might be near the position of an absolute minimum radar cross section.

5. Conclusions

The additional scattering measurements over those for the original open circuited element, a short circuited element, and an element shorted $\lambda/8$ behind the antenna terminals, resulted from the conclusion that if the absolute maximum and minimum return is not obtained from these measurements, the load dependent coefficient,B, and load independent coefficient, A, cannot be determined from measurements of only three configurations. Although in theory it is possible to solve for any number of unknowns from a corresponding set of simultaneous equations, the solution of a set of nonlinear equations is not always practical. Because of the complexity of the equations, it appeared more desirable to calculate A and B under the assumption that an absolute maximum and minimum radar cross-section measurement was obtained. The open and short circuit radar cross section of the antenna terminals was chosen for this calculation. However, only by additional measurements of various shorting terminations can the absolute maximum and minimum radar cross section be established and precise A and B values be obtained. The results of this effort indicated that the load dependent scattering of

the spiral antenna was far more significant than the load independent scattering.

E. RF EVALUATION OF SPIRAL ARRAYS

1. General

The primary effort during this portion of the program was concentrated on the following:

(1) Obtaining monostatic and bistatic scattering measurements of arrayed spiral antennas for different antenna spacings and reflecting surfaces.

(2) Establishing whether the single-port antenna scattering analysis can be adapted to arrayed antennas.

(3) Arriving at a method for computing the five unknown antenna parameters, A, B, γ, R_a, and X_a, under the assumption that the load impedance of the antenna is known.

2. Model Description

The spiral array models and the terminations that were used for the reflectivity measurements and analysis are presented in Table 22.

The individual spiral antenna characteristics that were used in the array were discussed earlier. The antenna array models for the free-space reflectivity range tests were three feet square. For ease in construction, the array panels were made in four 18-inch-square pieces that were spliced together. After assembly, the three-foot-square panels were within 0.22 of a wave length from a true plane surface. Figure 46 shows the dimensions of three panel configurations. The 0.75λ

Table 22. Arrayed Antenna Elements Used in RF Tests

Models	Bistatic Angle (degrees)	Spiral Termination				
		OC	SC	λ/8	λ/16	3λ/16
		Panel No.	Panel No.	Panel No.	Panel No.	Panel No.
1. Small Cups (1.312" Dia)	0	A	B	C	L	N
0.75λ Spacing	30		B			
Terminals Vertical	60		B			
2. Small Cups (1.312" Dia)	0		D			
1λ Spacing	30		D			
Terminals Vertical	60		D			
3. Small Cups (1.312" Dia)	0	E	F	G	M	O
1.25λ Spacing	30		F			
Terminals Vertical	60		F			
4. Plane Reflector	0	H	I	J	K	P
0.75λ Spacing	30		I			
Terminals Vertical	60		I			

Note: SC = short circuit. OC = open circuit. λ = wave length (2.348").

spacing arrays contained 400 elements that were spaced 1.761 inches from center to center. The 1λ spacing array contained 225 elements that were spaced 2.348 inches from center to center. The 1.25λ spacing arrays contained 144 elements that were spaced 2.935 inches from center to center.

Cross-sectional views of the spiral antenna reflecting surfaces are shown in Figure 47. Figure 48 shows the shorting strip tolerances.

3. Measurements

a. General. The measured data that was acquired consisted of scattering

patterns of arrays of spiral elements with various shorting configurations attached to the terminals.

b. Measurement Facilities. All array measurements were made on a 200-foot range with an asphalt surface. The monostatic measurements were made with a single circularly polarized 52-inch parabolic dish. The bistatic measurements were made with two circularly polarized 52-inch parabolic dishes. The 200-foot-range length satisfied the far-field criteria of $2D^2/\lambda$. Figure 49 shows the monostatic reflectivity range that was used for the array measurements. The small azimuth rotator was fitted with a specially designed foam support column. By judicious use of absorber material, the return from the rotator and a Rexolite support stud embedded in the top of the foam column was minimized.

The equipment block diagram is shown in Figure 50. The portion enclosed by dashed lines is used only for monostatic operation. The dotted lines indicate bistatic operation. The operation and tuning procedure for the monostatic and bistatic systems was covered earlier.

c. Measurement Procedure. After the system was properly tuned and checked out, the following procedure was followed to obtain the data patterns:

(1) With the target mount in position (no target), the background cancelling network was adjusted for a null.

(2) The background return was then recorded as the empty mount was rotated.

(3) A reference target (right-angle corner reflector) was positioned on the

mount, and its return (±30 degrees from the peak) was recorded.

(4) If the reference level was greater than the panel level under test, the calibration levels were recorded with the reference target positioned for peak return, using the precision attenuator in the receive line.

(5) The array panel was then positioned on the mount. The returned signal was peaked in elevation and recorded in azimuth (±30 degrees and then ±180 degrees).

(6) The target was then removed, and the background return was recorded. If the nulled background return had changed significantly, the entire series of measurements would be repeated.

The reference target used was a 24 x 24 inch aperture right-angle dihedral corner reflector. This reference was used so that the back-scatter patterns from one panel to the next could be compared in addition to determining the radar cross section of each array.

d. Measurement Results

(1) Monostatic Results. Back-scatter measurements were made on several spiral antenna arrays with three different spacings between individual elements and with various shorting configurations for each array, as outlined in Table 8.

As seen in Figure 51, the arrays with the 0.75λ spacing between elements had more return than the arrays with 1.00λ and 1.25λ spacing. However, the side-lobe levels for the 0.75λ spacing were high, and in most cases, turned into coma lobes (see Figure 52). Table 23 gives the relative return of the peak and the side-lobe levels for each panel.

Table 23. Three-Foot-Square Array Pattern Data -

Panel No.	Peak Level with Ref* (db)	Back-Ground	3-DB Beamwidth (degrees)	Position **	1st	2nd	3rd	4t
A	+1.8	41.9	1.8	(+)	9.9	16.4	21.1	23.
				Avg	9.5	16.5	20.6	22.
				(-)	9.2	16.5	20.1	21.
B	+2.8	34.0	1.8	(+)	6.5	13.0	16.5	20.
				Avg	6.9	12.8	19.4	20.
				(-)	7.2	12.6	22.2	20.
C	+2.4	37.0	2.0	(+)	7.3	11.6	21.2	19.
				Avg	7.3	12.4	21.6	19.
				(-)	7.2	13.2	21.9	19.
D	-3.0	37.6	1.9	(+)	17.0	21.8	25.0	24.
				Avg	17.3	21.2	24.9	22.
				(-)	17.6	20.5	24.7	20.
E	-8.4	31.6	1.8	(+)	8.1	18.6	15.9	18.
				Avg	8.0	17.3	16.2	22.
				(-)	7.8	16.0	16.4	26.
F	-10.3	46.0	1.7	(+)	8.2	16.1	18.4	18.
				Avg	8.6	15.8	18.2	18.
				(-)	9.0	15.4	17.9	17.
G	-7.6	27.4	1.7	(+)	8.4	12.5	20.5	21.
				Avg	8.6	12.1	21.0	19.
				(-)	8.8	11.7	21.4	18.
H	+1.6	36.0	2.2	(+)	6.3	15.8	18.3	25.
				Avg	6.4	15.7	18.0	23.
				(-)	6.5	15.6	17.7	20.
I	+0.1	32.3	2.2	(+)	4.9	10.8	15.0	18.
				Avg	5.0	11.8	16.1	19.
				(-)	5.0	12.4	17.2	20.

*Reference is 24" x 24" aperture dihedral corner reflector.
**-sign refers to right side of pattern; + sign refers to left side of pattern.

Notes: (1) Side-lobe levels and background are in db down from the peak retur
(2) See Figure 52.

Pattern Data - Monostatic Return (5030 MC, Circular Polarization)

Return - Side Lobes

3rd	4th	5th	6th	7th	8th	9th	10th	11th	12th	13th
21.1	23.7	23.2	23.7	21.7	22.7	28.8	23.3	29.9	24.8	
20.6	22.6	22.8	23.1	21.7	23.0	27.4	25.4	28.9	26.7	
20.1	21.4	22.4	22.5	21.7	23.3	26.1	27.5	27.9	28.6	
16.5	20.2	22.0	23.5	24.6	22.6	22.4	25.6	24.8		
19.4	20.2	23.3	23.8	26.4	21.9	24.5	24.4	25.4		
22.2	20.2	24.6	24.1	27.1	21.2	26.5	23.1	26.0	26.0	
21.2	19.2	26.4	19.6	23.7	23.2	27.3	24.2	24.0	28.1	
21.6	19.5	27.4	19.8	24.9	22.0	30.2	22.8	22.8	30.7	
21.9	19.8	28.4	20.0	26.0	21.2	23.0	21.3	21.6	33.2	
25.0	24.7	27.0	23.6	25.0	18.9	21.4	17.7			
24.9	22.7	28.2	22.1	24.0	17.8	20.5	16.4			
24.7	20.8	29.4	20.6	22.8	16.7	19.6	15.1	12.4	+0.9	
15.9	18.3	17.2	15.7	23.7	12.9	12.9	6.4			
16.2	22.2	16.4	16.2	20.2	11.6	8.6	8.3			
16.4	26.1	15.5	16.7	16.7	10.3	4.2	10.1			
18.4	18.9	23.0	21.0	26.3	18.4	15.9	7.1			
18.2	18.2	21.7	20.1	23.3	16.9	14.3	5.6			
17.9	17.5	20.4	19.2	21.2	15.4	12.7	4.0	13.1		
20.5	21.2	19.0	23.4	22.2	17.2	18.8	8.4	18.6		
21.0	19.6	21.5	20.1	20.0	18.6	15.4	7.8	15.3		
21.4	18.0	24.0	16.7	17.7	20.0	12.0	7.2	12.0		
18.3	25.8	22.0	33.5	23.4	24.4	23.8	28.4	24.3	25.3	
18.0	23.1	20.7	27.0	22.1	22.4	22.7	24.7	24.6	23.6	
17.7	20.4	19.3	20.5	20.7	20.4	21.6	21.0	24.8	21.8	
15.0	18.5	19.0	22.0	21.0	20.5	18.3	20.2	21.0	22.7	
16.1	19.6	20.4	22.6	22.3	21.7	19.7	22.0	22.5	23.9	
17.2	20.6	21.7	23.2	23.6	22.9	21.0	23.7	24.0	25.1	

side of pattern.

the peak return of the panel that was measured.

2

Table 23. Three-Foot Square Array Pattern Data - Monostatic Return (

Panel No.	Peak Level with Ref* (db)	Back-Ground	3-DB Beamwidth (degrees)	Position **	1st	2nd	3rd	4th	5th
J	+2.6	37.4	1.8	(+)	5.7	13.2	17.5	18.9	21.2
				Avg	6.0	13.9	18.6	20.4	21.7
				(-)	6.2	14.6	19.7	22.0	22.2
K	-0.1	33.4	2.0	(+)	5.0	12.6	15.8	19.6	20.3
				Avg	5.6	13.3	17.3	19.5	22.6
				(-)	6.2	14.0	18.8	19.4	24.9
L	+2.9	38.0	1.8	(+)	8.1	13.5	20.9	21.6	24.4
				Avg	8.0	13.5	20.2	20.8	24.6
				(-)	7.8	13.5	19.5	20.0	24.7
M	-9.3	27.7	2.3	(+)	3.8	12.3	13.2	16.0	18.3
				Avg	4.6	13.2	13.8	15.9	19.2
				(-)	5.3	13.9	14.3	15.7	20.1
N	0	32.5	2.1	(+)	5.9	12.6	19.7	20.9	22.6
				Avg	6.6	12.7	19.0	21.0	21.7
				(-)	7.2	12.8	18.3	21.1	20.7
O	-8.9	21.1	2.1	(+)	7.1	10.2	15.0	15.7	13.2
				Avg	6.9	11.4	14.8	15.9	13.8
				(-)	6.6	12.6	14.6	16.0	14.4
P	+2.0	37.6	2.2	(+)	4.3	11.9	17.4	21.6	24.0
				Avg	4.7	12.2	17.7	20.8	23.4
				(-)	5.0	12.4	17.9	20.0	22.8

*Reference is 24" x 24" aperture dihedral corner reflector.
**- sign refers to right side of pattern; + sign refers to left side of pattern.

Notes: (1) Side-lobe levels and background are in db down from the peak return of the panel
(2) See Figure 52.

leturn (5030 MC, Circular Polarization) (Continued)

Return - Side Lobes								
5th	6th	7th	8th	9th	10th	11th	12th	13th
21.2	21.6	21.6	23.7	21.6	22.8	22.0	24.4	24.0
21.7	22.8	22.3	24.2	21.9	23.5	22.9	25.4	24.2
22.2	23.9	22.9	24.6	22.1	24.1	23.8	26.3	24.3
20.3	24.6	20.8	24.6	21.1	26.0	20.9	27.0	
22.6	23.4	22.0	22.9	21.9	23.8	22.3	24.4	
24.9	22.2	23.1	21.1	22.7	21.5	23.6	21.7	25.3
24.4	24.1	25.1	25.0	30.8	27.3	32.9		
24.6	24.1	24.3	24.2	29.6	26.1	32.8		
24.7	24.1	23.4	23.3	28.3	24.8	32.7		
18.3	18.9	18.6	15.7	11.4	7.3			
19.2	16.6	20.2	18.2	11.7	9.3			
20.1	14.3	21.8	20.7	11.9	11.3	5.3	12.3	
22.6	20.6	24.0	21.0	23.3	30.6	24.3	26.8	
21.7	21.3	22.4	21.3	24.2	27.4	25.3	25.7	
20.7	22.0	20.9	21.6	25.0	24.1	26.3	24.5	
13.2	15.3	13.5	18.8	8.3	5.7			
13.8	17.0	13.5	15.2	9.9	8.2			
14.4	18.6	13.4	11.6	11.4	12.7	15.7		
24.0	18.3	18.1	23.2	23.8	25.7	30.0	25.2	
23.4	18.9	17.9	23.2	23.3	25.3	29.5	26.0	
22.8	19.4	17.7	23.2	22.8	24.9	28.9	26.7	

e panel that was measured.

2

The array with element spacing of 1.00λ had side-lobe levels down 17.0 db with the return 3 to 6 db lower than the return for the arrays with 0.75λ element spacing.

The return of the spiral antenna arrays with the 1.25λ spacing between elements was 7.5 to 13.0 db below the return of the arrays with 0.75λ element spacing. In general, the side-lobe levels were high and in most cases could be classified as coma lobes.

The panels used in these measurements were slightly distorted (see Figure 53) and may have caused some filling in of nulls and some deviations in side-lobe level.

(3) Bistatic Results. With the monostatic measurements being of prime importance, only a limited number of panels were measured at bistatic angles of 30 and 60 degrees (see Table 22). The results of these measurements are given in Tables 24 and 25 and shown in Figure 54.

The 30- and 60-degree patterns had peak back-scatter return for positions other than the dead-ahead or broadside return. This happened where the return from the elements in an array would add in phase, giving a peak. This was more pronounced where the return for the array was 3 to 6 db below the return of the reference (see Figures 55 and 56). Where the broadside return equaled or exceeded the peak return of the reference, the in-phase addition from the elements was minimized or virtually eliminated. As shown in Tables 24 and 25, the side-lobe levels for the broadside return are much higher for the panels exhibiting return in excess or equal to the return of the corner reflector.

Table 24. Three-Foot-Square Array Pattern Data - Thirty-Degree Bistatic Ret

Panel	Center Return					Elements in Phase - Return		
				1st Side Lobe				1st Side
	Position (degrees)	Peak Level with Ref (db)	Background Level with Peak (db)	Position with Peak ℄ (degrees)	Level (db)	Position with Peak ℄ (degrees)	Below Peak Level (db)	Position with Peak ℄ (degrees)
B	0	2.5	35.4	-2.8 +2.8	11.8 10.6	-43-1/2	3.8	-47-1/2 -39-1/2
D	0	5.2	37.5	-2.8 +2.8	15.7 15.0	-31	+3.0	-34-1/2 -27-1/2
F	0	5.8	35.8	-2.8 +2.8	18.1 18.3	-25	11.8	-28 -22
I	0	+0.6	38.0	-2.8 +2.8	9.3 9.3	-43-1/2	9.5	-47 -40

Notes: (1) Side-lobe level and background are in db down from the peak return

(2) See Figure 54.

ata - Thirty-Degree Bistatic Return (5030 MC, Circular Polarization)

Elements in Phase - Return (-)				Elements in Phase - Return (+)			
		1st Side Lobe				1st Side Lobe	
Position with Peak ℄ (degrees)	Below Peak Level (db)	Position with Peak ℄ (degrees)	Below Peak Level (db)	Position with Peak ℄ (degrees)	Below Peak Level (db)	Position with Peak ℄ (degrees)	Below Peak Level (db)
-43-1/2	3.8	-47-1/2 -39-1/2	19.4 15.8	+43-1/2	4.1	40 47	16.8 17.3
-31	+3.0	-34-1/2 -27-1/2	16.1 15.0	+31	3.2	27-1/2 34	15.2 15.0
-25	11.8	-28 -22	23.2 20.8	+25	11.0	22 28	21.1 14.1
-43-1/2	9.5	-47 -40	21.1 19.9	+43-1/2	10.5	40 47	20.1 21.9

in db down from the peak return of the panel that was measured.

2

Table 25. Three-Foot-Square Array Pattern Data - Sixty-Degre

Panel	Center Return					Elements in	
	Position (degrees)	Peak Level with Ref (db)	Background Level with Peak (db)	1st Side Lobe		Position with Peak ℄ (degrees)	Be P Le (
				Position with Peak ℄ (degrees)	Level (db)		
B	0	0	37.2	-3.0 +3.5	12.0 11.3	-49.3	
D	0	+0.2	36.4	-2.9 +3.3	12.2 13.0	-35	
F	0	5.8	29.8	-3.0 +3.3	17.0 16.2	-28	
I	0	+3.7	45.0	-2.8 +3.1	11.9 11.1	-52	2

Notes: (1) Side-lobe level and background are in db down from

(2) See Figure 54.

e Array Pattern Data - Sixty-Degree Bistatic Return (5030 MC, Circular Polarization)

		Elements in Phase - Return (-)				Elements in Phase - Return (+)			
1st Side Lobe				1st Side Lobe				1st Side Lobe	
Position with Peak ℄ (degrees)	Level (db)	Position with Peak ℄ (degrees)	Below Peak Level (db)	Position with Peak ℄ (degrees)	Below Peak Level (db)	Position with Peak ℄ (degrees)	Below Peak Level (db)	Position with Peak ℄ (degrees)	Below Peak Level (db)
-3.0	12.0	-49.3	6.7	-54.3	22.6	+50.5	6.7	46.1	15.5
+3.5	11.3			-44.7	14.5			55.7	23.6
-2.9	12.2	-35	8.0	-38.5	17.9	+35.2	7.0	31.6	18.3
+3.3	13.0			-31.3	17.2			39.0	20.1
-3.0	17.0	-28	4.5	-31.4	13.8	+27.8	5.0	24.3	13.3
+3.3	16.2			-24.2	13.0			31.5	12.2
-2.8	11.9	-52	23.1			+52	21.9		
+3.1	11.1								

nd background are in db down from the peak return of the panel that was measured.

4. Data Analysis

a. General. When antenna elements are placed in proximity to one another, the radiation from the individual elements is coupled to the adjacent elements of the array. As a result, differences occur between the measured array patterns and the theoretical array patterns, which are the product of the array factors and the isolated element patterns. As indicated in Reference 17, this interaction effect causes the antenna element impedance to change as a function of viewing aspect, which in turn causes a corresponding change in the effective element pattern.

The items discussed in this subsection include (1) an investigation to determine whether it is possible to compute the array element parameters, and especially the antenna impedance as a function of viewing using the single-port antenna scattering analysis, (2) an evaluation of the effective element pattern for the spiral antennas, and (3) the programing of a solution for the single-port antenna scattering equations.

b. Array Approach Investigation

(1) General. The array approach proposed for computing the array element parameters with mutual coupling effects was to measure the array scattering pattern, determine the effective element pattern, and then apply the single antenna analysis procedure to the effective element pattern. Several outside consultants were contacted in an effort to prove whether or not the single-port analysis for determining the antenna parameters from scattering data can also be applied to the elements in an array. Dr. E. M. Kennaugh and R. Garbacz of the Ohio State

University Antenna Laboratory were selected to provide this information. The general formulation of the problem is mainly attributed to Dr. Kennaugh, and the specific example is the result of Mr. Garbacz's work. The approach that was taken in their analysis was to compare the reflection coefficient of an N-terminal antenna to that of a single-terminal antenna and determine under what conditions they might be equal.

(2) General Formulation of Problem - Monostatic Scattering by a Multi-terminal Antenna or Array. The effect of load impedance upon the scattering from an antenna (in general, the antenna includes the object supporting the radiating structure as well) has been considered in some detail. In contrast, the analysis of scattering by an antenna with a number of terminal pairs (each with an arbitrary load) has received less attention. Such an antenna must be considered as a multimode system, where the strength and phasing of the various modes depend in a complicated manner upon the particular set of terminations as well as the polarization and direction of the exciting field. Even when a set of identical load impedances are placed at all the terminals and these are varied together, the variation in scattered field is not necessarily that of a single-mode antenna with the same load impedance.

The problem is approached by examining the parameters that determine the dependence of scattered field upon multiterminal loading of an antenna, and in particular, the case where all load impedances are alike. Consider the scattering antenna, with its N terminal pairs together with the terminal pair of the distant illuminating antenna, to be an N + 1 port network, and write the Z matrix of the network as

$$\begin{bmatrix} V_0 \\ V_1 \\ V_2 \\ \cdot \\ \cdot \\ \cdot \\ V_N \end{bmatrix} = \begin{bmatrix} Z_{00} & z_{01} & z_{02} & \cdots & z_{0N} \\ z_{10} & Z_{11} & Z_{12} & \cdots & Z_{1N} \\ z_{20} & Z_{21} & Z_{22} & \cdots & Z_{2N} \\ \cdot & \cdot & \cdot & & \cdot \\ \cdot & \cdot & \cdot & & \cdot \\ \cdot & \cdot & \cdot & & \cdot \\ z_{N0} & Z_{N1} & \cdots & & Z_{NN} \end{bmatrix} \begin{bmatrix} I_0 \\ I_1 \\ I_2 \\ \cdot \\ \cdot \\ \cdot \\ I_N \end{bmatrix} \quad (1)$$

The impedance matrix formed by striking out the first column and row of this matrix is the impedance matrix of the antenna, relating the voltages and currents at the N terminal pairs, assuming that the distant antenna associated with the zeroth terminal pair is open circuited, or in any event, does not influence the properties of the N-port antenna.

The term Z_{00} is the driving point impedance of the transmitting distant antenna with all the scattering antenna terminals open circuited, and the impedances z_{0j} are infinitesimal quantities (varying as 1/r) that measure the transfer impedance relating the current at the j^{th} antenna terminal to the induced open circuit voltage in the distant antenna, all other terminals of the N-port antenna being open circuited. The N + 1 dimensional Z matrix is complex symmetric in all cases.

Assume that each of the N terminals of the N-port antenna is loaded with an identical impedance, Z_L, and that we wish to determine the input impedance, Z_{in}, of the distant antenna. Then,

$$\begin{bmatrix} Z_{in}\, I_0 \\ -Z_L\, I_1 \\ -Z_L\, I_2 \\ \vdots \\ -Z_L\, I_N \end{bmatrix} = \begin{bmatrix} Z_{00} & z_{01} & z_{02} \cdots & z_{0N} \\ z_{10} & Z_{11} & Z_{12} \cdots & Z_{1N} \\ z_{20} & Z_{21} & Z_{22} \cdots & Z_{2N} \\ \vdots & \vdots & \vdots & \vdots \\ z_{N0} & Z_{N1} & Z_{N2} \cdots & Z_{NN} \end{bmatrix} \begin{bmatrix} I_0 \\ I_1 \\ I_2 \\ \vdots \\ I_N \end{bmatrix} \qquad (2)$$

Note: The polarity of V and I are chosen such that Re(VI*) measures power flow into the antenna; their relation at load Z_L is $V_n = -Z_L I_n$.

Combining the left and right sides of this matrix equation,

$$0 = \begin{bmatrix} Z_{00} - Z_{in} & z_{01} & z_{02} \cdots & z_{0N} \\ z_{10} & Z_{11} + Z_L & Z_{12} \cdots & Z_{1N} \\ z_{20} & Z_{21} & Z_{22} + Z_L \cdots & Z_{2N} \\ \vdots & \vdots & \vdots & \vdots \\ z_{N0} & Z_{N1} & Z_{N2} & Z_{NN} + Z_L \end{bmatrix} \begin{bmatrix} I_0 \\ I_1 \\ I_2 \\ \vdots \\ I_N \end{bmatrix} \qquad (3)$$

Clearly, the determinant of the array must vanish, which implies (expanding by minors using the first row)

$$0 = (Z_{00} - Z_{in})\, M_{00} + z_{01}\, M_{01} + z_{02}\, M_{02} + \cdots + z_{0N}\, M_{0N},$$

where M_{0j} denotes $(-1)^j$ times the determinant of the array formed by striking out the first row and $(j+1)^{st}$ column from the array in Equation 3.

Solving for Z_{in},

$$Z_{in} = Z_{00} + z_{01}\frac{M_{01}}{M_{00}} + z_{02}\frac{M_{02}}{M_{00}} + \cdots\cdots + z_{0N}\frac{M_{0N}}{M_{00}} \quad . \tag{4}$$

The M_{0j} are determinants of arrays, each of which includes the same first column, which is that of the first row in the array of Equation 3, less the first element ($Z_{00} - Z_{in}$). The minors, M_{0j}, can therefore be expanded in terms of the common first column, which explicitly brings out the factors z_{0j} as follows:

$$z_{01} M_{01} = - z_{01} \left[z_{10}\ m_{11} + z_{20}\, m_{21} + \cdots\cdots + z_{N0}\, m_{N1}\right]$$

$$z_{02} M_{02} = - z_{02} \left[z_{10}\ m_{12} + z_{20}\, m_{22} + \cdots\cdots + z_{N0}\, m_{N2}\right]$$

$$\vdots \qquad\qquad\qquad\qquad \vdots$$

$$z_{0N} M_{0N} = -z_{0N} \left[z_{10}\ m_{1N} + z_{20}\, m_{2N} + \cdots\cdots + z_{N0}\, m_{NN}\right]$$

or

$$Z_{in} = Z_{00} - \frac{1}{\Delta} \sum_{i=1}^{N} \sum_{j=1}^{N} z_{0i}\, z_{0j}\, m_{ij} \quad , \tag{5}$$

where Δ is the determinant of the array ($A = M_{00}$),

$$\begin{bmatrix} Z_{11} + Z_L & Z_{12} & \cdots & Z_{1N} \\ Z_{21} & Z_{22} + Z_L & \cdots & Z_{2N} \\ \vdots & \vdots & \ddots & \vdots \\ Z_{N1} & Z_{N2} & \cdots & Z_{NN} + Z_L \end{bmatrix} , \tag{6}$$

and m_{ij} is $(-1)^{i+j}$ times the determinant of the array formed by striking out the i^{th} and j^{th} column and row respectively from the array of Equation 6.

Since the element of interest is in the change in the input impedance of the distant antenna with changes in Z_L, the reflection coefficient can be defined as

$$\Gamma = \frac{Z_{in} - Z_{00}}{Z_{in} + Z_{00}} \approx \frac{Z_{in} - Z_{00}}{2Z_{00}} \quad \text{where } |Z_{in}| \approx |Z_{00}| .$$

If the distant antenna is "balanced" so as to detect no reflection when the multiterminal antenna has all ports open circuited, then it will measure a reflection coefficient, Γ, when all terminals are loaded with Z_L, given by

$$\Gamma = -\frac{1}{2\Delta Z_{00}} \sum_{i=1}^{N} \sum_{j=1}^{N} z_{0i}\, z_{0j}\, m_{ij} . \tag{7}$$

In particular, when $Z_L = 0$ (all antenna ports short circuited),

$$\Gamma = -\frac{1}{2Z_{00}} \sum_{i=1}^{N} \sum_{j=1}^{N} z_{0i}\, z_{0j}\, y_{ij}, \tag{8}$$

where y_{ij} is the admittance matrix of the N-port network.

For the case of arbitrary loads, Z_L, the formula, for Γ as a function of Z_L (Equation 7) is the ratio of two polynomials in Z_L:

$$\Gamma = -\frac{1}{2Z_{00}} \frac{P_{n-1}(Z_L)}{P_n(Z_L)} . \tag{9}$$

Thus, although one may, for a single port (N = 1), relate Γ to Z_L through a bilinear transform,

$$\Gamma = \frac{A}{Z_L + B} , \tag{10}$$

for a general N-port, a relation of the form,

$$\Gamma = \sum_{i=1}^{N} \frac{A_i}{Z_L + B_i} , \tag{11}$$

must be expected so long as the roots of the denominator are distinct and do not coincide with the roots of the numerator (in which case the number of terms is reduced).

The roots of the denominator B_i are nothing more than the eigenvalues of the impedance matrix Z_{ij}, or in other words, the B_i are given by

$$[B_i] \begin{bmatrix} I_1 \\ I_2 \\ \cdot \\ \cdot \\ \cdot \\ I_N \end{bmatrix} = \begin{bmatrix} Z_{11} & Z_{12} & \cdots & Z_{1N} \\ Z_{21} & Z_{22} & \cdots & Z_{2N} \\ \cdot & \cdot & & \cdot \\ \cdot & \cdot & & \cdot \\ \cdot & \cdot & & \cdot \\ Z_{N1} & Z_{N2} & \cdots & Z_{NN} \end{bmatrix} \begin{bmatrix} I_1 \\ I_2 \\ \cdot \\ \cdot \\ \cdot \\ I_N \end{bmatrix} . \tag{12}$$

The impedance matrix of a physical antenna must be positive definite; i.e., it has complex eigenvalues with positive real part, so that

$$\Gamma = \sum_{i=1}^{N} \frac{A_i}{Z_L + B_i}$$

becomes unbounded only for load impedances $Z_L = -B_i$ with negative real part (as would be expected from conservation of energy), but this does not happen for passive loads.

From Equation 11, A_i depends upon the location of the distant antenna (through the z_{0j}) as well as upon the Z matrix of the N-port antenna, while the B_i depend upon only the Z matrix of the N-port antenna. If, in the case of a planar array of identical elements, Equation 11 is to reduce to Equation 10, then two possibilities must be investigated:

(1) The A_i in Equation 11 may exhibit a dependence on the angular coordinates (θ, ϕ) of the distant antenna with respect to the array that is very sharp. Thus, for a given bearing of the distant antenna (θ_0, ϕ_0), all but one or two of the A_i are very small.

(2) The B_i in Equation 11 may differ only slightly, so that a number of terms can be combined (approximately) into a single term.

(3) Specific Example - Scattering by Multiport Arrays. The reflection coefficient at the input terminals to a probe antenna a far distance from the N-element array under study is given in general by

$$\Gamma = C \sum_{n=1}^{N} \frac{A_n}{Z_L + Z_n} \tag{13}$$

where C is a constant of proportionality, Z_L is the load placed on each of the array terminals, and Z_n is an eigenload equal to the eigenvalues of the matrix

$$[Z] = \begin{bmatrix} Z_{11} & Z_{12} \cdots Z_{1N} \\ Z_{21} & Z_{22} \cdots Z_{2N} \\ \vdots & \vdots \quad \ddots \quad \vdots \\ Z_{N1} & Z_{N2} \cdots Z_{NN} \end{bmatrix} .$$

If a load ($Z_L = -Z_n$) is placed on all the array terminals, an antenna power pattern will be produced which has a maximum in some direction in space (θ_n, ϕ_n). (Such loads will always be active loads for a physically realizable array.) The coefficient A_n will be equal to the value of this power pattern evaluated in the direction of the probe antenna. It is independent of the load Z_L.

Thus, for example, if we have an N-element array,

$$\Gamma = C\left(\frac{A_1}{Z_L + Z_1} + \frac{A_2}{Z_L + Z_2} + \cdots + \frac{A_m}{Z_L + Z_m} + \cdots + \frac{A_N}{Z_L + Z_N}\right).$$

Each of these terms is a bilinear form in Z_L. Therefore, if conditions could be found for which all the A's were zero except one, say A_m, then Γ would take the form

$$\Gamma = C\,\frac{A_m}{Z_L + Z_m} ,$$

which is a bilinear form. In this case all the theory constructed for the single-port antenna applies. However, it is not likely that such a case will exist. More likely, perhaps two or three terms will be significant, and all the others will be substantially smaller, i.e.,

$$\Gamma \cong C\left(\frac{A_{m-1}}{Z_L + Z_{m-1}} + \frac{A_m}{Z_L + Z_m}\right),$$

which is a sum of bilinear forms, not a bilinear form itself. If the eigenloads Z_{m-1} and Z_m are very close together, then as long as $|Z_L - Z_m|$ is large, the variation of Γ with Z_L will be very close to bilinear, and again, the single-port theory applies. However, since the exact values of the eigenloads (Z_{m-1} and Z_m) must be known if maximum radiation is to be produced in the directions θ_m, ϕ_m and θ_{m-1}, ϕ_{m-1}, the precise values of Z_{m-1} and Z_m must be known, and they are different. To determine these values with loads such that $|Z_L - Z_m|$ and $|Z_L - Z_{m-1}|$ are large and nearly equal would require great, perhaps too great, accuracy of measurement.

Just where the poles of Γ lie in the complex Z_L plane depends upon the array, its configuration, coupling, self-impedance, etc. The same may be said of the pattern functions, A_n.

A very special case of a linear (not planar) antenna of N identical elements equally spaced along a line was considered. Each element was considered to have an input impedance of Z_{11} when all the other elements were open circuited, and each element was coupled by an impedance, Z_c, to its nearest neighbors on each side. The element on each end were also considered to have an input impedance of Z_{11} and a coupling impedance of Z_c, but this is clearly an approximation. Such end effects were found to cause difficulties in the analysis; however, if the number of elements is large, these end effects become more and more negligible.

For this special case, the reflection coefficient, Γ , takes a form

$$\Gamma \cong -\frac{1}{2Z_{00}r^2} \sum_{n=1}^{N} \frac{\left\{\dfrac{\sin\left[\frac{Nkd}{2}(\cos\phi_n - \cos\phi_p)\right]}{\sin\left[\frac{kd}{2}(\cos\phi_n - \cos\phi_p)\right]}\right\}^2}{Z_{11} + Z_L - 2Z_c \cos\frac{n\pi}{N+1}} .$$

This is of the form

$$\Gamma = C \sum_{n=1}^{N} \frac{A_n}{Z_L + Z_n}$$

where

$Z_n = Z_{11} - 2Z_c \cos\frac{n\pi}{N+1}$, the eigenvalues of the $[Z]$ matrix,

and

$$A_n = \left\{\frac{\sin\left[\frac{Nkd}{2}(\cos\phi_n - \cos\phi_p)\right]}{\sin\left[\frac{kd}{2}(\cos\phi_n - \cos\phi_p)\right]}\right\}^2 ,$$

the power gain of the array in a direction ϕ_p when loaded with an eigenload $Z_L = -Z_n$. The maximum of the pattern when so loaded occurs at

$$\cos\phi_n = \frac{\lambda}{2d}\left(\frac{n}{N+1} - 1\right) .$$

The above expressions are only approximate in that approximate forms of the eigenvectors of $[Z]$ were used to determine the pattern functions, A_n.

It is important to remember that the above expressions are for a very special case of academic interest and not generally applicable. They are an

illustrative example of the more fundamental fact that associated with every array is a set of patterns in space in one-to-one correspondence with a set of loads, equal to the eigenvalues of $|Z|$ negated. The reflection coefficient seen by a probe at some position in space with respect to the array (θ_p, ϕ_p) is given by Equation 13, where the A_n are power gains, in that direction, of the respective patterns associated with the eigenloads.

Since even in the very special case of the linear array, approximations had to be made to arrive at a simple answer, it is unlikely that any realistic antenna array will be amenable to simple analysis. A computer solution is necessary to find the eigenvalues of the impedance matrix and the associated eigenvectors. Using these eigenvalues, Z_n, and using the eigenvectors to find the patterns, A_n, one can form the sum, Γ, and investigate the effect of varying Z_L. In some cases, perhaps the approximations suggested earlier hold, and their single-port theory may be applied. However, this can be determined only by a rather involved computer solution for Γ for the particular array of interest. General statements concerning arbitrary arrays could be made only after a much more thorough study of the problem.

c. Effective Element Patterns

(1) General. The effective element pattern of a large M x N array of identical scattering elements is the array scattering pattern divided by the array factor. Since the array is assumed to be large enough so that the edge effects are negligible, the effective element pattern would be the same for all the elements. The sizes of

the panels that were measured are 12 x 12, 15 x 15, and 20 x 20. As indicated in Reference 17, when large interaction occurs among the elements, five rows of elements might be required from the edge before a repetitive pattern is observed.

(2) Formulation of Problem. The linear power array factor (Reference 16) for the monostatic radar return is given by

$$A = \left| \sum_{K=1}^{N} M \; e^{i \frac{4\pi D}{\lambda} \sin\theta} \right|^2$$

$$= \frac{M^2 N^2 \left[\sin\left(\frac{2\pi DN}{\lambda} \sin\theta\right)\right]^2}{\left[\sin\left(\frac{2\pi D}{\lambda} \sin\theta\right)\right]^2}$$

where

N = number of element groups in the linear array,

M = number of elements in a group,

D/λ = element spacing/wave length,

θ = monostatic angle with respect to broadside direction.

The phase angle is twice that of an antenna array pattern because of the two-way propagation of the scattered radiation. This function is plotted in the Appendix of Reference 16 for N = 1 to N = 24.

The effective monostatic radar cross section values, $\sigma_e(\theta)$, for the elements might be obtained by dividing the array monostatic radar cross section values, $\sigma_a(\theta)$, by the power array factor on a point by point basis. However, this requires

exact values of the measured data near the null positions and also exact location of the measured null positions with respect to the theoretical null positions in order to obtain the element pattern. A better method of determining the equivalent element patterns is to divide the measured peak side-lobe levels of the array by the square of the total number of elements. The resultant levels are then compared to the theoretical peak side-lobe levels. As mentioned in Reference 18 (page 2-18), thetheoretical peak side-lobe levels are down approximately 13.2, 17.8, 20.8, 23.0, and 24.7 db from the main beam level when the number of elements in a row is large. The peak side-lobe return occurs when

$$\theta = \sin^{-1}\left[\frac{(1 + 2n)\lambda}{4DN}\right] \text{where } n = 0, 1, 2, 3 \ldots$$

(3) Resultant Patterns. Isolated spiral antenna patterns and the results of determining the effective element patterns for the spiral antennas are shown in Figures 57 through 61. The array side-lobe data that was used for this calculation is given in Table 23 along with the corresponding background levels. The accuracy of the computed effective element patterns was limited by the relative signal to background levels. The best measurement data was for panel F where all tabulated peak side-lobe levels were at least 19.7 db above its background level. Panel O, which had the smallest side lobe to background level, had a peak side-lobe level that is 1.9 db above the background level. Although restricting measurement consideration to the first two peak side lobes would give a theoretical measurement accuracy of approximately ±1 db for most of the panels, the complete set of side-lobe levels was used in determining the effective element patterns. The points where the effective element patterns were computed were connected by

straight lines. Different line representations are used to distinguish among the plots. For a given panel, the - sign points refer to the side-lobe levels on the right side of the original patterns and the + sign points refer to the side-lobe levels on the left side of the patterns.

As can be seen from these plots, the effective element patterns and the measured isolated patterns are different. The effective element patterns of the arrays with the cup reflectors should have been identical with the corresponding single-element patterns if the following were true:

(1) The reflectivity measurement accuracy was not restricted by background levels.

(2) There are no mutual coupling effects among the arrays.

(3) The array support return is negligible.

(4) The panels were perfectly flat.

(5) The elements were equally spaced on the panels.

(6) The load terminations were exactly the same for the single isolated elements and the elements of the array.

As a result, any of the above conditions could have resulted in some of the deviations. However, limiting the comparison to just the peak amplitude and the first two side-lobe levels, the fact that the equivalent element pattern of the cup array with the 0.75λ spacing differed from the equivalent patterns of the cup arrays with the 1λ and 1.25λ spacings indicates that either different mutual coupling effects or different structural scattering or both items might have taken place. The same conclusion is reached on comparing the 0.75λ spacing equivalent element patterns

for the arrays with the cups and the arrays with the plane surfaces at the same limited viewing aspects.

d. Antenna Parameter Computer Solution

(1) General. The development of a computer program for determining the antenna parameters, B, γ, R_a, and X_a, of single-port antennas with known antenna loads is described in the following paragraphs.

(2) Newton-Rathson Method. The problem is one of solving a set of five nonlinear, simultaneous equations for the five sets of σ_i, R_{Li}, and X_{Li}. The equations to be solved are

$$\sigma_i = \left| Ae^{j\gamma} + B \frac{Z^* - Z_{Li}}{Z + Z_{Li}} \right|^2 \quad \text{where } i = 1, 2, 3, 4, 5 \text{ (for 5 equations)} \qquad (14)$$

and

$$Z = R_a + jX_a, \quad Z^* = R_a - j X_a, \text{ and } Z_{Li} = R_{Li} + jX_{Li}.$$

The Newton-Rathson iterative method was employed to solve the equations. This technique is discussed in most text books on Numerical Analysis.

To use Newton's method we define function of the form,

$$F_i (A, B, \gamma, R_a, X_a) = \left| Ae^{j\gamma} + B \frac{Z^* - Z_{Li}}{Z + Z_{Li}} \right|^2 - \sigma_i \qquad (15)$$

$$= 0.$$

This equation then represents five functions with unknown A, B, γ, R_a, and X_a. The objective now is to determine the values of A, B, γ, R_a, and X_a such that

the functions $F_i(A, B, \gamma, R_a, X_a) = 0$. First, the values of A, B, γ, R_a, and X_a are estimated. Then $F_i(A, B, \gamma, R_a, X_a)$ are expanded by a Taylor series about the assumed values of the variables. (Assumed values are noted by $A = A_0$, $B = B_0$, $\gamma = \gamma_0$, $R_a = R_0$, $X_a = X_0$.)

$$F_i(A_0 + \delta A, B_0 + \delta B, \gamma_0 + \delta\gamma, R_0 + \delta R, X_0 + \delta X_a)$$

$$\cong F_i(A_0, B_0, \gamma_0, R_0, X_0) + \frac{\partial F_i}{\partial A}\ \delta A + \frac{\partial F_i}{\partial B}\ \delta B$$

$$+ \frac{\partial F_i}{\partial \gamma}\ \delta\gamma + \frac{\partial F_i}{\partial R_a}\ \delta R_a + \frac{\partial F_i}{\partial X_a}\ \delta X_a\ . \qquad (16)$$

Only first-order terms in δA, δB, . . . are kept, and the partial derivatives are evaluated at A_0, B_0, γ_0, R_0 and X_0. The functions $F_i(A_0 + \delta A, B_0 + \delta B, \ldots)$ are set equal to zero, resulting in a matrix equation of the form

$$F'\delta = -F \qquad (17)$$

where

$$F' = \begin{bmatrix} \frac{\partial F_1}{\partial A} & \frac{\partial F_1}{\partial B} & \frac{\partial F_1}{\partial \gamma} & \frac{\partial F_1}{\partial R_a} & \frac{\partial F_1}{\partial X_a} \\ \frac{\partial F_2}{\partial A} & \frac{\partial F_2}{\partial B} & \frac{\partial F_2}{\partial \gamma} & \frac{\partial F_2}{\partial R_a} & \frac{\partial F_2}{\partial X_a} \\ \frac{\partial F_3}{\partial A} & \frac{\partial F_3}{\partial B} & \frac{\partial F_3}{\partial \gamma} & \frac{\partial F_3}{\partial R_a} & \frac{\partial F_3}{\partial X_a} \\ \frac{\partial F_4}{\partial A} & \frac{\partial F_4}{\partial B} & \frac{\partial F_4}{\partial \gamma} & \frac{\partial F_4}{\partial R_a} & \frac{\partial F_4}{\partial X_a} \\ \frac{\partial F_5}{\partial A} & \frac{\partial F_5}{\partial B} & \frac{\partial F_5}{\partial \gamma} & \frac{\partial F_5}{\partial R_a} & \frac{\partial F_5}{\partial X_a} \end{bmatrix}$$

$$\delta = \begin{bmatrix} \delta A \\ \delta B \\ \delta \gamma \\ \delta R_a \\ \delta X_a \end{bmatrix}$$

and

$$F = \begin{bmatrix} F_1 (A_n, B_n, \gamma_n, R_n, X_n) \\ F_2 (A_n, B_n, \gamma_n, R_n, X_n) \\ F_3 (A_n, B_n, \gamma_n, R_n, X_n) \\ F_4 (A_n, B_n, \gamma_n, R_n, X_n) \\ F_5 (A_n, B_n, \gamma_n, R_n, X_n) \end{bmatrix}$$

(n denotes the nth iteration of the process.)

Solution of the five linear equations (Equation 17) gives δA, δB, $\delta \gamma$, δR_a, and δX_a.

The next set of answers for the variables A, B, γ, R_a, and X_a is then

$$A_1 = A_0 + \delta A$$

$$B_1 = B_0 + \delta B$$

$$\gamma_1 = \gamma_0 + \delta \gamma$$

$$R_1 = R_0 + \delta R_a$$

$$X_1 = X_0 + \delta X_a$$

The values A_1, B_1, γ_1, R_1, and X_1 are put into Equation 17, and a new set of δ's is obtained; thus the iteration. This process is repeated until answers for the variables are acceptable. The above solution was programmed for the digital

computer. The computer program for solving the equations has the following logical steps:

(1) Feed the initial estimate of the values of the variables into the computer.

(2) Calculate the matrices F' and F.

(3) Solve the matrix equation for the δ's.

(4) Calculate the new answers.

(5) Test for convergence (i.e., good answer).

(6) If test confirms good answer, print answer.

(7) If test says not a good answer, repeat the procedure starting with step 2 and iterate until step 5 confirms a good answer.

However, because of the degree of non-linearity of the initial equations, situations exist such that for some first estimates of the unknown variables, the program will not give good answers.

(3) Computer Program Development. Not only do situations exist that prevent the computer program from converging to a common root of the unknown variables for an arbitrary choice of the initial estimates of A, B, γ, R_a, and X_a, but also cases occur where the simultaneous equations do not have a real solution. Therefore, the following approaches to forcing the program to converge for a given set of σ_i, RL_i, and XL_i were considered:

(1) Trial of various unknown parameters to determine if the region of convergence can be obtained.

(2) Use of an auxiliary equation in four unknowns and fixed R_a to try to arrive at initial values for the unknown parameters.

(3) Use of the following three different expansions of the radar cross-section equation to determine if one form converged more readily:

(a) Trigonometric form in sin γ and cos γ.

(b) Cartesian form in u = cos γ and w = sin γ, where the highest order of the product of the unknown parameters is 6th order.

(c) Cartesian form in u = cos γ and w = sin γ, where the highest order of the product of the unknown parameters is 4th order.

(4) Incrementing the load impedances of a case with a known parameter solution to the theoretical load impedance of the case with the unknown parameter solution, using a constant set of radar cross sections.

(5) Incrementing the radar cross section of a case with a known parameter solution to the actual radar cross section of the case with the unknown parameter solution, using a constant set of load impedances.

(6) Dynamic programming technique to try to arrive at initial values for the unknown parameters.

(7) Manipulation of the radar cross section equations to try to arrive at initial values for the unknown parameters.

(8) Approximation of a point of nonconvergence by an elliptical paraboloid in 6-dimensional space.

The third form of the equation in item 3 was combined with the approaches in items 5 and 7 to form the final computer solution. The initial values of the five parameters are automatically chosen in the computer program to exactly satisfy the measured radar cross sections of the antennas with the short and open circuit

terminations and to approximately satisfy the third and fifth radar cross-section measurements. These five parameters are then used to obtain a set of calculated radar cross sections. After the parameters for these calculated radar cross sections are checked for convergence, the third and fifth radar cross sections are equated to their measured values. Using the calculated radar cross section parameters as its initial values, the antenna parameters for this new set of radar cross sections are determined in the loop employing the Newton-Rathson method. The fourth radar cross section in subsequent trials is incremented by 1/10 of the difference between the measured and calculated radar cross sections. The initial parameters for each of the trials are the results of the preceding trial. The incremental value is changed to 1/100 of the difference, if the parameters fail to converge before the fourth radar cross section reaches its measured value. The last set of radar cross sections in which the parameters converged is used as the starting point for the additional trials. The test for convergence for a set of parameters is whether

$$\left| \frac{\text{Calculated radar cross section using the parameters} - \text{specified radar cross section}}{\text{Specified radar cross section}} \right| < 10^{-10}$$

for each of the five radar cross sections. It is assumed in the computer program that the parameters will not converge for a specified set of radar cross section values if more than 19 iterations of the parameters are required using the Newton-Rathson method before convergence is obtained. If the load impedances are accurately known, the difference between the fourth measured radar cross section and the point at which the parameters fail to converge for a second time gives an

indication of the radar cross-section measurement accuracy that is necessary for convergence.

The analysis for determining the initial values of the parameters and the radar cross-section equation that was used for the Newton-Rathson method are presented in the following paragraphs.

The initial values of A and B were chosen using the equations

$$A = \left[0.25\,(\sigma_{max} + \sigma_{min}) \mp 0.5\,\sqrt{\sigma_{max}\,\sigma_{min}}\,\right]^{1/2}$$

$$B = \left[0.25\,(\sigma_{max} + \sigma_{min}) \pm 0.5\,\sqrt{\sigma_{max}\,\sigma_{min}}\,\right]^{1/2}$$

where the maximum and minimum values of the measured radar cross sections are selected automatically.

An expansion for the radar cross-section equation is

$$\sigma = A^2 + 2AB\,\frac{R_a^2 - R_e^2 - (X_a + X_e)^2}{(R_a + R_e)^2 + (X_a + X_e)^2}\cos\gamma - \frac{4A\,BR_a\,(X_a + X_e)}{(R_a + R_e)^2 + (X_a + X_e)^2}\sin\gamma$$

$$+ B^2\,\frac{(R_a - R_e)^2 + (X_a + X_e)^2}{(R_a + R_e)^2 + (X_a + X_e)^2}\,.$$

Solving for the load reactances gives

$$(X_a + X_e)^2\,(A^2 + B^2 - \sigma - 2AB\cos\gamma) + (X_a + X_e)\,R_a\,(-4AB\sin\gamma)$$

$$+ R_a^2\,(A^2 + B^2 - \sigma + 2AB\cos\gamma) + R_a\left[2R_e\,(A^2 - \sigma) - 2R_e\,B^2\right]$$

$$-2AB\,R_e^2\cos\gamma + (A^2 - \sigma)\,R_e^2 + B^2\,R_e^2 = 0.$$

When the load resistance is zero, such as for the open circuit and short circuit terminations, the solution for the quadratic equation becomes

$$(X_a + X_e) = R_a \frac{\sin\gamma \pm \sqrt{1 - \left[(A^2 + B^2 - \sigma)/2AB\right]^2}}{(A^2 + B^2 - \sigma)/2AB - \cos\gamma} .$$

A minus sign in the above equation and an initial value of

$$\gamma = \cos^{-1} \frac{A^2 + B^2 - \sigma_{\text{open circuit}}}{2AB}$$

satisfy the condition that the load reactance of an open circuit is minus infinity. The initial value of X_a is chosen to satisfy the reactance equation with a minus sign for the fixed value of $X_{e(\text{closed circuit})}$ and the selected values of A, B, and γ. The value of R_a is chosen from two other values of the measured radar cross sections.

The initial value for the fifth parameter, R_a, was determined by expressing the above general radar-cross section equation in powers of X_a. The X_a^2 term for two radar cross sections was eliminated by subtracting the two equations. The remaining X_a term was eliminated by substituting the expression for X_a of the short short circuit radar cross-section equation. The resulting quadratic in R_a then becomes

$$R_a^2 \left\{ \left[\frac{\sin\gamma - \sqrt{1 - \left[(A^2 + B^2 - \sigma_1)/2AB\right]^2}}{(A^2 + B^2 - \sigma_1)/2AB - \cos\gamma} \right] \left[\frac{-4AB \sin\gamma}{A^2 + B^2 - \sigma_3 - 2AB\cos\gamma} + \right. \right.$$

(Continued)

$$\frac{4AB \sin\gamma}{A^2 + B^2 - \sigma_5 - 2AB\cos\gamma}\Bigg] + \Bigg[\frac{A^2 + B^2 - \sigma_3 + 2AB\cos\gamma}{A^2 + B^2 - \sigma_3 - 2AB\cos\gamma}$$

$$- \frac{A^2 + B^2 - \sigma_5 + 2AB\cos\gamma}{A^2 + B^2 - \sigma_5 - 2AB\cos\gamma}\Bigg]\Bigg\}$$

$$+ R_a \Bigg\{ 2\left[\frac{\sin\gamma - \sqrt{1 - \left[(A^2 + B^2 - \sigma_1)/2AB\right]^2}}{(A^2 + B^2 - \sigma_1)/2AB - \cos\gamma}\right]\left[X_{e3} - X_{e5}\right]$$

$$- X_{e1}\left[\frac{-4AB\sin\gamma}{A^2 + B^2 - \sigma_3 - 2AB\cos\gamma} + \frac{4AB\sin\gamma}{A^2 + B^2 - \sigma_5 - 2AB\cos\gamma}\right]$$

$$+ \left[\frac{X_{e3}(-4AB\sin\gamma) + 2R_{e3}(A^2 - B^2 - \sigma_3)}{A^2 + B^2 - \sigma_3 - 2AB\cos\gamma}\right]$$

$$- \left[\frac{X_{e5}(-4AB\sin\gamma) + 2R_{e5}(A^2 - B^2 - \sigma_5)}{A^2 + B^2 - \sigma_5 - 2AB\cos\gamma}\right]\Bigg\}$$

$$+ \left\{-2X_{e1}\left[X_{e3} - X_{e5}\right] + \left[X_{e3}^2 - X_{e5}^2\right] + \left[R_{e3}^2 - R_{e5}^2\right]\right\} = 0$$

where the subscript 1 refers to the short circuit data and the subscripts 3 and 5 refer to the two other radar cross-section data. The solution for the quadratic equation in R_a in straighforward. It was found that the minus-sign solution gave the most realistic answers.

The third form of the radar cross-section equation appeared to cause the parameters to converge more readily than other forms of the equation. This equation, which was used to obtain the final parameters, is

$$\sigma = u^2 + w^2 + 2uB \frac{R_a^2 - R_e^2 - (X_a + X_e)^2}{(R_a + R_e)^2 + (X_a + X_e)^2} - \frac{4w B R_a (X_a + X_e)}{(R_a + R_e)^2 + (X_a + X_e)^2} +$$

$$B^2 \frac{(R_a - R_e)^2 + (X_a + X_e)^2}{(R_a + R_e)^2 + (X_a + X_e)^2}$$

where $u = A \cos \gamma$ and $w = A \sin \gamma$.

(4) Theoretical Loads. The solution of the actual parameters of a given antenna is dependent on the knowledge of the loads that are used to terminate the antennas. The shorting strips that terminate the spiral antennas consisted of U-shaped strips 3 mils thick and 30 mils wide. The nominal spacing between strips was 0.125 inch. The material was non-magnetic stainless steel, Type 302. Since shorting strips were used for the antenna loads, two possible choices result for the antenna load reactance. One is the standard transmission line reactance, and the other is a short wire reactance relationship. The load resistance might be considered to result from either transmission line losses or radiation losses.

The standard equation for the load impedance of a short circuited transmission line (without radiation losses) is

$$Z = jZ_0 \tan (\beta + j\alpha) s$$

$$= Z_0 \left[\frac{-\sinh 2\alpha s + j \sin 2\beta s}{\cosh 2\alpha s + j \cos 2\beta s} \right]$$

where

Z = load impedance,

Z_0 = characteristic impedance of the line,

$\beta = 2\pi/\lambda$,

λ = wave length,

α = attenuation coefficient per unit length,

s = transmission line length from the shorting position.

As mentioned in Reference 19, a fair approximation to the effective line length of a two-wire transmission line is the actual length to the shorting bend plus one half the wire to wire spacing. Since the nominal spacing between strips is 0.0533 wave length, large changes in the value of the calculated reactances can occur as a result of the choice for the effective strip length. As indicated in Reference 18 (page 30-15), the characteristic impedance for equal-width plates is given by

$Z_0 \approx 377\ (2h/b)$ for $2h \ll b$

$Z_0 \approx 276 \log_{10}(8h/b)$ for $2h \gg b$

where

h = one half the spacing between strips

b = total width of the strip.

In this case, $2h = 0.125$ inch $> b = 0.03$ inch.

The alternate short wire reactance relationship is given in Reference 20, pp 120 - 122 and 364 - 368. The equation for the reactance is

$$X_e = w\left(s\ell_0{}^e + L_S + L_T\right)$$

$$= 2\pi f\mu_0\left[\frac{s}{\pi}\cosh^{-1}\frac{2h}{2a} + \frac{2h}{2\pi}\left(\sinh^{-1}\frac{2h}{a} + \frac{a}{2h} - \sqrt{1+\frac{a^2}{(2h)^2}}\right) - \left(\frac{2h-a}{2\pi}\right)\right]$$

$s^2 \gg (2h)^2 \gg a^2$ and $(2\pi/\lambda)^2\, s^2 \ll 1$,

w = angular frequency,

ℓ_0^e = constant inductance power unit length of a uniform line,

L_S = theoretical isolated inductance of the bridge,

L_T = correction for actual nonuniformity of the inductance per unit length,

f = frequency,

μ_0 = $(4\pi/10^7)$ henrys/m,

s = transmission line length from the shorting position,

h = one half the spacing between strips,

a = wire radius,

λ = wave length

The equivalent radius of the shorting strip was approximated by equating the circumference of the strips to the circumference of an equivalent wire.

An evaluation of the transmission line loss of the shorting strips can be made by modifying Equation 43 of Reference 21 (p 165) for equal-width plates and zero thickness. The attenuation per unit length is

$$\alpha = \frac{\eta}{h}\left(\frac{\epsilon}{h}\right)^{1/2} \frac{\pi + 1 + \pi b/2h - 2\ln_e \delta/4}{1 + \pi b/2h + \ln_e (1 + \pi b/2h)} \quad \text{db/unit length}$$

where

$$\delta = -2 + 2(1 + t/h)^2 + 2(1 + t/h)\left[(1 + t/h)^2 - 1\right]^{1/2},$$

$$\eta = (\pi \mu f/\sigma_c)^{1/2},$$

ϵ = permitivity of free space,

μ = permeability of free space,

b = total width of strip,

t = thickness of strip,

h = one half the spacing between strips,

σ_c = conductivity of the strips.

The numerical results of the attenuation per unit length indicate that the dissipation losses are negligible.

The radiation resistance of a small wire loop of any shape that is fed from a single point is given in Reference 18 (p 6-12) and 22 p(227) as

$$R_e = 20\ \beta^4\ A^2 = 320\pi^4\ A^2/\lambda^4 \text{ for } \beta d \leq 1$$

where

R_e = radiation resistance,

A = area enclosed by the loop,

d = distance around the loop

Absolute reliance on the radiation resistance equation is not possible because of the large width to thickness ratio of the strips and the fact that the shorting strips are not a closed loop.

Although some of the shorting strips, which vary from a short circuit to 3/16 wave length in length, do not satisfy the length and width conditions of the short wire reactance relationship, it is believed that this relationship is more representative of the actual load reactances. The validity of a given load calculation might be established by applying it and the corresponding measured returns of isolated elements to the computer program. The resultant value of R_a would then

be compared to the known value. The stated value of R_a was 62 ohms for the spiral antennas that were considered. This approach was tried for both the transmission line and short wire reactance relationship, but the answers did not converge for the input data. The final resistances that were computed in both cases differed from 62 ohms. The difference between the stated resistance and the last computed resistances (before the parameters failed to converge) might be caused by one or more of the following factors:

(1) The measured data might not be sufficiently accurate to result in a correct value of resistance.

(2) The single element data that was used for this calculation was obtained from spiral antennas that had hand-made strip line terminations. These termination dimensions might not be sufficiently exact to give accurate reflectivity data and calculated antenna loads.

(3) There is a question as to what is the exact reactance between the open circuit and short circuit termination.

(4) As opposed to a linear relationship, the nonlinear equation for the radar cross sections has multiple roots for the antenna parameters. There is the possibility that the root that was attempted was not the one that applies to the physical situation.

(5) As indicated previously, there are uncertainties in the theoretical strip line loads.

Because of the limited extent of the investigation, the above ambiguities were not resolved for the particular spiral and strip line combination. However, this approach of solving for five antenna parameters from five scattering measurements

can be applied to any single-port antenna for which there is accurate input data.

(5) Computer Program and Example. The final computer program, which computes the initial parameters and then evaluates the final parameters using the Newton-Rathon method is written in Fortran IV and can be readily adapted to most digital computers. A sample input data sheet is shown in Figure 62. A listing of the computer program is given in Figure 63. As written, the program assumes that the B coefficient is larger than the A coefficient. Another solution, where A is greater than B, can be found by interchanging the first A and B symbols after statement 4 in the Fortran listing.

The approximate running time of the 1410 computer is as follows:

(1) Compilation time - 2 minutes.

(2) Each iteration pass - 6 to 7 seconds.

(3) Each set of radar cross section values (requires an estimated 5 to 15 passes for convergence, depending on the accuracy of the initial estimate of the parameters) - 30 to 105 seconds.

(4) Ten increments of radar cross section to the measured return (if each set converges) - 300 to 1050 seconds

The input data of a sample problem is included in Figure 63, and the computer results are shown in Figure 64. The input radar cross section data is in db with respect to one square meter and refers to the single-spiral antenna measurements given in Table 16 for the 0-degree viewing aspect. The $\sigma(3)$, $\sigma(4)$, and $\sigma(5)$ values correspond to the $3/32\lambda$, $1/8\lambda$, and $5/32\lambda$ terminations respectively. The

antenna load resistances were computed using the wire loop radiation resistance equation, and the load reactances were computed using the short wire reactance relationship. The steps indicating how the computer results are obtained were described earlier in this section. As stated previously, the parameters $u = A \cos \gamma$ and $w = A \sin \gamma$ were substituted for A and γ in the equation that was used to determine the antenna parameters from the Newton-Rathson method. The 10 columns after the "ESTIMATED ANSWERS" for the parameters list the respective trial parameters, u, w, B, R_a, and X_a, and the resulting

$$\frac{\text{calculated radar cross section using the parameters} - \text{specified radar cross section}}{\text{specified radar cross section}}$$

for $\sigma(1)$ through $\sigma(5)$. After the parameters converge, the values of A and γ are computed and the final parameters are printed along with the resulting calculated radar cross sections. The last $\sigma(4)$ value where the parameters converged is within 0.82 db of its measured value. The antenna resistance for this radar cross section is 56.6 ohms.

5. Conclusions

The following items resulted from the array scattering investigation:

(1) Further knowledge on array antenna scattering theory was obtained from the work of the consultants from Ohio State University. Their analysis indicates that the computer program is not suitable for calculating the mutual coupling impedances of general array antennas.

(2) Comparison of the equivalent element pattern of an array to its isolated

element pattern is one method for determining if mutual coupling effects occurred for this type of array. Evaluation of the effective element patterns of the spiral antenna arrays indicates that mutual coupling effects might have occurred among the array elements.

(3) The effect of element spacing and type of reflector surface on the scattered radiation is shown by comparing the equivalent element patterns rather than by directly comparing the measured array pattern. The large differences in the measured peak amplitudes for the same load terminations were primarily due to the differences in the number of elements in the arrays, while the equivalent element patterns are normalized to account for this fact. All the peak amplitudes of the equivalent element patterns were within 3.4 db of each other and were within 4.8 db of the measured isolated element patterns. As mentioned previously, the equivalent element pattern values from the measured peak amplitude and the first two side-lobe levels of the cup array with the 0.75λ spacing differed from the corresponding values of the cup arrays with the 1λ and 1.25λ spacing. This indicates that either different mutual coupling effects or different structural scattering or both items might have taken place. The same conclusion was reached on comparing the 0.75λ spacing equivalent element patterns for the arrays with the cups and the arrays with the plane surfaces at the same limited viewing aspects.

(4) A Fortran program, which was not previously available, was developed that can be used to determine the parameters of single-port antennas from scattering measurements. As opposed to standard antenna

impedance measurement techniques, this program can be used to calculate other antenna parameters besides impedance of any single-port antenna whose load can be defined. The use of the radar cross-section approach for determining antenna impedances is especially useful when the antenna test leads change the antenna characteristics, such as for small antennas, or when there are problems in the bridge and slotted line techniques due to radiation coupling to the measurement equipment. The computer program, which requires five measurements for a solution, can also be used where the three-measurement technique of the Ohio State University Laboratory cannot be used, such as when the antenna load impedance cannot be continuously adjusted for an absolute maximum and minimum return. This new approach should be a valuable tool in the investigation of the antenna parameters of various single-port antennas.

SECTION 3

CONCLUSIONS

A flexible thermal coating suitable for spacecraft applications has been fabricated and tested under simulated operating and space conditions, resulting in no significant deleterious effects. Although test results were encouraging, this investigation must be considered preliminary, and additional characterization work must be done for a specific application to get a full evaluation.

Test results have indicated that a lightweight, flexible solar sail material having solar absorptance characteristics on one side and solar reflectance characteristics on the other side along with corresponding infrared emittance properties is feasible. The optical phenomena of the sail sides have been widely studied for similar hard-surface applications; however, this was one of the first attempts to utilize a flexible substrate and packageable approach.

This program attempted to establish the antenna parameters (which include the impedances) of small spiral antennas with unusual terminations through the application of new antenna scattering techniques. This effort has been partially successful in that a computer program has been developed, using the fundamental equations of this technique, to calculate these parameters. Due to problems of multiple roots, mechanical tolerances, uncertainties in the theoretical loads, or possibly measurement uncertainties, this program has not produced a useful set of antenna parameters from the measured antenna data. It has produced correct results for hypothetical cases, and it should be possible to refine either the program or the measurements to produce correct results for single elements.

An investigation of the applicability of the theory to arrays has shown that, while the arbitrary general array does not meet the bilinear condition that is required for use of the single-port scattering technique for determining antenna parameters, array configurations might exist for which the approach is suitable. A complete analysis of the physical situations that satisfy this bilinear requirement was not considered a part of this program.

The measurement part of the program was successful in that all required measurements have been completed. The data is reported herein. In addition there are indications, if not positive proof, that mutual coupling does exist for the arrays considered.

The inability to compute these mutuals and the self-impedances of the array elements is a result of the discovery during the program that there was a limitation on the direct applicability of this scattering approach. However, this discovery does not rule out the eventual possibility of using scattering measurements for determining impedances of array elements. Rather, the disclosure indicates that additional fundamental work must be done in this field before a scattering approach can be applied to arrays. As a result of the exposure given this field during the current program, it is believed that important new work can and should be done in this technical discipline.

SECTION 4

RECOMMENDATIONS

A. GENERAL

There are three possible approaches for further rf work. These lie in the areas of (1) a pure theoretical analysis to either establish the criteria for when the single-port antenna approach applies to arrays under the assumption of bilinearity, or develop suitable modified expressions relating impedances and scattering data for a general array; (2) a combined theoretical and empirical approach, which would employ simpler elements to obtain the same results; and (3) employment of a "scale down" technique to establish the impedance characteristics of the spiral element in a small array. Although the last solves the immediate problem, and the first will provide the greatest depth of understanding, it is believed that the second will provide the greatest amount of general useful engineering information in the shortest time and with the least expenditure. The three approaches are covered in greater detail in the following paragraphs.

B. PURE THEORETICAL APPROACH

As discussed in Section 2, valuable insights into the problem may be obtained through an investigation of the eigenvalues of the matrix of a simplified "line array" for several particular antenna array configurations. This would be done for various assumptions of mutual coupling and for different element spacings. The basis for a more general examination of two dimensional arrays would be laid by this work. Depending on the scope of this program, the development of an approach to the latter case might be attempted.

Any antenna array of N elements can be described in an N x N impedance matrix, but this matrix becomes quite complex for the general case. For a one-dimensional array (line array), the non-zero elements can be arranged to fall on and near the diagonal and manipulation of the matrix becomes quite straightforward. For a two-dimensional array with some mutual coupling, non-zero elements will appear throughout the matrix and mathematical manipulation is extremely difficult.

Therefore, this effort might also include an investigation of the properties and matrix manipulations of a three-dimensional matrix. This matrix, illustrated in Figure 65, can be constructed so that all of the non-zero terms lie in a "tube" around the diagonal to the matrix. (In Figure 65, only the case of mutual impedances between adjacent elements is illustrated.) This arrangement provides conceptual simplicity and could eventually lead to ease of mathematical manipulation of the matrix of the general two-dimensional antenna array case.

C. COMBINED THEORETICAL-EMPIRICAL APPROACH

A significant problem, which hindered the development of a fuller understanding of the array impedance characteristics, was the compactness and unusual nature of the elements. While it was these very elements that led to the requirement in the beginning, the exploration of the problem indicates that much useful work can be done in understanding the fundamental theory of mutual coupling effects if simpler configurations are considered first. For example, if small horns and variable short circuits were used, a measurement program could be devised to support a theoretical investigation of first the line array and then the two-dimensional array. One result of such a study would be the establishment of the

requirements, which must be satisfied, for an array to be considered to be "quasi-bilinear"; i.e., the types of arrays for which the bilinear relationship between scattering and impedance is approximately satisfied, so that a computer-aided approach of the type developed in this investigation would be applicable. In addition, it might also be possible to develop a modified expression for this relationship which would, for other array configurations, permit computation of the various antenna parameters involved in these relationships.

As outlined above, this approach offers a comprehensive exploration of the problem with the promise of yielding useful results within a relatively short time.

D. "SCALE DOWN" TECHNIQUE

In view of the extreme precision with which small antennas can be reproduced using techniques that were either developed or used on the current program, it should be possible to build extremely accurate models scaled up in size and to a lower frequency. By taking extreme care to maintain resistances and antenna reactive impedances, the models should have the same characteristics as the original antennas. The transmission lines of these models may then be probed using standard techniques for parallel wire lines or by other techniques to establish the impedances. By measuring the center element in a sufficiently large array (25 or more elements) for different angles of incident energy, the antenna impedance can be obtained.

In addition, the larger size should permit accurate termination of the antenna in both resistive and reactive loads for scatter or other measurement. In

particular, by putting a variable load on the antenna, the techniques developed by OSU can be applied to permit quick and accurate determination of the parameters of single antennas.

A further advantage of this techniques lies in the fact that antenna parameters can be varied more easily than they can with the smaller antennas, for which the requirements for reproducibility demand that all elements be constructed from special tooling.

Since the current program has succeeded in defining a new field of investigation, it is recommended that programs along the lines suggested above should be initiated. In addition to the applicability to the pseudo-passive program, this work would have important implications to radar vulnerability of airborne, ground-based, and shipboard arrays, and to the design of configurations such as arrays of "Antennafier" elements (antennas combined with mixer, amplifiers, or frequency converters); it might find applicability to normal arrays by virtue of the large dependence of the mutual impedances to the phasing angles of such arrays.

REFERENCES

1. Study of a Passive Communication, Gravity-Gradient Stabilized, Lenticular Satellite, Interim Summary Report. GER 11893. Goodyear Aerospace Corporation, Akron, Ohio, January 1965.

2. Green, R. B., The Effect of Antenna Installations upon the Echo Area of an Object. Report 1109-3. Antenna Laboratory, Ohio State University Research Foundation, 29 September 1961.

3. Green, R. B., The General Theory of Antenna Scattering. Report 1223-17. Antenna Laboratory, Ohio State University Research Foundation, 30 November 1963.

4. Moffatt, D. L., Determination of Antenna Scattering Properties from Model Measurements. Report 1223-12. Antenna Laboratory, Ohio State University Research Foundation, 1 January 1964.

5. Pseudo-Passive Satellite Technique Study - Evaluation of Lenticular Spiral Array. Progress Reports. GER 11750. Goodyear Aerospace Corporation, Akron, Ohio, October 1964 - October 1965.

6. Olson, R. L., et. al., The Effects of Ultraviolet Radiation on Low α_s/ϵ Surfaces. ASD Symposium on Thermal Radiation of Solids. San Francisco, California, March 1964.

7. Thermophysics Design Handbook. Lockheed Missiles and Space Company, Sunnyvale, California.

8. Zerlaut, G. A., Ultraviolet Radiation in Vacuum of White Spacecraft Coatings. ASD Symposium on Thermal Radiation of Solids. San Francisco, California, March 1964.

9. Progress in Developing Stable Thermal-Control Coatings for Space Applications. GER-10906. Goodyear Aerospace Corporation, Akron, Ohio, June 1963.

10. Zerlaut, C. A., and Harada, Y., Stable White Coatings. Interim Report ARF 3207-14. Armour Research Foundation of IIT, 13 November 1962.

11. Hass, G., Schroeder, H. H., Turner, A. F.,"Mirror Coatings for Low Visible and High Infrared Reflectance." Journal of the Optical Society of America, Vol 46, No. 1, January 1956.

12. Dyson, John D., "The Equilangular Spiral Antenna". IRE Transactions on Antennas and Propagation. 1959. p. 181.

13. Pseudo-Passive Satellite Technique Study. RADC-TDR-64-157. Contract No. AF30(602)-2957. Sylvania Electronic System - Control, Williamsville, N.Y., October 1964.

14. Pseudo-Passive Program Technical Report. Item II - RF Evaluation of Single Spiral Antenna Elements. GER-12125. Goodyear Aerospace Corporation, 22 March 1965.

15. Buckley, E. F., "Microwave Reflectivity Measurements - Theory and Practice." Electronic Design, 15 March 1962.

16. Kraus, J.D., Antennas. McGraw-Hill Book Company, Inc., 1950.

17. Allen, J.R., "Array Antennas and New Applications for an Old Technique." IEEE Spectrum, Vol 1, No. 11, November 1964.

18. Jasik, H., Antenna Engineering Handbook. McGraw-Hill Book Company, Inc., 1961.

19. Skilling, H.H., Electric Transmission Lines. McGraw-Hill Book Company, Inc., 1951. p 321.

20. King, R.W.P., Transmission-Line Theory. Dover Publications, Inc., 1965.

21. Assadourian, F., and Rimai, E., "Simplified Theory of Microstrip Transmission Systems. "Proceedings of the IRE. December 1952.

22. King, R.W.P., Mimno, H.R., and Wing, A.H., Transmission Lines, Antennas and Waveguides. McGraw-Hill Book Company, Inc., 1945.

23. Schmitt, R.G., and Hirt, R.C., Studies on the Protective Ultraviolet Absorbers in a Space Environment III. ASD-TR-61-298. 1962.

24. RCA Electron Tube Handbook, HB-3.

25. Tinsley Laboratories Glass Color Filters Catalog, Bulletin CF-1.

26. National Bureau of Standards Report of Calibration of Two Standards of Spectral Radiance for GAC. NBS Test No. 2. 1/167675. 21 July 1961.

27. General Electric Company Bulletin, GET-12481.

28. Fressell, W.P., Trido, J.J., and Henningen, J.H., A Dynamic Thermal Vacuum Technique for Measuring the Solar Absorptance and Thermal Emittance of Spacecraft Coatings. NASA TN D-1716.

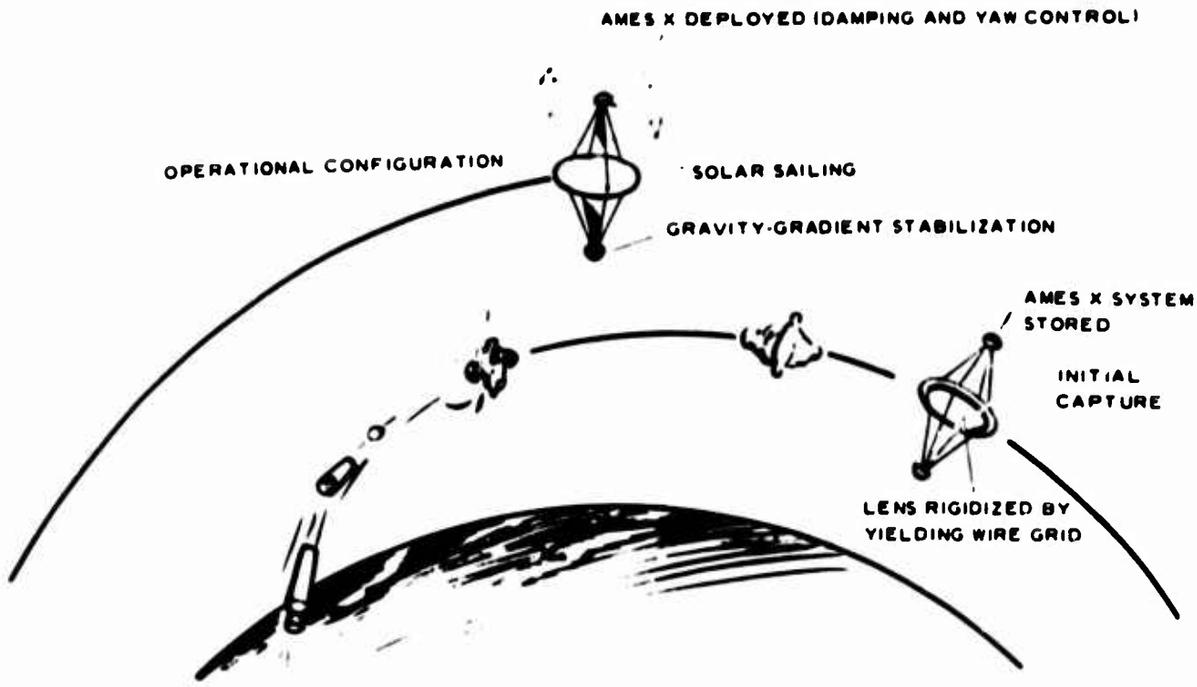

Figure 1. Lenticular Configuration Principle

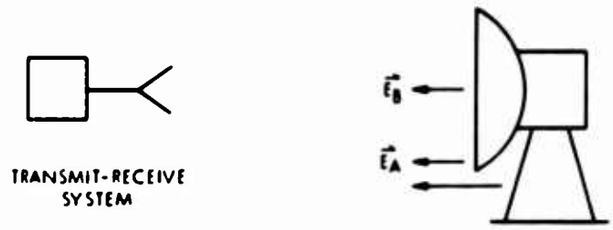

$$\sigma \propto |\vec{E}_A + \vec{E}_B|^2$$

$\vec{E}_A$ = SCATTERED FIELD THAT IS REFLECTED FROM THE ANTENNA STRUCTURE WHEN THE ANTENNA IS MATCHED ITS MAGNITUDE IS DIRECTLY PROPORTIONAL TO A, THE LOAD INDEPENDENT COEFFICIENT, AND VARIES AS A FUNCTION OF VIEWING ASPECT

$\vec{E}_B$ = SCATTERED FIELD THAT IS REFLECTED FROM THE ANTENNA LOAD IT VARIES BOTH IN AMPLITUDE AND PHASE AS THE LOAD IS VARIED ITS MAGNITUDE IS DIRECTLY PROPORTIONAL TO $B\,|(Z_0^* - Z_{in})/(Z_0 + Z_{in})|$ THE LOAD DEPENDENT COEFFICIENT, B, VARIES AS A FUNCTION OF VIEWING ASPECT

Figure 2. Parameter Interaction of Scattering Antenna

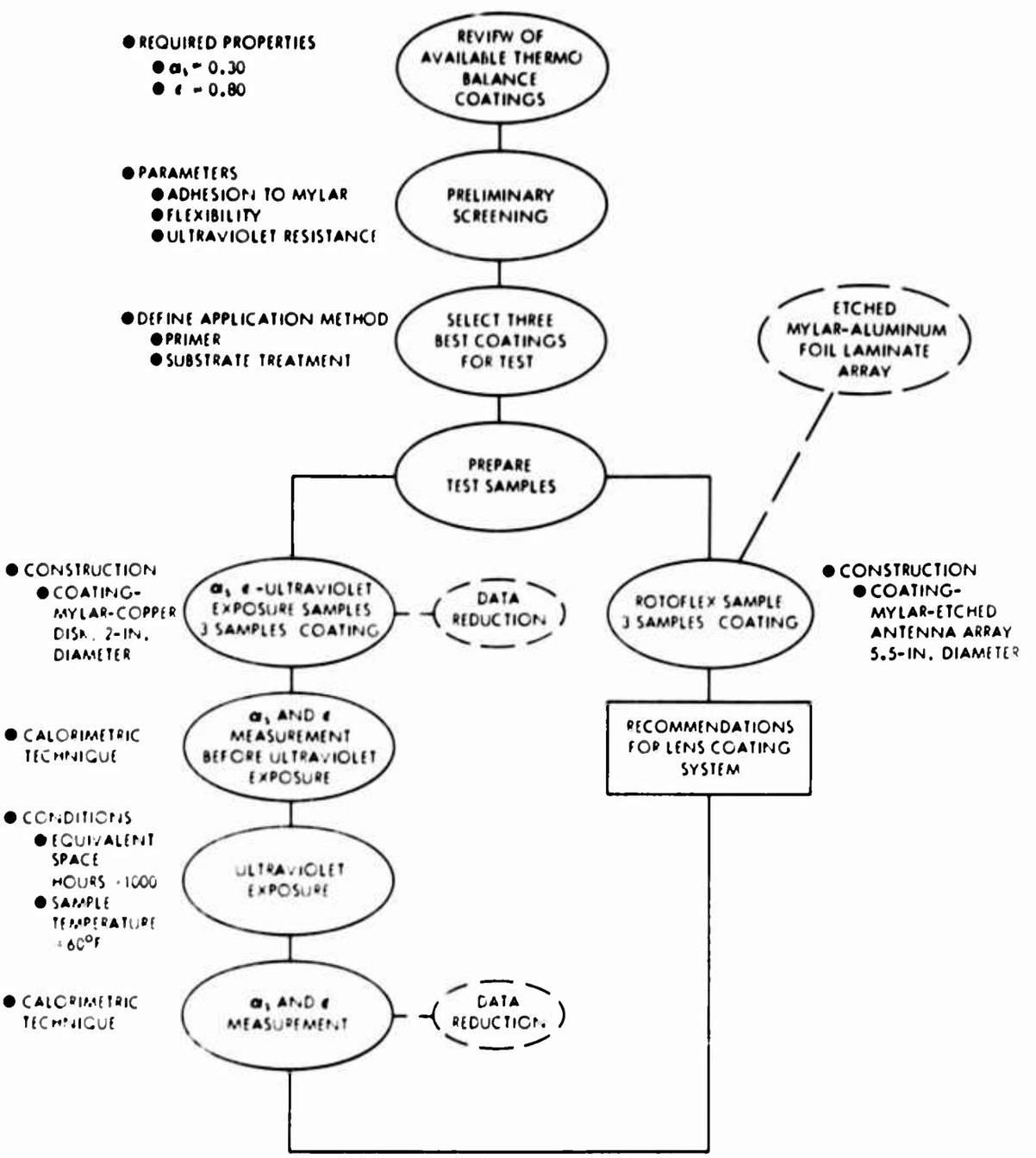

Figure 3. Work Flow Chart for Coatings Investigation

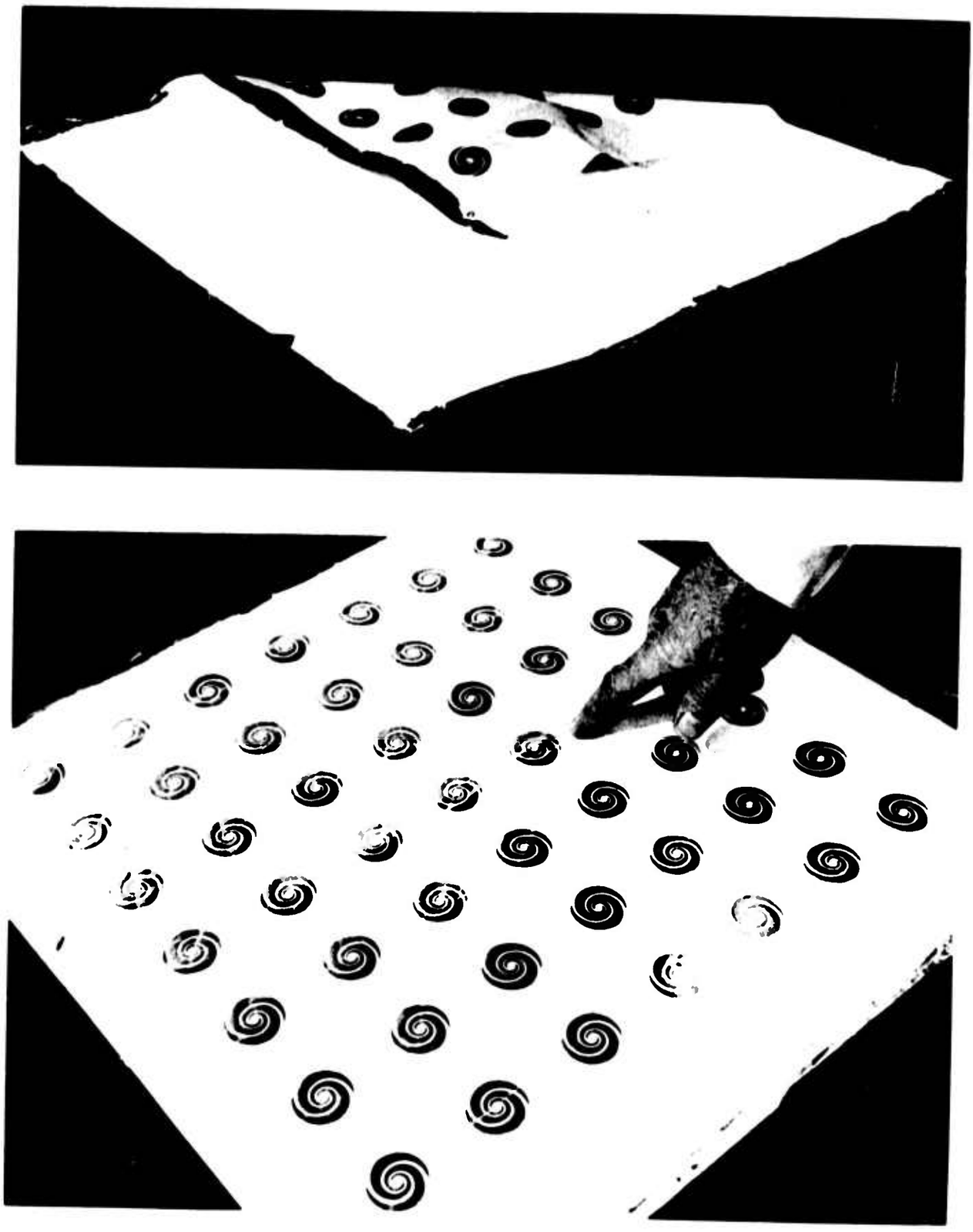

Figure 4. Photographs of Coated Lens Material

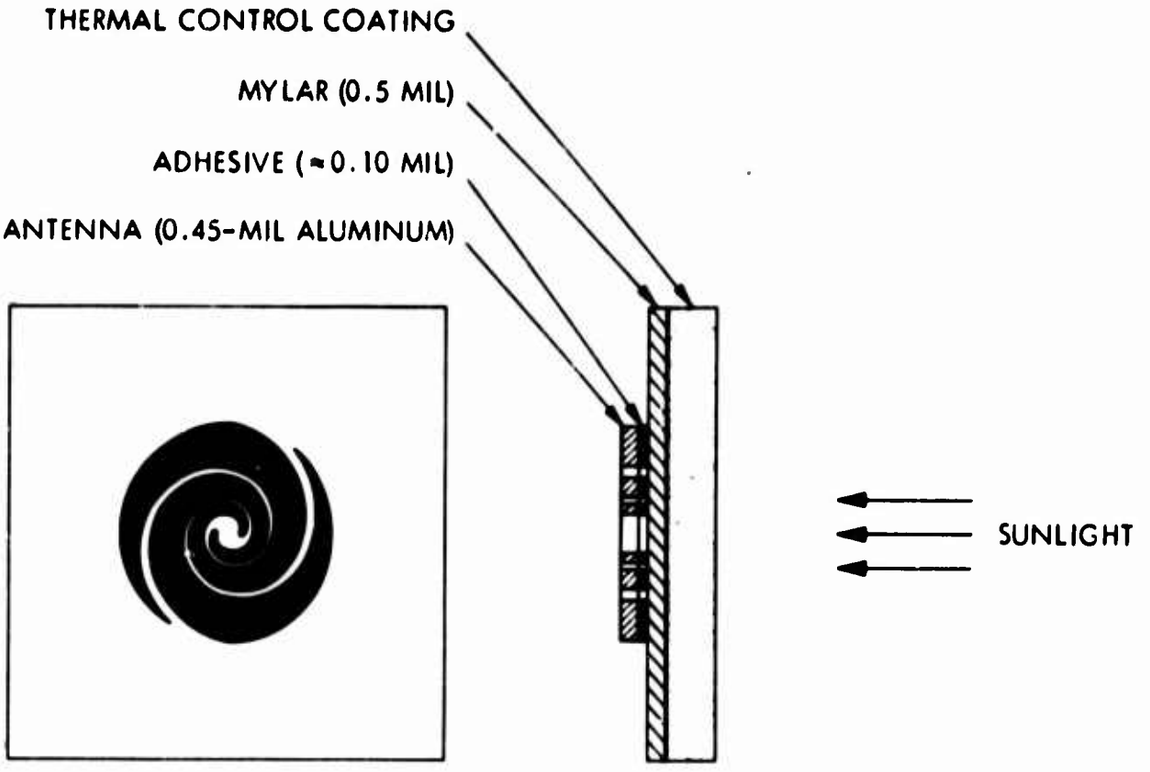

Figure 5. Typical Cross Section of Panel

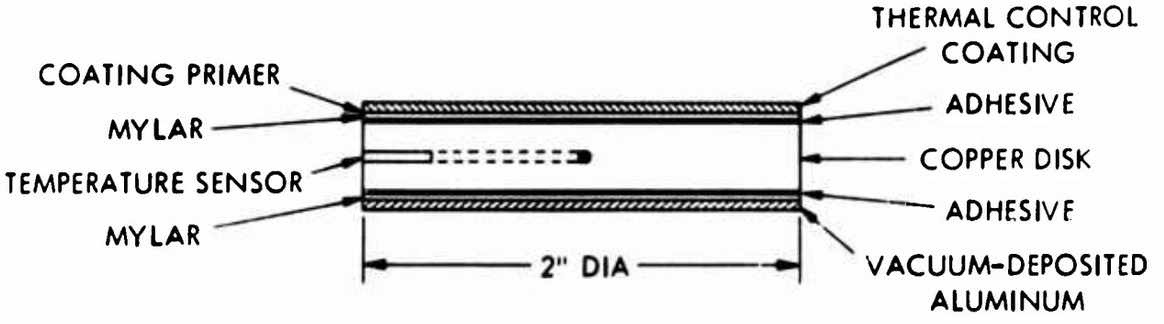

Figure 6. Cross Sectional View of Absorptance-Emittance Sample

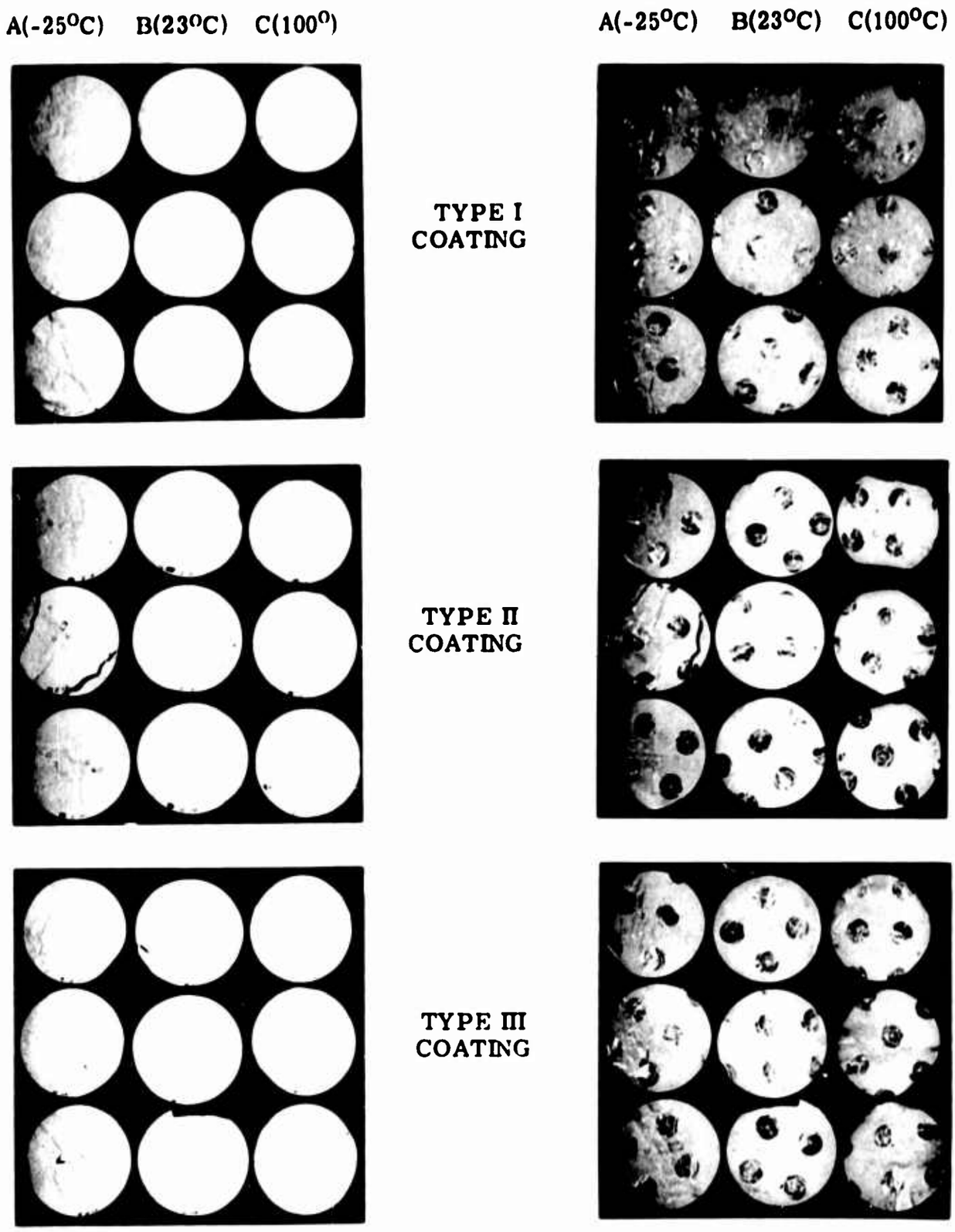

Figure 7. Photographs of Rotoflex Samples after 2000 Cycles

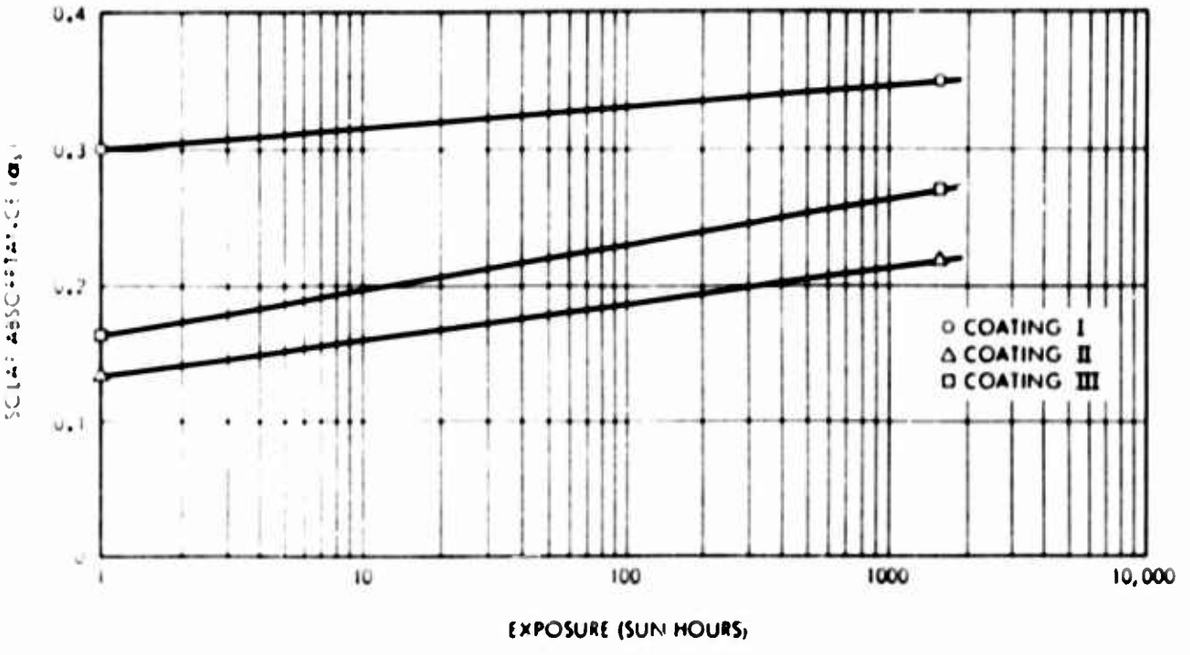

Figure 8. Solar Absorptance versus Exposure Time for Flexible Thermal Control Coatings

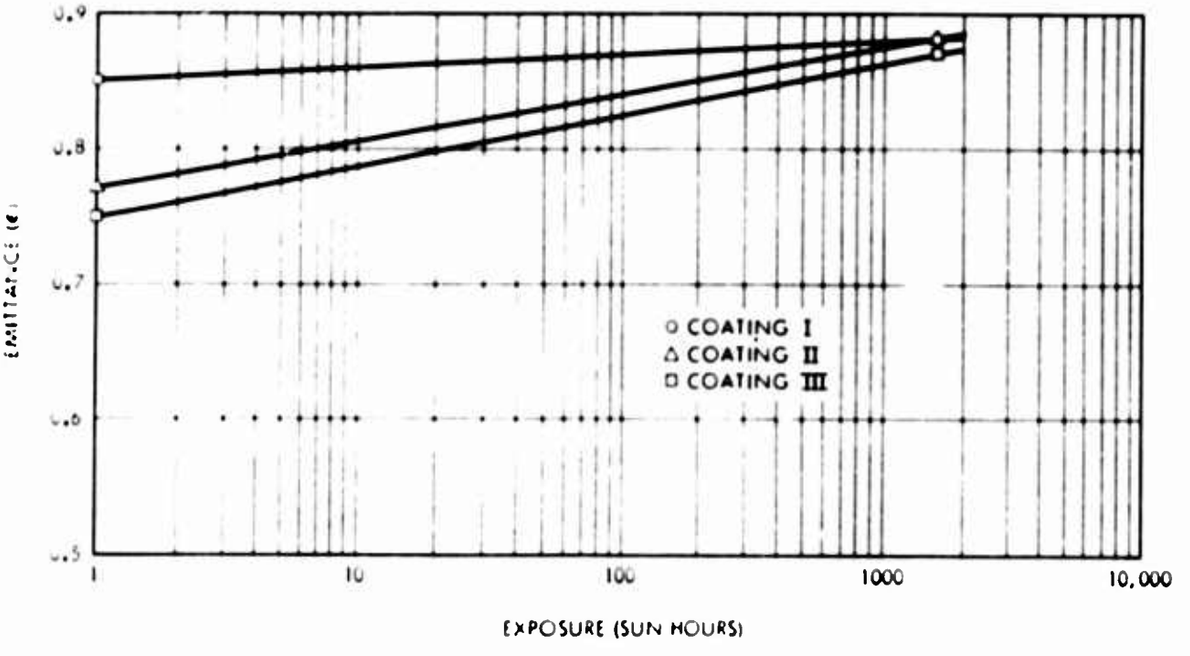

Figure 9. Emittance versus Exposure Time for Flexible Thermal Control Coatings

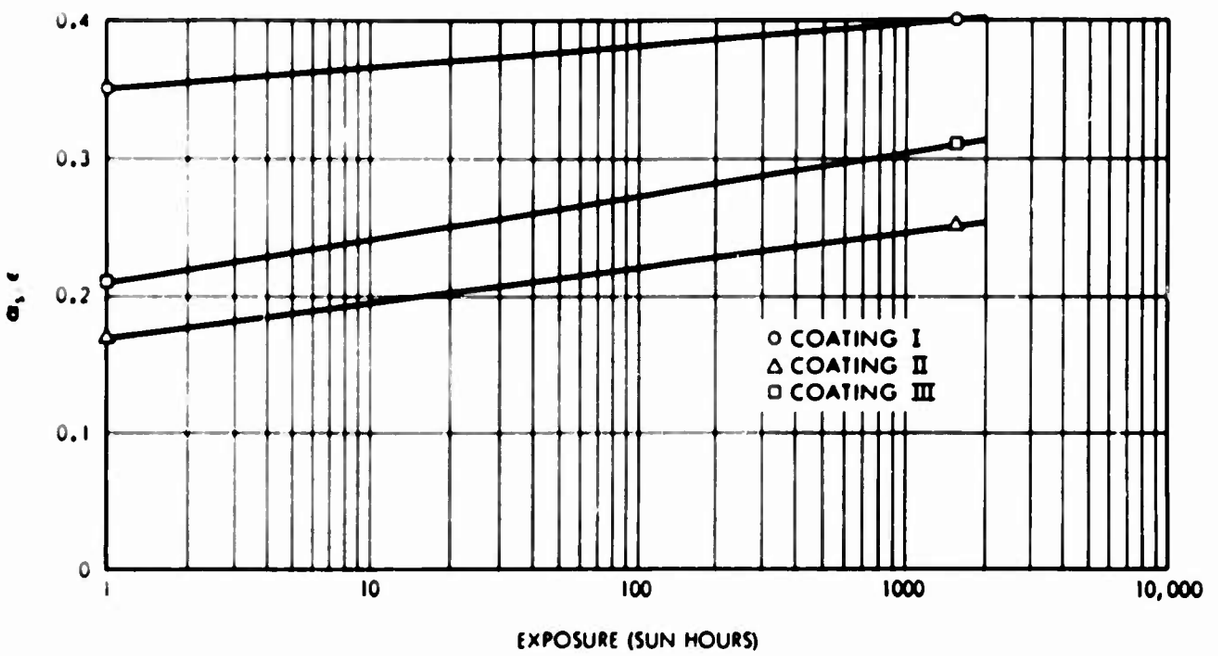

Figure 10. α_s/ϵ Ratio versus Exposure Time for Flexible Thermal Control Coatings

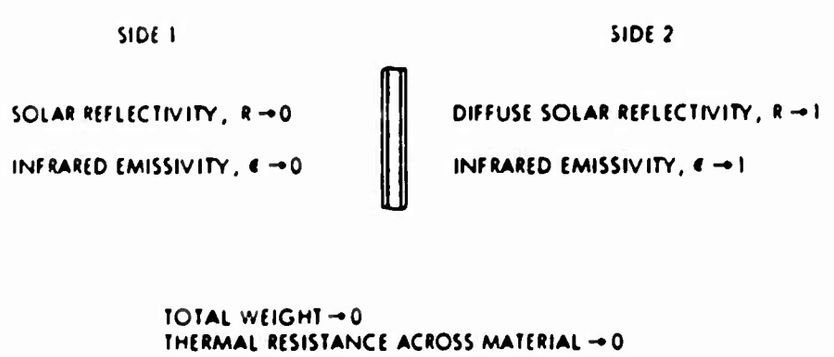

Figure 11. Optimum Solar Sail Material

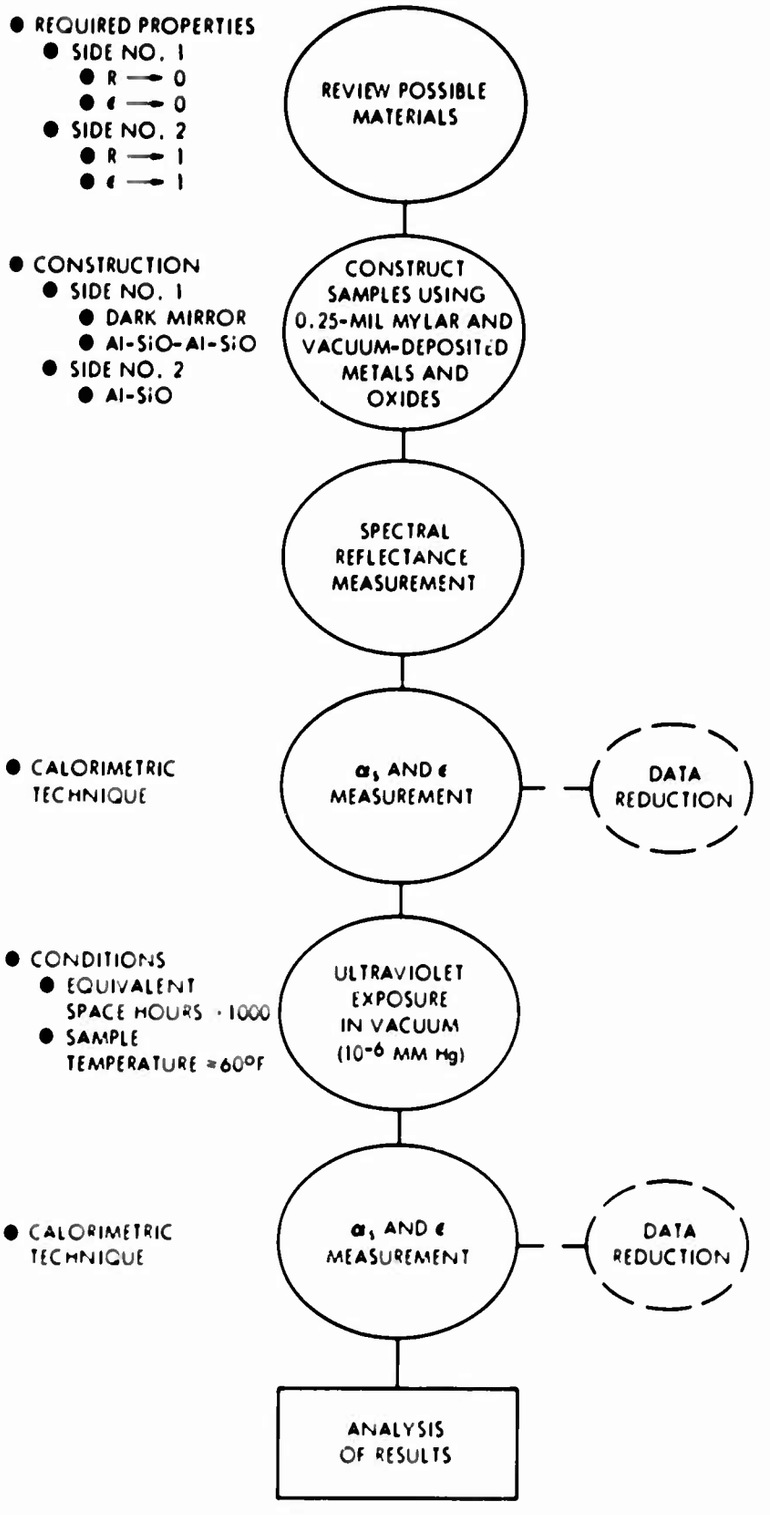

Figure 12. Work Flow Chart for Solar Sail Investigation

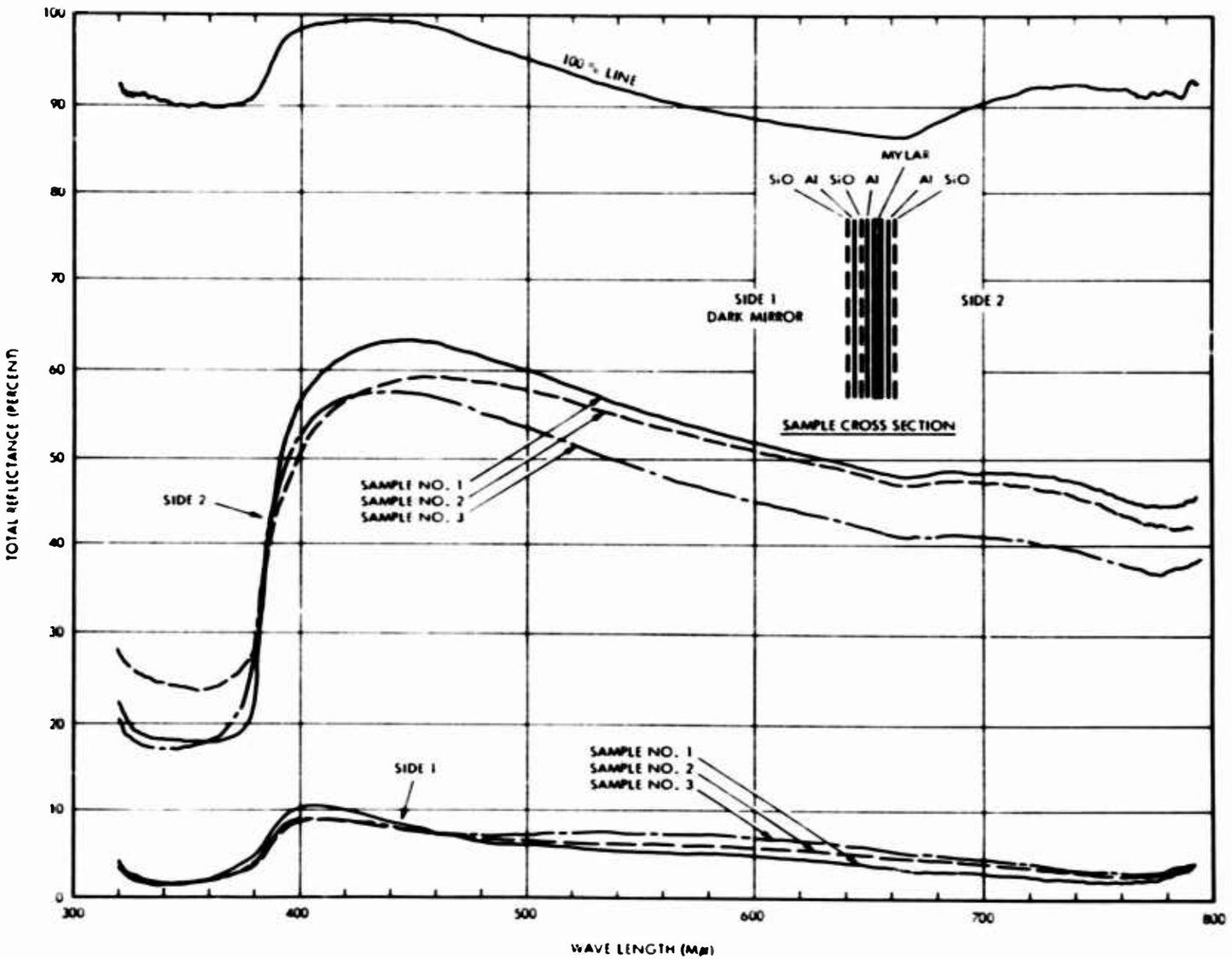

Figure 13. Spectral Reflectance of Solar Sail Samples

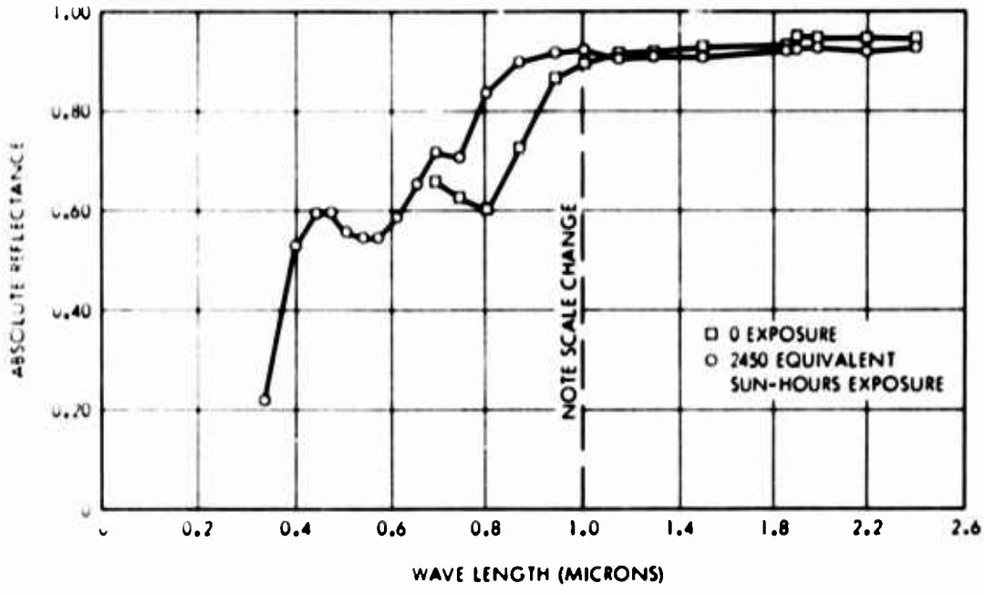

Figure 14. Absolute Reflectance of Al-SiO Coating before and after Ultraviolet Exposure

ARRAY SPACING (λ)	ANTENNA TERMINAL CONDITION					TYPE OF REFLECTING SURFACE (λ 2 THICK)	
	OPEN	SHORT	STUB SHORT 1 8 IN. x			POCKET OR CUP	PLANE
			x = λ 8	x = λ 16	x = 3λ/16		
0.75	A	B	C	L	N	A,B,C,L,N	H,I,J,K,P
1.0	-	D	-	-	-	D	
1.25	E	F	G	M	O	E,F,G,M,O	

TEST FREQUENCY = 5030 MC (λ = 2.348 INCHES)
USE CIRCULAR POLARIZATION
SPIRAL DIAMETER = 1.185 INCHES
MONOSTATIC TESTS - ALL MODELS
BISTATIC TESTS - MODELS B, D, F, AND I - 30 AND 60 DEGREES

Figure 15. Summary of Three-Foot-Square RF Test Models

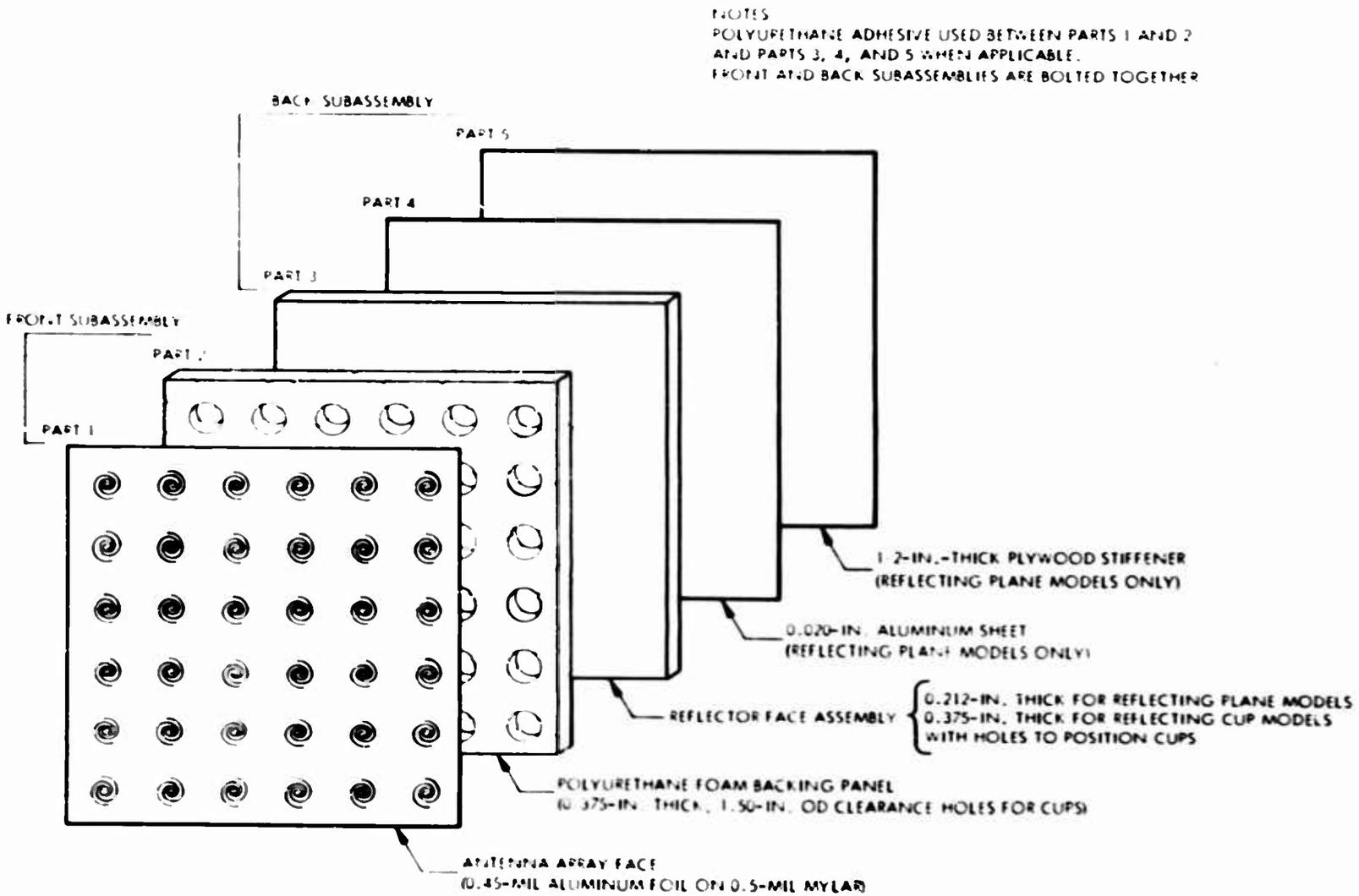

Figure 16. Schematic of Three-Foot-Square Flat Panel Models for RF Evaluation

A. TYPICAL CONSTRUCTION FOR MODELS A, B, C, D, E, F, G, L, M, N, AND O

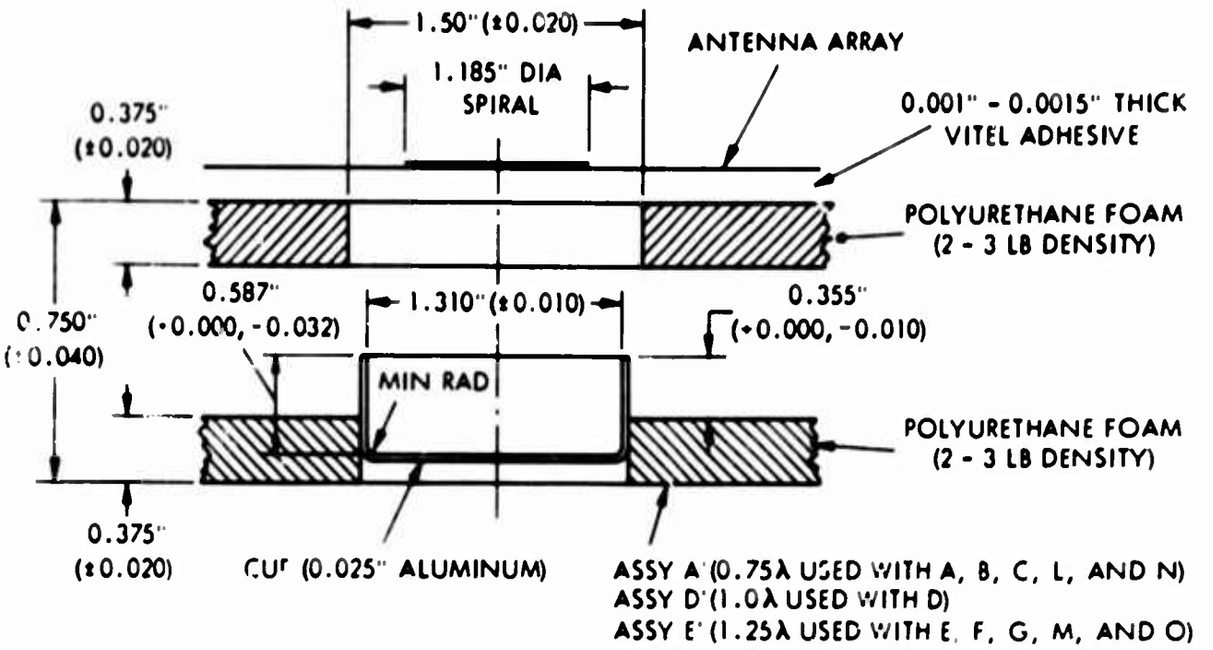

B. TYPICAL CONSTRUCTION FOR MODELS H, I, J, K, AND P

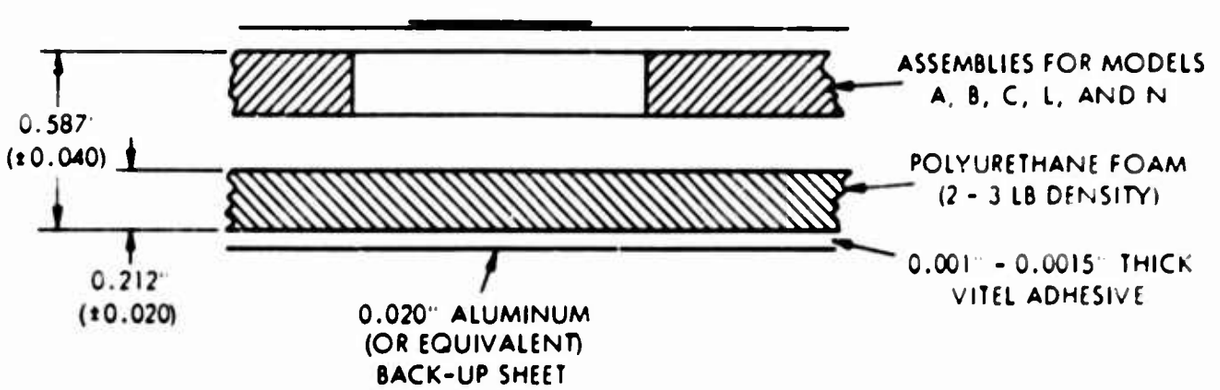

Figure 17. Design Details for Pocket or Cup and Plane Reflecting Types of Surfaces

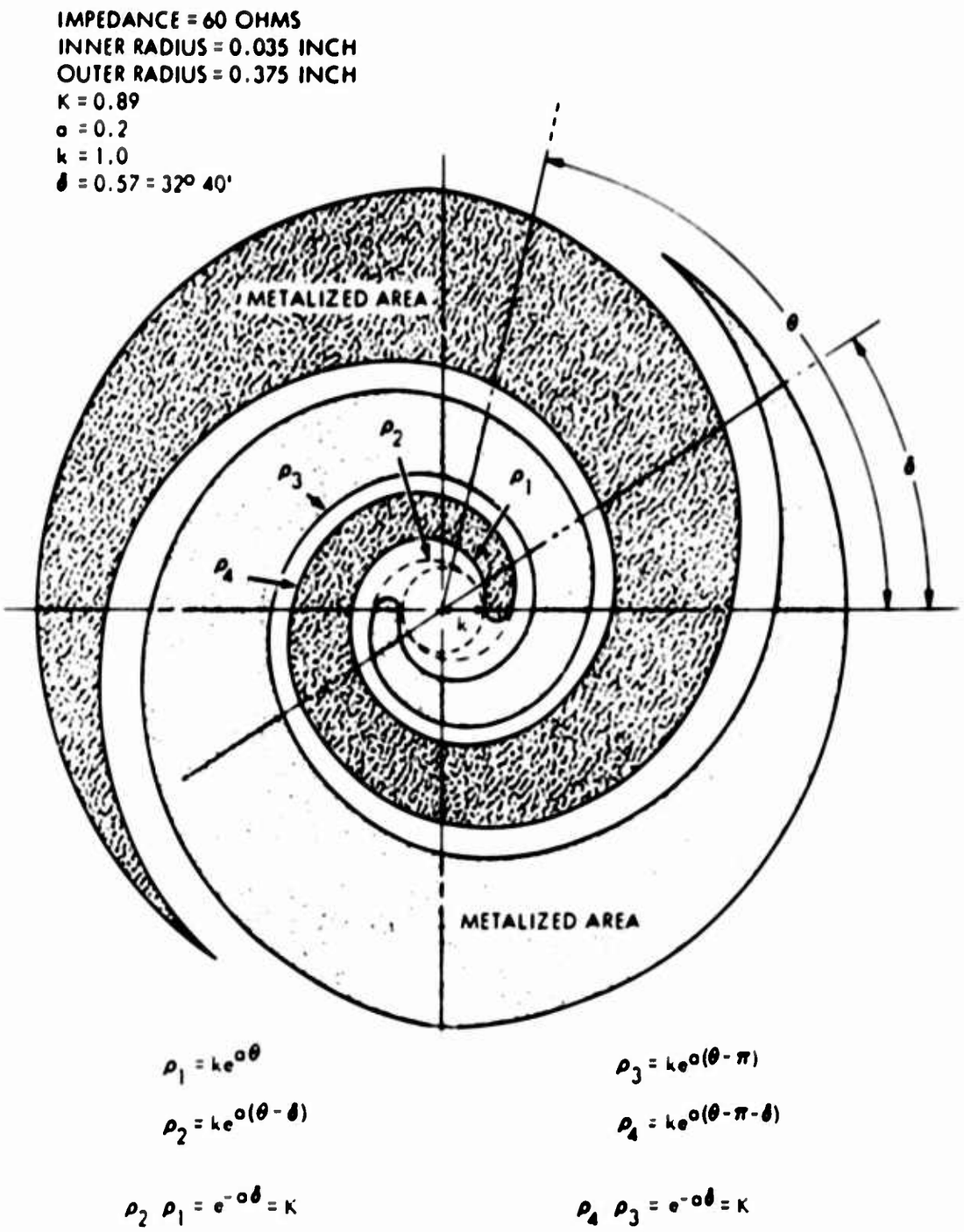

Figure 18. Definition of Spiral Antenna Characteristics

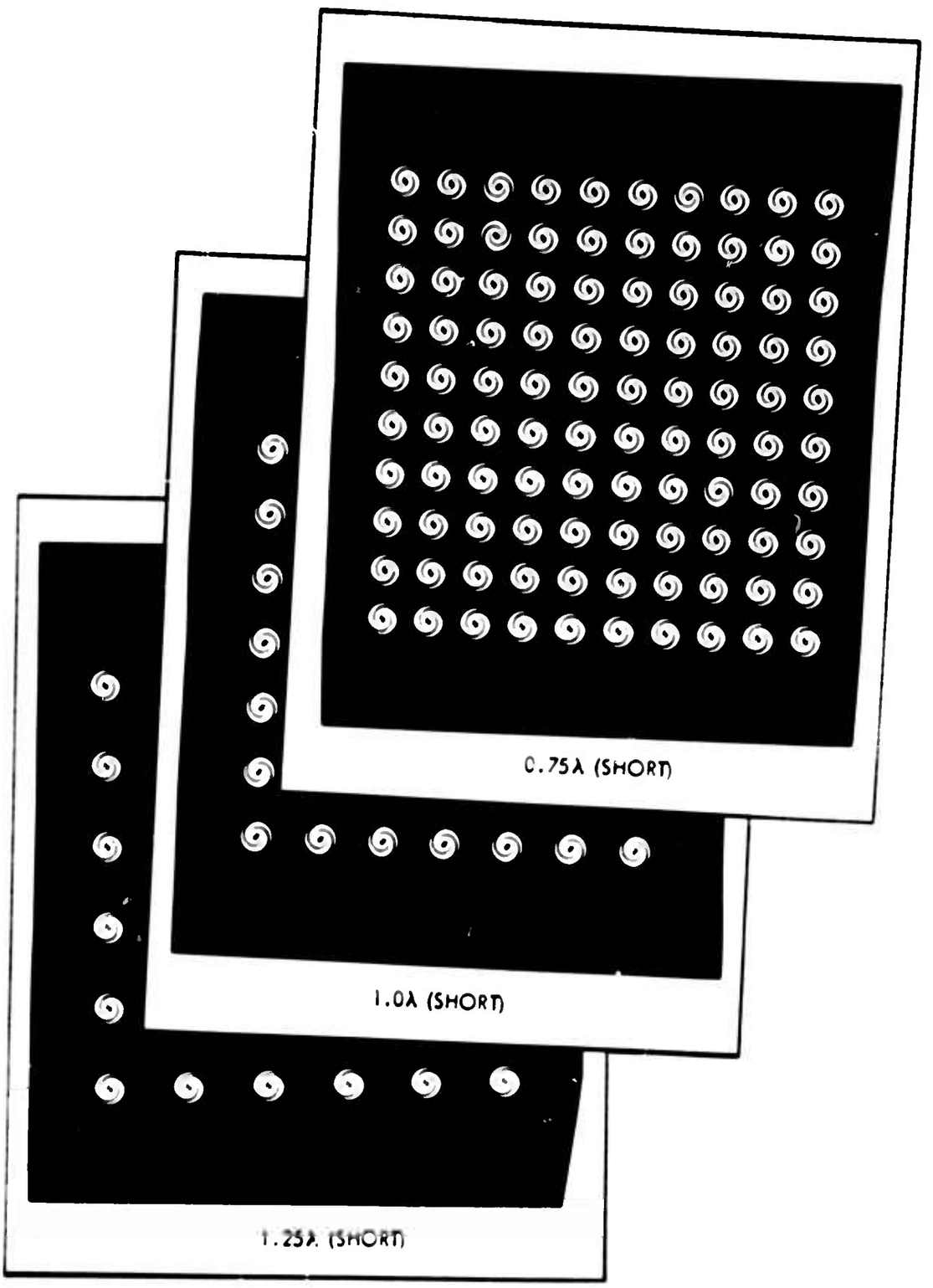

Figure 19. Master Patterns for 18-Inch-Square Quarter Panels with 0.75λ, 1.0λ, and 1.25λ

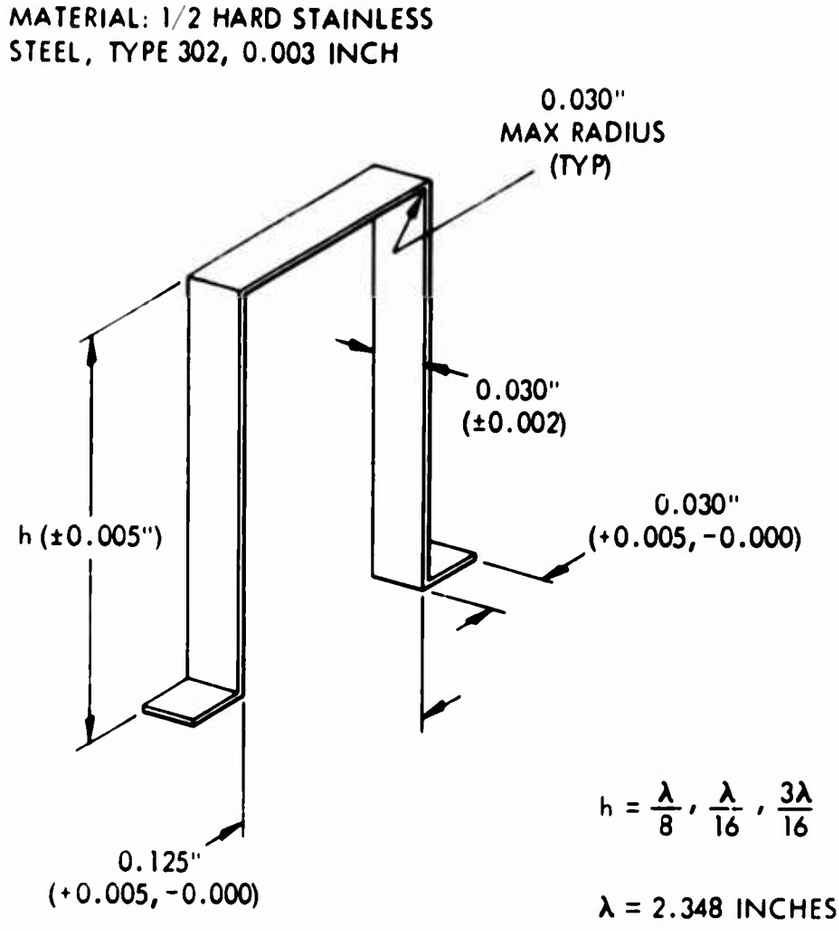

Figure 20. Sketch of Stub Short Details

Figure 21. Partially Welded Quarter Section Showing Protective Channels

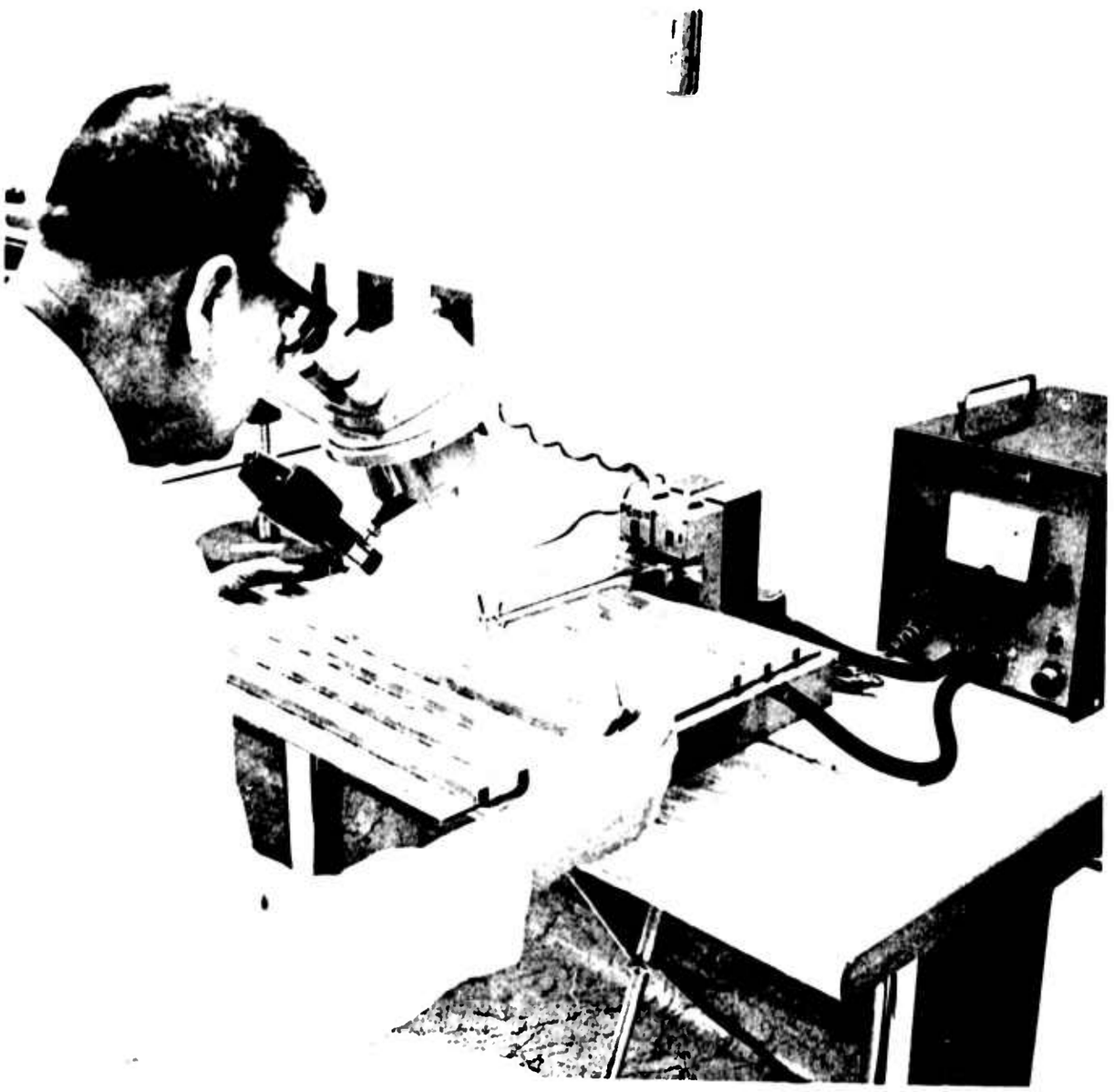

Figure 22. Clean-Room Welding Installation

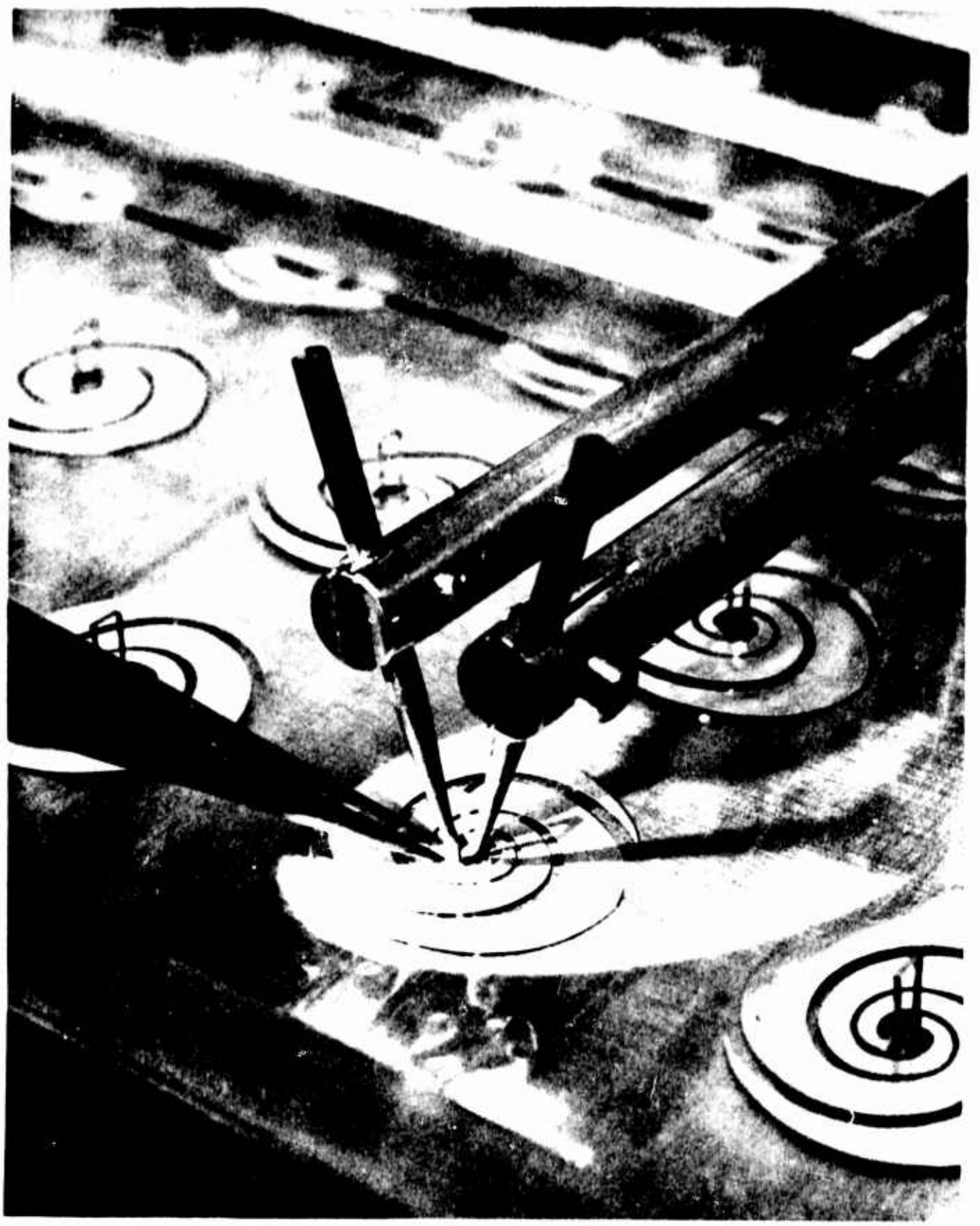

Figure 23. Close-Up of Welding Operation

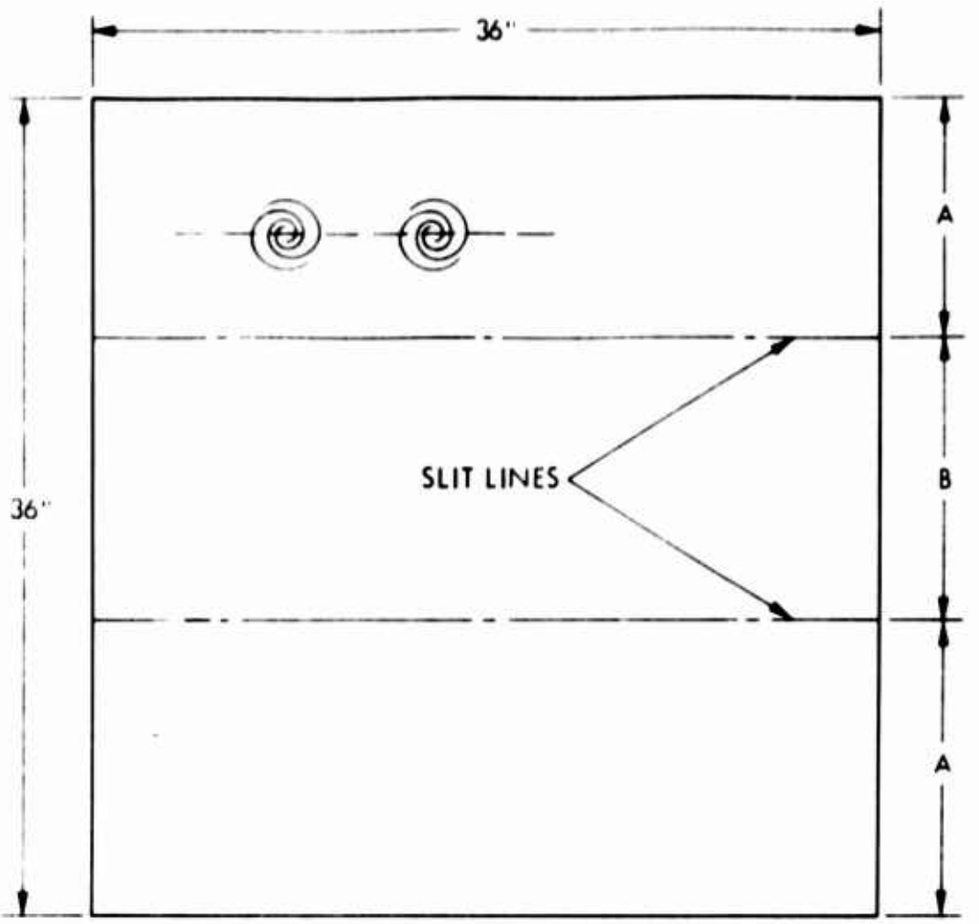

PANEL NO.	DIMENSIONS A	B
M (1.25λ)	12.63"	11.74"
O (1.25λ)	12.63"	11.74"
L (0.75λ)	12.71"	11.58"
N (0.75λ)	12.71"	11.58"

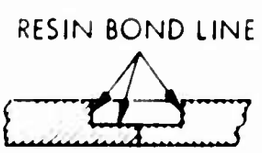

SECTION THROUGH JOINT

Figure 24. Panel Division for Welding Operation

Figure 25. Welding Stub Shorts through Foam Cutouts

Figure 26. Electrodes in Welding Position as Viewed through Binoculars

Figure 27. Foot of Stub Short as Viewed through Mylar at 50X

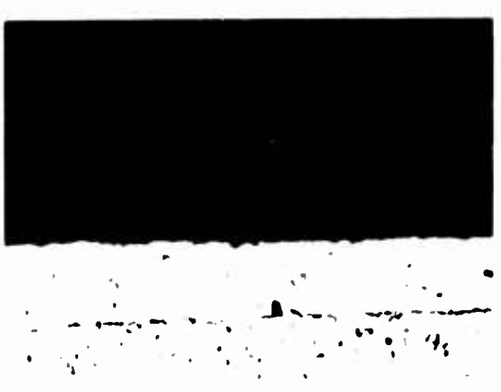

Figure 28. Sectional View through Weld at 1000X

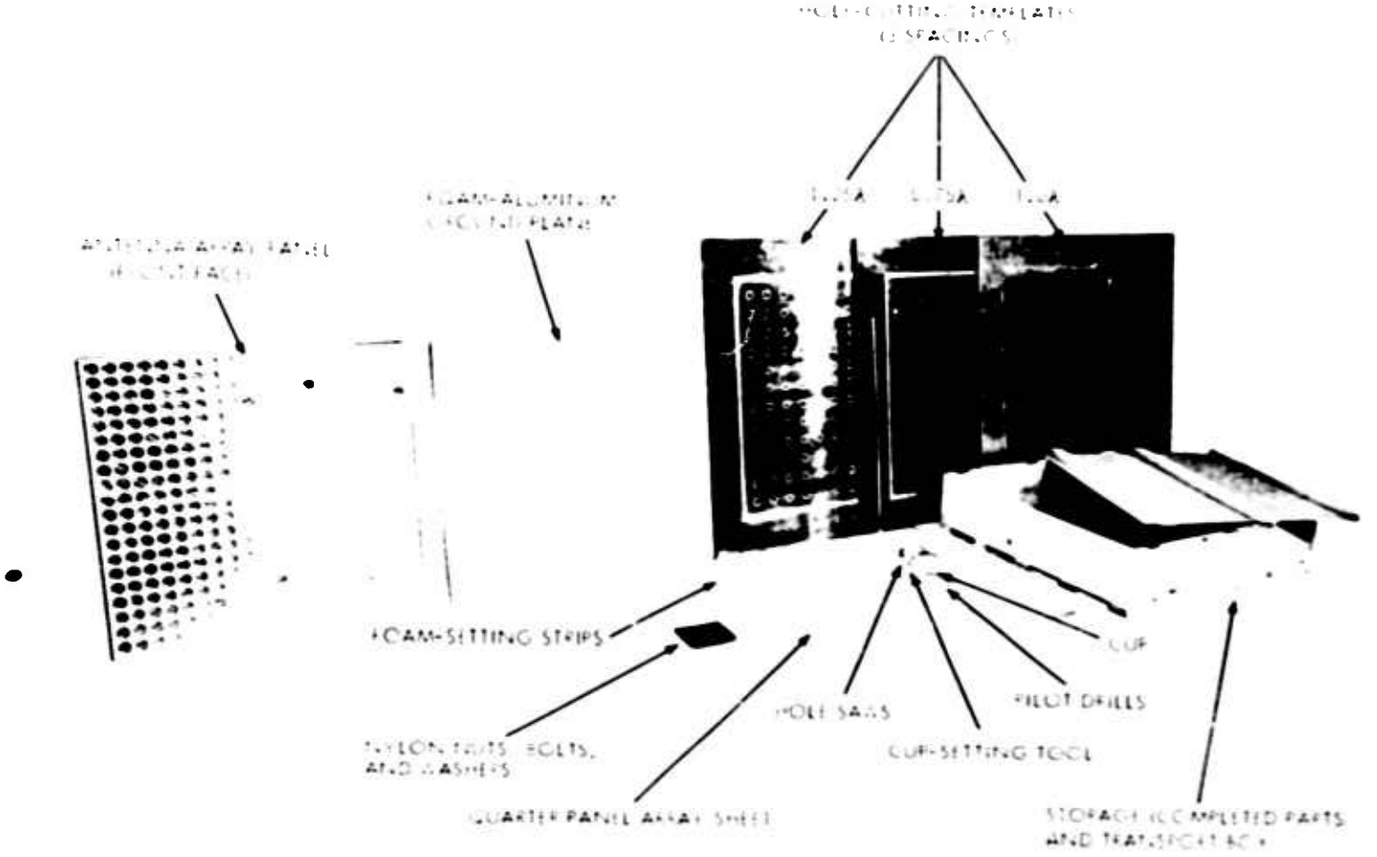

Figure 29. Test Panel Tools, Materials, Equipment, and Assemblies

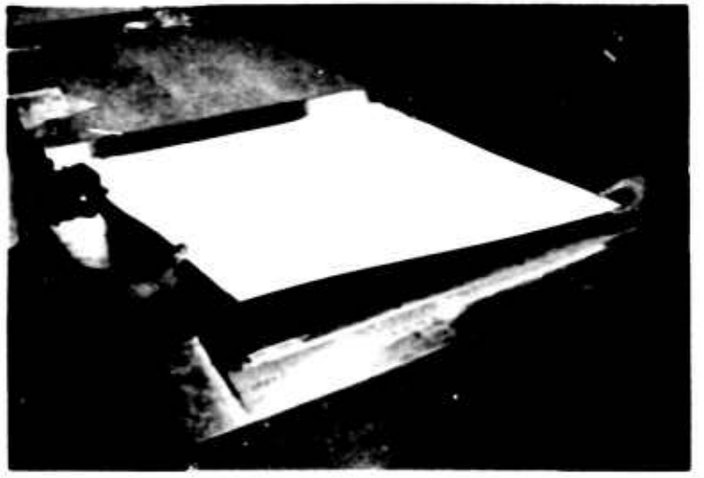

(A) Placing Foam Panel in Drill Fixture

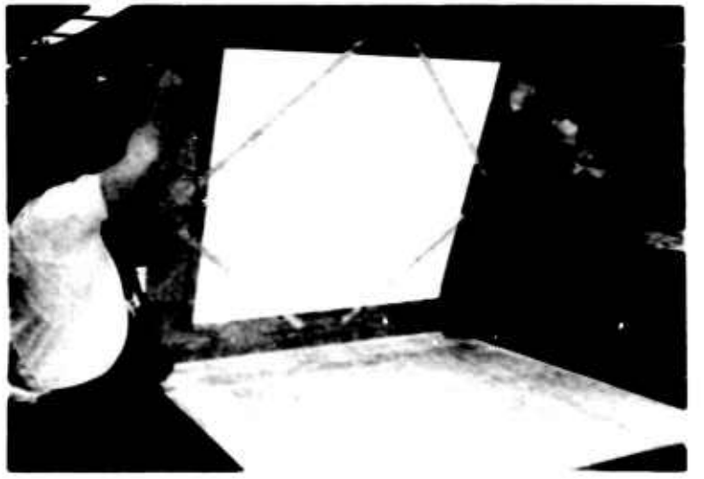

(B) Turnover of Drill Fixture - Foam Panel in Place

(C) 1/4-Inch Pilot Drill through Foam

(D) Hole Cutout in Foam

Figure 30. Foam Support Preparation

HOLE SPACING	a	b
0.75λ	$\frac{0.75\lambda}{2}$	1.27
[illegible]	0	1.56
1.25λ	$\frac{1.25\lambda}{2}$	1.86

λ = 2.348

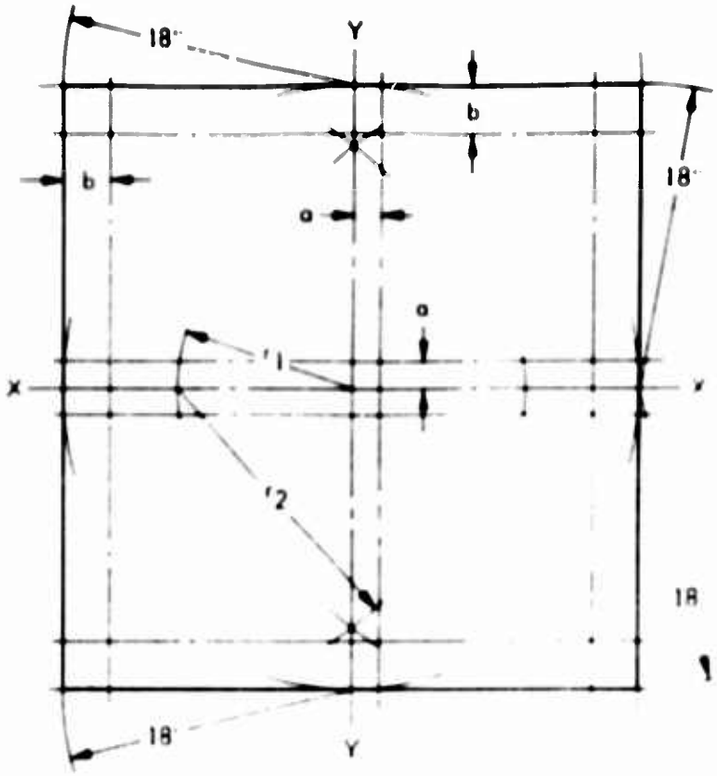

1. DRAW AXIS X - X.
2. CONSTRUCT AXIS Y - Y PERPENDICULAR TO AXIS X - X, USING RADII r_1 AND r_2.
3. ESTABLISH OUTER PERIPHERY USING 18" RADIUS AS SHOWN.
4. CONSTRUCT ARRAY CENTERLINES AS SHOWN FOR EACH ARRAY SPACING.

Figure 31. Layout Procedure for RF Panel Array

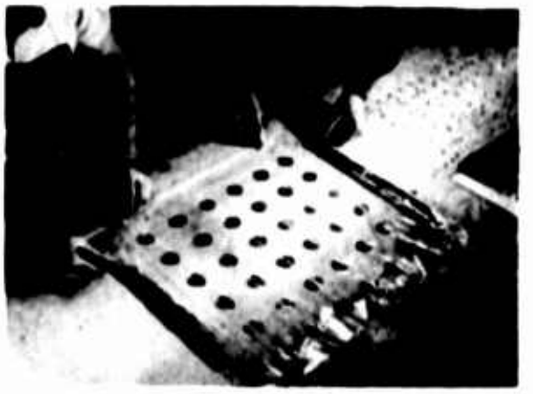

(A) First Quarter Panel Placement

(B) Second Quarter Panel Placement

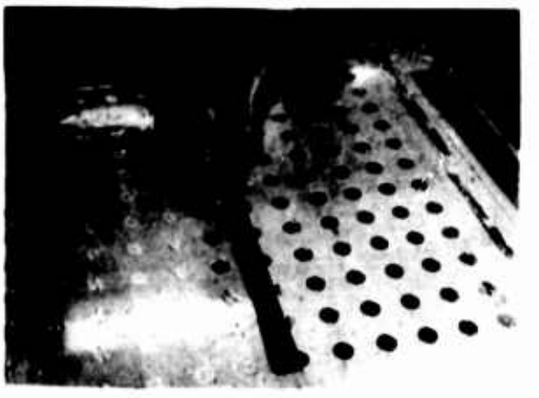

(C) Center Trim Operation

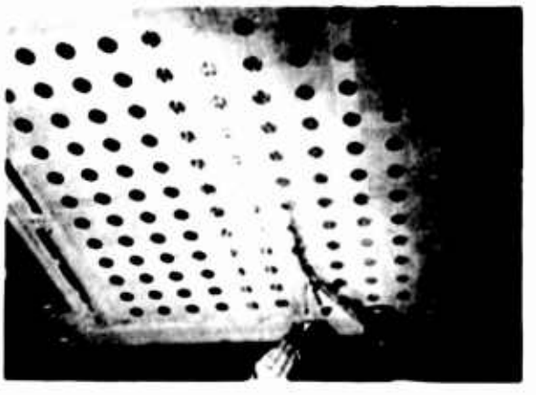

(D) Removal of Trim-Off

(E) Taping of Center Butt Seam

Figure 32. Antenna Array Assembly

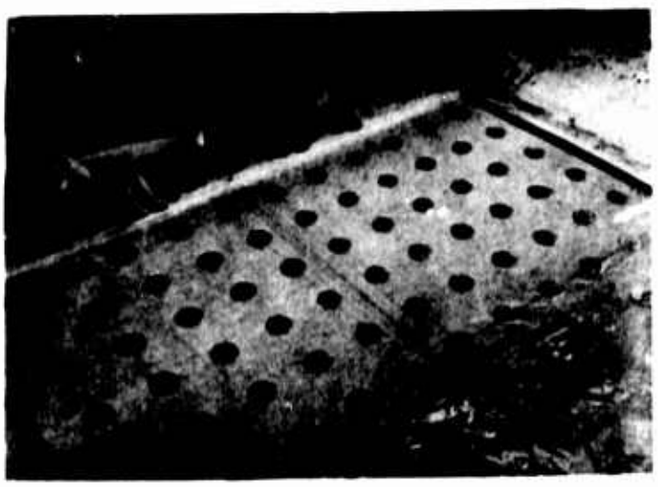

(A) Setting of Foam Guide Strips

(B) Application of Polyurethane Elastomer Adhesive

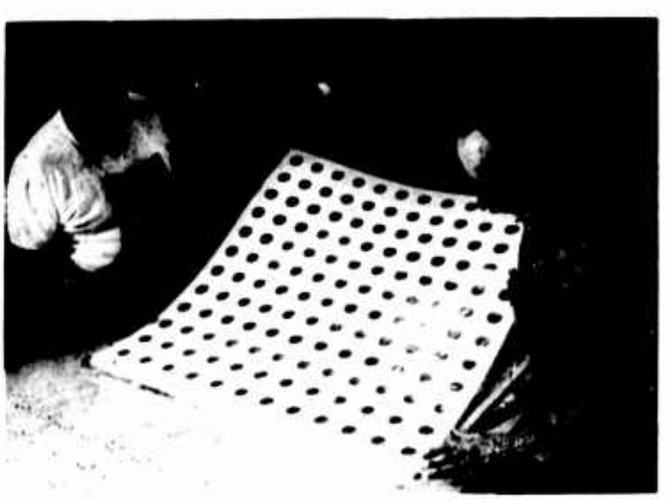

(C) Placing Foam Panel on Etched Array

Figure 33. Assembly of Foam Backing to Array Panel

(A) Application of Adhesive to Inside of Holes

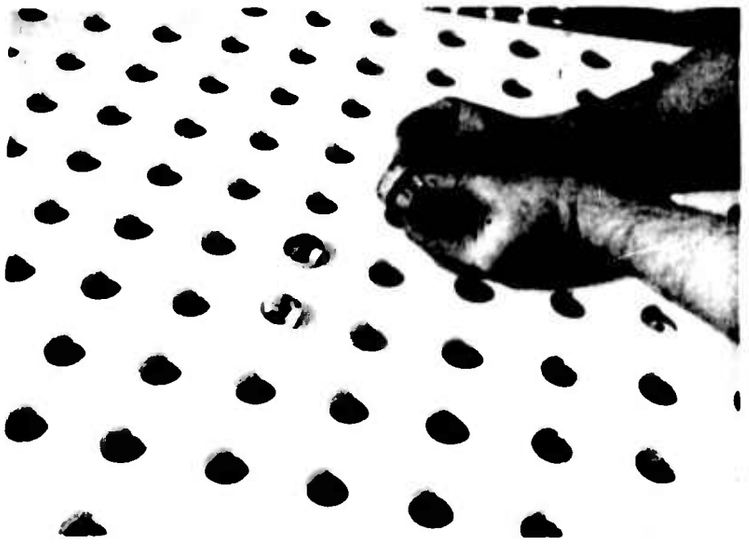

(B) Placing Cup in Cup-Setting Holders

(C) Installation of Cup

Figure 34. Reflector Face Assembly

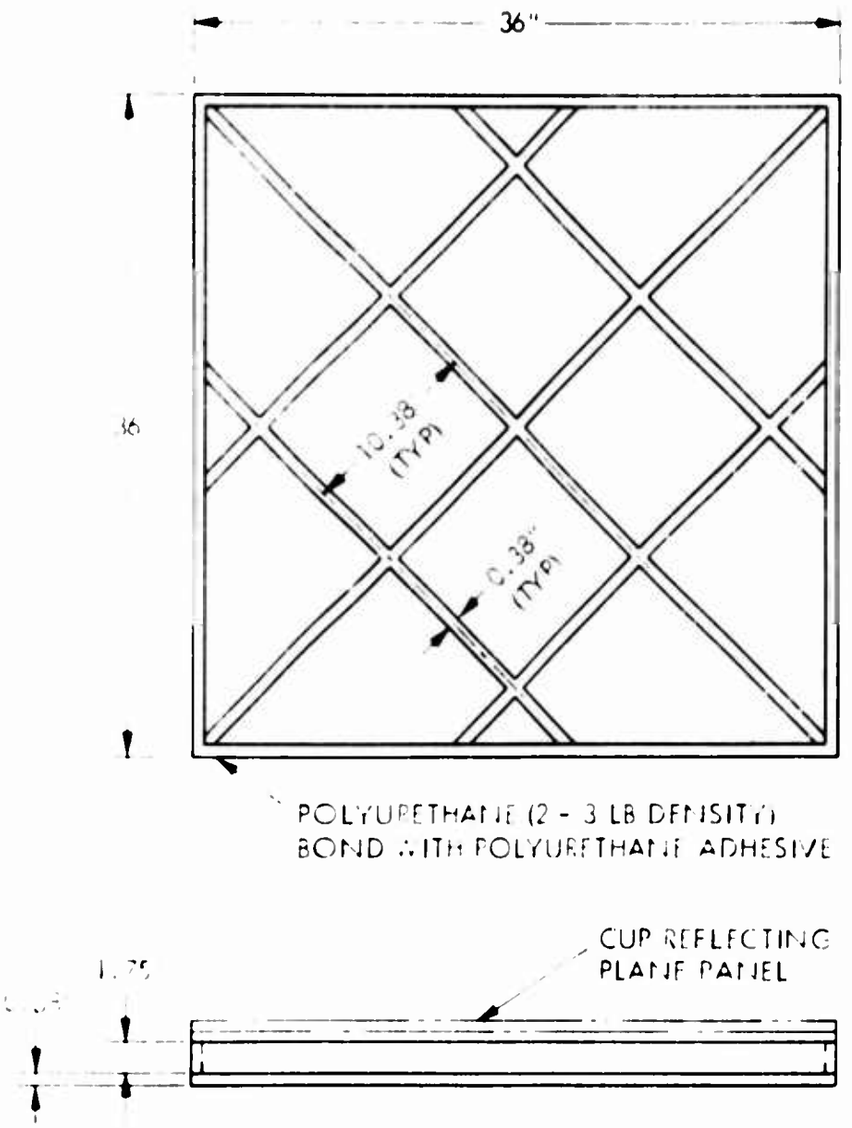

Figure 35. Structural Back-Up for Parts A', D' and E'

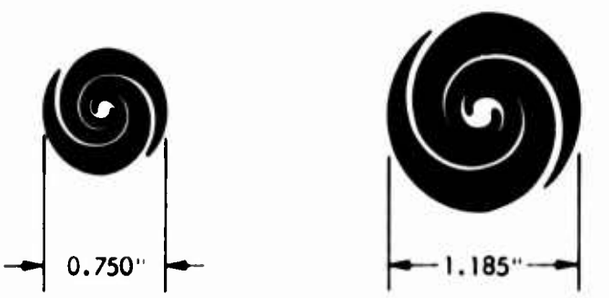

Figure 36. Single-Spiral Antenna Element Design

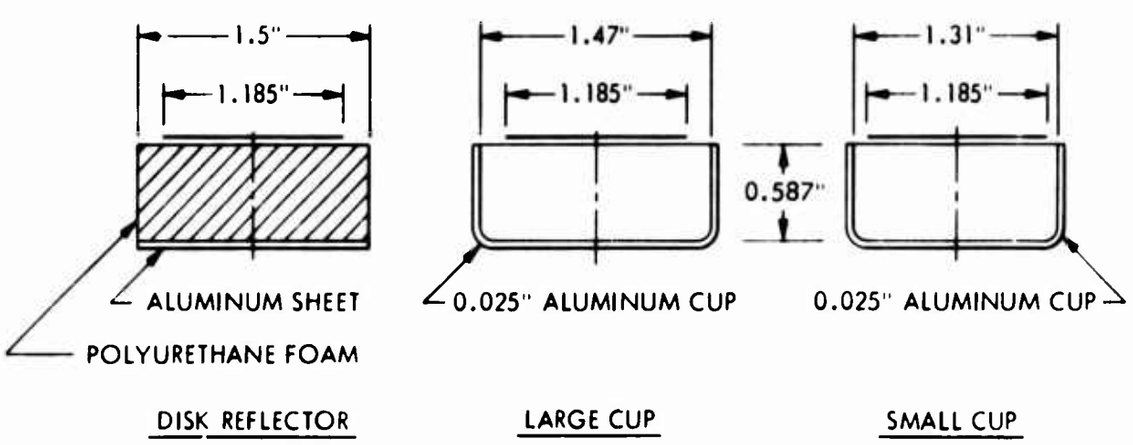

Figure 37. Reflecting Surfaces for Single-Spiral Antennas

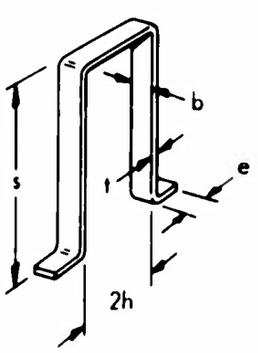

NONMAGNETIC STAINLESS STEEL, TYPE 302

$s = \lambda/16 = 0.147"$	$t = 0.003"$
$s = 3\lambda/32 = 0.220"$	$b = 0.030"$
$s = \lambda/8 = 0.294"$	$2h = 0.125"$
$s = 5\lambda/32 = 0.367"$	$e = 0.030"$
$s = 3\lambda/16 = 0.440"$	

Figure 38. Nominal Dimensions of Single-Spiral Antenna Shorting Strip

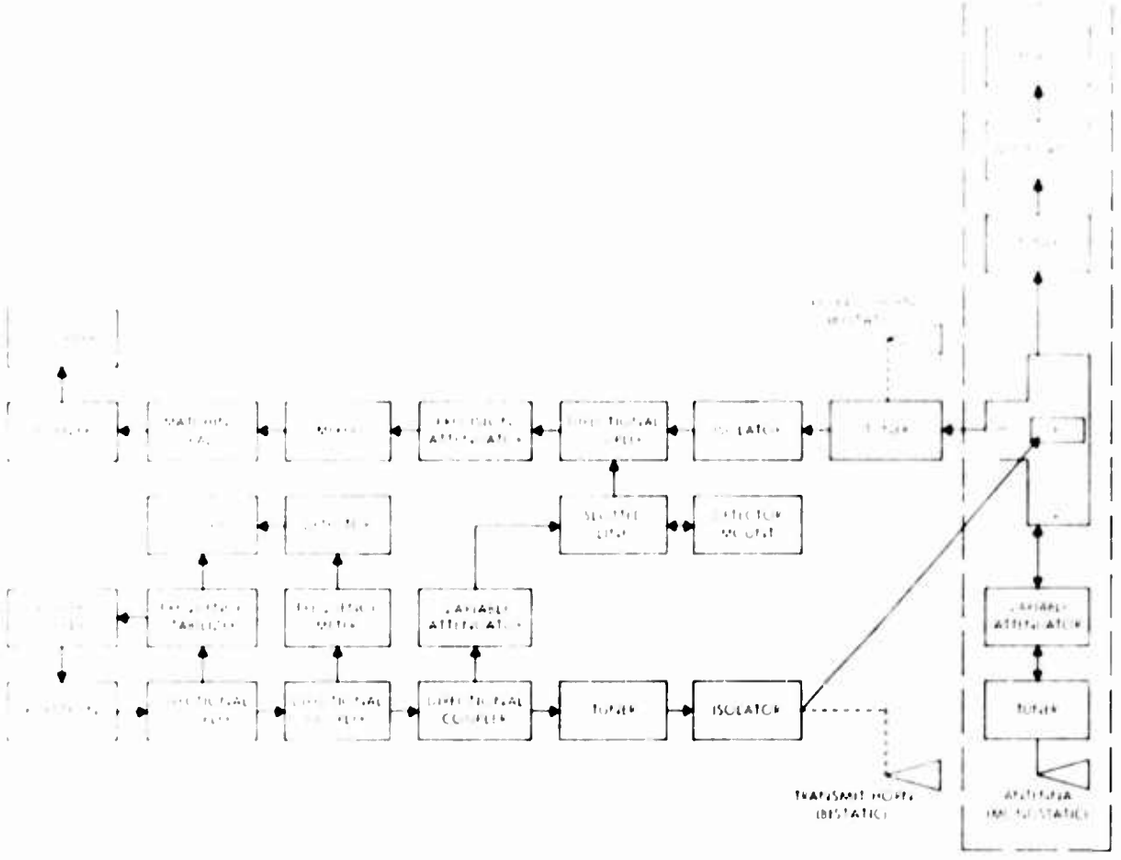

Monostatic and Bistatic Block Diagram

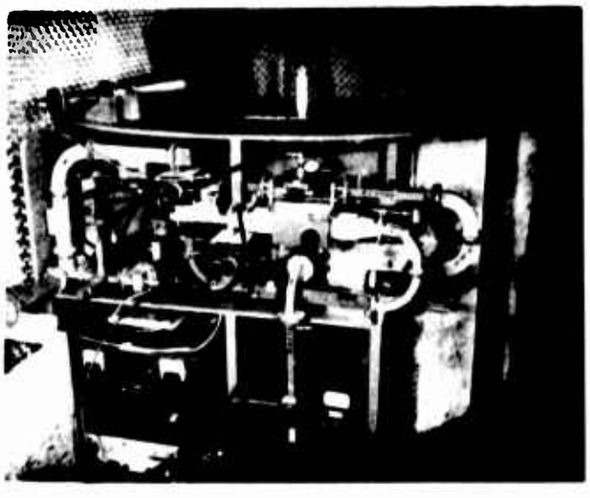

Monostatic Setup

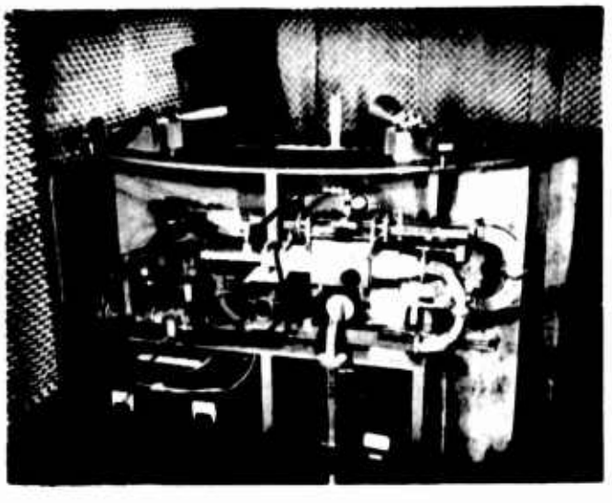

Bistatic Setup

Figure 39. Reflectivity Measurement Instrumentation for Single-Spiral Antennas

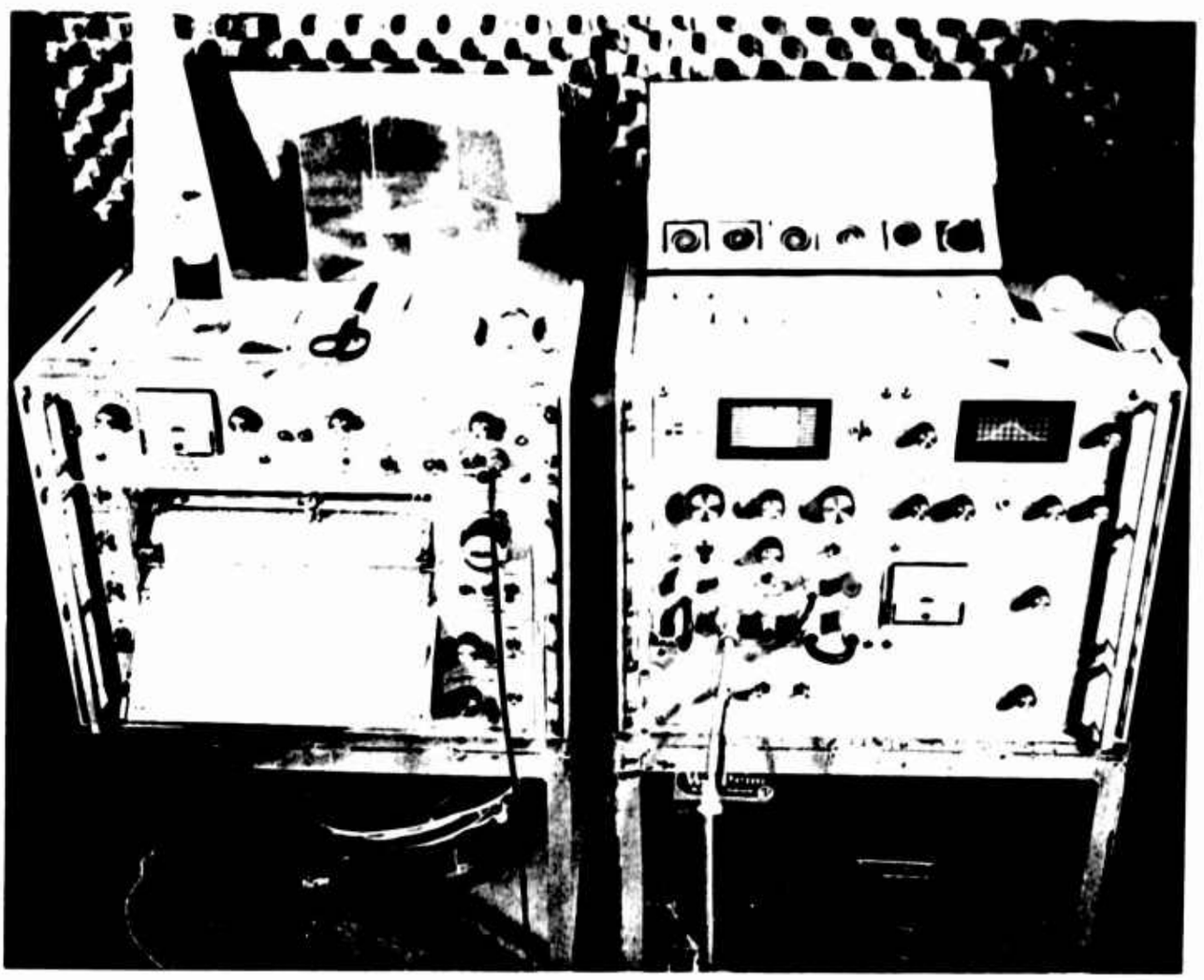

Figure 40. Recorder, Receiver, Standard Targets, and Spiral Elements

Figure 41. A^2, B^2, $(A/B)^2$, and Shorted Element Pattern for Monostatic Return

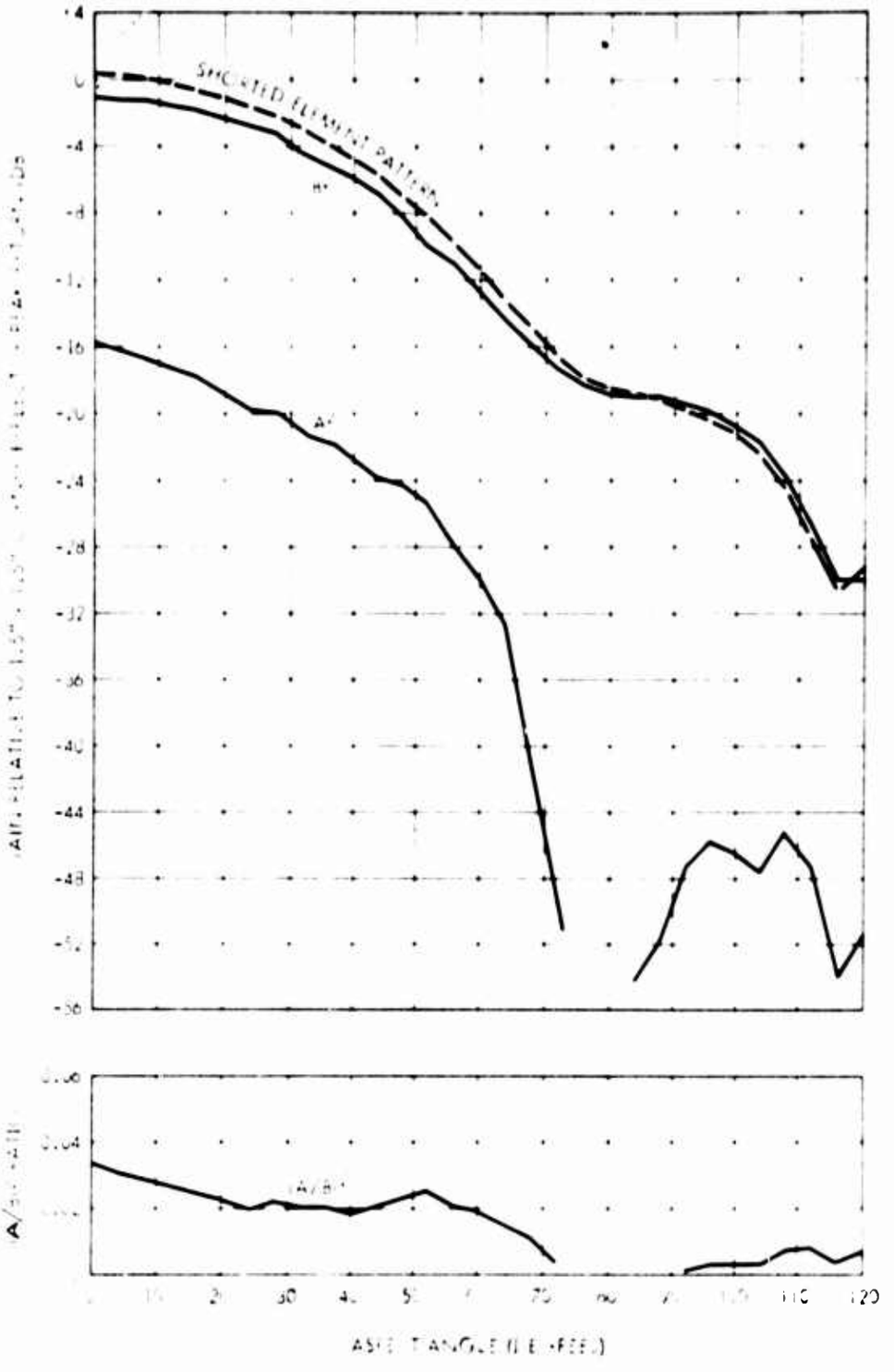

Figure 42. A^2, B^2, $(A/B)^2$, and Shorted Element Pattern for 15-Degree Bistatic Return

Figure 43. A^2, B^2, $(A/B)^2$, and Shorted Element Pattern for 30-Degree Bistatic Return

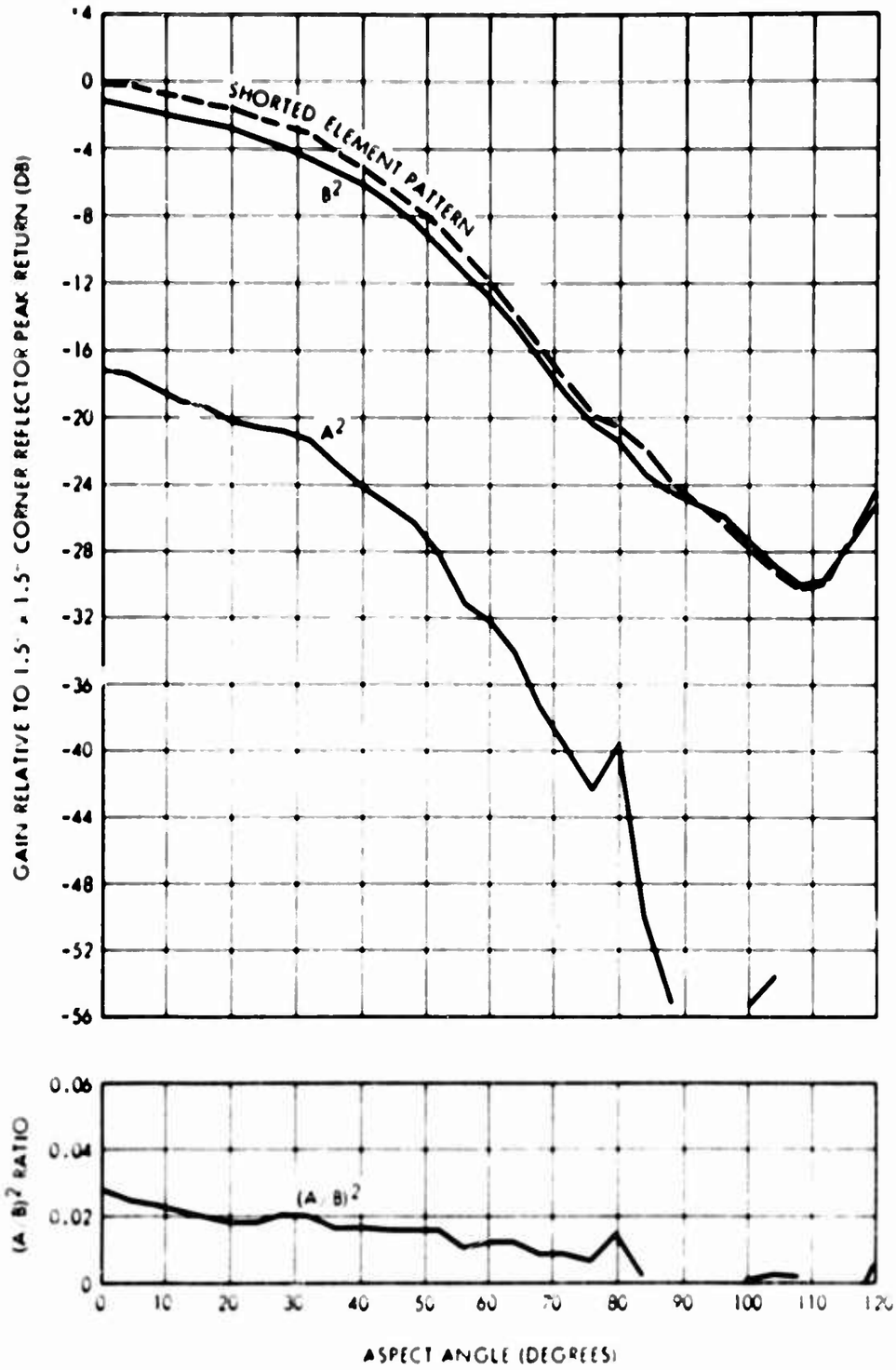

Figure 44. A^2, B^2, $(A/B)^2$, and Shorted Element Pattern for 45-Degree Bistatic Return

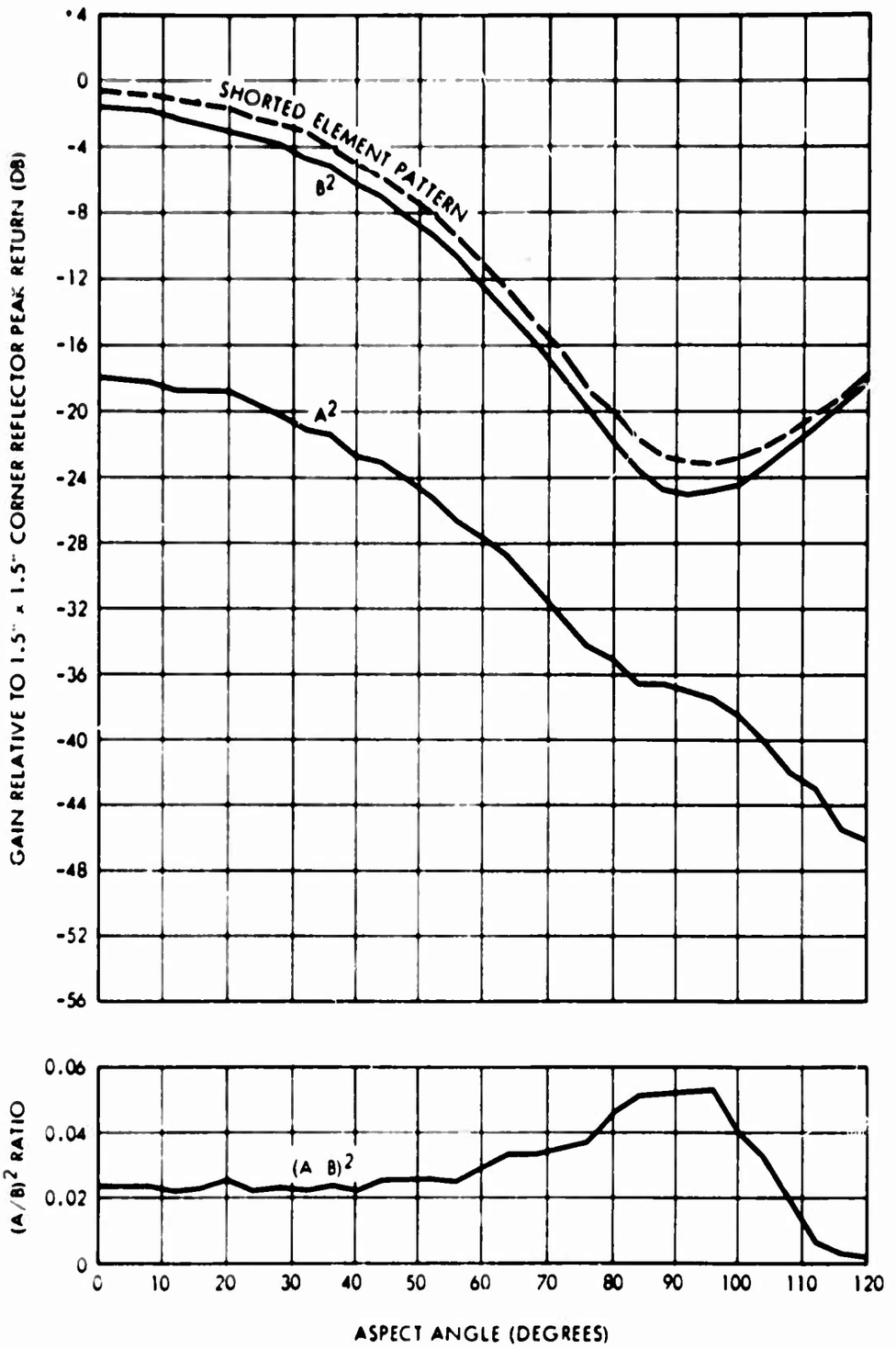

Figure 45. A^2, B^2, $(A/B)^2$, and Shorted Element Pattern for 60-Degree Bistatic Return

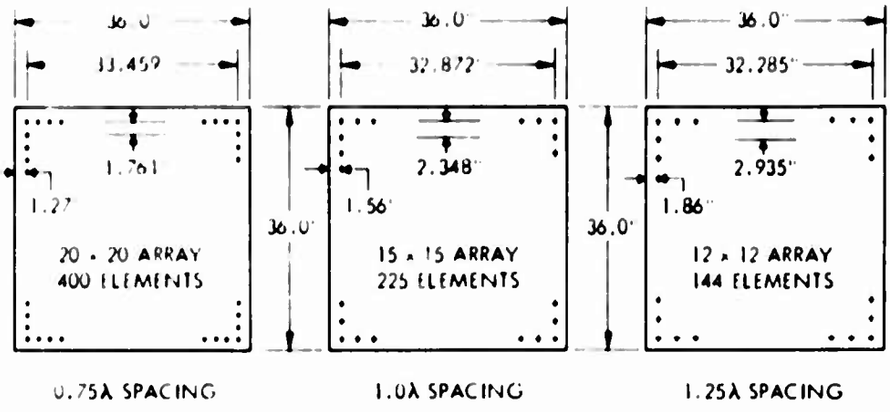

Figure 46. Panel Configurations for Arrayed Elements

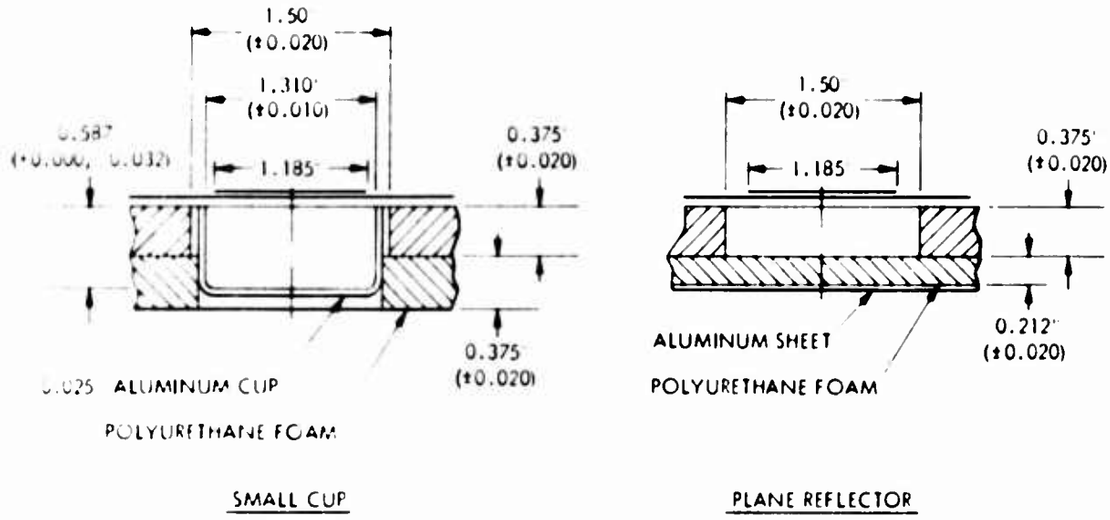

Figure 47. Reflecting Surfaces for Arrayed Elements

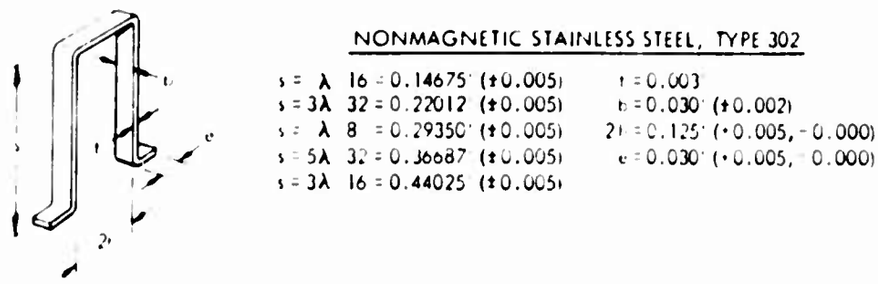

Figure 48. Shorting Strip Dimensions for Arrayed Elements

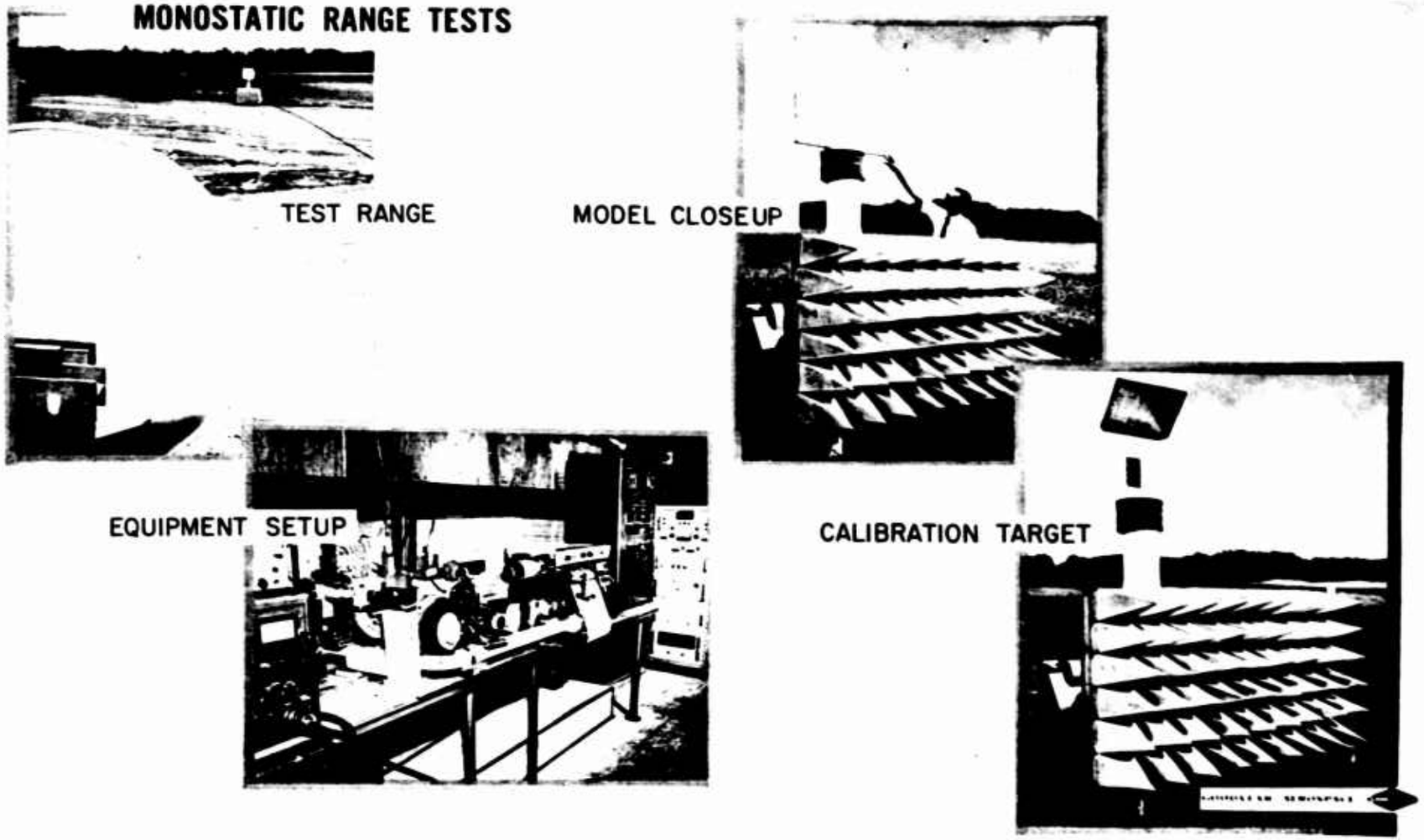

Figure 49. Monostatic Range Tests

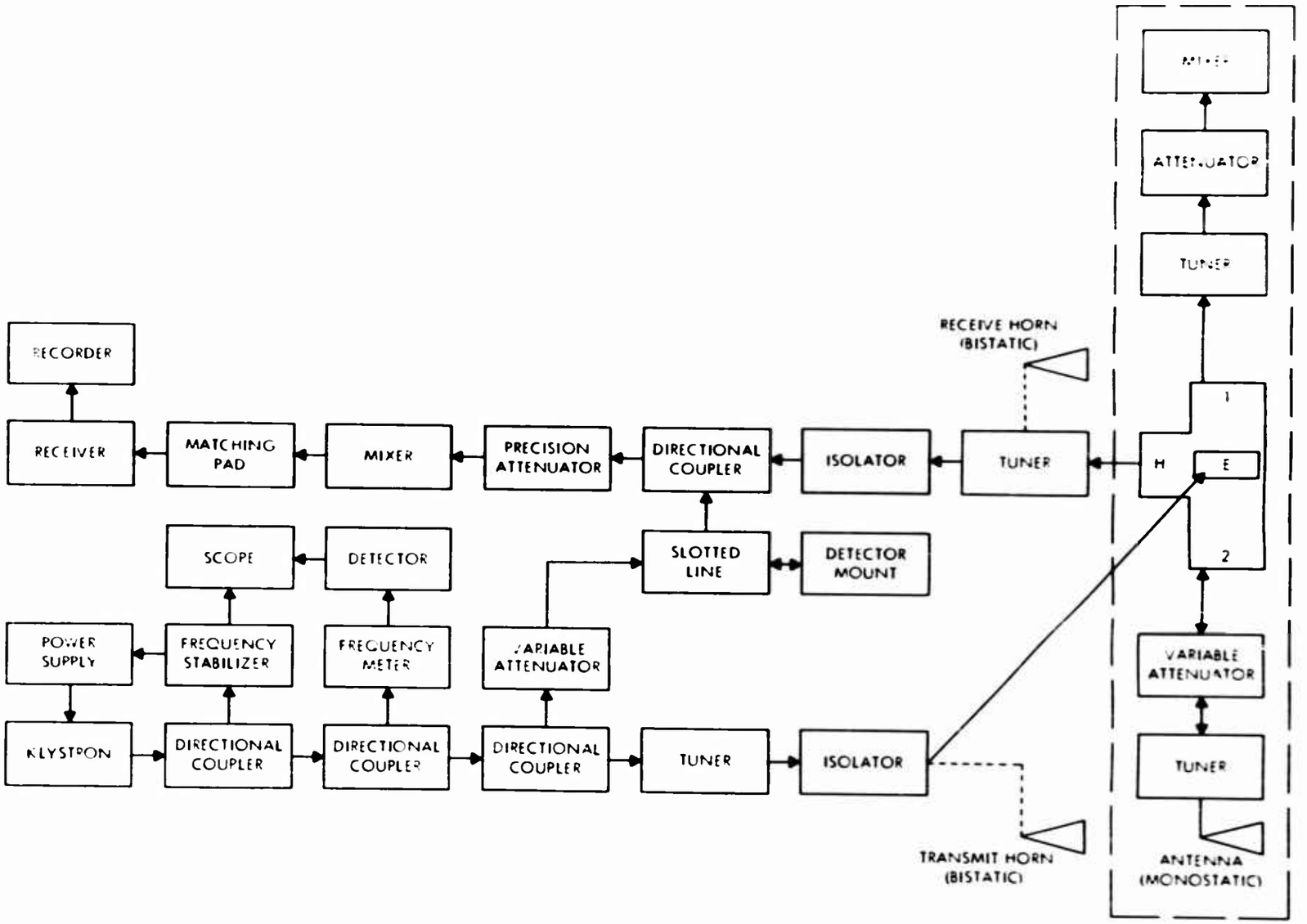

Figure 50. System Block Diagram

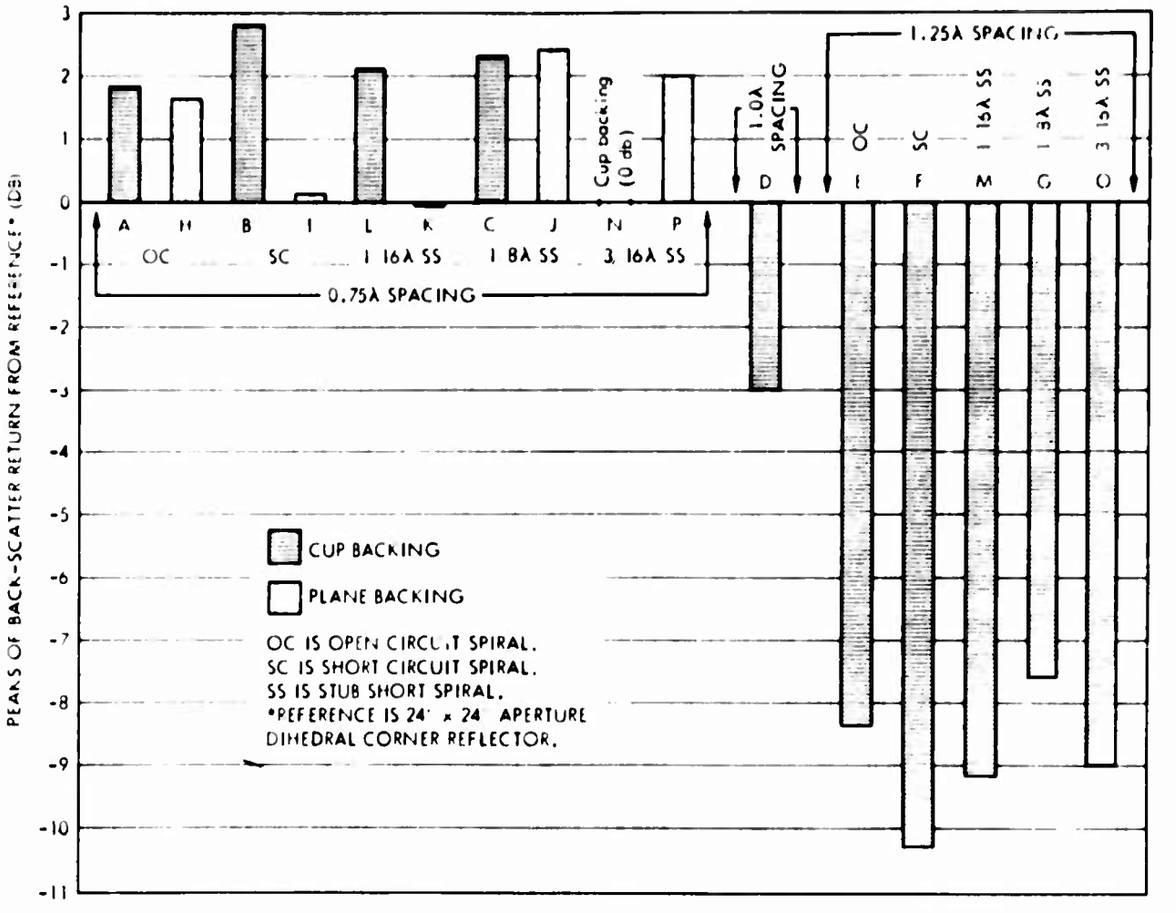

Figure 51. Deviation of Panel Radar Cross Section from Reference Radar Cross Section

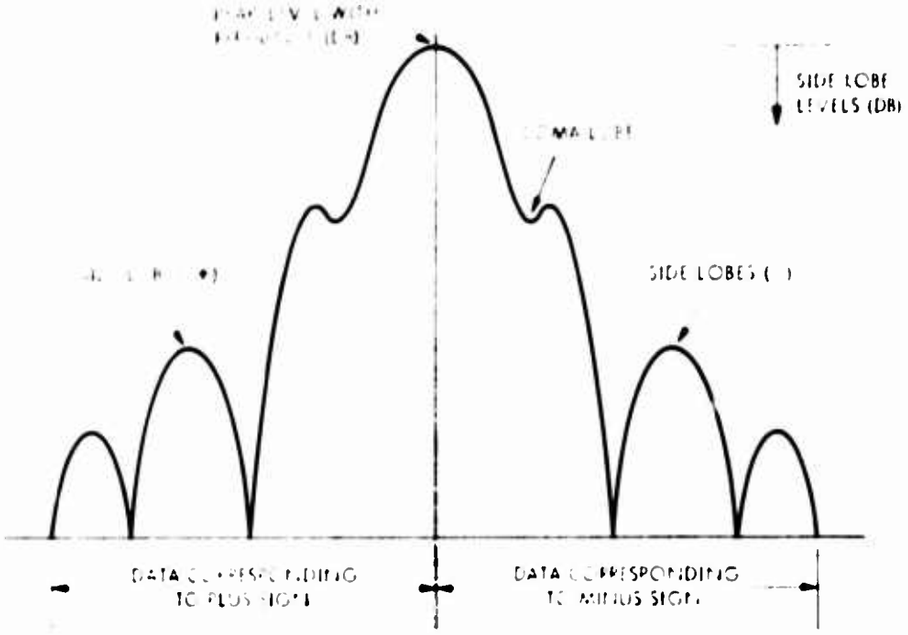

Figure 52. Sketch Illustrating Monostatic Scattering from Panel Array

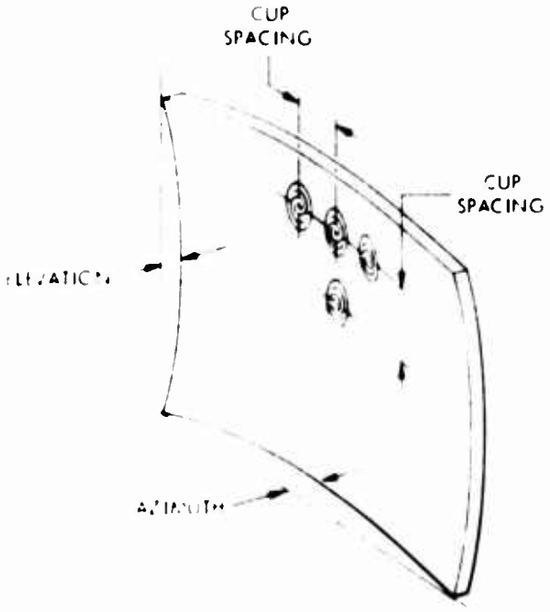

	ELEVATION	AZIMUTH
[illegible] CUP SPACING	1 16	5 16
[illegible] CUP SPACING	1 8	3 16
CONDUCTING PLANE	1 2"	1 4"

Figure 53. Panel Distortion

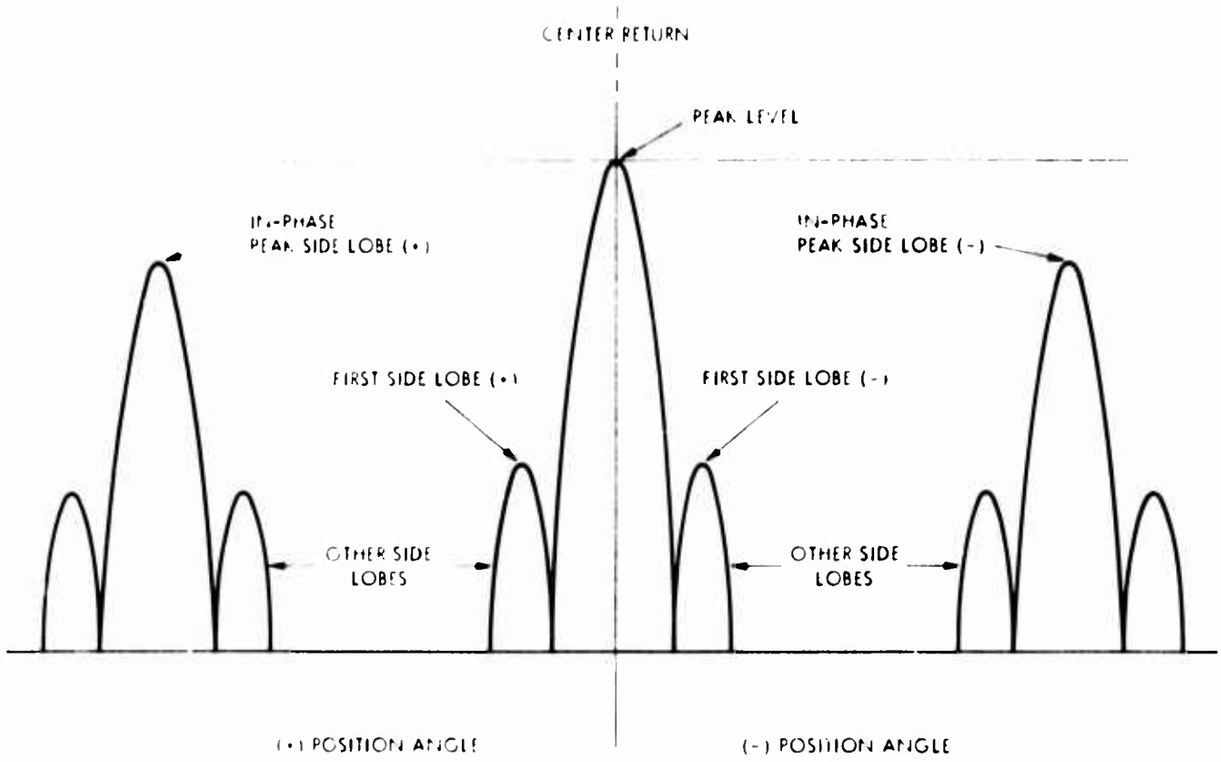

Figure 54. Sketch Illustrating Bistatic Scattering from Panel Array

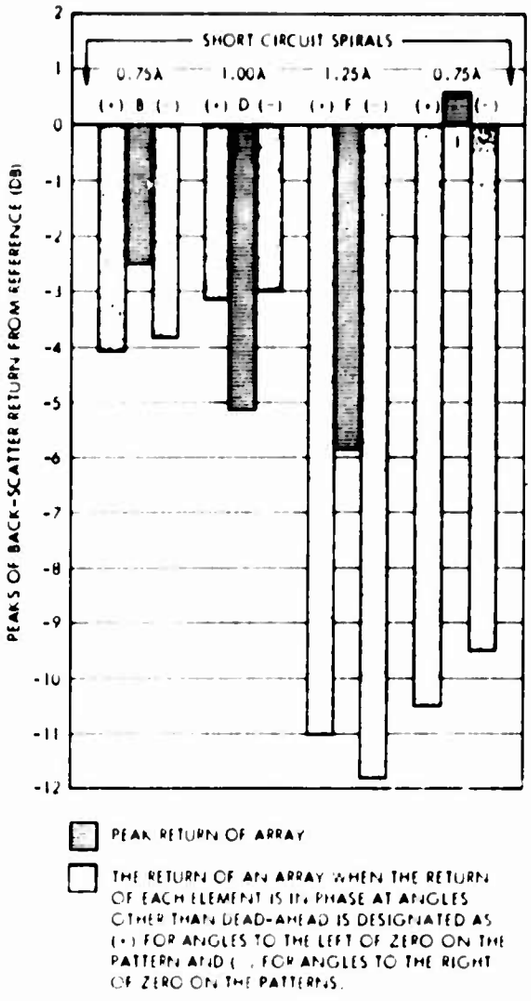

Figure 55. Thirty-Degree Bistatic Peak Returns

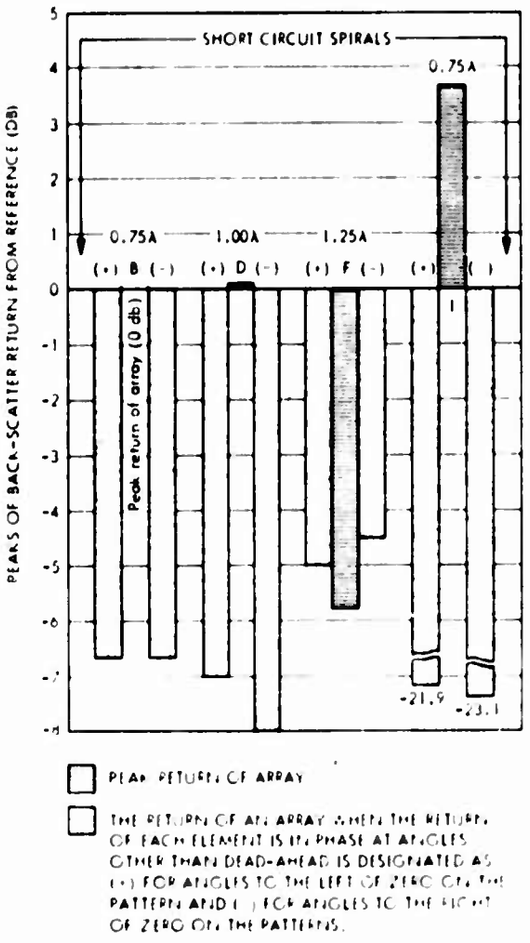

Figure 56. Sixty-Degree Bistatic Peak Returns

Figure 57. Isolated and Effective Spiral Element Patterns for Short Circuit Termination

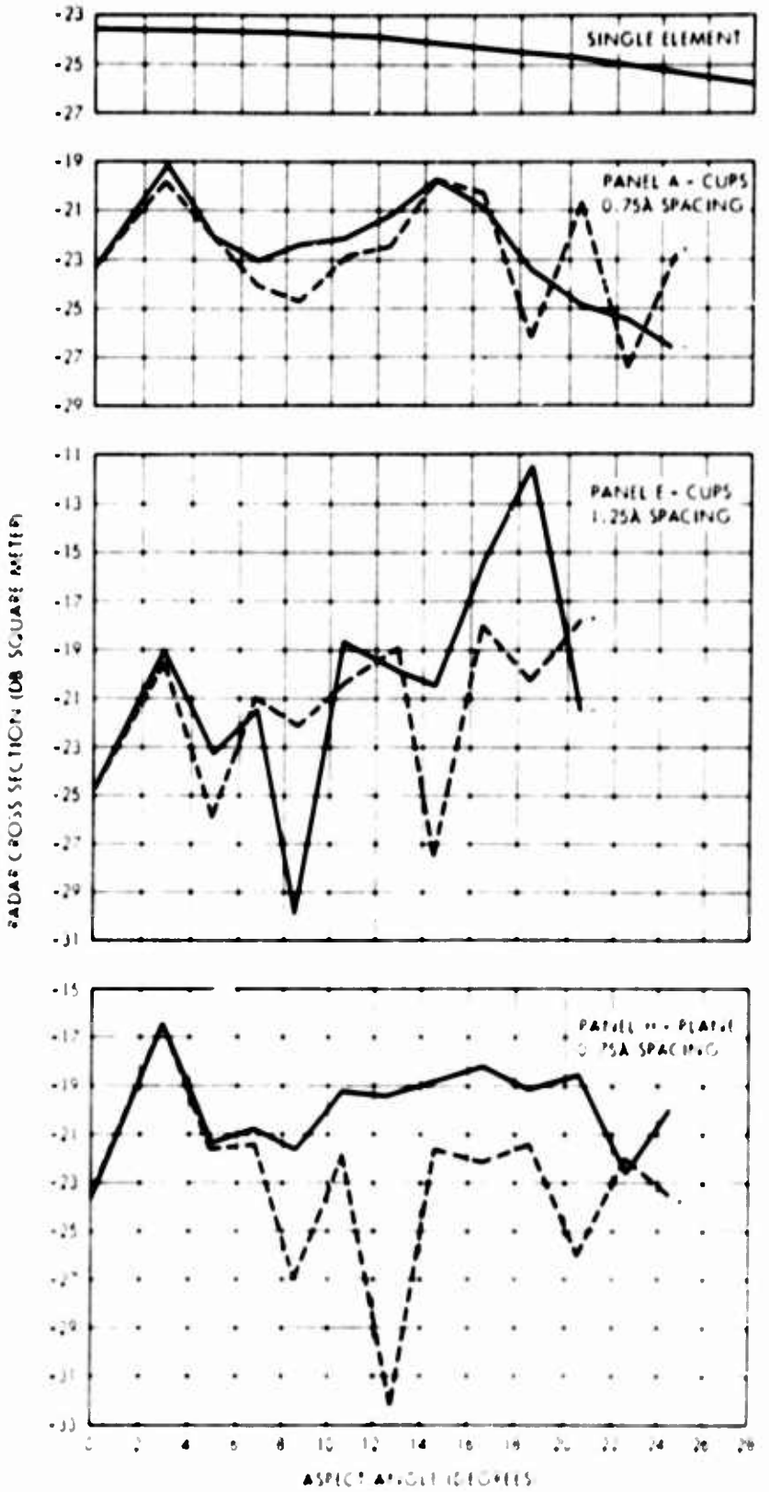

Figure 58. Isolated and Effective Spiral Element Patterns for Open Circuit Termination

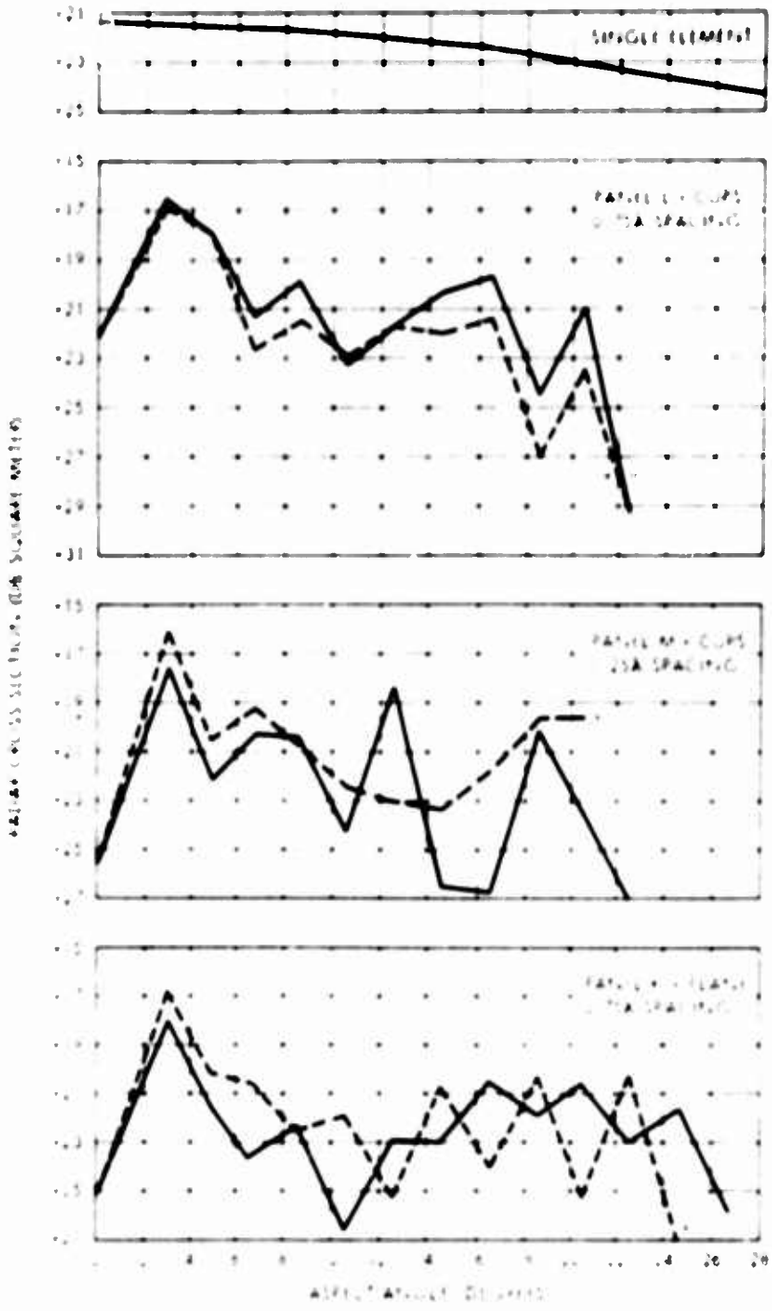

Figure 59. Isolated and Effective Spiral Element Patterns for λ/16 Termination

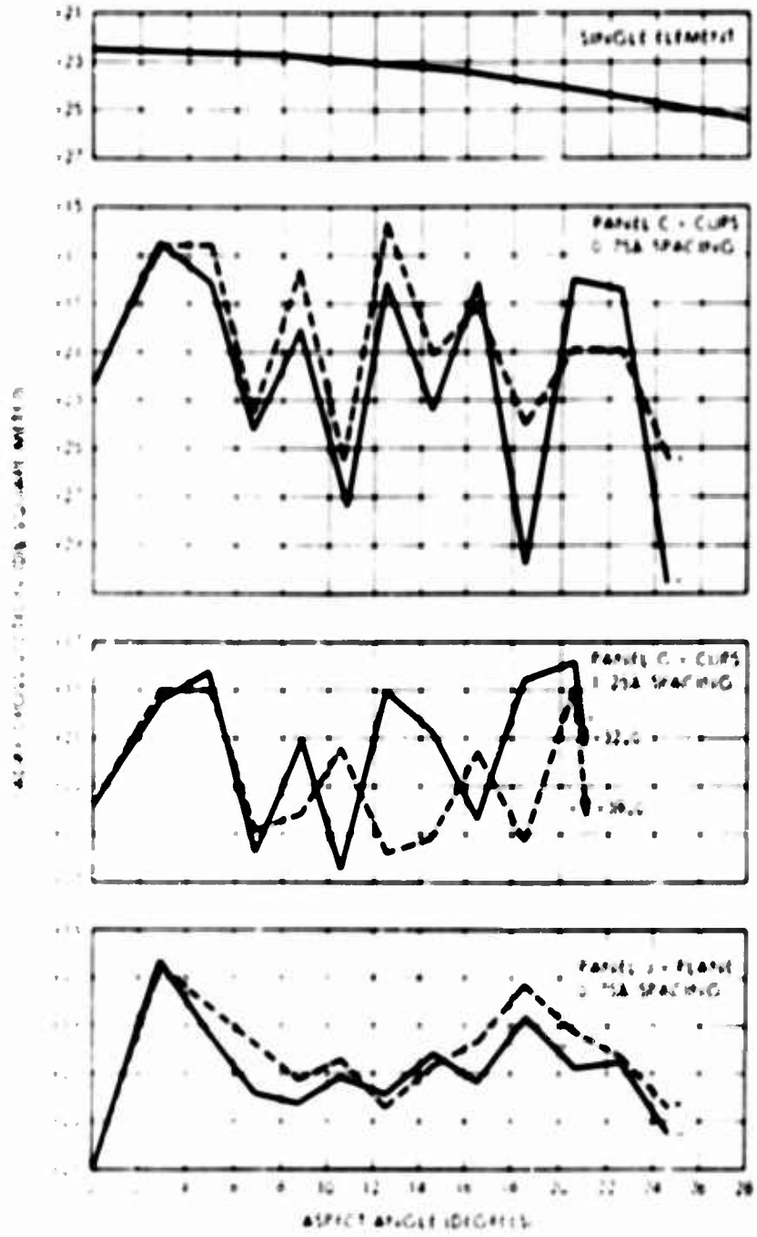

Figure 60. Isolated and Effective Spiral Element Patterns for λ/8 Termination

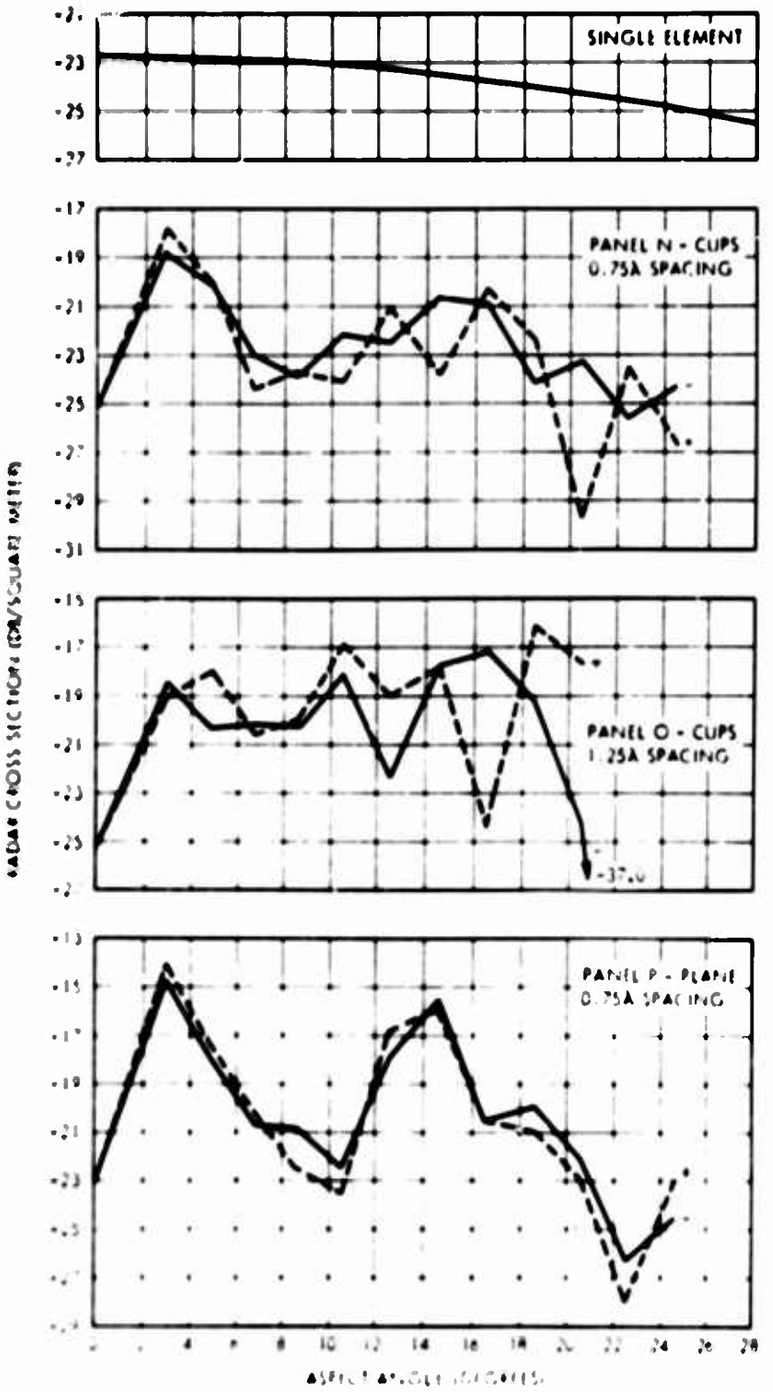

Figure 61. Isolated and Effective Spiral Element Patterns for 3λ/16 Termination

Four cards are required for one set of data.

(1) Your title or identification (no more than 50 spaces)

(2) $\sigma(1)$ through $\sigma(5)$ in db with respect to reference.

Note: $\sigma(1)$ is the location for the short circuit data.
$\sigma(2)$ is the location for the open circuit data.

(3) RL(1) through RL(5).

(4) XL(1) through XL(5).

As many sets of four cards each can be used as required.

Card No	1	11	21	31	41
1	1. EVALUATION OF EFFECTIVE REACTANCE				
2	-19.8	-23.5	-22.3	-22.5	-24.5
3	0	0	0.7775	1.382	2.160
4	19.39	-1.E10	55.73	71.83	87.95
1					
2					
3					
4					
1					
2					
3					
4					
1					
2					
3					
4					
1					
2					
3					
4					

Figure 62. Input Data Format

```
      DIMENSION F(5,6),DB(5),SIG(5),TITLE(8), S(5),RL(5),XL(5), SF(5)
      DIMENSION DELS(5),SI(5), RATIO(5)
      COMMON FU(5),FW(5),FB(5),FR(5),FX(5),DL(5)
      EQUIVALENCE(F(1),FU(1))
  100 FORMAT(8A10)
  101 FORMAT(1HT,8A10)
  102 FORMAT(5F10.5)
  103 FORMAT(//20X,10HINPUT DATA///17X,1HN,10X,5HSIGMA,10X,2HRL,8X,2HXL/)
  104 FORMAT(I3,10 3E13.3)
  105 FORMAT(1HL,19X,17HESTIMATED ANSWERS/15X,1HU,9X,1HW,9X,1HB,
     19X,1HR, 9X,1HX)
  106 FORMAT(10X, 5F10.5/)
  107 FORMAT(I10, 10SF11.3,3X,5E11.3)
  108 FORMAT(20X,1P5E14.4)
  109 FORMAT(33HK                    FINAL ANSWERS/130HK                U
     1              W                B              K                   X
     /                    A          GAMMA            /1HK,7F18.8)
  111 FORMAT(10X,30HSIGMAS FROM FINAL ANS AS CHECK//22X,5HSIGMA/)
  112 FORMAT(1H1,8A10)
  113 FORMAT(//20X,10HNEXT TRIAL///17X,1HN,10X,5HSIGMA,10X,2HRL,8X,2HXL/)
  115 FORMAT(39X,6E12.5)
    1 READ(1,100) TITLE
      READ(1,102) DB, RL, XL
      WRITE(3,112)TITLE
      WRITE(3,103)
      DO 4 N = 1, 5
   10 SF(N)= 10.** (DB(N)/10.)
    4 WRITE(3,104) N, SF(N), RL(N), XL(N)
      SMAX = AMAX1(SF(1), SF(2), SF(3), SF(4), SF(5))
      SMIN = AMIN1(SF(1), SF(2), SF(3), SF(4), SF(5))
      SM = .25*(SMAX + SMIN)
      SH = .5*SQRT(SMAX*SMIN)
      A     =SQRT( SM - SH )
      B     =SQRT( SM + SH )
      TMP=A*A+B*B
      TMP1=TMP-SF(2)
      TMP2=2.*A*B
      TMP3=TMP1/TMP2
      TMP4=SQRT((TMP2*TMP2-TMP1*TMP1)/TMP2
      U= A*TMP3
      W=A*TMP4
      TMP1=TMP-SF(1)
      TMP6=TMP1/TMP2
      TMP7=((TMP4-SQRT(1.-TMP6*TMP6))/(TMP6-TMP3))
      ST0=TMP-SF(3)
      ST1=ST0-TMP2*TMP3
      ST2=-2.*TMP2*TMP4
      ST3=ST0+TMP2*TMP3
      ST4=2.*RL(3)*(A*A-B*B-SF(3))
      SS0=TMP-SF(4)
      SS1=SS0-TMP2*TMP3
      SS2=ST2
```

Figure 63. Fortran IV Computer Program Listing (Sheet 1 of 5)

```
      SS3=SS0+TMP2*TMP3
      SS4=2.*RL(5)*(A*A-B*B-SF(5))
      SR1=TMP7*(ST2/ST1-SS2/SS1)
      SR2=ST3/ST1-SS3/SS1
      SR3=2.*TMP7*(XL(3)-XL(5))
      SR4=-XL(1)*(ST2/ST1-SS2/SS1)
      SR5=(XL(3)*ST2+ST4)/ST1
      SR6=-(XL(5)*SS2+SS4)/SS1
      SR7=-2.*XL(1)*(XL(3)-XL(5))
      SR8=XL(3)*XL(3)-XL(5)*XL(5)
      SR9=RL(3)*RL(3)-RL(5)*RL(5)
      AAA=SR1+SR2
      BBB=SR3+SR4+SR5+SR6
      CCC=SR7+SR8+SR9
      R=(-BBB-SQRT(BBB*BBB-4.*AAA*CCC))/(2.*AAA)
      X=R*TMP7-XL(1)
      DO 9 I   = 1, 5
      XXL = (X + XL(I))
      RRL = R + RL(I)
      DUM=U*RRL-W*XXL+B*(R-RL(I))
      DUM1=(U-B)*XXL+W*RRL
      DUM3=RRL*RRL+XXL*XXL
      S(I)=(DUM*DUM+DUM1*DUM1)/DUM3
    9 DELS(I) = (SF(I) - S(I))/10.
      DO 3 K = 1, 11
      WRITE(3,112)TITLE
      WRITE(3,113)
      DO 2 N = 1, 5
    2 WRITE(3,104)  N, S(N), RL(N), XL(N)
      WRITE(3,105)
      WRITE(3,106)U,W,A,R,X
      DO 20 I=1,20
      B2=B*B
      DO 30 J=1,5
      T1=R-RL(J)
      T2=R+RL(J)
      T4=X+XL(J)
      A1=U*T2-W*T4+B*T1
      A2=U*T4+W*T2-B*T4
      A3=T2*T2+T4*T4
      SI(J)=S(J)*A3
      DL(J)=-A1*A1-A2*A2+S(J)*A3
      RATIO(J) = DL(J)/SI(J)
      FU(J)=2.*(A1*T2 + A2*T4)
      FW(J)=2.*(-A1*T4+A2*T2)
      FB(J)=2.*(A1*T1-A2*T4)
      FR(J)=2.*(A1*(U+B)+A2*W-S(J)*T2)
   30 FX(J)=2.*(-A1*W+A2*(U-B)-S(J)*T4)
      WRITE(3,107)I,U,W,B,R,X,(RATIO(J),J=1,5)
      IF(ABS(DL(1)/SI(1)) .GT. 1.E-10)GO TO 12
      IF(ABS(DL(2)/SI(2)) .GT. 1.E-10)GO TO 12
      IF(ABS(DL(3)/SI(3)) .GT. 1.E-10)GO TO 12
      IF(ABS(DL(4)/SI(4)) .GT 1.E-10)GO TO 12
```

Figure 63. Fortran IV Computer Program Listing (Sheet 2 of 5)

```
      IF(ABS(DL(5)/SI(5)) .GT. 1.E-10)GO TO 12
      GO TO 14
   12 CALL INVERT(F,5,6,5)
      U=U+DL(1)
      W=W+DL(2)
      B=B+DL(3)
      R=R+DL(4)
   20 X=X+DL(5)
      GO TO 60
   14 GAMMA = ARGD(W, U)
      A = SQRT(W*W + U*U)
      WRITE(3,109)U,W,B,R,X, A, GAMMA
      WRITE(3,111)
      DO 40 J=1,5
      DUM1=R+RL(J)
      DUM2=X+XL(J)
      A1=DUM1*DUM1+DUM2*DUM2
      A2=R*R-RL(J)*RL(J)-DUM2*DUM2
      A3=(R+R)*DUM2
      DUM1=U+B*A2/A1
      DUM2=W-B*A3/A1
      SIG(J)=DUM1*DUM1+DUM2*DUM2
   40 WRITE(3,108)SIG(J)
      UVL=U
      WVL=W
      BVL=B
      RVL=R
      XVL=X
      S(3)=SF(3)
      S(5)=SF(5)
    3 S(4)=S(4)+DELS(4)
      GO TO 1
   60 DELS4=(S(4)-SIG(4))/10.
      S(4)=SIG(4)+DELS4
      U=UVL
      W=WVL
      B=BVL
      R=RVL
      X=XVL
      DO 70 K=1,11
      WRITE(3,112)TITLE
      WRITE(3,113)
      DO 22 N=1,5
   22 WRITE(3,104)N,S(N),RL(N),XL(N)
      WRITE(3,105)
      WRITE(3,106)U,W,B,R,X
      DO 21 I=1,20
      B2= 2.*B
      DO 31 J=1,5
      T1=R-RL(J)
      T2=R+RL(J)
      T4=X+XL(J)
      A1=U*T2-W*T4+B*T1
```

Figure 63. Fortran IV Computer Program Listing (Sheet 3 of 5)

```
      A2=U*T4+W*T2-B*T4
      A3=T2*T2+T4*T4
      SI(J)=S(J)*A3
      DL(J)=-A1*A1-A2*A2+S(J)*A3
      RATIO(J) = DL(J)/SI(J)
      FU(J)=2.*(A1*T2 + A2*T4)
      FW(J)=2.*(-A1*T4+A2*T2)
      FB(J)=2.*(A1*T1-A2*T4)
      FR(J)=2.*(A1*(U+B)+A2*W-S(J)*T2)
   31 FX(J)=2.*(-A1*W+A2*(U-B)-S(J)*T4)
      WRITE(3,107)I,U,W,B,R,X,(RATIO(J),J=1,5)
      IF(ABS(DL(1)/SI(1)).GT.1.E-10) GO TO 42
      IF(ABS(DL(2)/SI(2)).GT.1.E-10) GO TO 42
      IF(ABS(DL(3)/SI(3)).GT.1.E-10) GO TO 42
      IF(ABS(DL(4)/SI(4)).GT.1.E-10) GO TO 42
      IF(ABS(DL(5)/SI(5)).GT.1.E-10) GO TO 42
      GO TO 44
   42 CALL INVERT(F,5,6,5)
      U=U+DL(1)
      W=W+DL(2)
      B=B+DL(3)
      R=R+DL(4)
   21 X=X+DL(5)
      GO TO 1
   44 GAMMA=ARGD(W,U)
      A = SQRT(W*W + U*U)
      WRITE(3,109)U,W,B,R,X, A, GAMMA
      WRITE(3,111)
      DO 41 J=1,5
      DUM1=R+RL(J)
      DUM2=X+XL(J)
      A1=DUM1*DUM1+DUM2*DUM2
      A2=R*R-RL(J)*RL(J)-DUM2*DUM2
      A3=(R+R)*DUM2
      DUM1=U+B*A2/A1
      DUM2=W-B*A3/A1
      SIG(J)=DUM1*DUM1+DUM2*DUM2
   41 WRITE(3,108)SIG(J)
   70 S(4)=S(4)+DELS4
      GO TO 1
      END
```

Figure 63. Fortran IV Computer Program Listing (Sheet 4 of 5)

```
      SUBROUTINE INVERT(A, L, N, M)
      DIMENSION A(1)
      DO 5 I = 1, L
      MI = M*I - M
      II = MI + I
      IF(A(II).EQ.0.0)A(II)=.1E-10
      A(II) = 1./A(II)
      DO 2 J = 1,L
      IF(J.EQ.I) GO TO 2
      JI = MI + J
      A(JI) =-A(JI)*A(II)
    2 CONTINUE
      DO 3 J = 1, L
      IF(J.EQ.I) GO TO 3
      DO 4 K = 1, N
      IF(K.EQ.I) GO TO 4
      MK = M*K-M
      JK = MK + J
      JI = MI + J
      IK = MK + I
      A(JK) = A(JK) + A(JI)*A(IK)
    4 CONTINUE
    3 CONTINUE
      DO 1 J = 1, N
      IF (J.EQ.I) GO TO 1
      IJ = M*J + I - M
      A(IJ) = A(IJ)*A(II)
    1 CONTINUE
    5 CONTINUE
      RETURN
      END
```

Figure 63. Fortran IV Computer Program Listing (Sheet 5 of 5)

1. EVALUATION OF EFFECTIVE REACTANCE

INPUT DATA

N	SIGMA	RL	XL
1	1.047E-02	0.000E-00	1.939E 01
2	4.467E-03	0.000E-00	-1.000E 10
3	5.888E-03	7.775E-01	5.573E 01
4	5.623E-03	1.382E-00	7.183E 01
5	3.715E-03	2.160E-00	8.795E 01

1. EVALUATION OF EFFECTIVE REACTANCE

NEXT TRIAL

N	SIGMA	RL	XL
1	1.047E-02	0.000E-00	1.939E 01
2	4.467E-03	0.000E-00	-1.000E 10
3	5.836E-03	7.775E-01	5.573E 01
4	4.361E-03	1.382E-00	7.183E 01
5	3.727E-03	2.160E-00	8.795E 01

ESTIMATED ANSWERS

U	W	B	R	X
0.01609	0.01301	0.08164	36.06675	-32.14940

1	1.609E-02	1.301E-02	8.164E-02	3.607E 01	-3.215E 01	-6.525E-12	-4.477E-12	-8.955E-12	-1.540E-11	-1.173E-11

FINAL ANSWERS

U	W	B	R	X	A	GAMMA
0.01608547	0.01300934	0.08164149	36.06675077	-32.14939789	0.02068780	38.96468265

SIGMAS FROM FINAL ANS AS CHECK

SIGMA

1.0478E-02
4.4668E-03
5.8358E-03
4.3613E-03
3.7270E-03

1. EVALUATION OF EFFECTIVE REACTANCE

NEXT TRIAL

N	SIGMA	RL	XL
1	1.047E-02	0.000E-00	1.939E 01
2	4.467E-03	0.000E-00	-1.000E 10
3	5.888E-03	7.775E-01	5.573E 01
4	4.498E-03	1.382E-00	7.183E 01
5	3.715E-03	2.160E-00	8.795E 01

ESTIMATED ANSWERS

U	W	B	R	X
0.01609	0.01301	0.08164	36.06675	-32.14940

1	1.609E-02	1.301E-02	8.164E-02	3.607E 01	-3.215E 01	-6.525E-12	-4.477E-12	8.935E-03	2.812E-02	-3.131E-03
2	1.534E-02	1.609E-02	8.028E-02	5.352E 01	-2.565E 01	5.150E-02	-2.215E-03	2.296E-02	1.149E-02	8.521E-03
3	1.655E-02	1.607E-02	8.142E-02	5.038E 01	-2.564E 01	5.346E-03	-1.224E-06	4.367E-03	3.368E-03	2.469E-03
4	1.669E-02	1.610E-02	8.156E-02	5.028E 01	-2.564E 01	1.278E-05	-1.029E-07	1.282E-05	1.091E-05	8.520E-06
5	1.669E-02	1.610E-02	8.156E-02	5.028E 01	-2.564E 01	3.720E-12	-2.239E-12	4.835E-12	4.640E-12	-4.058E-12

FINAL ANSWERS

U	W	B	R	X	A	GAMMA
0.01668966	0.01609577	0.08155693	50.28210113	-25.63880378	0.07318661	43.86222961

SIGMAS FROM FINAL ANS AS CHECK

SIGMA

1.0471E-02
4.4668E-03
5.8884E-03
4.4875E-03
3.7154E-03

Figure 64. Computer Results (Sheet 1 of 4)

1. EVALUATION OF EFFECTIVE REACTANCE

NEXT TRIAL

N	SIGMA	RL	XL
1	1.047E-02	0.000E-00	1.939E 01
2	4.467E-03	0.000E-00	-1.000E 10
3	5.884E-03	7.775E-01	5.573E 01
4	4.614E-03	1.382E-00	7.183E 01
5	3.715E-03	2.160E-00	8.795E 01

ESTIMATED ANSWERS

U	W	B	R	X
0.01669	0.01610	0.08156	50.28210	-25.63880

1	1.669E-02	1.610E-02	8.156E-02	5.028E 01	-2.564E 01	3.720E-12	-2.239E-12	4.835E-12	2.735E-02	-4.058E-12
2	2.495E-02	3.235E-02	8.578E-02	1.168E 02	1.518E 01	8.327E-02	-6.278E-02	-1.338E-02	-3.554E-02	-3.734E-02
3	2.859E-02	2.881E-02	8.900E-02	9.115E 01	1.541E 01	5.018E-02	-2.845E-03	3.141E-02	2.506E-02	2.050E-02
4	3.054E-02	2.897E-02	9.077E-02	8.762E 01	1.545E 01	3.970E-03	-1.374E-05	3.709E-03	3.903E-03	3.235E-03
5	3.067E-02	2.899E-02	9.089E-02	8.755E 01	1.545E 01	2.520E-06	-3.907E-08	2.371E-06	2.214E-06	1.995E-06
6	3.067E-02	2.899E-02	9.089E-02	8.755E 01	1.545E 01	2.151E-12	4.477E-12	2.639E-12	4.188E-12	-1.436E-12

FINAL ANSWERS

U	W	B	R	X	A	GAMMA
0.0306679R	0.0289R648	0.0908R941	87.54768280	15.4526?427	0.04219883	43.38540643

SIGMAS FROM FINAL ANS AS CHECK

SIGMA

1.0471E-02
4.466RE-03
5.88A4E-03
4.6137E-03
3.7154E-03

1. EVALUATION OF EFFECTIVE REACTANCE

NEXT TRIAL

N	SIGMA	RL	XL
1	1.047E-02	0.000E-00	1.939E 01
2	4.467E-03	0.000E-00	-1.000E 10
3	5.884E-03	7.775E-01	5.573E 01
4	4.740E-03	1.382E-00	7.183E 01
5	3.715E-03	2.160E-00	8.795E 01

ESTIMATED ANSWERS

U	W	B	R	X
0.03067	0.02899	0.09084	87.54768	15.45270

1	3.067E-02	2.899E-02	9.089E-02	8.755E 01	1.545E 01	2.151E-12	4.477E-12	2.639E-12	2.663E-02	-1.436E-12
2	-1.216E-02	1.420E-03	5.435E-02	3.535E 01	-9.198E 01	5.383E-01	-2.095E-01	3.721E-01	4.637E-01	6.203E-01
3	-1.523E-01	-7.238E-02	-8.373E-02	-1.721E 02	-9.619E 01	-3.150E-00	-1.225E-00	-8.025E-00	-1.105E 01	-1.532E 01
4	-1.784E-01	-3.701E-02	-1.124E-01	-5.293E 01	-8.503E 01	-1.790E-00	-2.816E-01	-9.358E-00	-1.593E 01	-2.385E 01
5	-5.120E-01	-3.166E-02	-4.525E-01	4.970E 01	-9.284E 01	-5.901E 01	-1.595E-02	-1.390E 02	-1.84AE 02	-2.39AE 02
6	-9.455E-01	-1.061E-02	-8.759E-01	-3.826E 01	-1.155E 02	-4.349E 01	-1.244E-01	-1.684E 02	-3.177E 02	-6.366E 02
7	-3.757E-00	-1.038E-02	-3.691E-00	1.019E 02	-7.936E 01	-3.339E 03	-3.470E-03	-8.815E 03	-1.133E 04	-1.422E 04
8	-1.117E 01	-6.872E-03	-1.111E 01	-1.522E 02	-2.620E 02	-1.33?E 04	-5.915E-04	-2.982E 04	-4.118E 04	-5.861E 04
9	3.752E 01	-2.878E-03	9.759E 01	-1.5??E 03	7.171E 02	-2.?74E 05	-?.316E-04	-5.197E 06	-6.407E 06	-8.112E 06
10	-1.678E 03	-1.759E-03	-1.478E 03	-3.233E 04	-6.899E 04	-2.436E 08	-2.382E-02	-4.332E 08	-5.483E 08	-6.871E 08
11	4.391E 04	-4.553E-03	4.391E 04	-4.060E 05	3.669E 05	-6.100E 11	-1.123E 04	-1.085E 12	-1.344E 12	-1.719E 12
12	3.?87E 04	-8.550E-04	3.887E 04	-4.954E 05	-7.646E 05	-1.707E 11	-3.327E 03	-3.036E 11	-3.771E 11	-4.811E 11
13	-2.349E 02	1.286E-03	-2.391E 02	-7.461E 05	1.817E 06	-3.155E 06	-3.439E-00	-5.610E 06	-6.969E 06	-8.890E 06
14	-8.609E 01	-7.981E-04	-9.600E 01	-4.196E 05	7.231E 05	-1.981E 06	-5.582E-01	-3.523E 06	-4.377E 06	-5.583E 06
15	2.676E 02	-2.571E-03	2.676E 02	-3.001E 06	-2.578E 06	-9.472E 06	-3.687E-00	-1.684E 07	-2.093E 07	-2.670E 07
16	1.907E 02	-2.891E-03	1.908E 02	-1.744E 06	-1.009E 06	-1.041E 07	-3.933E-01	-1.852E 07	-2.300E 07	-2.935E 07
17	-3.411E 01	-3.517E-03	-3.405E 01	-2.328E 06	1.042E 06	-2.134E 05	3.771E-04	-3.795E 05	-4.714E 05	-6.014E 05
18	4.612E 01	-4.234E-03	4.614E 01	-4.356E 06	-5.113E 06	-5.320E 05	-1.501E-00	-1.053E 06	-1.308E 06	-1.668E 06
19	6.178E-00	-4.149E-03	6.234E-00	-1.141E 07	9.260E 06	-8.878E 03	-3.608E-04	-1.579E 04	-1.961E 04	-2.502E 04
20	-9.261E-00	-2.532E-04	-9.194E-00	-3.405E 07	-1.030E 07	-1.815E 04	-8.072E-01	-3.227E 04	-4.008E 04	-5.115E 04

Figure 64. Computer Results (Sheet 2 of 4)

1. EVALUATION OF EFFECTIVE REACTANCE

NEXT TRIAL

N	SIGMA	RL	XL
1	1.047E-02	0.000E-00	1.939E 01
2	4.467E-03	0.000E-00	-1.000E 10
3	5.888E-03	7.775E-01	5.573E 01
4	4.626E-03	1.382E-00	7.183E 01
5	3.715E-03	2.160E-00	8.795E 01

ESTIMATED ANSWERS

U	W	B	R	X
0.03067	0.02899	0.09089	87.54768	15.45270

1	3.067E-02	2.899E-02	9.089E-02	8.755E 01	1.545E 01	2.151E-12	4.477E-12	2.639E-12	2.728E-03	-1.436E-12
2	3.800E-02	3.340E-02	9.610E-02	9.590E 01	3.264E 01	7.340E-03	-5.361E-03	1.047E-03	6.611E-05	2.450E-04
3	3.863E-02	3.316E-02	9.665E-02	9.402E 01	3.266E 01	5.204E-04	-1.345E-05	4.608E-04	4.369E-04	4.128E-04
4	3.865E-02	3.316E-02	9.667E-02	9.400E 01	3.266E 01	[illegible]	-3.448E-10	1.482E-07	1.447E-07	1.386E-07
5	3.865E-02	3.316E-02	9.667E-02	9.400E 01	3.266E 01	-8.[illegible]	[illegible]	-6.067E-12	-4.320E-12	-1.357E-11

FINAL ANSWERS

U	W	B	R	X	A	GAMMA
0.03864766	0.03316201	0.09667452	94.00247966	32.65523068	0.05092505	40.63157773

SIGMAS FROM FINAL ANS AS CHECK

SIGMA

1.0471E-02
4.4668E-03
5.8884E-03
4.6264E-03
3.7154E-03

1. EVALUATION OF EFFECTIVE REACTANCE

NEXT TRIAL

N	SIGMA	RL	XL
1	1.047E-02	0.000E-00	1.939E 01
2	4.467E-03	0.000E-00	-1.000E 10
3	5.888E-03	7.775E-01	5.573E 01
4	4.639E-03	1.382E-00	7.183E 01
5	3.715E-03	2.160E-00	8.795E 01

ESTIMATED ANSWERS

U	W	B	R	X
0.03865	0.03316	0.09667	94.00248	32.65523

1	3.865E-02	3.316E-02	9.667E-02	9.400E 01	3.266E 01	-8.272E-12	0.000E-00	-6.067E-12	2.721E-03	-1.357E-11
2	5.440E-02	4.036E-02	1.083E-01	1.025E 02	6.389E 01	2.927E-02	-1.540E-02	1.646E-02	1.446E-02	1.425E-02
3	5.730E-02	3.987E-02	1.109E-01	9.744E 01	6.393E 01	5.236E-03	-1.104E-05	5.115E-03	5.055E-03	4.963E-03
4	5.754E-02	3.987E-02	1.112E-01	9.731E 01	6.393E 01	7.123E-06	-2.407E-08	6.874E-06	6.638E-06	6.288E-06
5	5.754E-02	3.987E-02	1.112E-01	9.731E 01	6.393E 01	-5.813E-12	6.716E-12	2.128E-11	7.652E-12	8.166E-12

FINAL ANSWERS

U	W	B	R	X	A	GAMMA
0.05754391	0.03987203	0.11118212	97.30573789	63.93325002	0.07000772	34.71798964

SIGMAS FROM FINAL ANS AS CHECK

SIGMA

1.0471E-02
4.4668E-03
5.8884E-03
4.6390E-03
3.7154E-03

Figure 64. Computer Results (Sheet 3 of 4)

```
I. EVALUATION OF EFFECTIVE REACTANCE

                NEXT TRIAL

          N          SIGMA          RL          XL

          1      1.047E-02     0.000E-00     1.939E 01
          2      4.467E-03     0.000E-00    -1.000E 10
          3      5.888E-03     7.775E-01     5.573E 01
          4      4.652E-03     1.382E-00     7.183E 01
          5      3.715E-03     2.160E-00     8.795E 01

                ESTIMATED ANSWERS
             U          W          A          R          X
       0.05754    0.04987    0.11118   97.80574   63.93325

 1  5.756E-02  4.987E-02  1.112E-01  9.731E 01  6.393E 01   -5.819E-12  6.716E-12  2.128E-11  2.713E-03  8.166E-12
 2  1.118E-01  5.687E-02  1.543E-01  9.318E 01  1.383E 02    2.520E-01 -7.815E-02  2.380E-01  2.381E-01  2.604E-01
 3  1.582E-01  5.353E-02  1.984E-01  6.367E 01  1.382E 02    2.985E-01 -1.667E-03  3.090E-01  3.175E-01  3.142E-01
 4  1.981E-01  5.361E-02  2.380E-01  5.719E 01  1.378E 02    3.427E-02 -1.164E-05  3.257E-02  3.116E-02  2.921E-02
 5  2.043E-01  5.407E-02  2.436E-01  5.659E 01  1.381E 02    4.453E-04 -1.278E-04  4.412E-04  4.303E-04  4.112E-04
 6  2.043E-01  5.407E-02  2.436E-01  5.658E 01  1.381E 02    1.378E-07 -2.759E-08  1.356E-07  1.331E-07  1.269E-07
 7  2.043E-01  5.407E-02  2.436E-01  5.658E 01  1.381E 02    6.823E-12 -2.239E-12 -8.315E-12  4.536E-12 -1.681E-11

                FINAL ANSWERS

       U                  W                  B                  R                  X                  A              GAMMA

0.20434604         0.05406824         0.24363294        56.58129259       138.07087255         0.21137804        14.82035951
 SIGMA, FROM FINAL ANS AS CHECK

                SIGMA

                1.047E-02
                4.466E-03
                5.888E-03
                4.652E-03
                3.715E-03

I. EVALUATION OF EFFECTIVE REACTANCE

                NEXT TRIAL

          N          SIGMA          RL          XL

          1      1.047E-02     0.000E-00     1.939E 01
          2      4.467E-03     0.000E-00    -1.000E 10
          3      5.888E-03     7.775E-01     5.573E 01
          4      4.664E-03     1.382E-00     7.183E 01
          5      3.715E-03     2.160E-00     8.795E 01

                ESTIMATED ANSWERS
             U          W          A          R          X
       0.20435    0.05407    0.24363   56.58129 138.07087

 1  2.043E-1   5.407E-02  2.436E-01  5.659E 01  1.381E 02    6.823E-12 -2.239E-12 -8.315E-12  2.706E-03 -1.681E-11
 2  2.706E-00  1.305E-01  2.660E-00 -4.596E 02  5.065E 02   -1.246E 03 -3.787E-00 -2.064E 03 -2.525E 03 -3.072E 03
 3 -1.445E 01  8.710E-02 -1.444E 01 -3.256E 03 -2.864E 03   -4.557E 04 -8.235E-01 -8.195E 04 -1.040E 05 -1.312E 05
 4  8.225E 02  5.310E-02  8.526E 02 -1.476E 05  2.161E 05   -1.263E 08 -2.179E-01 -2.245E 08 -2.836E 08 -3.559E 08
 5  7.819E 02  2.857E-02  7.819E 02 -1.150E 05  7.670E 04   -1.616E 08 -1.249E-02 -2.476E 08 -3.627E 08 -4.553E 08
 6  5.128E 03  1.627E-02  5.127E 03  5.818E 05  9.763E 05   -2.640E 09 -8.611E 01 -4.696E 09 -5.926E 09 -7.443E 09
 7  5.047E 03  9.865E-03  5.047E 03  1.000E 05  5.496E 05   -2.234E 09 -2.148E 01 -3.972E 09 -5.014E 09 -6.294E 09
 8  4.267E 03  7.134E-03  4.267E 03  1.964E 05  3.214E 05   -1.891E 09 -4.529E-00 -3.362E 09 -4.243E 09 -5.327E 09
 9  3.159E 03  6.643E-03  3.157E 03 -3.496E 04  3.519E 05   -1.902E 08 -1.806E-01 -3.381E 08 -4.268E 08 -5.357E 08
10  3.476E 03  6.036E-03  3.475E 03 -1.598E 04  1.553E 05   -2.209E 08 -1.505E-01 -3.927E 08 -4.957E 08 -6.222E 08
11  5.894E 04  5.562E-03  5.074E 04  8.346E 04  6.506E 04   -6.143E 11 -1.696E 02 -1.092E 12 -1.378E 12 -1.730E 12
12  3.531E 04  4.165E-03  3.531E 04  6.751E 04  8.822E 05   -2.773E 09 -5.132E 01 -4.930E 09 -6.224E 09 -7.813E 09
13 -5.338E 03  3.671E-03 -5.338E 03  1.115E 05  4.653E 05   -5.907E 08 -2.642E-00 -1.050E 09 -1.326E 09 -1.664E 09
14 -3.225E 03  2.701E-03 -3.955E 03  8.460E 04  1.668E 05   -1.223E 09 -1.147E-00 -2.176E 09 -2.746E 09 -3.446E 09
15 -3.  5E 03  1.925E-03 -3.565E 03  5.064E 04  1.538E 04   -3.262E 09 -2.466E-01 -5.797E 09 -7.316E 09 -9.181E 09
16 -2.633E 03  1.432E-03 -2.633E 03  3.456E 04 -1.367E 05   -1.952E 08 -9.700E-02 -3.473E 08 -4.384E 08 -5.506E 08
17 -2.625E 03  4.769E-04 -2.625E 03 -8.356E 04 -7.868E 04   -1.488E 10 -6.144E-00 -3.359E 10 -4.241E 10 -5.325E 10
18 -3.711E 04  5.415E-04 -3.711E 04  1.459E 05 -8.548E 05   -2.625E 10 -4.641E 02 -4.668E 10 -5.894E 10 -7.399E 10
19 -2.  E 04  2.511E-04 -2.677E 04  5.961E 05 -4.491E 05   -1.048E 12 -1.695E 04 -1.499E 12 -2.534E 12 -3.211E 12
20  1.  7E 05 -5.660E-01  1.477E 05 -8.472E 05  5.520E 04   -3.163E 07 -2.762E 05 -5.625E 07  7.103E 07  9.435E 07
```

Figure 64. Computer Results (Sheet 4 of 4)

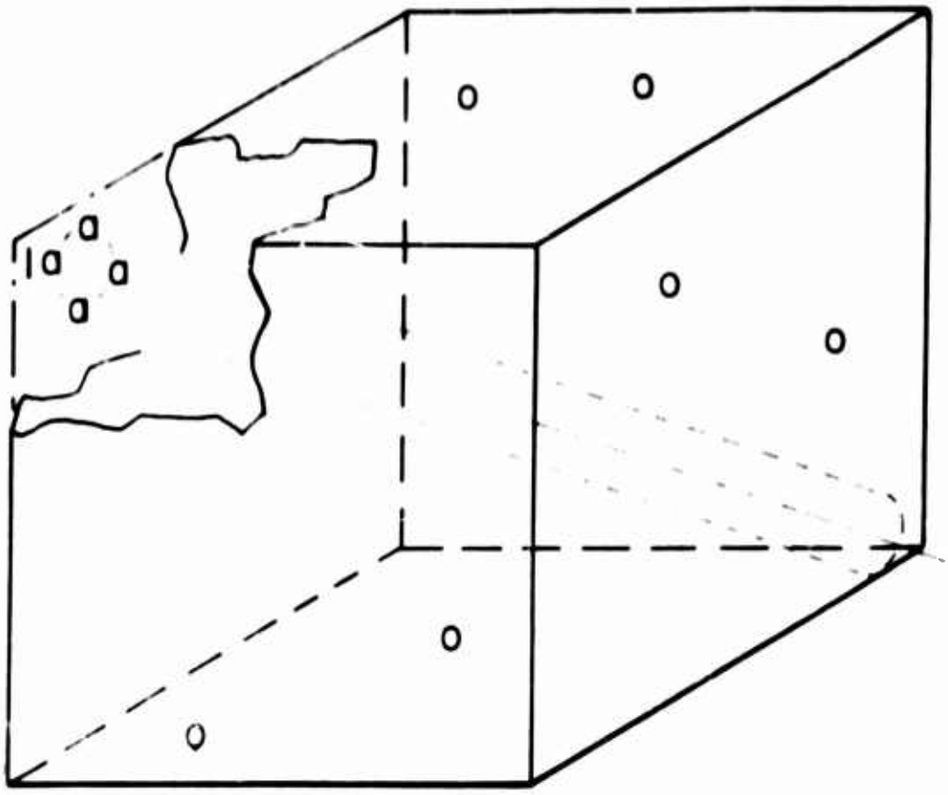

Figure 65. Three-Dimensional Matrix

APPENDIX I

ROTOFLEX TESTING APPARATUS AND PROCEDURE

A. APPARATUS

The rotoflex test apparatus (Figure 66) is a device designed and fabricated by Goodyear Aerospace for the purpose of providing continuous flexing of samples of materials under a controlled temperature environment. Two jaws mounted one above the other are used to hold the test specimen. The bottom jaw is fixed in a stationary position,and the upper jaw is mounted to permit rotation through an arc of up to 270 degrees in either the clockwise or counterclockwise direction through a plane perpendicular to the centerlines of the two jaws. Figure 67 shows a sample in the test apparatus with the jaws in the extreme positions. Rotation or oscillation of the upper jaw is controlled in both frequency and amplitude by a regulated air motor and limit switches.

B. PROCEDURE

A series of nine rotoflex tests was conducted using identical samples of material and coating on each sample. Three of the samples were tested in a temperature environment of -25^{o}C, three at 23^{o}C, and three at 100^{o}C. Most samples were flexed through 2000 cycles at a rate of 135 cycles per minute. A thorough inspection of the sample was made at the conclusion of each increment of the cyclic period.

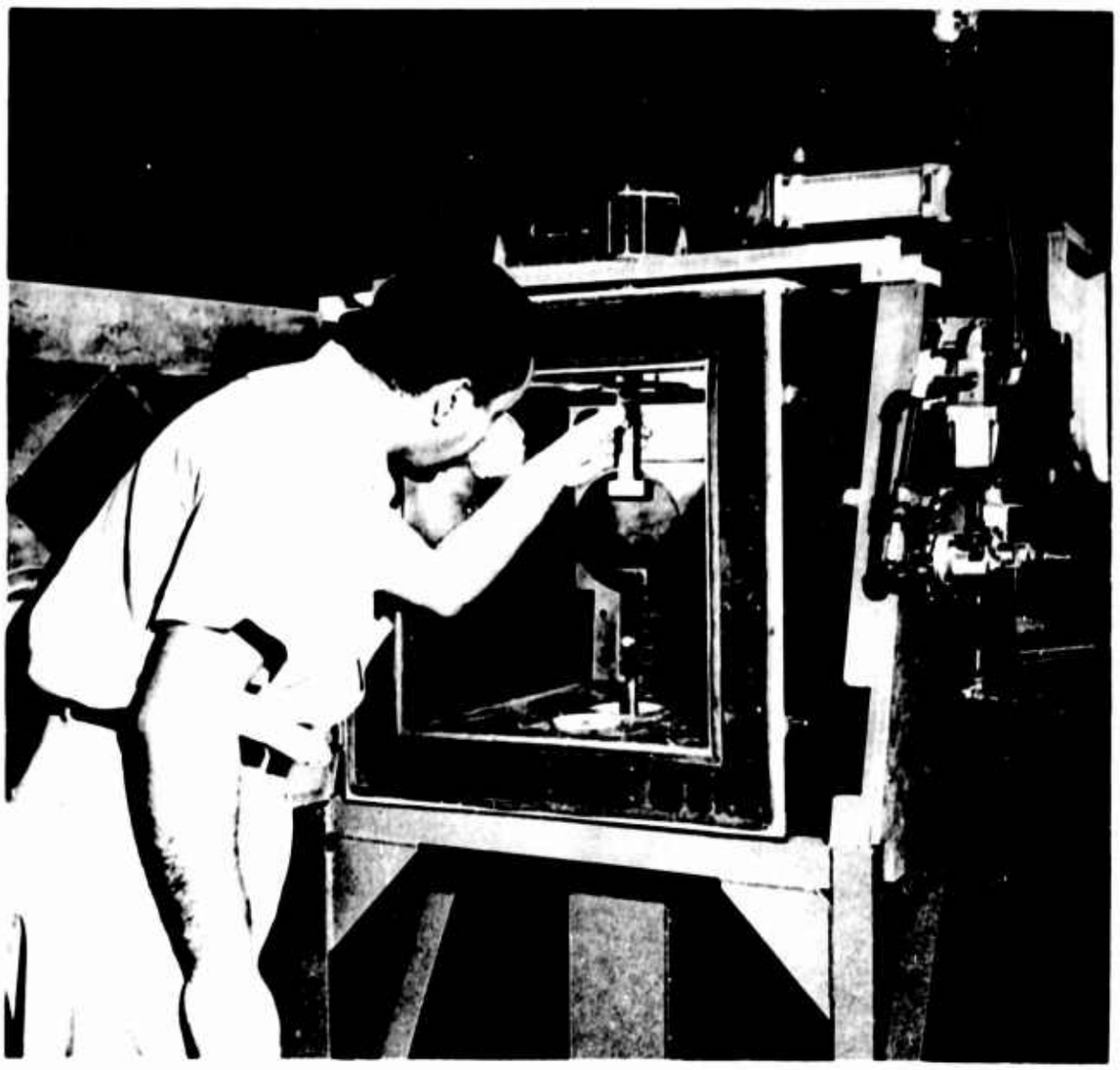

Figure 66. Rotoflex Test Apparatus

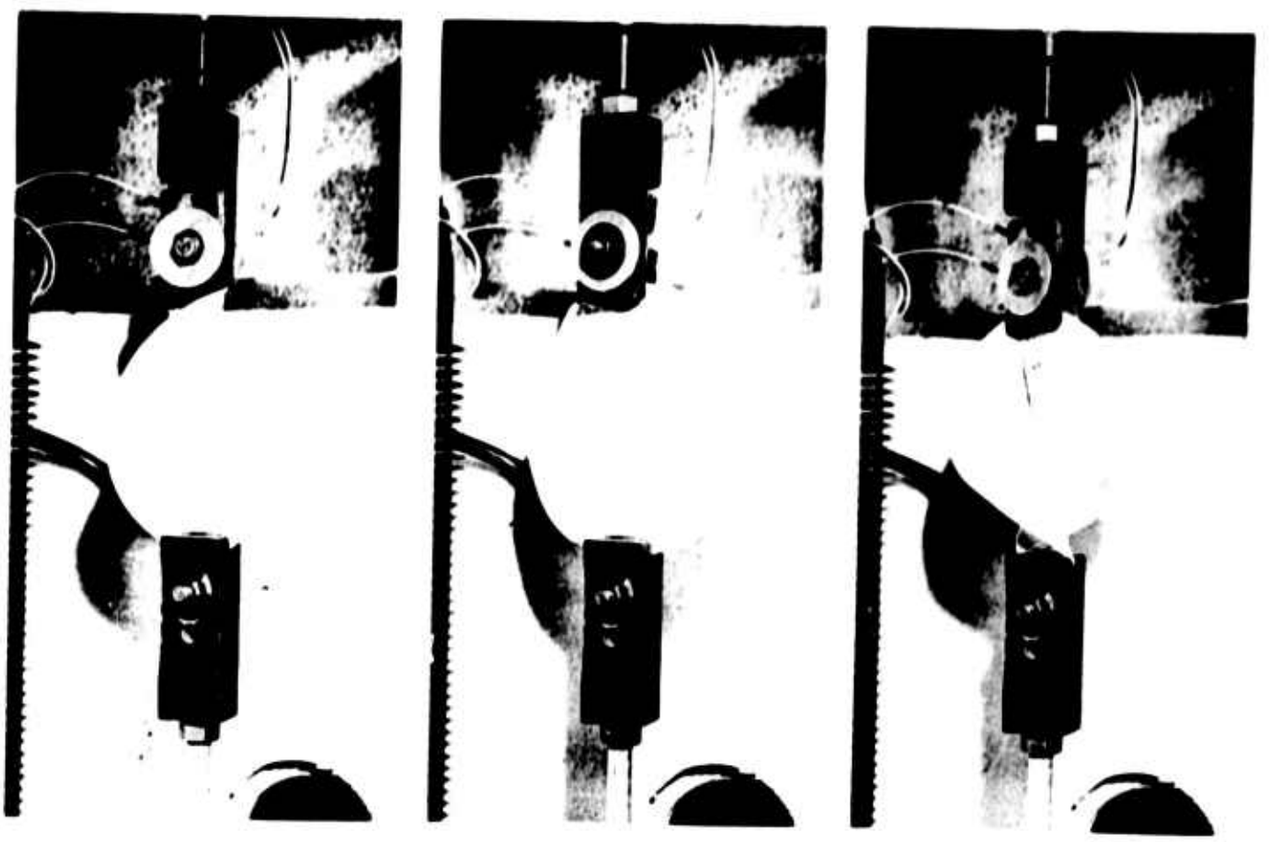

Figure 67. Rotoflex Sample in Test Apparatus

APPENDIX II

ULTRAVIOLET IRRADIATION OF SAMPLES

A. IRRADIATION APPARATUS

1. General

The apparatus used in the irradiation experiments is illustrated in Figure 68. The apparatus comprised a high-vacuum system, an ultraviolet source and detector assembly, a sample holder, and associated controls and instrumentation. The components are described in the following paragraphs.

2. Vacuum System

A Consolidated Vacuum Corporation oil-diffusion pumped system, Type LC 1-18B, was used to obtain the required test pressure. The base plate of this system was provided with feed-through into the bell jar for thermcouples and fluid connections to the sample holder. The bell jar was a stainless steel unit that was provided with a 4-inch-diameter quartz probe extending from the top through the center point of the jar. This unit was specially designed to support the AH-6 lamp assembly and permit the lamp to be changed without breaking vacuum on the samples.

3. Ultraviolet Source

A General Electric Company water-cooled mercury arc lamp, Type A-H6, was used for the ultraviolet radiation source. The overall length of the lamp is 3-1/4 inches long and 3/16 inch in diameter. The actual source of light is an enclosed arc approximately 1 inch long by 1/16 inch in diameter.

Because of the lamp geometry and the desire to uniformly irradiate as many samples as possible during each test run, the lamp is mounted in a vertical position at the center of the bell jar base plate with the center of the arc located at the same level as the midpoint of the samples. The lamp is operated in a General Electric Company A154G11 water jacket equipped with quartz velocity tube and jacket tube assembly supplied by the George W. Gates Company.

A refrigerated, recirculating, cooling water system, shown in Figure 69, was used to furnish the required water flow to the lamp. The water is recirculated through a 25-gallon tin-coated storage tank using a stainless steel pump. All plumbing is 3/8-inch stainless steel with stainless steel fittings and valves throughout. The unit is equipped with a continuous-bypass-type water purification system consisting of a submicron filter and inorganic and organic removal cartridges. This system, designed and constructed by GAC for use with the A-H6 lamp, has eliminated most of the lamp operating problems having to do with deposits forming on the lamp and inside of the water jacket.

The total ultraviolet incident on the samples, placed at a distance of five inches from the lamp, is approximately five times the intensity of solar ultraviolet radiation of zero air-mass. A comparison of the spectral distribution of the A-H6 lamp with that of the sun was made by Schmitt and Hirt (Reference 23) and is presented in Table 26.

4. Sample Holder

A special water-cooled holder assembly was designed and fabricated to

position and control sample temperature during ultraviolet irradiation. Through the use of this fixture, it was possible to maintain the nine sample disks at 70 (±5)°F through the exposure period.

Baffle plates were installed between each group of three samples and above the diffusion pump port to reduce possible migration of degradation products from one group to another.

Table 26. Comparison of Spectral Energy Distribution of A-H6 Lamp and the Solar Spectral Energy Distribution*

Wave Length Region (mμ)	Solar Energy (mw/cm^2)	A-H6 Lamp (mw/cm^2)
200 - 210	0.01	0.02
210 - 220	0.02	0.06
220 - 230	0.03	0.15
230 - 240	0.05	0.50
240 - 250	0.06	1.60
250 - 260	0.10	1.61
260 - 270	0.20	2.02
270 - 280	0.24	3.84
280 - 290	0.34	4.19
290 - 300	0.63	6.05
300 - 310	0.63	7.12
310 - 320	0.76	9.56
320 - 330	1.04	3.79
330 - 340	1.05	3.34
340 - 350	1.13	1.86
350 - 360	1.14	1.41
360 - 370	1.20	9.64
370 - 380	1.26	4.37
380 - 390	1.15	2.29
390 - 400	1.23	1.97
	12.27	65.41

*See Reference 23.

5. Ultraviolet Detector

The detector assembly consisted of an RCA Type 935 phototube and a Corning Glass Company Filter No. 9863, ultraviolet-transmitting, visible absorbing filter. The filter and phototube were mounted in a small metal enclosure that was fitted with a small aperture sized to provide optimum detector sensitivity. The detector was secured to the sample holder so that the aperture position relative to the source was identical with that of the samples. A shield was placed in front of the detector assembly to confine exposure to a small area around the aperture. An integrated 50-volt d-c power supply and vacuum tube microammeter were designed to power and monitor the detector.

B. TEST PROCEDURE

1. Ultraviolet Detector Calibration

To use the detector for ultraviolet measurements, the following must be known:

(1) The relative spectral response of the detector.

(2) The sensitivity of the detector.

(3) The spectral distribution of the source.

The curve representing the radiation response of the filter photometer is shown in Figure 70. The instrument has a peak sensitivity of 340 millimicrons (mμ) and falls off on both sides to zero at 220 and 440 mμ. Here every ordinate corresponds to equal amounts of energy. The curve shown in Figure 70 was obtained by multiplying the relative response of the phototube (Reference 24) by the

Table 27. Tabulated Phototube and Filter Transmission Data

Wave Length (mμ)	P*	T**	S_λ*** (PxT)
200	10	0	0
220	40	0	0
240	74	0.22	16.3
260	76	0.67	51.0
280	80	0.87	69.6
300	90	0.97	87.3
320	97	1.00	97.0
340	100	0.99	99.0
360	97	0.95	92.1
380	92	0.78	71.8
400	87	0.23	20.0
420	82	0.11	9.0
440	75	0	0
460	68	0	0
480	60	0	0
500	54	0	0
520	46	0	0
540	37	0	0
560	28	0	0
580	16	0	0
600	9	0	0
620	6	0	0
640	3	0	0
660	2	0	0
680	1	0.19	0.19
700	0	0.44	0

*P = relative response of RCA Type 935 phototube.
**T = relative transmission of Corning Glass No. 9863 filter.
***S_λ = relative response of filter photometer.

relative transmission of the filter (Reference 25). A tabulation of this data is presented in Table 27.

The sensitivity of the detector is determined by exposing the instrument to a source of known radiance. A diagram of this experimental setup is shown in

Figure 71. The filament of the tungsten lamp (GE Type 30A/T24/3) and the aperture of the detector assembly were placed at the radius of curvature (60 cm) of the 7.5-cm-diameter front-surface aluminized mirror. The angle between incident and reflected radiation was approximately 10 degrees. This arrangement permitted the focusing of radiation from the lamp filament onto the detector aperture with a minimum distortion of lamp filament image. The instrument reading was then recorded. The instrument sensitivity was determined from the expression:

$$S = \frac{R}{\frac{\rho A}{d^2}\int_{\lambda_1}^{\lambda_2} S_\lambda N_\lambda \, d\lambda} \qquad (18)$$

where

S = instrument sensitivity,

R = instrument reading,

ρ = reflectance of spherical mirror,

A = area of spherical mirror,

d = distance from spherical mirror to detector aperture,

S_λ = spectral sensitivity of the instrument,

N_λ = spectral radiance of tungsten lamp,

$\lambda_1\lambda_2$ = practical wave length limits of the instrument (220 to 440 mμ).

The evaluation of the integral in Equation 18 was performed arithmetically as shown in Table 28. The values of lamp radiance for the wave length bands indicated were obtained from values of spectral radiance of the tungsten lamp reported by the National Bureau of Standards (Reference 26). The values for S were obtained from the curve shown in Figure 70.

Table 28. Tabulated Values for Tungsten Lamp Radiance (N_λ) and Filter Photometer Radiation Response (S_λ)

Wave Length Band (mμ)	N_λ μw/ster - mm^2	S_λ (percent)	$(N_\lambda) \times (S_\lambda)$
245 - 255	0.050	32.2	0.016
255 - 265	0.100	46.0	0.046
265 - 275	0.242	58.0	0.139
275 - 285	0.440	69.0	0.304
285 - 295	0.750	78.0	0.585
295 - 305	1.23	87.3	1.07
305 - 335	8.49	90.0	7.64
335 - 365	25.50	94.0	24.00
365 - 375	15.40	84.0	12.03
375 - 425	166.50	48.0	79.50
425 - 475	435.00	2.5	11.0
	653.702		137.230

The detector was used to measure the total ultraviolet radiant flux from the General Electric Type A-H6 mercury arc lamp. The instrument reading was recorded and converted to a radiant flux value according to the relationship:

$$\phi = R\,(D/S) \tag{19}$$

where

ϕ = total radiant flux from A-H6 lamp,

R = instrument reading,

S = instrument sensitivity as defined in Equation 18,

D = A-H6 mercury lamp spectral energy distribution factor.

The factor D was introduced in Equation 19 to compensate for the difference in spectral energy distribution between the A-H6 lamp and the tungsten lamp. The factor D is expressed mathematically as:

$$D = \frac{\int_{\lambda_1}^{\lambda_2} f_\lambda d\lambda}{\int_{\lambda_1}^{\lambda_2} f_\lambda S_\lambda d\lambda} \qquad (20)$$

where

f_λ = relative spectral energy distribution of A-H6,

S_λ = spectral response of the instrument,

λ_1 = 220 mμ,

λ_2 = 401 mμ.

The evaluations of the integrals in Equation 20 were performed arithmetically as shown in Table 29. The values for f_λ and S_λ were obtained from Reference 27 and Figure 70 respectively.

By substitution in Equation 18,

$$S = \frac{(R = 0.0148)}{\frac{(0.87)(25.5)}{3600} \times 137.2} = 0.0175\ \mu a/\mu w\text{-}mm^2.$$

by substitution in Equation 19,

$$\phi = R\left[\frac{1.26}{0.0175}\right] = 72\ R_{\mu a}\ \mu w/mm^2$$

$$= 7.2\ R_{\mu a}\ mw/cm^2.$$

2. Sample Exposure

The ultraviolet radiation level was recorded on an average interval of 4 hours. The AH-6 lamp was replaced after an average of 80 hours of operation.

Table 29. Tabulated Values for A-H6 Lamp Energy Distribution (f_λ) and Filter Photometer Radiation Response (S_λ)

Wave Length Band (mμ)	f_λ	S_λ (percent)	$(f_\lambda) \times (S_\lambda)$	Wave Length Band (mμ)	f_λ	S_λ (percent)	$(f_\lambda) \times (S_\lambda)$
222 - 223	0.00003	1.2	0.000	270 - 274	0.346	60.6	0.210
223 - 225	0.00020	2.0	0.000	274 - 278	0.414	64.9	0.268
225 - 227	0.00077	3.1	0.000	278 - 282	0.488	69.0	0.337
227 - 229	0.00385	4.5	0.000	282 - 286	0.480	73.0	0.350
229 - 231	0.0132	6.0	0.000	286 - 290	0.576	77.0	0.444
231 - 233	0.0206	7.4	0.001	290 - 294	0.483	80.4	0.388
233 - 234	0.0124	9.3	0.001	294 - 299	1.06	84.9	0.900
234 - 236	0.0310	10.4	0.003	299 - 305	1.16	89.0	1.03
236 - 238	0.108	13.0	0.014	305 - 310	1.76	92.2	1.62
238 - 241	0.128	16.2	0.020	310 - 316	1.73	94.8	1.64
241 - 243	0.143	19.7	0.028	316 - 322	1.17	97.1	1.14
243 - 245	0.153	22.7	0.035	322 - 329	0.76	98.5	0.75
245 - 247	0.212	26.1	0.055	329 - 336	0.94	99.0	0.93
247 - 249	0.274	29.5	0.081	336 - 343	0.656	98.5	0.645
249 - 252	0.236	33.5	0.078	343 - 351	0.526	96.7	0.508
252 - 255	0.095	38.0	0.004	351 - 360	0.481	93.7	0.450
255 - 257	0.00033	41.2	0.000	360 - 369	3.00	89.0	2.67
257 - 260	0.008	44.3	0.004	369 - 379	1.75	79.5	1.39
260 - 263	0.0736	47.7	0.003	379 - 390	0.95	60.5	0.575
263 - 267	0.191	52.0	0.099	390 - 396	0.408	39.0	0.159
267 - 270	0.289	56.5	0.163	396 - 401	0.463	25.5	0.118
					21.593		17.111

$$D = \frac{\Sigma f_\lambda}{\Sigma f_\lambda S_\lambda} = \frac{21.594}{17.111} = 1.262.$$

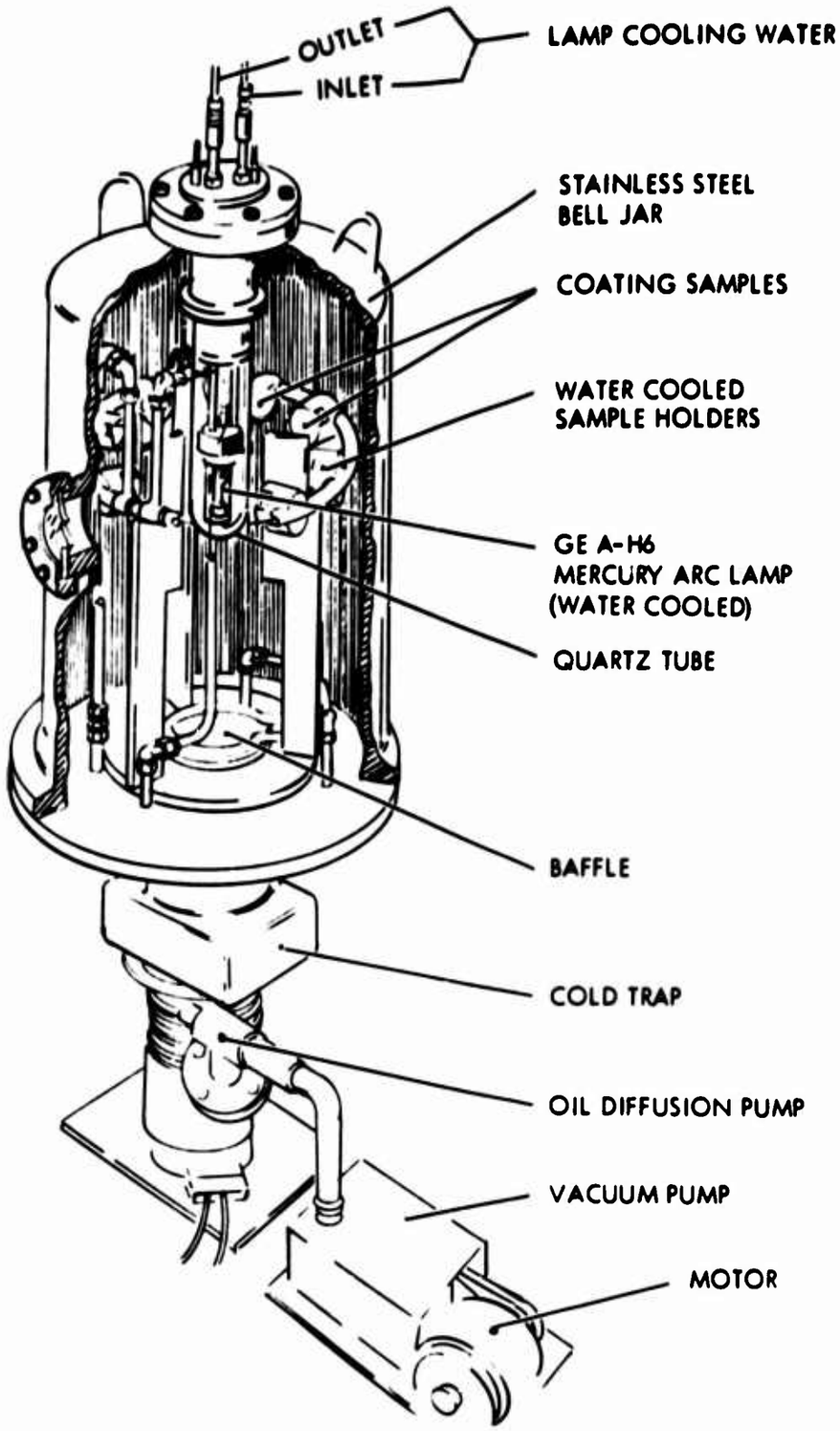

Figure 68. Ultraviolet Irradiation Apparatus

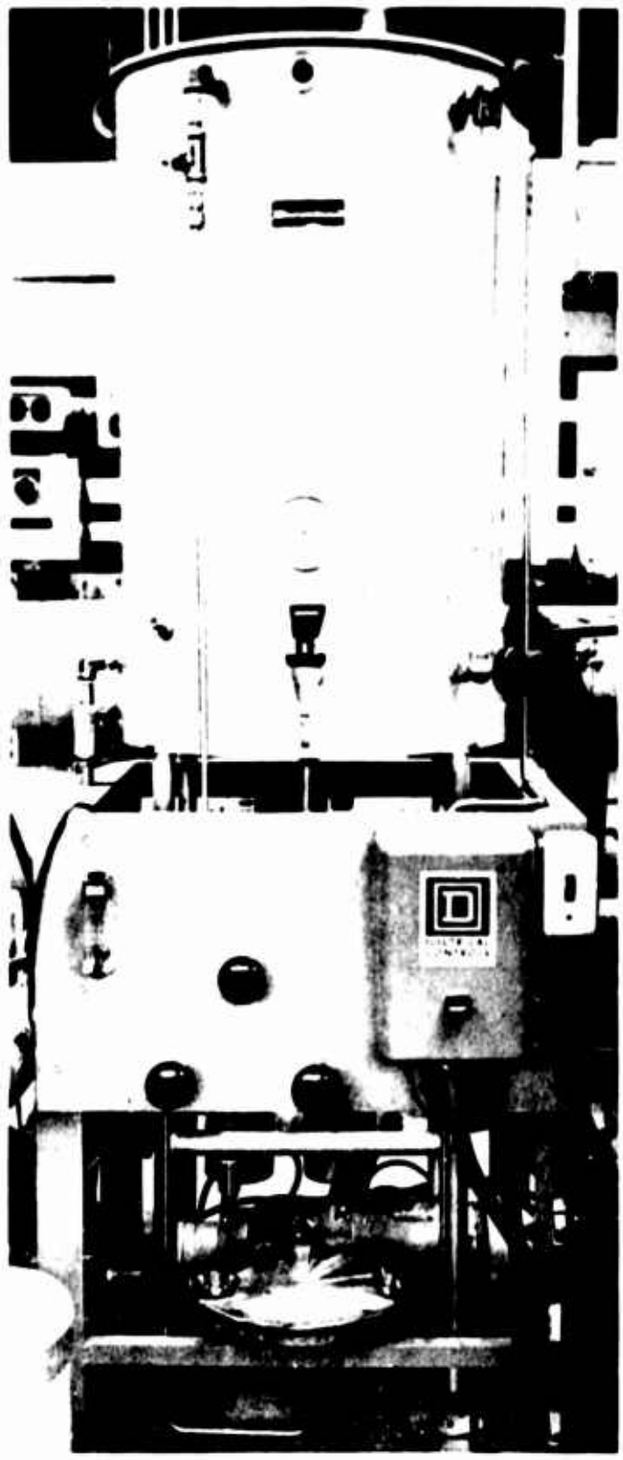

Figure 69. A-H6 Lamp Recirculating Cooling Water System

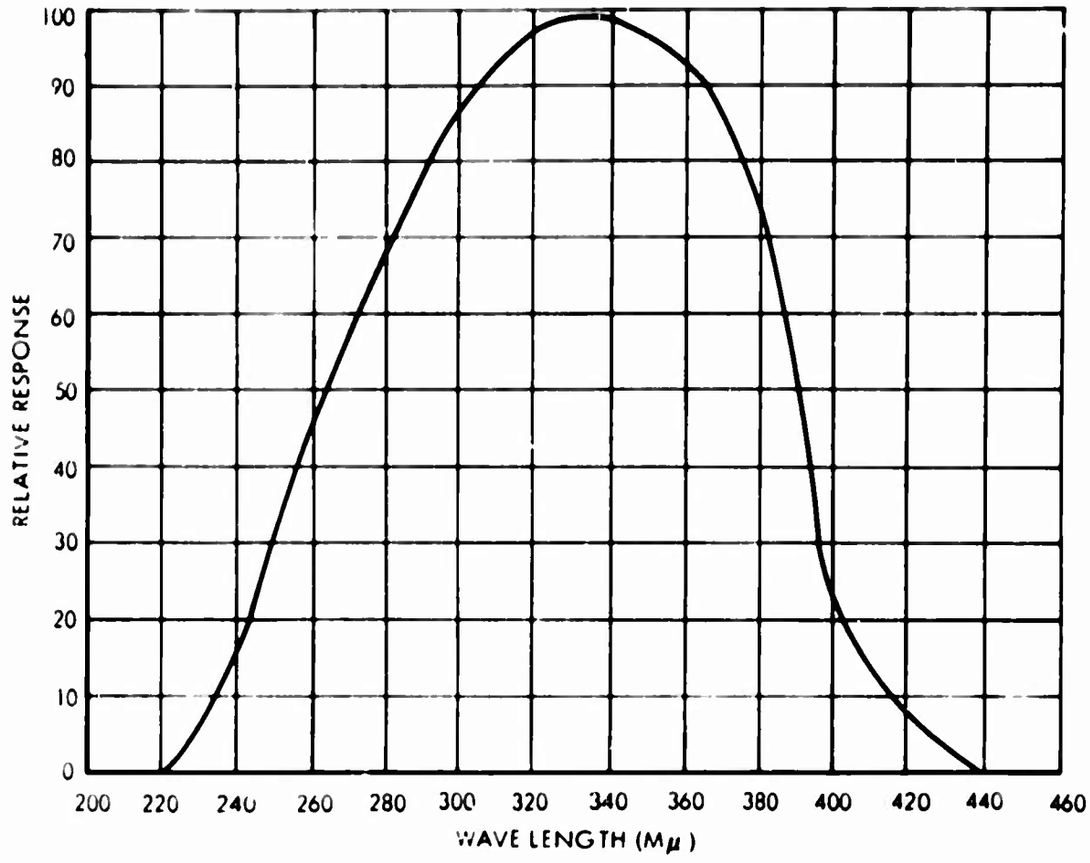

Figure 70. Filter Photometer Radiation Response

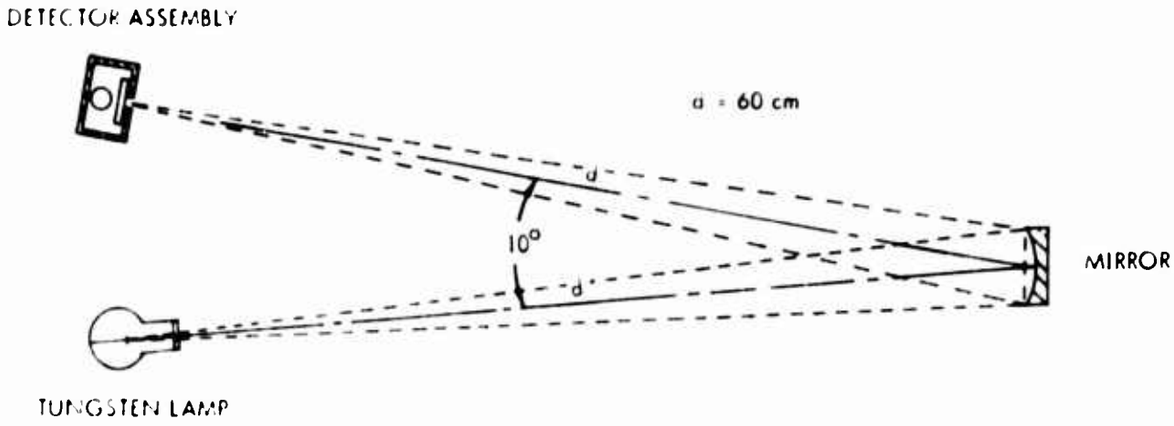

Figure 71. Diagram of Experimental Setup for Determining Filter Photometer Sensitivity

APPENDIX III

SPECTROPHOTOMETRIC MEASUREMENTS

A. APPARATUS

Spectral reflectance measurements are made using an integrated-sphere type of reflectometer.

Actually, the reflectometer is composed of the following four major sub-assemblies:

(1) Integrating sphere

(2) Prism monochromator

(3) Radiation source assembly

(4) Radiation detection assembly

The complete system is shown in Figure 72.

During operation, radiation from the exit slit is projected through apertures in the sphere wall for near normal irradiation of the specimen or reference. The reflected energy is then measured with a detector mounted in the wall of the sphere.

B. ABSOLUTE REFLECTANCE MEASUREMENT

Measured values of reflectance were obtained by comparing the measured reflectance of the specimen to that of a magnesium-oxide reference.

The absolute reflectance of each of the nine specimens was then calculated from the following relationship:

$$\rho_s = \rho_R \frac{B_s}{B_r}$$

where

ρ_s = absolute reflectance of the specimen,

ρ_R = absolute reflectance of the reference,

B_s = apparent brightness of energy reflected by the specimen,

B_r = apparent brightness of energy reflected by the reference.

The total error in reflectance measurements is estimated to be ±5 percent.

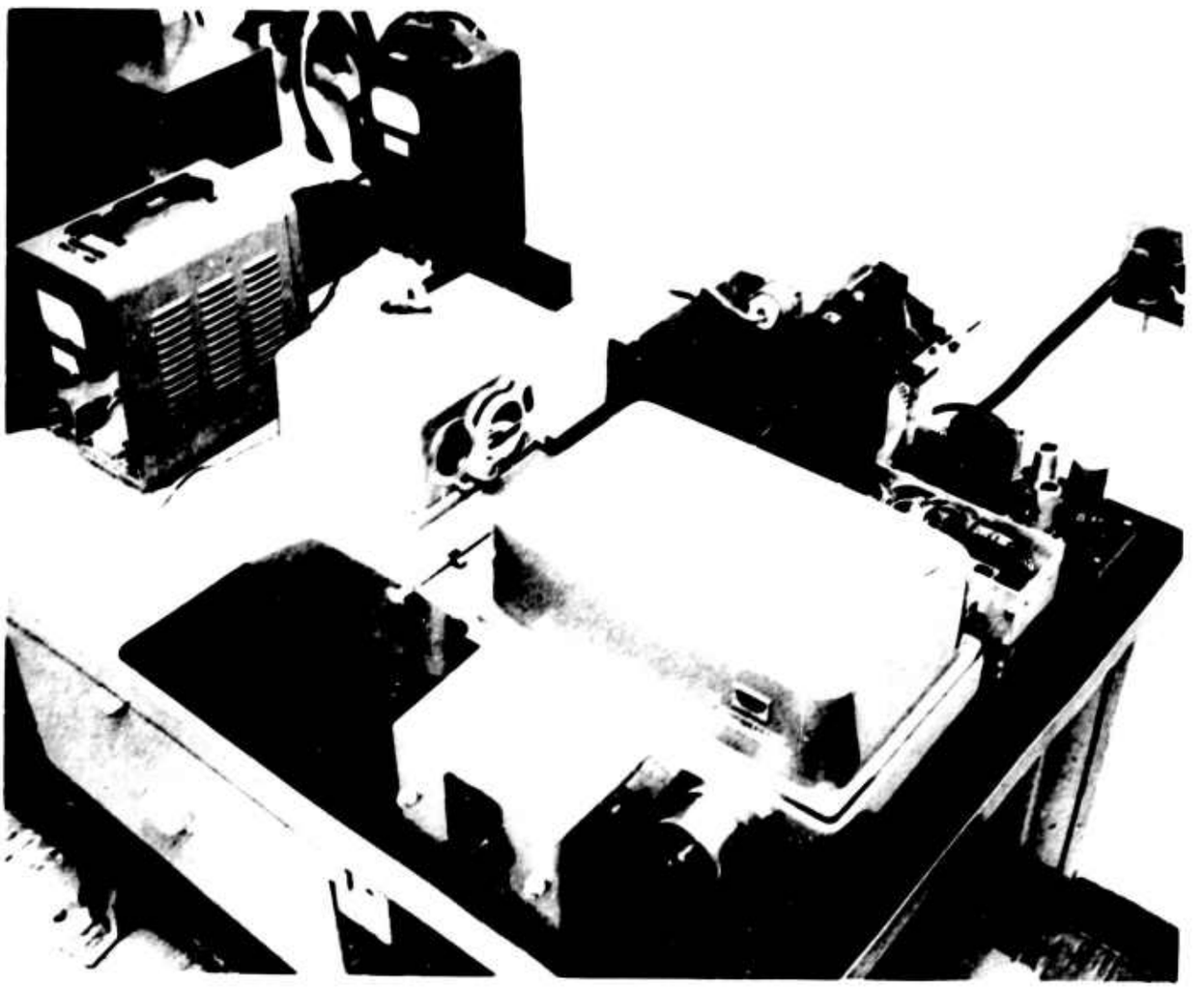

Figure 72. Spectral Reflectance Apparatus

APPENDIX IV

OPTICAL PROPERTIES MEASUREMENTS

The optical properties, solar absorptance and infrared emittance, were determined by using a method called the dynamic thermal vacuum technique, similar to the technique outlined in Reference 28. The experimental apparatus used in this technique is shown in Figures 73 and 74.

The thermal coating was applied on just one side of the specimen. The other side was vacuum-deposited aluminum on Mylar, which had an infrared emittance of only 0.043 whereas the thermal coating had an infrared emittance of about 0.80. Therefore, since only the thermal coating side received heat flux from the carbon arc, the temperature rise curves would be faster and the temperature drop curves would be slower with only one side coated. Both of these were desirable for thermal coatings whose ratio of solar absorptance to infrared emittance was small, as was the case. Another reason for coating only one side was that exposing both sides to ultraviolet radiation was more difficult.

The analysis of each specimen, to determine solar absorptance (α) and infrared emittance (ϵ) of the applied thermal coating, was accomplished by performing an energy balance during heating and cooling of the specimen. The heating was accomplished by letting the heat flux from the carbon arc strike the thermal coated side of specimen. The temperature as a function of time was then recorded. In time, the specimen reached a maximum temperature, not necessarily equilibrium temperature, at which time the carbon arc was shut off. The specimen then

began to cool down, and temperature as a function of time was again recorded. Typical heating and cooling curves are shown in Figure 75.

To analyze these curves, the following energy balance equation was used:

$$\frac{\Delta Q}{\Delta t} - \frac{\Delta R}{\Delta t} = \frac{\Delta U}{\Delta t}$$

where

$\Delta Q/\Delta t$ = rate at which heat was added to the specimen,

$\Delta R/\Delta t$ = rate at which specimen lost heat,

$\Delta U/\Delta t$ = rate of change of heat content of specimen.

The rate at which heat was added to the specimen during heating is

$$\frac{\Delta Q}{\Delta t} = I\alpha A + C_o$$

where

I = heat flux intensity of the carbon arc,

α = solar absorptance of the thermal coating,

A = area of specimen receiving heat flux,

C_o = heat exchange with chamber.

During cooling, of course, $\Delta Q/\Delta t = C_o$. In a similar manner, the rate of change of heat content of the specimen was written as

$$\frac{\Delta U}{\Delta t} = CM \frac{\Delta T}{\Delta t}$$

where

C = specific heat of the specimen,

M = mass of the specimen,

$\Delta T/\Delta t$ = time rate of change of the specimen temperature.

The rate heat lost by the specimen was due entirely to radiation and hence was written as:

$$\frac{\Delta R}{\Delta t} = (\epsilon_1 A + \epsilon_2 A + \epsilon_2 a)\sigma T^4$$

where

ϵ_1 = infrared emittance of thermal coating,

ϵ_2 = infrared emittance of copper surface,

a = edge area of specimen,

σ = Stefan-Boltzmann constant,

T = specimen temperature.

These were then written into the following form:

$$I_0 A + C_0 = CM \frac{\Delta T}{\Delta t} + (\epsilon_1 A + \epsilon_2 A + \epsilon_2 a)\sigma T^4$$

for the heating curve and

$$C_0 = CM \frac{\Delta T}{\Delta t} + (\epsilon_1 A + \epsilon_2 A + \epsilon_2 a)\sigma T^4$$

for the cooling curve. The heating and cooling curve was now analyzed to determine $\Delta T/\Delta t$ as a function of T. From the data obtained, plots were made of

$$\frac{CM}{A}\frac{\Delta T}{\Delta t} \quad \text{versus } \sigma T^4$$

for the heating and cooling curves (see Figure 76). These plots were straight lines of the following form:

$$S_2 - S_1 = Ia$$

$$a = \frac{S_2 - S_1}{I}$$

$$Ia = \left[\epsilon_1 + \epsilon_2(1 + a/A)\right](r_2 - r_1) = S_2 - S_1$$

$$\epsilon_1 = \frac{S_2 - S_1}{r_2 - r_1} - \epsilon_2 (1 + a/A).$$

This analysis was carried out on each specimen before and after exposure of the specimen to ultraviolet light. A comparison was then made between the solar absorptance before and after ultraviolet exposure and also the infrared emittance before and after ultraviolet exposure.

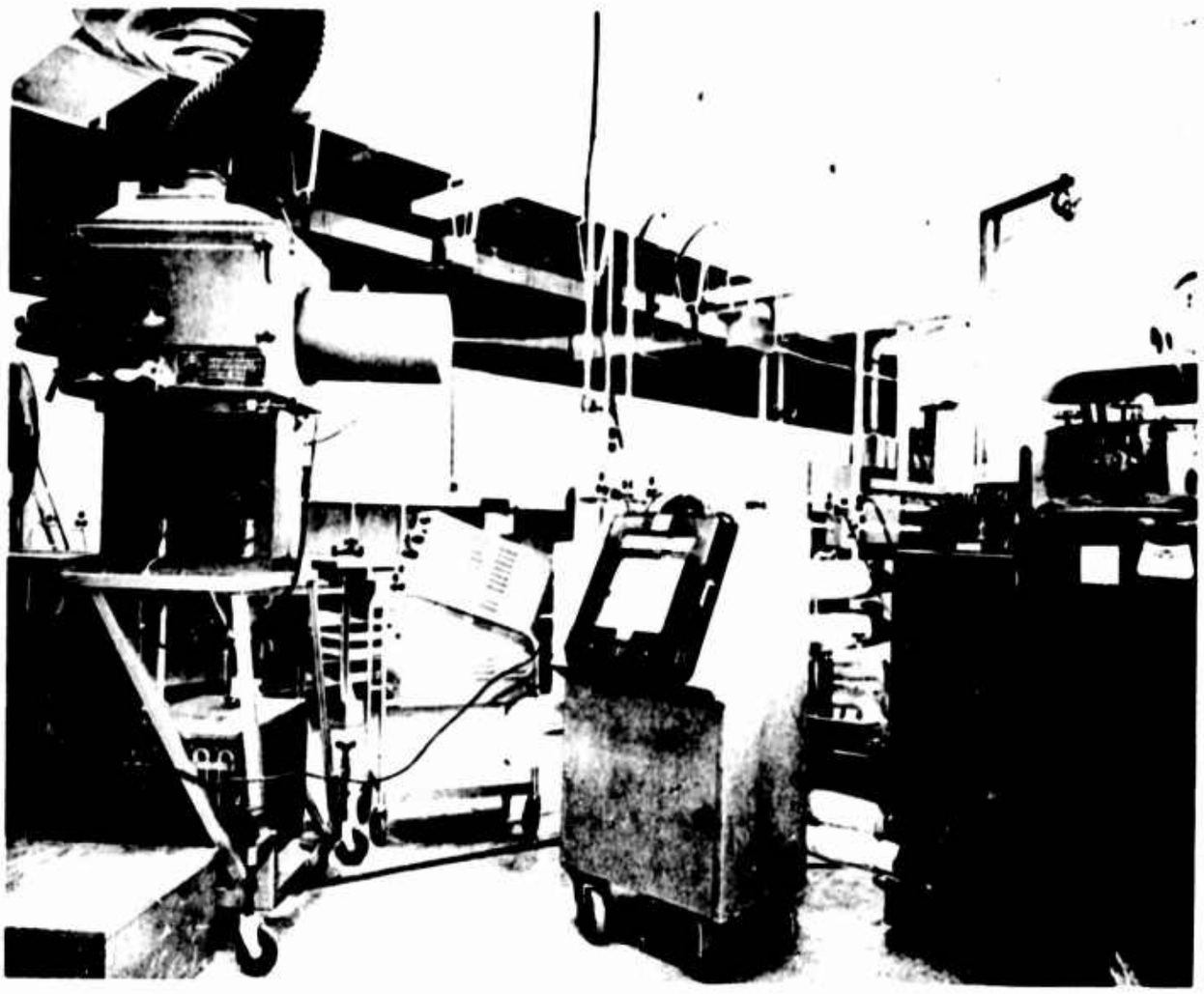

Figure 73. Carbon Arc Solar Radiation Simulator Test Setup in Operation

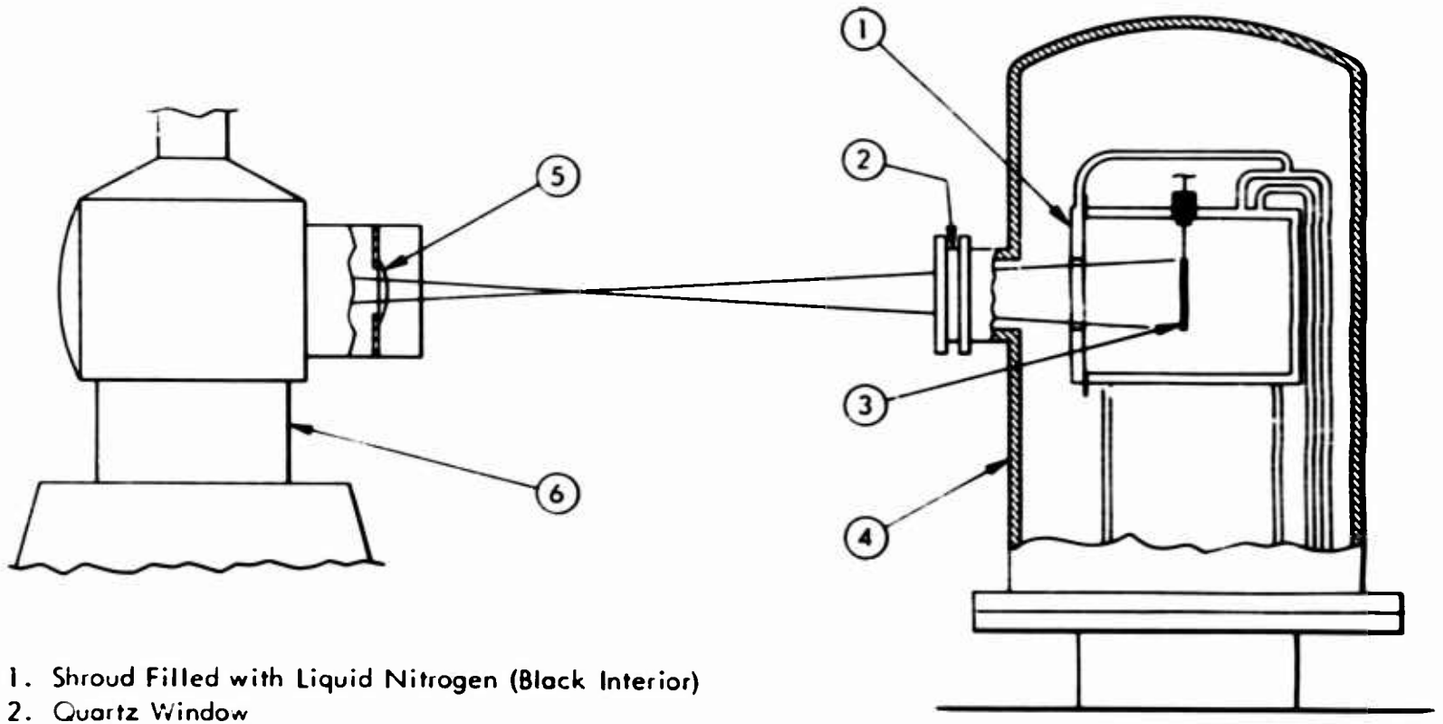

1. Shroud Filled with Liquid Nitrogen (Black Interior)
2. Quartz Window
3. Sample Suspended by Thermocouple Wires
4. Ultek 18-Inch Stainless Steel Bell Jar
5. Quartz Lens
6. Carbon Arc Solar Simulator

Figure 74. Diagram of Solar Simulator Test Setup

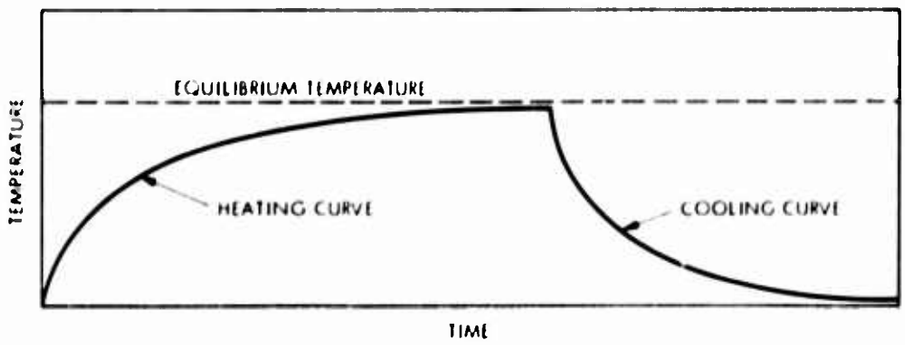

Figure 75. Typical Heating and Cooling Curves for α_S and ϵ Measurement

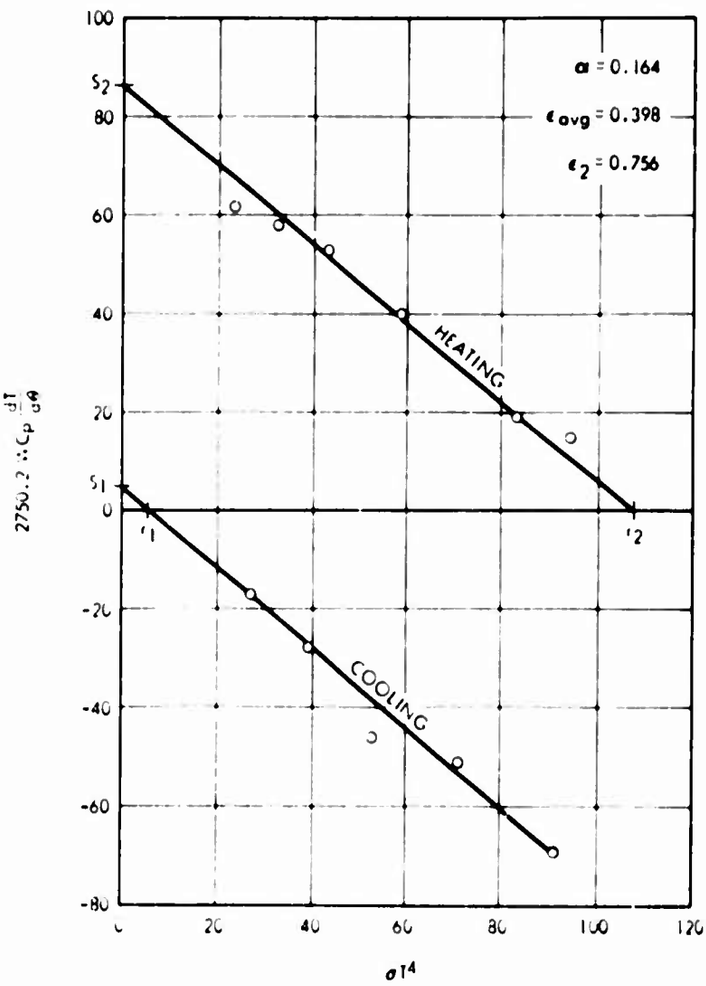

Figure 76. Dynamic Response Curves for Typical Sample

APPENDIX V

GENERAL DESCRIPTION OF PHOTO-LIGHT PAINTING PROCESS

A flow chart of the procedure for obtaining fine-line artwork by GAC's photo-lighting painting process without the use of the photographic reduction method is shown in Figure 77. This process can be of great help, specifically if the 1 to 1 scale design is exceptionally large and/or the photo-reduction errors can be tolerated.

The photo-light painting process is much the same as photographic contact printing. However, a special printer is used to vacuum a negative or positive film to the bottom surface of a glass plate, and the film to be exposed is vacuumed to the top surface of a controlled oscillating plate below the glass plate.

When a wide line is required, a negative film is used as a tool to photo-paint (see Figure 78). The machine is put into motion, and an overhead pinpoint light is used to make the time exposure (1 to 5 minutes). By presetting the machine to a specific oscillation or radius of rotation, a wider and cleaner line is obtained. When a smaller line width is required, a positive film is used as a tool (see Figure 79) and the radius of rotation is preset to give the required amount of line shrinkage.

In addition to having the capability of spreading or shrinking a line width, this process has a very unique advantage that no other photographic process has. This is the ability to start with a ragged pencil, ink, or scribed line and clean the edges so that they are still sharp under 100-power microscope. In other words, the artwork would be equal to a 100 : 1 artwork. The amount of clean-up is in direct

proportion between the edge raggedness and the radius of rotation of the photo-painting machine. Sketches illustrating good clean-up and poor clean-up are shown in Figure 80.

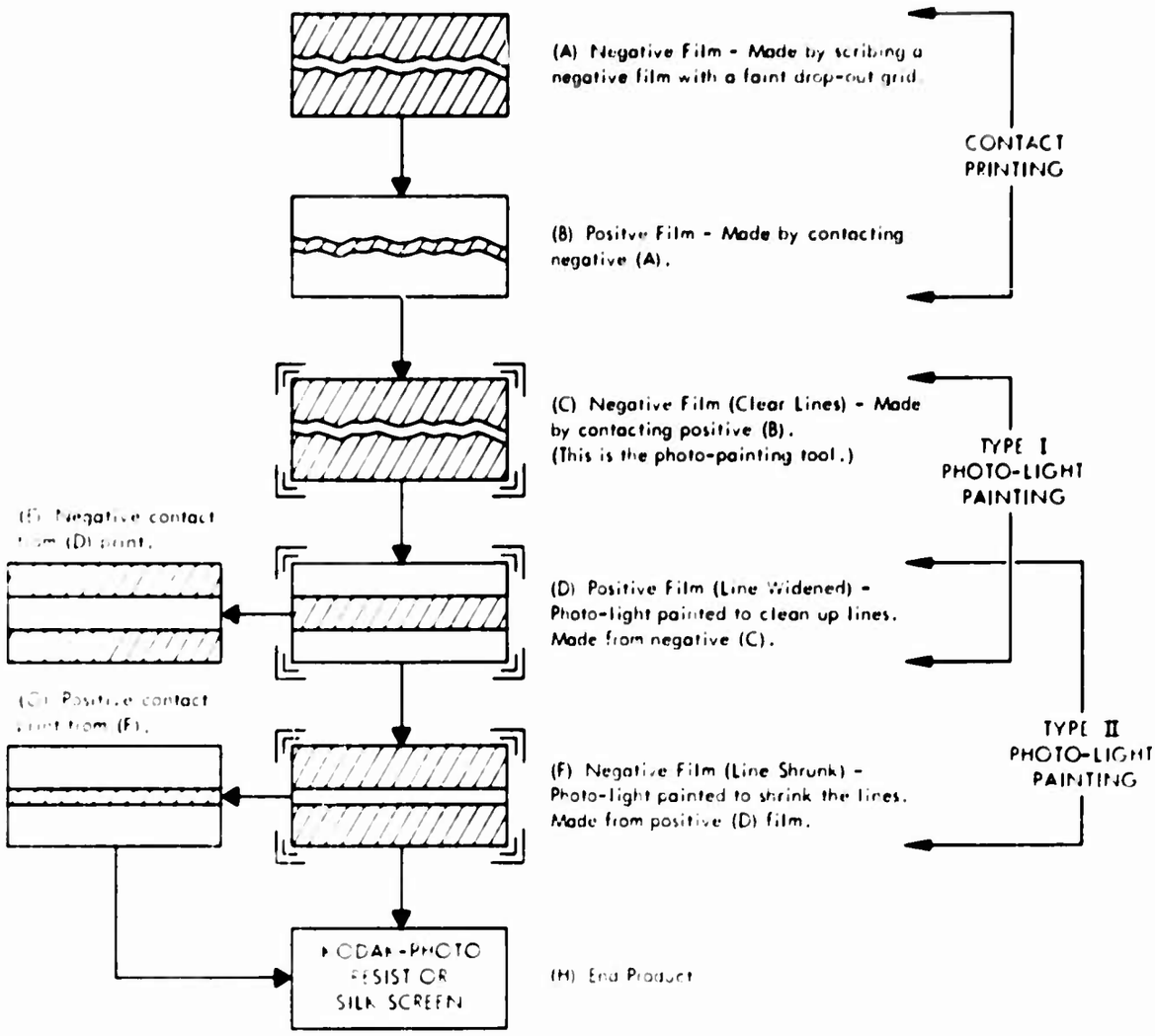

Figure 77. Photo-Light Painting Flow Chart (Types I and II)

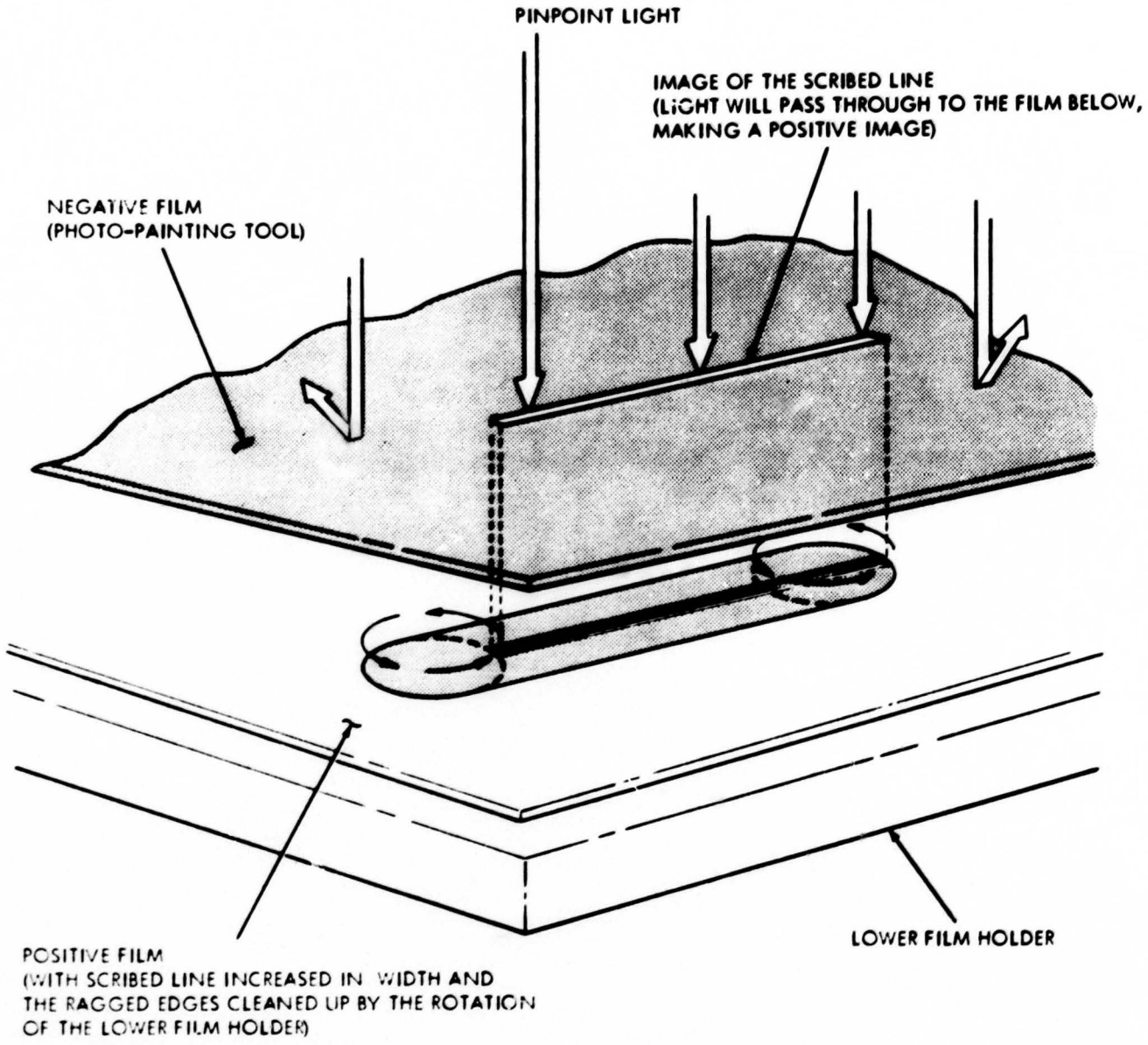

Figure 78. Type I Photo-Light Painting

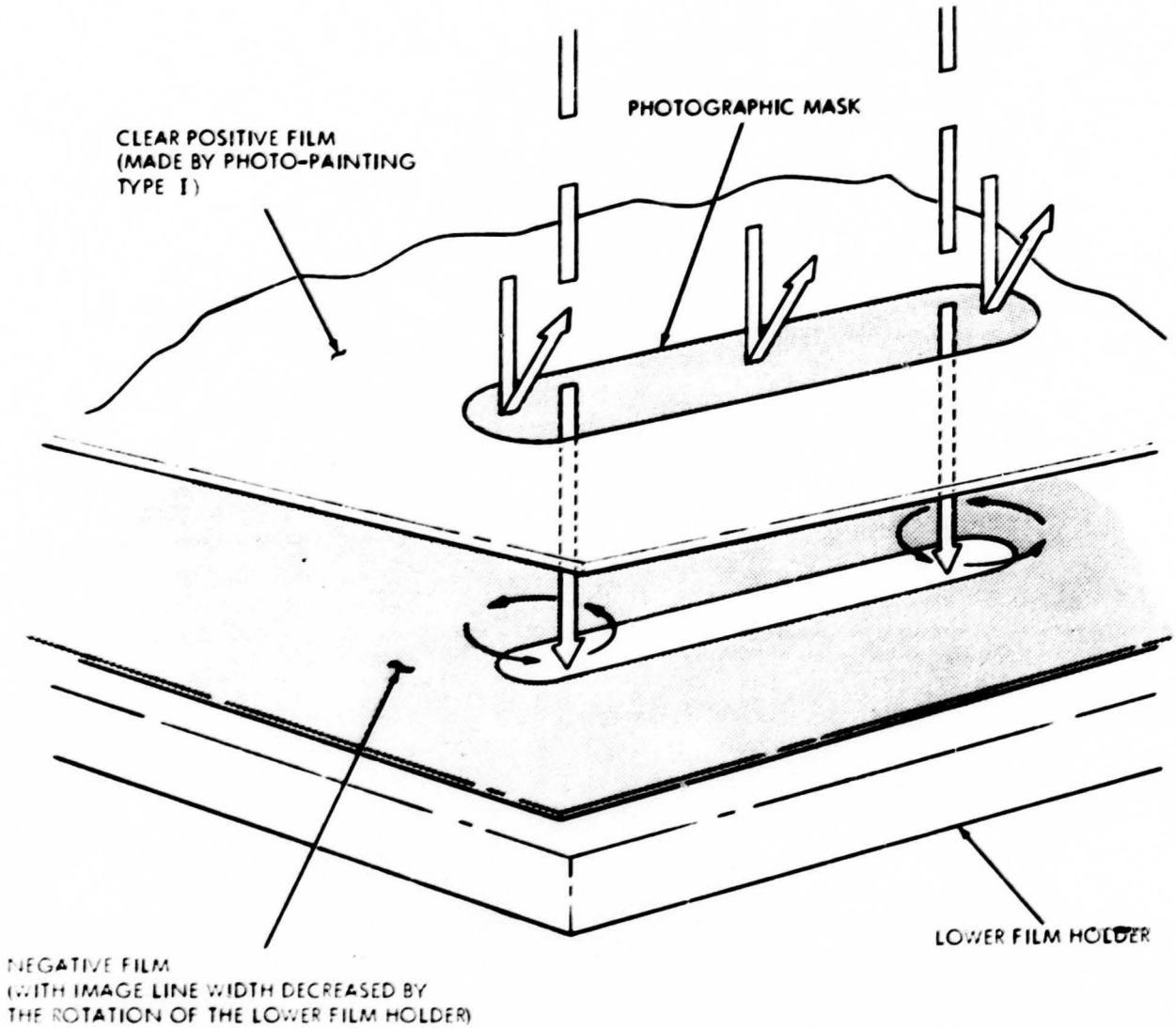

Figure 79. Type II Photo-Light Painting

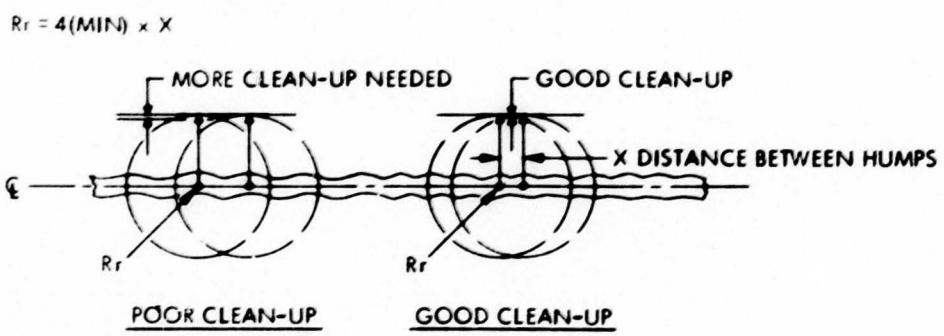

Figure 80. Etching Clean-Up Technique

UNCLASSIFIED

Security Classification

DOCUMENT CONTROL DATA - R&D

(Security classification of title, body of abstract and indexing annotation must be entered when the overall report is classified)

1. ORIGINATING ACTIVITY (Corporate author)
Goodyear Aerospace Corporation

2a. REPORT SECURITY CLASSIFICATION
None

2b. GROUP
N/A

3. REPORT TITLE
Evaluation of Lenticular Spiral Array

4. DESCRIPTIVE NOTES (Type of report and inclusive dates)
Final Report (From Sep 1964 through Dec 1965)

5. AUTHOR(S) (Last name, first name, initial)
F. J. Stimler

6. REPORT DATE	7a. TOTAL NO. OF PAGES	7b. NO. OF REFS
March 1966	202	28

8a. CONTRACT OR GRANT NO.	9a. ORIGINATOR'S REPORT NUMBER(S)
AF 30(602)-3486	GER 12369
b. PROJECT NO. 4519	
c. Task: 451901	9b. OTHER REPORT NO(S) (Any other numbers that may be assigned this report)
d.	RADC TR 66-61

10. AVAILABILITY/LIMITATION NOTICES
This document is subject to special export controls and each transmittal to foreign governments or foreign nationals may be made only with prior approval of RADC (EMCRR), GAFB, N.Y. 13440.

11. SUPPLEMENTARY NOTES	12. SPONSORING MILITARY ACTIVITY
	RADC (EMCRR) Griffiss AFB NY 13440

13. ABSTRACT

The program was initially let to support the launch of a pseudo passive satellite. Part of the requirements include the capability to add energy to the satellite orbit through absorbtion or reflection of solar energy (solar sail) and the temperature stabilization of tunnel diode amplifiers in a space environment. A lightweight packageable solar sail material possessing optical characteristics of low reflectivity and high emissivity on one side and high reflectivity and high emissivity on the opposite side was then tested under simulated space conditions. A flexible termal coating containing zinc oxide was rotoflex tested for material reliability at various test temperatures and then tested under simulated space conditions.

The goals of the procurement were then changed as the satellite requirements were negated. Scattering characteristics, load dependent and load independent, of spiral antennas in arrays and under isolated conditions were to be determined. A computer program (Fortran IV) was developed to determine the parameters of single antenna elements. The program did not produce a useful set of antenna parameters from the measured data but it should be possible to refine either the computer program or the measurements to produce correct results for single elements. Additional fundamental work must be done in this field before a scattering approach can be applied to arrays.

DD FORM 1 JAN 64 1473

UNCLASSIFIED

Security Classification

14 KEY WORDS	LINK A		LINK B		LINK C	
	ROLE	WT	ROLE	WT	ROLE	WT
Spiral Antennas Antenna Radiation Patterns Coupled Antennas Scattering Materials Solar Radiation Temperature Control Optical Properties						

INSTRUCTIONS

1. ORIGINATING ACTIVITY: Enter the name and address of the contractor, subcontractor, grantee, Department of Defense activity or other organization *(corporate author)* issuing the report.

2a. REPORT SECURITY CLASSIFICATION: Enter the overall security classification of the report. Indicate whether "Restricted Data" is included. Marking is to be in accordance with appropriate security regulations.

2b. GROUP: Automatic downgrading is specified in DoD Directive 5200.10 and Armed Forces Industrial Manual. Enter the group number. Also, when applicable, show that optional markings have been used for Group 3 and Group 4 as authorized.

3. REPORT TITLE: Enter the complete report title in all capital letters. Titles in all cases should be unclassified. If a meaningful title cannot be selected without classification, show title classification in all capitals in parenthesis immediately following the title.

4. DESCRIPTIVE NOTES: If appropriate, enter the type of report, e.g., interim, progress, summary, annual, or final. Give the inclusive dates when a specific reporting period is covered.

5. AUTHOR(S): Enter the name(s) of author(s) as shown on or in the report. Enter last name, first name, middle initial. If military, show rank and branch of service. The name of the principal author is an absolute minimum requirement.

6. REPORT DATE: Enter the date of the report as day, month, year, or month, year. If more than one date appears on the report, use date of publication.

7a. TOTAL NUMBER OF PAGES: The total page count should follow normal pagination procedures, i.e., enter the number of pages containing information.

7b. NUMBER OF REFERENCES: Enter the total number of references cited in the report.

8a. CONTRACT OR GRANT NUMBER: If appropriate, enter the applicable number of the contract or grant under which the report was written.

8b, &c, & 8d. PROJECT NUMBER: Enter the appropriate military department identification, such as project number, subproject number, system numbers, task number, etc.

9a. ORIGINATOR'S REPORT NUMBER(S): Enter the official report number by which the document will be identified and controlled by the originating activity. This number must be unique to this report.

9b. OTHER REPORT NUMBER(S): If the report has been assigned any other report numbers *(either by the originator or by the sponsor)*, also enter this number(s).

10. AVAILABILITY/LIMITATION NOTICES: Enter any limitations on further dissemination of the report, other than those imposed by security classification, using standard statements such as:

(1) "Qualified requesters may obtain copies of this report from DDC."

(2) "Foreign announcement and dissemination of this report by DDC is not authorized."

(3) "U. S. Government agencies may obtain copies of this report directly from DDC. Other qualified DDC users shall request through _____."

(4) "U. S. military agencies may obtain copies of this report directly from DDC. Other qualified users shall request through _____."

(5) "All distribution of this report is controlled. Qualified DDC users shall request through _____."

If the report has been furnished to the Office of Technical Services, Department of Commerce, for sale to the public, indicate this fact and enter the price, if known.

11. SUPPLEMENTARY NOTES: Use for additional explanatory notes.

12. SPONSORING MILITARY ACTIVITY: Enter the name of the departmental project office or laboratory sponsoring *(paying for)* the research and development. Include address.

13. ABSTRACT: Enter an abstract giving a brief and factual summary of the document indicative of the report, even though it may also appear elsewhere in the body of the technical report. If additional space is required, a continuation sheet shall be attached.

It is highly desirable that the abstract of classified reports be unclassified. Each paragraph of the abstract shall end with an indication of the military security classification of the information in the paragraph, represented as *(TS), (S), (C), or (U)*.

There is no limitation on the length of the abstract. However, the suggested length is from 150 to 225 words.

14. KEY WORDS: Key words are technically meaningful terms or short phrases that characterize a report and may be used as index entries for cataloging the report. Key words must be selected so that no security classification is required. Identifiers, such as equipment model designation, trade name, military project code name, geographic location, may be used as key words but will be followed by an indication of technical context. The assignment of links, rules, and weights is optional.